Examining the diversity of Apollo 12 basalts through geochemical and mineralogical studies of basaltic coarse fines from the Apollo 12 soil sample 12023,155 L. Alexander[1, 2] (l.alexander@bbk.ac.uk), J.F. Snape[2, 3], I.A. Crawford[1, 2], K.H. Joy[2,3, 4, 5] and R. Burgess[6]. [1]Birkbeck College, London, UK. [2]CPS at UCL-Birkbeck, London. [3]Department of Earth Sciences, UCL, London, UK. [4]CLSE, The Lunar and Planetary Institute, USRA, Houston, TX 77058, USA. [5]The NASA Lunar Science Institute. [6]SEAES, University of Manchester, UK.

Introduction: The Apollo 12 mission landed in the Eastern region of Oceanus Procellarum in November 1969 and returned 34 kg of mainly basaltic samples. Crater size-frequency distribution measurements [1] indicate that a large number of individual basaltic flows are located within the Oceanus Procellarum, including some of the youngest mare basalts on the Moon (~1.2 Ga). The potential for lateral transport of material across the lunar surface as a result of impacts [2,3] allows the possibility that some of this young basaltic material may have been sampled by the Apollo 12 mission. Therefore, further analysis of the Apollo 12 sample collection may help to constrain the duration of lunar volcanism and provide new insights into the magmatic evolution of the Moon. Here we present textural characteristics, bulk chemical compositions and mineral chemistries for lunar soil sample 12023,155 consisting of 12 basaltic coarse fines ~ 2mm in diameter. In particular, 4 potentially atypical samples will be discussed.

Methods: Each grain was split in two with the larger split retained for petrographic analysis and the smaller split allocated for radiometric dating. Textures were examined using a JEOL JXA-8100 electron microprobe with an Oxford Instrument INCA energy dispersive system (EDS) to produce backscattered electron (BSE) images and elemental maps. Modal mineralogies were obtained from BSE images and elemental maps using imaging software to identify the phases. Bulk compositions were calculated using multiple raster beam analyses (RBA) across the samples that were corrected for differences in phase densities in accordance with [4]. These methods have been previously tested on known samples [5] and found to be in good agreement. Individual mineral grain analyses were obtained with an integrated wavelength dispersive system (WDS).

Sample Descriptions: The samples studied are all holocrystalline basalts. Samples are low-Ti basalts in accordance with the compositional scheme of [6]. In addition, most of the samples have chemical and textural similarities to other known Apollo 12 basalts [7] in that these coarse fines are generally typical of Apollo 12 low-Ti olivine, pigeonite and ilmenite basalts [2]. Four samples (155_2A, 8A, 9A and 10A) are similar to olivine basalts with highly varied textures from subophitic to porphyritic to microgabbroic and modal percentages of olivine (Fo_{48-74}) between 7.8 and 13.9%. Pyroxenes are zoned with highly variable compositions ($En_{1-63}Fs_{20-84}Wo_{8-39}$), with the exception of the microgabbroic sample, 155_8A which appears to have a more equilibrated ($En_{39-56}Fs_{22-39}Wo_{11-38}$) composition and shows little zoning. Two samples (155_3A and 155_7A) are similar to ilmenite basalts with higher modal abundances of ilmenite (4.2 and 6.5% respectively) and intermediate TiO_2 contents >5 wt% (table 1). In addition, 155_7A exhibits a schlieren-like texture together with small pools of sulphides and this may indicate a degree of shock processing. Plagioclase compositions in 155_7A (An_{76-93}) are more varied than in other samples and olivines are more fayalitic (Fo_{34-55}). A further two samples (155_6A and 155_12A) bulk compositions indicate that they are similar to Apollo 12 pigeonite basalts (table 1), with textures which are dominated by large, highly zoned pyroxenes ($En_{0-67}Fs_{22-87}Wo_{7-37}$), partially enclosing plagioclase (An_{87-93}) and ilmenite laths. Minor olivine (Fo_{65-73}) is present in 155_6A (5.9% of the sample). In addition, exceptions to these standard lithological groups are noted which warrant further investigation:

12023,155_1A. We identify this sample as a coarse-grained pyroxene cumulate, consisting mainly of pyroxene (93%), in which ilmenite is absent. The sample consists of orthopyroxene ($En_{53-65}Fs_{26-35}Wo_{7-12}$) which encloses olivine (Fo_{60-68}) together with minor augite ($En_{45}Fs_{24}Wo_{30}$), plagioclase (An_{83}) and spinel. This is the most magnesian sample with a bulk Mg# composition of 65.33 (table 1).

Sample	155_1A	155_2A	155_3A	155_4A	155_5A	155_6A
Na_2O	0.31 ± 0.02	0.42 ± 0.01	0.55 ± 0.02	0.46 ± 0.01	0.50 ± 0.02	0.42 ± 0.02
MgO	20.28 ± 0.03	12.72 ± 0.12	6.34 ± 0.04	7.47 ± 0.08	7.83 ± 0.02	10.29 ± 0.02
Al_2O_3	2.31 ± 0.03	8.66 ± 0.17	10.65 ± 0.07	11.91 ± 0.08	12.29 ± 0.26	10.61 ± 0.10
SiO_2	51.48 ± 0.06	43.86 ± 0.10	44.31 ± 0.03	45.30 ± 0.09	46.54 ± 0.23	44.12 ± 0.08
K_2O	0.01 ± 0.02	0.07 ± 0.01	0.07 ± 0.01	0.07 ± 0.01	0.12 ± 0.02	0.09 ± 0.02
CaO	5.10 ± 0.01	8.05 ± 0.06	10.80 ± 0.06	10.50 ± 0.06	10.21 ± 0.01	9.66 ± 0.02
TiO_2	0.90 ± 0.04	3.05 ± 0.08	5.69 ± 0.08	3.95 ± 0.07	3.65 ± 0.08	3.26 ± 0.05
FeO	19.18 ± 0.07	23.06 ± 0.16	21.65 ± 0.12	19.07 ± 0.08	17.67 ± 0.01	20.67 ± 0.03
Total	99.56	99.89	100.06	98.73	98.81	99.13
Mg #	65.33 ± 0.21	49.58 ± 0.52	34.3 ± 0.27	41.12 ± 0.19	44.13 ± 1.65	47.02 ± 0.51
Sample	155_7A	155_8A	155_9A	155_10A	155_11A	155_12A
Na_2O	0.38 ± 0.01	0.46 ± 0.02	0.44 ± 0.01	0.51 ± 0.01	0.49 ± 0.02	0.43 ± 0.02
MgO	10.17 ± 0.01	12.26 ± 0.06	12.54 ± 0.23	14.41 ± 0.09	3.71 ± 0.04	6.99 ± 0.04
Al_2O_3	5.56 ± 0.08	9.84 ± 0.15	8.67 ± 0.15	7.13 ± 0.09	11.57 ± 0.09	10.52 ± 0.07
SiO_2	44.21 ± 0.11	45.88 ± 0.11	42.11 ± 0.15	45.22 ± 0.16	43.78 ± 0.17	46.89 ± 0.12
K_2O	0.14 ± 0.07	0.03 ± 0.01	0.05 ± 0.01	0.05 ± 0.01	0.14 ± 0.01	0.09 ± 0.01
CaO	9.69 ± 0.01	10.39 ± 0.07	8.01 ± 0.13	8.14 ± 0.07	10.91 ± 0.05	10.65 ± 0.06
TiO_2	5.18 ± 0.09	1.32 ± 0.06	3.25 ± 0.05	2.51 ± 0.07	5.29 ± 0.12	2.93 ± 0.06
FeO	24.91 ± 0.03	19.43 ± 0.16	23.83 ± 0.19	21.62 ± 0.16	23.96 ± 0.14	19.70 ± 0.11
Total	100.24	99.61	98.88	99.59	99.84	98.20
Mg #	42.12 ± 0.39	52.94 ± 0.34	48.4 ± 1.12	54.3 ± 0.40	21.63 ± 0.24	38.74 ± 0.28

Table 1. Bulk chemical compositions in wt% oxide for samples 12023,155_1A to 12A. Mg# = Mg/(Mg+Fe) atomic ×100. Errors for major element oxides are 1δ standard deviation. Propogation of errors is used to calculate the error for Mg#

12023,155_4A and 5A. These samples are likely to be from the same parent rock, given similarities in their bulk chemical compositions (table 1) and min-

eral chemistries. They have a sub-ophitic texture, consisting of large fractured pyroxenes (41.2% by mode) which are highly zoned with variable compositions ($En_{2-58}Fs_{22-86}Wo_{8-36}$) partially enclosing blocky plagioclase (An_{88-92}) Minor embayed olivine (Fo_{64-69}) is present in both samples (4.8 and 2.8% by mode, respectively). Interstitial silica is common accounting for up to 7% modally. Opaque phases are seen mainly in the form of ilmenite (up to 4.9%) but occasional rounded spinels are also present. Pyroxenes also contain tiny opaque inclusions of Fe-Ni metal and sulphides (troilite) occur in trace amounts, associated with ilmenite. These samples are similar to feldspathic basalts or evolved pigeonite basalts, which have low-Ti contents (<4 wt% TiO_2, table 1) and have higher Al concentrations (11.91 and 12.29 wt% Al_2O_3 respectively). Both samples have relatively high modal plagioclase contents (42.3 and 36.6%) which together with the bulk chemistry of these samples, indicate that they are feldspathic in nature.

12023,155_11A. This is an unusual variolitic sample consisting of Fe-rich pyroxene (43.5%), plagioclase (42.8%), ilmenite (4.5%) and silica (9%). No olivine is present. This sample exhibits an apparently evolved composition with a very low Mg# (21.63) compared with the other Apollo 12 material studied here. 155_11A also contains relatively high Al (11.57 wt% Al_2O_3) and Ti (8.29 wt% TiO_2) abundances. Pyroxenes are zoned with variable compositions ($En_{0-43}Fs_{40-85}Wo_{12-33}$) but are distinct from all other samples (figure 2d), with no Fe-poor pyroxenes detected, further attesting to the evolved nature of the melt from which it crystallized.

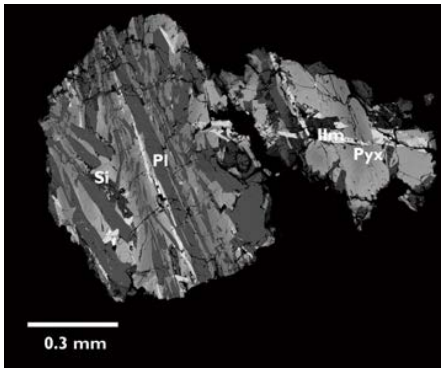

Figure 1: BSE image of 12023,155_11A illustrating distinct differences in textures within the sample. Si = silica, Pl = plagioclase, Pyx = pyroxene, Ilm = ilmenite

Summary: Most of the basaltic fines presented in this study have chemical and textural similarities consistent with olivine, pigeonite or ilmenite Apollo 12 low-Ti basalt lithological groups, but noted exceptions may require contributions from separate lava flows. The acquisition of trace element mineral chemistries (ongoing) will complete the chemical analysis of these samples. Results can then be evaluated together with Ar-Ar dating in order to gain a better understanding of the petrogenesis and source regions of these samples.

References: [1] Hiesinger, H. et al. 2003. JGR 108, E7. [2] Li, L. and Mustard, J.F. 2005. JGR, 110, E11002-E11018. [3] Petro, N.E. and Pieters, C.M. 2007. LPS XXVII Abstract #2069. [4] Warren, P.H. 1997. LPS XXVIII Abstract #1497. [5] Snape, J.F. et al. 2011. LPS XLII Abstract #2011. [6] Neal, C.R. and Taylor, L.A. GCA. Vol 56. pp.2177-2211 [7] Papike, J.J. et al. 1998. Lunar Samples. Reviews in Mineralogy, 36, pp 5-1 – 5-234.

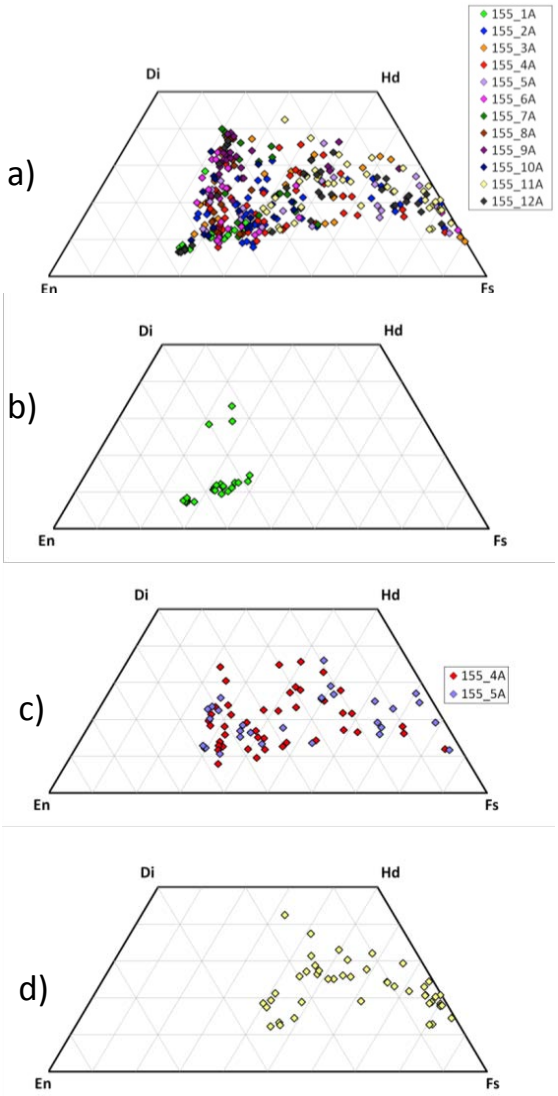

Figure 2: Pyroxene compositions in 12023,155. a) Pyroxene compositions from all samples showing a typical range for lunar basalts. b) Pyroxene compositions in 155_1A, a cumulate textured pyroxenite. Compositions are more equilibrated and Mg-rich than other samples. c) Pyroxene compositions in 155_4A and 155_5A, showing a wide range of compositions d) Pyroxene compositions in the evolved sample 155_11A which are all Fe-rich.

The Abundance, Distribution, and Source(s) of Water in the Moon M. Anand[1,2] and R. Tartèse[1], [1]Planetary and Space Sciences, The Open University, Walton Hall, Milton Keynes, MK7 6AA, UK. [2]The Natural History Museum, Cromwell Road, London, SW7 5BD, UK. (M.Anand@open.ac.uk)

Introduction: Recently, we have witnessed a paradigm shift in our understanding of the history of water on the Moon. Currently, there is less disagreement over the presence of water in the lunar interior as documented by sample analysis. However, uncertainties exist regarding the abundance, distribution, and the source(s) of water in the lunar interior. The giant-impact origin of the Moon is thought to have involved a lunar magma ocean (LMO) phase. Much of any water present during the accretion of the Moon would presumably have been lost to space because of high-temperatures but some primordial water may have been sequestered in minerals and rocks formed by LMO solidification. Mare basalts (and volcanic glasses) derived by partial melting of the lunar mantle have erupted episodically onto the lunar surface. Any evidence for the presence of water in the lunar mantle is likely to be preserved in mare basalts as water behaves incompatibly during mantle partial-melting and is thus partitioned preferably into the melt. The Apollo missions collected a range of lunar samples including those of primary LMO products (e.g., anorthosites, Mg-suite rocks etc.) and a variety of mare basalts with crystallization ages predominantly ranging from ~ 3.9 to ~ 3.1 Ga [1].

Results to date: There has been several reports on the discovery of variable amounts of hydroxyl/water in lunar volcanic glasses [2], melt inclusions [3] and in apatites from mare basalts [4-9]. Direct analyses in melt inclusions in high-Ti glasses yielded a pre-eruptive H_2O content of 270 - 1202 ppm [3]. Glass beads themselves contain 10 ± 4 ppm H_2O, corresponding to a pre-eruptive H_2O content of ca. 490 ± 160 ppm. In very low-Ti glasses, H_2O content is more heterogeneous (0.4 - 30 ppm [2]) and corresponds to pre-eruptive H_2O contents of ca. 20 - 1600 ppm. Water content of apatites, in which it is present in OH form, range from a few ppm to more than 1 wt. % OH [4-9]. In a few cases, the hydrogen isotopic composition of the lunar water has also been measured indicating significantly elevated D/H ratios compared to terrestrial values. In addition, significant intra-sample variability in terms of water content at roughly constant δD value seems to characterize a number of lunar samples. Furthermore, comparison of apatite OH contents with the age of mare-basalts reveal two interesting features: (1) the mean OH content tends to increase from older to younger basalts (2) there is far larger intra-sample variability in the OH content of the younger (< 3.5 Ga) low-Ti basalts (Fig. 1). Interestingly, samples of the lunar crust, some of which correspond to the earliest LMO products, contain the lowest amounts of water [5] suggesting late addition of water to the Moon.

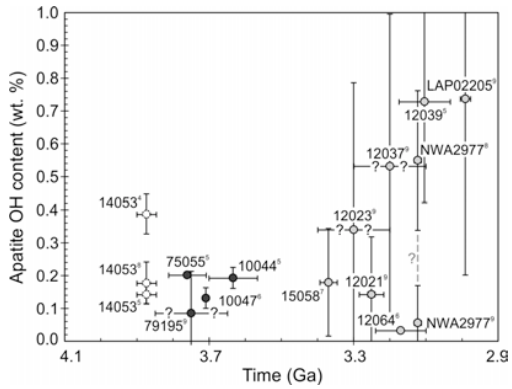

Figure 1: OH content of apatites from mare basalts plotted against mare basalt ages. Vertical error bars represent intra-sample variability (standard deviation of the mean). Superscript numbers after sample numbers correspond to the references given in the reference list.

Discussion: The existing dataset for water contents in a range of lunar rock types strongly suggest heterogeneous distribution of water inside the Moon. Although relatively fewer data points exist for the hydrogen isotopic composition of water in these lunar samples, it is increasingly becoming obvious that lunar samples have highly fractionated δD values compared to terrestrial samples. This specific signature has been interpreted in terms of cometary source for lunar water [5] although it is also possible to generate such fractionated δD values through degassing of hydrogen from a cooling magma body. At the very low fO_2 in the lunar interior (IW-2), H_2 is likely to be the dominant H-bearing species in the lunar magma. Degassing of H_2 could generate highly fractionated D/H ratios in the cooling magma, and, it could be that water/OH only becomes stable in lunar magmas towards the very end of their crystallization, coinciding with the onset of apatite crystallization, which then becomes the main carrier phase of OH. If this scenario is correct then it is possible that the current estimates for the water contents of the bulk-Moon are overestimated and these figures need to be revised downwards.

References: [**1**] Papike, J.J. et al. (1998) *Rev. Mineral. Geochem. 36,* 5001-5234. [**2**] Saal, A.E. et al. (2008) *Nature 454,* 192-195. [**3**] Hauri, E.H. et al. (2011) *Science 333,* 213-215. [**4**] Boyce, J.W. et al. (2010) *Nature 466,* 466-469. [**5**] Greenwood, J.P. et al. (2011) *Nat. Geosci. 4,* 79-82. [**6**] Greenwood, J.P. et al. (2012) *LPSC XLIII*, Abs# 2089. [**7**] McCubbin, F.M. et al. (2010) *Am. Min. 95,* 1141-1150. [**8**] McCubbin, F.M. et al. (2010) *PNAS 107,* 11223-11228. [**9**] McCubbin, F.M. et al. (2011) *GCA 75,* 5073-5093.

THE EARLY MOON: IMPACT RECORD AND OTHER PARAMETERS. V. A. S. M. Fernandes and J. P. Fritz, Museum für Naturkunde, Leibnitz Institut an der Humboldt Universität zu Berlin, Invalidenstr. 43, 10115 Berlin; veraafernandes@yahoo.com; joerg.fritz@mfn-berlin.de;

Introduction: The ancient lunar crust bears testimony of an early (>3.7 Ga) period that is characterized by frequent hypervelocity impacts of 10´s to 100´s km sized projectiles that detonated ~40 basin sized (>300 km diameter) impact structures into the lunar crust [e.g., 1]. By implication, a larger number of such massive impact events affected the early Earth [2], but the traces of these events are erased by crustal recycling of our geological active planet. An important debate in lunar and planetary science relates to the period of time during which these lunar basins formed. The finding that ~3.9 Ga old impact reset rocks were collected on all 6 Apollo landing sites gave rise to the concept of a "Late Heavy Bombardment (LHB)" or "terminal lunar cataclysm" where most or all of the basins formed during a <200 Ma time interval centered around 3.9 Ga [3-6]. The LHB hypothesis gained popularity with dynamical models presenting celestial mechanisms for a "late" reconfiguration of the Solar System architecture that could provide abundant projectiles for such a "late" event [7, 8].

However, the interpretation that samples collected by the Apollo and Luna missions and lunar meteorites bear evidence for a "terminal lunar cataclysm" is repeatedly criticized [i.e. 9- 11]. Currently the dominance of ~3.9 Ga ages in Apollo and Luna mission samples is thought to be due to either 1) the resetting of the different radiogenic chronometers (e.g. Rb/Sr, Ar/Ar) around 3.9 Ga by a large number of impacts at that time [i.e. 12], or 2) because all Apollo missions mainly sampled Imbrium ejecta [9,10].

In order to contribute to the aims of the lunar community for acquiring a more comprehensive view of the impact history of the Earth-Moon system, we briefly 1) revisit the first 800 Ma of lunar history, 2) review radiometric ages (including correction for K-decay and monitor ages as appropriate; [13-15]), 3) review petrography of Apollo and Luna samples and 4) discuss four different approaches for constraining the time interval during which the lunar basins formed.

1) Relating impact melt rocks to specific basins by geological arguments – The Nectaris case -

The age of the Nectaris basin (and it difference in age to Imbrium basin) is considered key for testing the putative LHB [16]. Proposed ages for Nectaris formation range between 4.2 Ga [17] and 3.85 Ga [18]. The assignment of a 3.9 Ga [19] and 3.85 Ga[18] age for Nectaris are based on forma-tion age (minimum age given by the youngest clast within the breccia) of rock sized breccias collected on the rim of the North Ray Crater (NRC). Later, Norman et al. [20] reported KREEP-rich impact melt clasts of 3.85 Ga within some of the NRC breccias. They concluded that this breccias bear no information for the age of Nectaris, because the KREEP signature should be indicative of Imbrium derived ejecta.

A 4.2 Ga age was proposed for Nectaris to account for the variety of lithologies related to the Descartes formation [17]. In addition, different publications report rocks with impact reset ages up to 4.3 Ga for samples collected by Apollo 16 astronauts [21, 22], (Fig. 1). Thus, the Moon surface was impacted before 4.0 Ga ago. Moreover, a variety of impact craters, including basins Tranquilitatis, Nectaris, Serentiatis and Imbrium, delivered material to the Apollo 16 landing site. Thus, relating individual samples collected from the lunar surface with a specific impact basin will always be ambiguous. Therefore, additional information is required to constrain the heavy bombardment of the Moon.

The lunar curst: Understanding the formation, thickening and cooling of the lunar crust is essential to constrain the:

1) formation time when impacts could leave lasting marks, i.e., it provides a maximum age for lunar basins.

2) thickening time after which the crust was too thick for the delivery of meteoritic PGE´s to the mantle by even the largest impact events, i.e., the 0.02 % of lunar mass equiva-lent of meteoritical material required to explain the chondritic PGE signature in lunar basalts [23] had to be delivered be-fore that time .

3) cooling time of the lunar crust which increases viscosity and by this the support for retaining the topographic relief of impact structures for the past ~4 billion years [i.e. 9. 24].

2) Time estimates based on geological independent processes:

In order to estimate the time lapse between formation of different basins, Baldwin [9, 24] argued that the ages of lunar basins can be deduced by comparing the topographic relief of the impact structures (categorized from young to old correspond to class 1 to 10, respectively). The older crater structures (>161 km diameter) that formed in a less viscous (warmer) lunar crust would display a higher degree of topographic smoothing compared to younger crater structures that formed on a cooler and thus a more supportive lunar crust. At about 3.7 Ga ago, the viscosity of the lunar crust had increased to high values allowing it to support the prominent topographic relief of Imbrium and Orientale for billions of years. Baldwin [9, 24] argued that the prominent morphological differences of Orientale (class 2) and Nectaris (class 7) require that the latter basin to be older by a few 100´s Ma.

3) Impact exhumation scenario: Basin-sized impacts into a warm and less viscous lunar crust [9, 24] would be consistent with an impact exhumation scenario for some lunar rocks by considering: 1) crystallization in deep and warm crustal areas with an open system behaviour for some isotopic systems, followed by impact-exhumation by large impacts, and then cooling on or near the lunar surface. This impact exhumation scenario can explain the difference between the Sm-Nd crystallization age and the K-Ar age for FAN rock 60025 with crystallization at 4.44 Ga and resetting of the K-Ar system at ~4.2 Ga [25-27]. It could also explain the 4.36 Ga Pb-Pb age, and 4.32 Ga ^{146}Sm-^{142}Nd ages re-ported recently for 60025 [28] within

the petrological context of the standard lunar magma ocean (LMO) model. The stan-dard LMO model [29, and refs. therein] interprets FAN rocks as flotation cumulates that formed during crystallization of the LMO. Hence, the FAN rock 60025 must have formed earlier than the 4.36 Ga Pb-Pb ages since the LMO crystalli-zation is constrained to have been completed before 4.42 Ga ago, as given by the isotopic age of the KREEP reservoir [29]. The impact excavation model could explain the isotopic age of FAN rocks being younger than the reservoir age of the KREEP source. 60025 could have formed early (>4.42 Ga) during the LMO crystallization at deep crustal levels where temperatures remained for an extended period above the closing temperatures of the different isotopic systems. The 4.2 Ga Ar-age of FAN rock 60025 [21,22, 25-27] would then date the time of a basin sized impact.

4) Impact age frequencies for meteorites from the Moon and the asteroid belt can provide another test for an extreme intense bombardment during a putative LHB. Statistical age distribution for impact reset H and L chondrites and HED [30] and lunar [11] meteorites provide no evidence for a brief (<200 Ma) and extremely high impact rate centered around 3.9 Ga. Instead, the impact ages distribution shows a similar number of impact ages between 4.2 and ~3.0 Ga.

Conclusion: The currently available lunar impact record dates back to [at least] 4.3 Ga ago [31], Figure 1. The lithologic variety of impact reset rocks older than 4.0 Ga show that not all basins formed around 3.9 Ga ago. Despite that some of the large lunar basins (Imbrium and Orientale) formed "late", it has to be seriously considered that a large number of lunar basins formed are older than 4.0 Ga (see also [59 & 60], i.e., could reasonably be part of the tail end of planetary accretion [61].

Acknowledgement: VASMF and JPF thank ISSI for supporting an international Team of discussion on the lunar bombardment. Financial support of JF by the Helmholtz Alli-ance "Planetary Evolution and Life", and VASMF thanks financial support from the DFG-ICDP FE-130074.

References: [1] Wilhelms (1987) U.S.G.S. Prof. Paper 1348. [2] Maher & Stevenson (1988) Nature 331, 612-614. [3] Tera et. al. (1974) EPSL 22, 1-21. [4] Turner et al. (1973) PLPSC IV, 1889-1914 [5] Ryder (1990) EOS 71, 322-323. [6] Cohen et al.(2005) MaPS 40, 755-777. [7] Gomes et al. (2005) Nature, 435, 466. [8] Morbidelli et al. (2007) AJ, 134, 1790. [9] Baldwin (1974) Icarus 23, 157-166. [10] Haskin et al. (1998) MaPS 33, 959-975. [11] Chapman et al. (2007) Icarus 189, 233-245. [12] Stöffler & Ryder (2001) Space Sci. Rev. 96, 9-54, 2001. [13] Steiger & Jäger (1977) EPSL 36, 359–362. [14] Jourdan & Rene (2007) GCA 71, 387–402. [15] Schwarz & Trieloff (2007) Chem.Geol. 242 218–231. [16] Norman (2009) Elements 1, 23-28. [17] Schäffer et al. (1976) PLPSC VII, 2067-2092. [18] Stöffler et al. (1985) PLPSC XV 90, C449-C506. [19] James (1981) LPSC XII, 503-505. [20] Norman et al. (2010) GCA 74, 763-783. [21] Fernandes et al. (2008) Early S.S. Impact Bombard. I, abst. #3028. [22] Fernandes & Fritz (2011) LPSC XLII, #1189. [23] Day et al. (2007) Science 315, 217-219. [24] Baldwin (2006) Icarus 184, 308-318. [25] Carlson & Lugmair (1988) EPSL 90, 119-130. [26] Schäffer & Husain (1973) PLPSC IV, 1847-1863. [27] Schäffer & Husain (1974) PLPSC V, 1541-1555. [28] Borg et al. (2011) Nature 477, 70–72. [29] Shearer et al. (2006) Rev. Mineral. Geochem. 60, 365-518. [30] Bogard (2011) Chem. der Erde 71, 207-226. [31] Fernandes et al. (submitted). [32] Kirsten et al. (1973) PLPSC IV, 1757-1784. [33] Kirsten & Horn (1974) PLPSC V, 1451-1475. [34] Cadogan & Turner, 81976) PLPSC VII, 2267-2285. [36] Schäffer & Schäffer (1977) PLPSC VIII, 2253-2300. [37] Maurer et al. (1978) GCA 42, 1687-1720. [38] Staudacher et al. (1978) PLPSC IX 1098-1100. [39] McGee et al. (1978) PLPSC IX, 743-772. [40] Dalrymple & Ryder (1996) JGR 101, 26,069-26,084. [41] Culler et al. (2000) Science 287, 1785-1788. [42] Levine et al. (2005) GRL 32, L15201, doi:10.1029/2005GL022874. [43] Barra et al. (2006) GCA 70, 6016–6031. [44] Norman et al. (2006) GCA 70, 6032–6049. [45] Zellner et al. (2006) LPSC XXXVII, #1745. [46] Norman et al. (2007) XXXVIII, # 1991. [47] Hudgins et al. (2008) 72, 5781–5798. [48] Fernandes et al. (2000) MaPS 35, 1355-1364. [49] Fernandes et al. (2004) XXXV #1514. [50] Fernandes et al. (2008) Goldschmidt Conf. #A264. [51] Fernandes et al. (2009) MaPS 44, 805-821. [55] Gnos et al. (2004) Science 305, 657-660. [56] Burgess et al. (2007) XXXVIII # 1603. [57] Haloda et al. (2009) GCA 73, 3450-3470. [58] Sokol et al. (2009) GCA 72, 4845-4873. [59] Frey (2011) GSA Spec. Paper 477, 53-75. [60] Spudis et al. (2011) doi:10.1029/2011JE003903 [61] Morbidelli et al. (2012) Early S.S. Impact Bombard. II, abst. #4014.

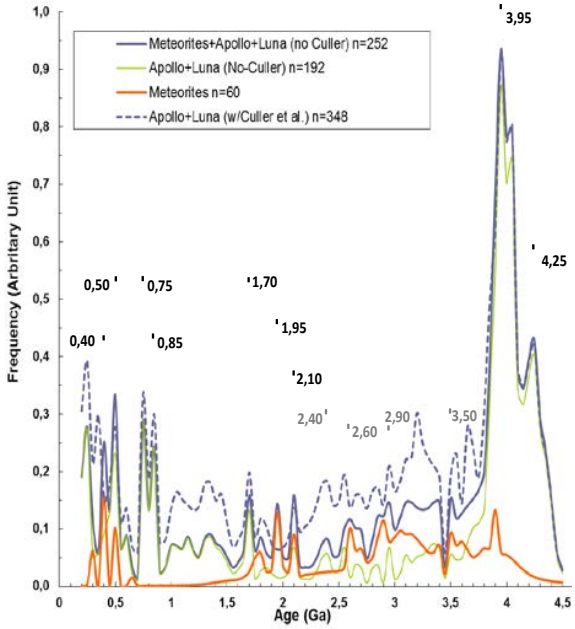

Figure 1: Gaussian probability curve calculated using published 40Ar/39Ar impact ages obtained for samples from Apollo 12, 14, 16 and 17 and Luna 16 and 24 missions [26, 27, 31-47] and lunar meteorites [7, 48-58]. To calculate this curve, the sample age and error were combined in bins of 0.05 Ga (50 Ma) which is representative of the average error in $^{40}Ar/^{39}Ar$ age determination. Where necessary, the age was corrected for monitor age and decay-constant. Orange line is the cumulative ompact ages for lunar meteorites; the green line is the cumulative impact ages for Apollo and Luna missions samples; the thick blue line is the cumulative impact ages for Apollo, Luna and meteorites and does not include the [41] due to uncertainty in the glass origin, i.e., volcanic or impact. However, for comparison, the same line with the [41] data is plotted and shown using the thin blue dotted line.

MOON SUB-SURFACE EXPLORER 'MOUSE' - THE COMPLEX INSTRUMENT FOR GEOTECHNICAL PARAMETERS DETERMINATION OF THE LUNAR REGOLITH.

M. Banaszkiewicz[1] J. Grygorczuk[1], K. Seweryn[1], R. Wawrzaszek[1] [1]Space Research Centre Polish Academy of Sciences (18a Bartycka str. 00-716 Warsaw Poland, marekb@cbk.waw.pl).

Introduction: Space exploration is a global endeavour with many technical challenges to be taken. Its main objective is to extend our civilization to other bodies of the Solar System, starting with the neighbouring ones, by sending to them robotic as well as human missions.

Preparation for the space bodies exploration requires systematic scientific investigations that enlarge our knowledge about target bodies and in consequence allows to exploit its results for the benefit of future exploration programs, but it also requires development of available technologies. One example is research of dust on the Moon surface. The lunar surface is covered by dust particles with micro and nanometer size [1]. Fraction of dust grains is often ionized and interacts with solar wind leading to interesting dusty plasma effects [2]. Except the purely scientific interest, such effects can have an important consequence for astronauts working on lunar surface, for instance can be a source of different kinds of human illnesses [4]. The problem is aggravated by the local increase of dust density due to the interaction between man-made devices like robotic arms, sampling devices, rovers or astronauts activities on the lunar surface. Since the source of dust is the surface layer of the regolith, the studies of mechanical properties (structure, cohesion, strength) of the regolith are important from both the scientific and technical point of view.

Subsurface layers of the Moon: Investigation of subsurface layers of the lunar regolith can provide clues for solving a number of important scientific questions [3], such as: (i) the nature of impactors (comets?, asteroids?) that produced lunar craters in the period of late have bombardment, (ii) the origin, evolution and circulation of volatiles in the regolith, (iii) internal structure of the Moon, (iv) transformation of the regolith at different time scales due to meteoroid and micrometeoroid impacts as well as interaction with cosmic rays and solar wind ions. In order to answer these questions, complex in-situ measurements should be carried out, covering elemental, molecular and mineralogical analysis, but also studies of physical processes, such as heat and mass transfer or surface-exosphere interaction. It is of much importance to perform these measurements in many points on the lunar surface and at many depths in the regolith.

Technological challenges: Such requirement poses a challenge for technical tools that have to be developed for comprehensive exploration of the Moon. Not a single lander or rover but a network of

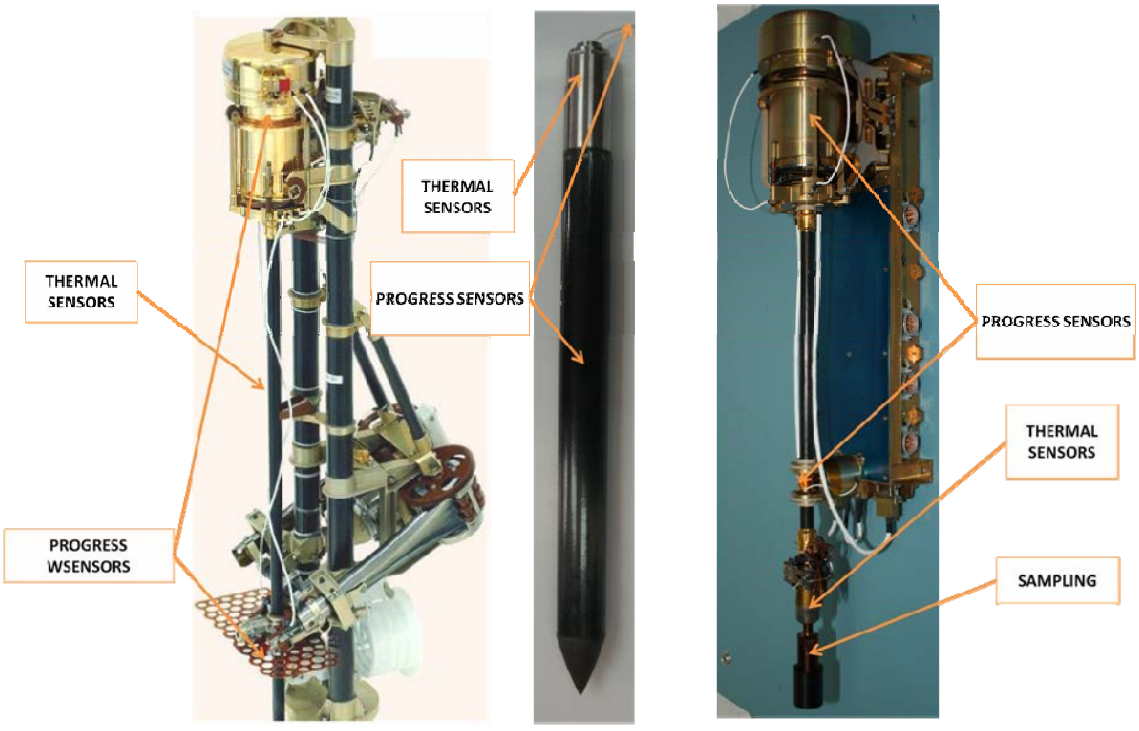

Figure 1. Penetrometers developed in SRC PAS: starting from left – MUPUS instrument for Rossetta mission, mole KRET instrument, CHOMIK instrument for Phobos Grunt mission

monitoring stations and swarms of autonomous vehicles will be required to collect data in quantity that is necessary to make substantial progress in understanding the fundamental processes that have shaped our natural satellite from the time of its origin till now. Such an approach will be beneficial from the point of view of future exploitation of the Moon. Knowing where to look for valuable minerals or sources of energy (eg He3) will allow to optimize future prospecting and mining efforts. From the perspective of human bases on the Moon it is important to find out source of water (polar regions of the Moon) and minerals that could be used to produce fuel (e.g O2 + H2). Any constructions on the Moon will require comprehensive engineering knowledge about properties of lunar rocks and regolith that will be used as potential building blocks.

Penetrometers: Space Research Centre is ready to get involved in the international cooperation on preparing the future exploration and exploitation of the Moon. The assets we can offer comprise mechanical devices for penetrating the subsurface layers and taking the samples of the regolith as well as deployment devices that can provide means to set the penetartors at desired points on the surface [5]. Several types of penetrating devices have been developed in SRC, including MUPUS penetrator for Rosetta mission [6], [11], Chomik sample taker delivered for Fobos-Grunt mission [7] or new generation of moles with very efficient performance [8]. These units are equipped with measuring probes, for instance, temperature and thermal conductivity sensors [9] and progress sensor [10] – details on figure 1. Basing on these heritage, SRC is ready to extend its expertise to include a number of new sensors and tools that will be used to address the following scientific issues:

- thermal budget of the Moon
- composition (gas and solid components) of Moon's surface layers in its natural state
- geotechnical properties of Moon's surface layers in its natural state

In the presentation, the concept of complex instrumental suite MOUSE that will allow for subsurface investigations will be presented. The existing penetrators will be described and concepts of accommodating new instruments will be provided. In the attached figure examples of devices developed are shown, while in the Table 1, the matrix illustrating the research objectives of planned instruments is given.

References:

[1] Stubbs, T. J., et al. (2005), ESA SP-643, p.239-243. [2] J. S. Halekas, et al. (2008), LPSC XXXIX. [3] National Research Council, (2007) The Scientific Context for the Exploration of the Moon, National Academies Press. [4] D. Linnarson et al. (2012), Scientfic Preparation for Lunar Exploration, ESTEC/ESA. [5] Grygorczuk, J. et al. (2011), 11th ASTRA, ESTEC/ESA. [6] Spohn, T. et al. (2007), Space Sci. Rev, 128. [7] Grygorczuk, J. et al. (2010), 1st Moscow Solar System Symposium, Moscow. [8] Seweryn et al. (2011) LPSC XVII. [9] Banaszkiewicz, M et al. (2007) *Adv. Space Res. 40(2)* 226-237. [10] Seweryn et al. (2012) Scientfic Preparation for Lunar Exploration, ESTEC/ESA. [11] Grygorczuk, J. et al. (2007) *J. Tel. Inf. Techn.* 1/2007.

Table.1 Potential set of instrumentation and it's impact on determination of properties of lunar surface/subsurface matter basing on SRC expertise. Level of impact: H: high; M-H: medium high; M-L: medium low; L: low

Measurement goals / Hardware component	Heat conductivity, diffusivity and capacity	Density of lunar regolith	Porosity of lunar regolith	Local seismic waves velocity in lunar surface (+ echo sounding)	Mechanical and geotechnical properties of lunar surface	Lunar surface mineralogy	Actual maturity of technology (TRL)
Penetrator with thermal active and passive sensors	**H**	**M-H**	**M-H**	**L**	**M-L**	**M-L**	**4**
Penetrator with progress measurement device	**L**	**M-H**	**M-H**	**L**	**H**	**M-H**	**3**
Penetrator + matrix of geophones	**L**	**M-L**	**L**	**H**	**H**	**M-H**	**2**
Electrical permeability probe	**M-L**	**M-H**	**M-H**	**L**	**H**	**M-H**	**3**
Radioactive source and detector	**L**	**H**	**H**	**L**	**H**	**M-H**	**3**
Microcamera	**M-L**	**H**	**H**	**L**	**H**	**M-H**	**2**
VIR spectrometer	**L**	**L**	**M-L**	**L**	**M-L**	**H**	**1**

ENERGETIC NEUTRAL ATOMS FROM THE MOON. REVIEW OF THE CHANDRAYAAN/SARA OBSERVATIONS AND FUTURE INVESTIGATIONS. S. Barabash[1], Y. Futaana[1], M. Wieser[1], and C. Lue[1], P. Wurz[2], A. Vorburger[2], A. Bhardwaj[3], M. B. Dhanya[3], R. Sridharan[3], K. Asamura[4], [1]Swedish Institute of Space Physics, Box 812, SE-98128 Kiruna, Sweden; stas@irf.se, [2]Physikalisches Institut, University of Bern, Sidlerstrasse 5, CH-3012 Bern, Switzerland, [3]Space Physics Laboratory, Vikram Sarabhai Space Centre, Trivandrum, 695022, India, [4]Institute of Space and Astronautical Science, 3-1-1 Yoshinodai, Sagamihara, Japan.

Introduction: The Moon does not possess a global magnetic field and collisional atmosphere but only a surface –bound tenuous exosphere. The lunar surface is thus exposed to the solar wind. The interaction of the solar wind particles with the lunar regolith and exosphere results in the production of fast (velocities higher than the escape velocity) neutrals, energetic neutral atoms (ENA). The solar wind particles may be neutralized by the surface and backscattered, cause sputtering of regolith atoms, or charge – exchange on the exosphere. Detecting ENAs remotely provides a diagnostic tool to study the plasma – surface interaction processes and image the global plasma distribution. Mechanisms of the ENA production at the Moon [1][2] and Mercury are similar and the ideas of ENA imaging of the Moon is based on the earlier analysis performed for Mercury [3].

SARA Instrument: SARA (Sub-keV Atom Reflecting Analyzer) is a package of an ENA imager and ion spectrometer flown onboard the Indian Chandrayaan-1 mission [4]. The ENA imager provides measurements of ENA fluxes in the energy range 10 eV - 3.3 keV and field-of-view 15° x 160° divided into 7 angular pixels in the fan configuration. Each pixel is about 7° x 45° (full-width-half-maximum). The ion spectrometer monitors the ion fluxes in the energy range 10 eV – 15 keV. SARA operated on a circular 100 km polar orbit from January to July 2009.

ENAs from the Moon: Detection of backscattered hydrogen from the Moon occurred almost simultaneously by an ENA detector onboard NASA IBEX [5], an Earth orbiting satellite to observe heliospheric ENAs, and SARA [6]. The fluxes observed are high 10^6-10^7 cm^{-2} sr^{-1} s^{-1} and correspond to 10% - 20% of the solar wind protons backscattered as hydrogen. The detailed analysis of the scattering function [7] revealed that the scattering occurs preferentially backwards not forward, and becomes shallower for larger solar zenith angles. It is uniform over azimuth but becomes more peaked for large solar zenith angles. The ENA energy spectrum is best fitted by a Maxwellian distribution with a temperature of 60 – 160 eV depending on the solar wind velocity [8]. The physics of the solar wind – regolith interaction behind the observed features is still not clear. No observations of the charge – exchange ENAs were reported so far. IBEX seems to observe a few oxygen atoms emitted from the Moon, which are likely to be sputtered products of the solar wind – regolith interaction (P. Wurz, private communication).

ENA Imaging: ENA provided a very effective tool to image lunar magnetic anomalies, which, as turned out, create voids (50% reduction) in the solar wind flux reaching the surface as observed at an anomaly at the Gerasimovich crater [9]. This first ENA image of the lunar mini-magnetosphere revealed a complex structure including the solar wind void surrounding by the enhanced flux region, an analogy to the terrestrial magnetosphere and magnetosheath. ENA imaging of the anomalies showed [10] that these structures are highly variable and the morphology is fully controlled by the solar wind dynamic pressure.

Future Investigations: The future investigations and observations of the lunar ENAs should be focused on understanding (1) microphysics of the solar wind – regolith interaction, and (2) global ENA imaging of the solar wind – magnetic anomaly interaction. To address the question (1) one would require detailed measurements of the ENA scattering function, energy spectra, and dependences on the solar wind from a lander. For global ENA imaging one would require high (at least 5° x 5°) angular resolution measurements from an orbiter. There investigations are planned to be conducted onboard the Russian Luna-Globe lander and Luna-Globe orbiter scheduled for launch in 2015.

References: [1] Futaana Y. et al. (2006) *Planet. Space Sci.*, *54* (2), 132–143. [2] Futaana Y. et al. (2008) *J. Geophys. Res.*, *113*, doi: 10.1029/ 2008JA013356. [3] S. Barabash, et al. (1997), Proceedings of the Mercury workshop, Kiruna, Sweden, IRF Scientific Report 244, 51 – 64. [4] Barabash S. et al. (2009) *Current Science*, *96*, 526–532. [5] McComas D. J. et al. (2009) *Geophys. Res. Lett.*, *36*, doi:10.1029/2009GL038794. [6] Wieser M. et al. (2009), *Planet. Space Sci.*, *57*, 2132–2134 and Wieser M. et al. (2011) *Planet. Space Sci.*, *59* (8), 798–799. [7] Schaufelberger A. et al. (2011) *Geophys. Res. Lett.*, *38*, doi:10.1029/2011GL049362. [8] Futaana Y. et al. (2012) *J. Geophys. Res.*, *submitted*. [9] Wieser M. et al. (2010) *Geophys. Res. Lett.*, *37* (5), doi:10.1029/2009GL041721. [10] Vorburger A. et al. (2012) *J. Geophys. Res.*, *submitted*.

Lunar volatiles: An examination of hydrogen isotopes and hydroxyl content. J. J. Barnes[1], M. Anand[1,2], I. A. Franchi[1], N. A. Starkey[1], R. Tartèse[1], Y. Sano[3] and S. S. Russell[2]. [1]Planetary and Space Sciences, The Open University, Walton Hall, Milton Keynes, MK7 6AA, UK. [2]The Natural History Museum, Cromwell Road, London, SW7 5BD, UK. [3]Atmosphere and Ocean research institute, The University of Tokyo, 5-1-5, Kashiwanoha, Chiba, 277-8564, Japan. Email: jessica.barnes@open.ac.uk

Introduction: A re-investigation of Apollo rock samples has up-ended the long standing consensus that the Moon is an anhydrous planetary body[1]. This has been spurred by the findings of water in apatite grains from a range of Apollo rock samples, glass beads and melt inclusions[2-7]. Currently the maximum recorded water content is from apatite in Apollo 12 mare basalt 12039 which contains up to 1.13 wt.% OH, and the maximum recorded δD thus far is +1010 ‰, also from the same sample[7].

Here we report our latest results of ion microprobe analyses of D/H ratio and OH content of apatite in mare basalt 12064 and troctolite 76535. We also present the findings of an experiment designed to test the effects of scanning electron microscopy on volatiles in lunar apatites prior to ion probe analysis.

Materials: We used as a primary standard a homogenous apatite, Morocco, which is characterized by a δD of -84.9 ‰ and an OH content of 0.26 wt.%. For calibration we used a homogenous apatite, Imaichi, which has an OH content of 0.019 wt.% and an unknown δD value.

Method: Apatite grains were identified using the FEI Quanta 200 3D scanning electron microprobe at the Open University. Ion microprobe analyses were conducted using the Cameca NanoSIMS 50L at the Open University. A large Cs^+ beam of 250 pA current was used, and each analysis was preceded by a 3 minute pre-sputter. The beam was rastered over a 12 ×12 µm area, but the data were only collected from the central 5 × 5 µm area. The negative secondary ions of ^1H, ^2H, ^{13}C and ^{18}O were collected simultaneously. An electron gun was used for charge compensation.

Results: Figure 1 shows the NanoSIMS results and errors are reported as 2⎵. Apatite grains in Apollo basalt 12064 have a δD range from +768 ‰ to +998 ‰ and the OH content ranges from 0.033 wt.% to 0.14 wt.%. Troctolite 76535 has a δD signature ranging from -113 ‰ to +557 ‰ and an OH content ranging from 0.0026 wt.% to 0.0073 wt.%.

Discussion: Interestingly, the maximum δD value recorded from 12064 overlaps with the highest previously reported δD value from mare basalt 12039[7]. It has been suggested that this high δD may be attributed to cometary input to mare source regions[7]. However, alternative hypotheses involving magma degassing could also explain the high δD and low OH contents of these samples[8,9]. Finally, these fractionated D/H signatures could have been inherited from the proto-lunar disc evolution.

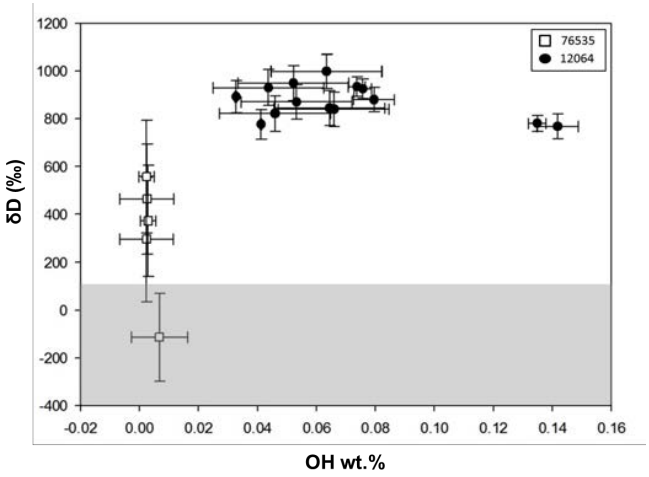

Figure 1. Results from ion microprobe analysis of apatites in 12064 and 76535 samples. Errors are reported at 2⎵. The grey box corresponds to the range of terrestrial δD.

Conclusion: Mare basalt 12064 has among the highest δD recorded thus far from Apollo samples. The samples studied here have δD signatures above the range of terrestrial δD (except for one analysis of troctolite) and contain relatively low hydroxyl contents. The lunar crustal rocks appear to have lower δD and hydroxyl contents than mantle derived rocks. A further study is in progress to collect additional hydroxyl and hydrogen isotope data for a range of lunar samples, which will aid our understanding of these preliminary results.

Acknowledgments: We thank CAPTEM and MWG for sample allocation. This research has been funded by the Science and Technology Facilites Council (STFC) and the UK Cosmochemical and Analytical Network (UKCAN).

References: [1] Papike, J.J. (1998) *Min. Soc. Of America* [2] Saal, A.E. et al. (2008) *Nature*., 454, 192-195 [3] Hauri, E.H. et al. (2011) *Scienceexpress*., 333, 1-4 [4] Boyce, J.W. et al. (2010) *Nature*., 466, 466-469 [5] McCubbin, F.M. et al. (2010) *PNAS*., 107, 11223-11228 [6] McCubbin, F.M. et al. (2011) *GCA*., 75, 5073-5093 [7] Greenwood, J.P. et al. (2011) *Nat. Geoscience*., 4, 79-82 [8] Ustunisik, G. et al. (2011) *Am. Min*., 96, 1650-1653 [9] Greenwood, J. P. et al. (2012) *LPSC XLIII* Abstract # 2089.

THE NA EXOSPHERE OF THE MOON DURING PERSEID 2009 METEOR SHOWER. A. A. Berezhnoy[1], O. R. Baransky[2], K. I. Churyumov[2], T. K. Churyumova[2], V. V. Kleshchenok[2], V. Mangano[3], V. O. Ponomarenko[2], Yu. I. Velikodsky[4], [1]Sternberg Astronomical Institute, Universitetskij pr., 13, Moscow, 19991 Russia ber@sai.msu.ru , [2]Shevchenko National University, Kiev, Ukraine, [3]Institute of Astrophysics and Planetology from Space, INAF, Rome, Italy, [4]Institute of Astronomy, Kharkiv National University, 35 Sumskaya Street, Kharkiv, 61022 Ukraine

Observations: Observations of Na resonance lines (5890 and 5896 Å) in the lunar exosphere at the 2-m Zeiss Terskol telescope (Kabardino-Balkaria, Russia) were performed during 2008 – 2010 years. The most successful observations were performed on August 12-13, 2009 and August 13-14, 2009 during maximum of Perseid meteor shower (see Table). According to [1] maxima of Perseid meteor shower on Earth occurred on Aug. 12, 2009 at 8 and 18 UT and Aug. 13, 2009, 6 UT. Six eshelle spectra were obtained at the distances of 50″, 150″, and 250″ (90, 270, and 455 km, respectively) from the lunar limb above the north pole which was bombarded by Perseid's meteoroids. Spectral resolution was equal to 15 000, the exposure time of each spectrum was equal to 1 800 s. Height of the slit is 10″, width of the slit is 2″. For calibration purpose star HD214923 was observed.

Time of observations, UT	Distance from the surface, km	Position angle, degrees	Intensity of Na D2 line, R
Aug. 12, 23:13 - 23:43	90	-19	11.4
Aug. 12, 23:54 – Aug. 13, 0:24	270	-19	12.2
Aug. 13, 0:43 -1:13	455	-19	9.4
Aug. 13, 23:22 – 23:52	90	-15	10.6
Aug. 13, 23:53 – Aug. 14, 0:23	270	-15	8.1
Aug. 14, 0:26 – 0:56	455	-15	4.8

Table 1. Parameters of observations of the Moon.

Discussion: To subtract solar spectrum we use high-resolution solar spectrum [2] averaged to spectral resolution of Terskol's telescope (see Fig. 1). The signal-to-noise ratio of obtained spectra is about 50. Spectral transpearency of Earth's atmosphere at 600 nm was taken as 75 % in accordance with [3]. Based on D1/D2 line area ratio accuracy of measurements of Na line areas is estimated as 3 %. Brightness of Na lines at 270 and 455 km from the limb is 107 % and 83 % in comparison with that at 90 km on Aug. 12/13, 2009. Brightness of Na lines at 270 and 455 km from the limb is 77 % and 45 % in comparison with that at 90 km on Aug. 13/14, 2009. Brightness of reflected solar spectrum at 270 and 455 km is 75 % and 54 % in comparison with that at 90 km on Aug. 12/13 and 13/14, 2009.

Temperature of Na atoms is estimated as 2100±400 K on Aug. 13/14. Temperature of Na atoms on Aug. 12/13 is higher than 3000 K. Obtained results can be explained as evidence of quick variability of brightness of Na lines during maximum of Perseid meteor shower which is responsible for additional intensity of Na D2 line of about 5 R on Aug. 13, 2009 at 0-1 UT. It corresponds to zenith column density of impact-produced Na atoms of about 4×10^{7} cm^{-2}. Taking properties of Perseid's impacts from [4] our results can be explained by single impact of Perseid meteoroid with mass of about 1.2 kg or additional mass flux of small meteoroids of about 5×10^{-18} g cm^{-2} s^{-1}.

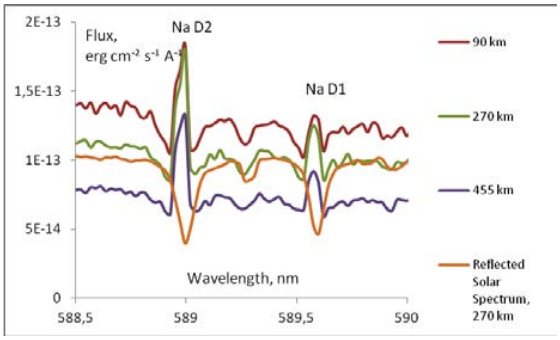

Fig. 1. Obtained spectra of the lunar exosphere on Aug. 12,978 UT, 13,006 UT and 13,04 UT, 2009.

Conclusions: Quick variability of brightness of Na lines during maximum of Perseid 2009 meteor shower is detected and explained by impacts of Perseid meteoroids. Maximum of activity of Perseid's meteor shower on the Moon is observed on Aug. 13, 2009 at 0-1 UT.

Acknowledgments: This research was supported by joint RFBR grant 11-02-90440-Ukr_f_a and DFFD grant F40 2087. Authors would like to thank A. Mozgovaya and staff of Terskol Observatory.

References:

[1] IMO (2009). http://www.imo.net/live/perseids2009 [2] Kurucz R.L. et al. (1984) National Solar Observatory Atlas No. 1. *NOAO*, Sunspot, NM [3] www.water.kg/Issyk_Kul/AST.htm [4] Berezhnoy A.A. et al. Astronomical School's Report, V. 7, Is. 2, p. 185-189, 2011

Multiple reflected seismic lunar waves and core of the Moon

O. B. Khavroshkin[1], V. V. Tsyplakov[2]
Institute Phisics of the Earth, RAS
khavole@ifz.ru

[1] Head of Nonlinear Seismology Laboratory, Schmidt Institute of Physics of the Earth, Russian Academy of Sciences. B.Gruzinskaya 10, 123995 Moscow D242 Russia, E-mail: khavole@ifz.ru

[2] Senior Reaseacher of Nonlinear Seismology Laboratory, Schmidt Institute of Physics of the Earth, Russian Academy of Sciences. B.Gruzinskaya 10, 123995 Moscow D242 Russia, E-mail: tspl@mail.ru

The initial stage of development of nonlinear seismology was sufficient for attempt to transfer terrestrial experience on studying of lunar seismicity and the analysis lunar seismograms. Features of geological structures of the Moon and the form of records seismograms became the precondition and the certificate of existence strong modulation effect. As well as in the general physics modulation in lunar seismology (as well as in terrestrial) - change under the known law (the law of external influence) in time of parameters of a seismic wave field. Therefore understanding of that and the account of nonlinearly of processes have resulted in reception of significant results on cosmology and to an internal structure of the Moon. The above-stated results and the common understanding have allowed to accept not only nonlinear model of seismicity of the Moon but also existence of seismic acoustic processes and first time seismic acoustic emission. Studying of forms and structures seismograms allows to draw the following conclusions: (1) lunar seismogram as records of a seismic signal or event usually consist of one or several parts of which duration and quantity is connected to energy of initial event; (2) the characteristic forms of lunar seismogram similar to forms of seismic acoustic emission on records of seismic acoustic noise on the Earth especially for seismic active zones and during activation of the nearest faults; (3) lunar sites of records seismogram as well as envelope of seismic acoustic emission signals on the Earth records satisfy to the typified forms of signals inherent in processes of micro - and macro destruction and plastic deformation of a firm body and rocks, and are characterized by a similar range of frequencies and energy. Therefore for lunar records of signals with the big amplitude the seismogram will analize on three components. This is a clue for search and select of lunar seismograms which is a result of a multiple reflected waves (MRW) exist. Deep faults of the Moon will help to existing of that waves. In accordance to property of MRW and lunar faults only code of Z component of seismic signal will be contents peculiarity which connect with existing of MRW. Really despite of a lot of significant spectral peaks of realization codes X components kepstrum of this spectrum has not strongly pronounced significant peaks and represents smooth enough falling down curve that testifies to absence in researched process of multiple waves, or proves absence of lamination (reflecting borders) in a direction X component. Thus spectral peaks are caused or free Moon oscillation, or own oscillations of registration region. On the other hand, the spectrum of realizations Z making has powerful strongly pronounced spectral peaks, as well as its kepstrum. The last proves existence of horizontal lateral lamination or reflecting borders in region of registration which are the reason appear of a multiple reflected waves too. The seismic data of two impact of meteorites was used. Statistic analyze (spectrums, kepstrums) of all seismograms was presented on 10 tables but the results of discovered of a multiple reflected waves presents by one table where is the comparison between the recorded characteristics times (periods) of that waves and known periods which received from known geologic models of the Moon .

The general conclusions.

1. Deep breaks of the Moon promote formation from powerful impact sources of multiple waves such as type PKiKP, and also PcP etc.
2. Time characteristics processes of modulation by lunar oscillations and multiple waves are an authentic material for research of an internal structure of the Moon.
3. The place of landing of lunar stations is necessary for choosing in view of registration of multiple waves.

Recommended Literature

1. Nakamura I . Structure of the lunar mantl // J/ Geophys. Res. 1976. vol. 81,№26.
2. Toksoz M. Planetary seismology and interiors//Rev. Geoph. space phys,1979.Vol.17.№ 7.
3. Khavroshkin O.B., Tsyplakov V.V. Meteoroid stream impacts on the Moon: information of duration of seismograms // Proc. Conf. "Meteoroids 2001" (ESA SP-495). Noordwijk, The Netherlands: ESA Publ. Division., 2001.
4. Koper K. D., Pyle M. L. Observation of PKiKP / PcP amplitude ratios and implications for Earth structure at the boundaries of liquid core. J of Geoph. Res., Vol.109, B03301,2004, p.p.1-13.
5. Mizutani H. Lunar A Mission. Intern. Symposium on Atmospheres and Surfaces of Mars and Venus. The Inst. Of Space and Astronautical Science. Sagamihara, Kanagawa, Japan, 1993, 241-254 p.p.

An overview of the Diviner Compositional Investigation - from the lab to the Moon and back again. N. E. Bowles[1], B. T. Greenhagen[2], T. J. Warren[1], I. R. Thomas[1], and the Diviner Science Team. [1]Atmospheric, Oceanic and Planetary Physics Dept., University of Oxford, Oxford, UK (Thomas@atm.ox.ac.uk), [2]Jet Propulsion Laboratory, California Institute of Technology, Pasadena, CA, USA.

Introduction: This presentation will provide an overview of the surface compositional investigation that forms part of the Diviner Lunar Radiometer Experiment and new laboratory spectra to assist with their interpretation.

In addition to its six channels for albedo and temperature sensing, Diviner has three channels between with spectral band passes centred on 7.8, 8.25 and 8.53 μm designed to measure the position of the Christiansen Feature (CF). The CF is an emissivity maximum that shifts to shorter wavelengths with increasing silicate polymerisation and thus provides diagnostic information on lunar surface lithology, with highest sensitivity to plagioclase and olivine composition (Figure 1, [1]).

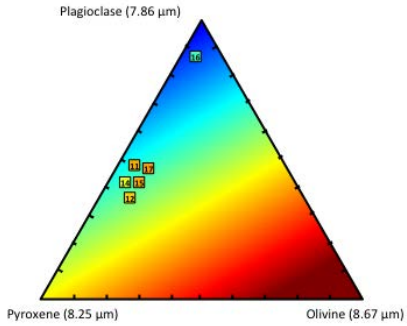

Figure 1: Ternary diagram of major lunar mineralogy with the observed CF values of Apollo sites for comparison[from 1].

A combination of the fine particulates in the top layers of the regolith, differential heating and cooling due to shortwave absorption to depths of a few 100 μms, and thermal emission from the surface impose near-surface thermal gradients in the regolith, leading to shifts in the strength and position of the CF (figure 2) and other mid-infrared spectral features.

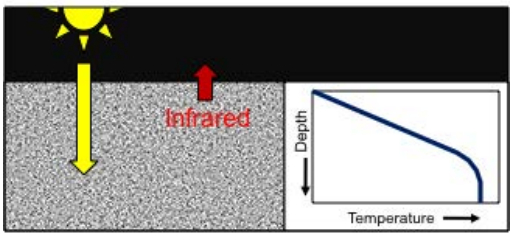

Figure 2: Schematic of heating to depth by shortwave insolation and cooling from the surface, leading to a steep near-surface thermal gradient.

Diviner CF Maps: Diviner maps of silicate mineralogy are available via the PDS Geosciences Node. These products consist of 32 pixel per degree mosaics for the region bounded by 60°N and 60°S. Two products are available: a standard CF map for the entire first year of mapping and a map that corrects for some latitudinal and local time variations ("normalized to equatorial noon" or NEN) using a subset of the dataset [described in 1].

The Diviner dataset shows significant compositional diversity. These data have been used to identify new compositional complexity on the lunar surface, including silica-rich (quartz or alkali feldspar), unusual plagioclase compositions, and the FeO content of unsampled pyroclastic deposits [6, 7 and 1]. Unlike near-infrared spectroscopy, the CF parameter is extremely sensitive the plagioclase abundance and can be used to estimate the feldspar-mafic ratio [8].

Rigerous quantitative analysis requires a better understanding of the behaviour of mineral powders, regolith simulants, and Apollo samples measured under controlled simulated lunar environment (SLE) conditions in labs here on Earth.

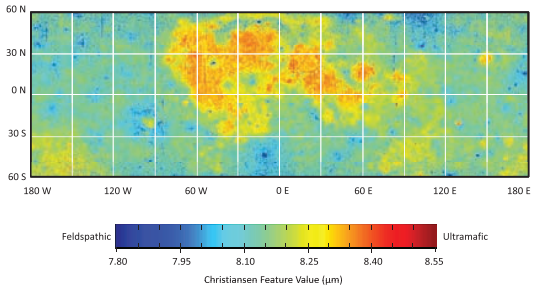

Figure 3: CF Value Map of Silicate Mineralogy [from 1].

Laboratory Experiments To simulate the near-surface thermal gradient, a new SLE chamber has been developed at the Planetary Spectroscopy Facility (PSF) in the Univeristy of Oxford Department of Physics, UK.

Limited laboratory experiments have been made in the past (e.g. [3], [4], [5]) but using the new capabilites at PSF, a more comprehensive study is now underway. This study includes a range of lunar analog minerals (quartz, plagioclase feldspars, pyroxenes, and olivines), lunar simulants, and returned Apollo soils (Apollo 11, 12, 15, 16 x2, and 17). The results of this study are critical to an improving the interpretation of Diviner compositional data.

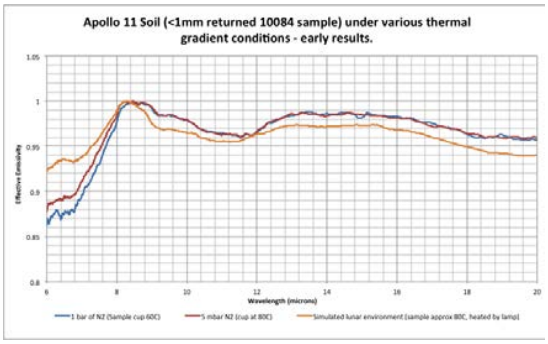

Figure 4: The effect of the induced thermal gradient is to cause a systematic shift in the position of the CF to shorter wavelengths. The size of the effect can be estimated by comparing an Apollo 11 soil sample (<1mm 10084) when measured under different local thermal environments.

References: [1] Greenhagen et al 2010 *Science vol 329 p1507 10.1126/science.1192196*; [2] Nash D. B. et al. 1993 J. Geophys. Res., 98, 23535-23552; [3] Henderson & Jakosky 1997 J. Geophys. Res., 102, 6567-6580; [4] Logan et al. 1973 J. Geophys. Res., 78, 4983-5003; [5] Henderson et al. (1996) J. Geophys. Res., 101, 14969-14975;[6] Glotch et al 2010 *Science* 329, 1510 DOI: 10.1126/science.1192148; [7] Allen et al 2012, LPI Contribution No. 1659, p.1504; [8] Lucey and Greenhagen 2012, LPI Contribution No. 1659, p.1736

LROC DIGITAL ELEVATION MODELING OF KEY SCIENCE TARGETS. K.N. Burns, T. Tran, M.S. Robinson, S.J. Lawrence, E.J. Speyerer, J. Stopar. School of Earth and Space Exploration, Arizona State University, Tempe, AZ, 85281. (knburns1@asu.edu)

Introduction: One of the primary objectives of the Lunar Reconnaissance Orbiter Camera (LROC) [1] is to gather Narrow Angle Camera (NAC) stereo observations to generate digital elevation models (DEMs). Although not designed for stereo observations, off-nadir slews of the spacecraft of ~20° enable stereo NAC observations acquired from adjacent orbits. Since off-nadir rolls interfere with data collection of the other instruments, LROC slew opportunities are limited to four per day. From an altitude of 50 km the NAC acquires images with a pixel scale of 0.5 meters and cover approximately 5 km cross-track by 25 km down-track. The low altitude was common during the nominal and first half of the science mission (September 2009 to December 2011). Images acquired during the commissioning phase and those acquired from the fixed orbit (after 11 December 2011) have pixel scales that range from 0.35 meters to 2 meters. In order to maintain a vertical precision of less than 1 meter and rarely above 2 meters, the convergence angle between image sets are ideally between 12° and 45°.

Method: A combination of USGS Integrated Software for Image and Spectrometers (ISIS) and SOCET SET® from BAE Systems software packages are used to generate DEMs. ISIS routines ingest the images, perform a radiometric correction, and export the image data in SOCET SET data format. SOCET SET includes a NAC specific a push broom sensor model to relate the image space to ground coordinates. A bundle adjustment is performed on the images to correct for offsets in camera pointing using a multi-sensor triangulation (MST) algorithm. MST is used to update camera pointing, improve registration between areas of stereo coverage, and ground truth using tie-points, sensor position, and camera pointing. Tie points relate a point in the overlapping area of two or more images. Selected parameters, such as the position, velocity, and pointing angles of the cameras are adjusted so that the root mean square errors for all the tie points are minimized. In order to improve accuracy between the images and ground truth, Lunar Orbiter Laser Altimeter (LOLA) data are used to define the geodetic reference frame for the DEMs. The images are shifted in relation to their original latitude, longitude, scale, elevation, and horizontal and vertical rotation, using a script in MATLAB, in order to better fit the LOLA data.

Once the images are adequately registered to each other, as well as the LOLA data, the process of extracting DEMs can begin with NGATE (SOCET SET- Next Generation Automatic Terrain Extraction). NGATE performs image correlation and edge matching for every pixel in the image to create a dense model. The DEM is then resampled to at least three times the ground sampling distance of the image (typically 2 meters for nominal phase images) [3]. Orthorectified images can be created upon completion of the DEM using Orthophoto Generation. The DEM and orthorectified images are converted into ISIS cube format for future analysis. In addition, a hill shade image, color shaded relief image, slope map and confidence map are provided in GeoTIFF format. These products are made using the Geospatial Data Abstraction Library (GDAL).

Application: NAC DEMs are the highest resolution topographical data set of the lunar surface. Because these products provide a three-dimensional view of the surface, they can be used for site selection and hazard avoidance for any future missions. Traverse planning can be modeled in order to minimize energy and ensure that time spent on the surface yields a high return of data. Geologists can measure parameters such as elevation, slope, and volume to place constraints on composition and geologic history to make sure that smaller regions of interest can be identified before launch.

Release: Arizona State University has produced DEMs of more than 120 stereo pairs for 11 Constellation Program sites and 50 other regions of scientific interest. The ASU and LROC team have released a collection of 68 DEMs in January 2012, which includes 11 of the 50 CxP sites. We currently plan to continue releasing NAC DEMs to the Planetary Data System (PDS) over the next year.

References: [1] Robinson et. al. (2010) *Space Sci Rev, 150,* 81-124. [2] Cohen, B.A. et al., (2008) LPSC XXXIX, Abstract #1640. [3] Tran, T. et al., (2010) *ASPRS/CaGIS 2010*.

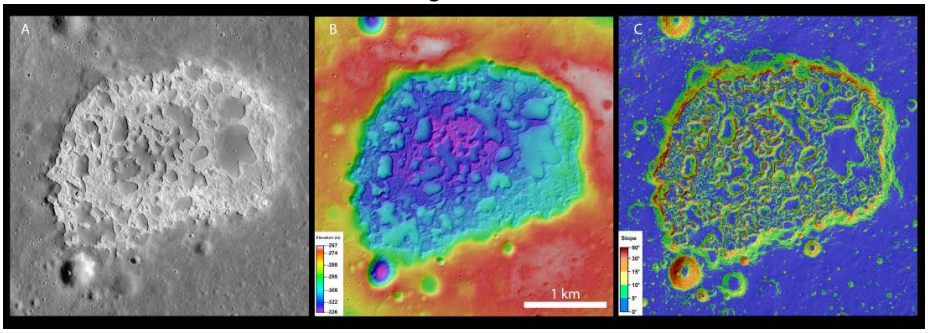

Figure 1. Products derived from NAC DEMs include: (A) Orthophoto (B) Color shaded Relief (C) Slope map.

LUNAR BISTATIC RADAR OBSERVATIONS USING THE ARECIBO OBSERVATORY & MINI-RF. D. B. J. Bussey[1], R. Schulze[1], C. V. Jakowatz[2], M. Nolan[3], R. Jensen[1], F. S. Turner[1], D. E. Wahl[2], D. A. Yocky[2], J. T. S. Cahill[1], R. K. Raney[1], G. W. Patterson[1], and the Mini-RF Team, [1]Applied Physics Laboratory, Laurel MD 20723, [2]Sandia National Laboratory, Albuquerque NM, [3]Arecibo Observatory, Arecibo PR.

Introduction: The Mini-RF team is acquiring bistatic radar measurements that will test the hypothesis that permanently shadowed areas near the lunar poles contain water ice. Additionally these measurements can be used for studies of the composition and structure of pyroclastic deposits, impact ejecta and melts, and the lunar regolith. These bistatic observations involve the Arecibo Observatory Planetary Radar (AO) transmitting a 12.6 cm wavelength signal, which is reflected off of the lunar surface and received by the Mini-RF instrument on LRO. These observations will be the first lunar non beta-zero radar images ever collected.

Rationale: Typically, orbital radar observations use the same antenna to both transmit and receive a signal. The angle between the transmitted and received signals, (the bistatic, or beta angle), for these observations is therefore zero, these are called monostatic observations. By using the AO radar as the transmitter and Mini-RF as the receiver, we are collecting data for the Moon with beta angles other than zero. These measurements provide the best possible test of the water ice hypothesis with current Earth-based and/or luanr assets.

The Circular Polarization Ratio (CPR) is the ratio of the powers of received signal in the same sense transmitted divided by the opposite sense. Mini-RF transmits a left circular polarized (LCP) signal; a normal reflection from a dry randomly rough surface is dominated by Bragg backscatter, hence it results in RCP since in effect it is "single-bounce". Typical dry lunar surface has a CPR value less than unity [1]. Higher CPR signals can result from multiple-bounce backscatter from rocky surfaces or from the combined volume scattering and coherent backscatter opposition effects (CBOE) from an ice/regolith mixture. CBOE is the interferometric addition of same sense reflections caused by ice radio frequency (RF) transparency [2]. CBOE occurs only around zero phase (beta=0) and accounts for both the high CPR and radar brightness of ice in typical monostatic radar observation.

Mini-RF monostatic data shows many craters with high CPR values. Most of these features are associated with fresh, young craters and display elevated CPR both inside and outside their rims. Some permanently shadowed craters near both poles show elevated CPR inside the crater rims but low CPR outside the crater rim (Figure 1). These properties are consistent with RF backscatter caused by surface roughness in the former case and water ice in the latter [1].

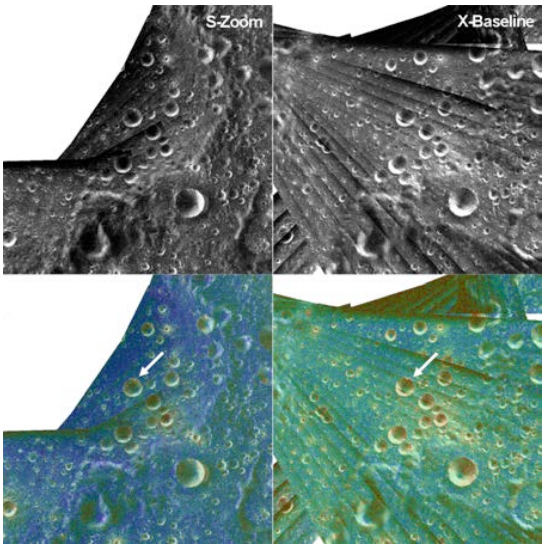

Figure 1. Mini-RF mosaics showing multiple small craters on the floor of Peary crater which have elevated CPR values only in their interiors (Arrow points to one example). These represent prime candidates for the location of ice deposits. The elevated CPR is seen in both the 12.6cm (S) and 4.2 cm (X) radar bands.

The physics of radar scattering predict that high CPR caused by a rocky surface will be relatively invariant to the beta angle, whilst high CPR caused by ice will be very sensitive to beta, with elevated CPR values dropping off abruptly at beta angles greater than about 1-2° (Figure 2).

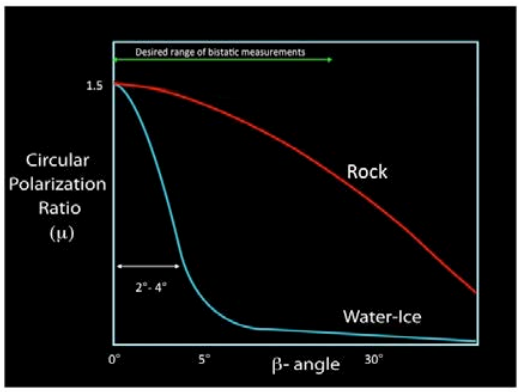

Figure 2. Predicted behavior of CPR versus beta angle for both rock terrains and an ice/regolith mixture.

The exact shape of the CPR-β curve for an ice-regolith mixture is a function of the amount and purity of the ice. However we do not need to measure this curve to

differentiate between high CPR from rocks versus ice, by measuring at beta angles in the 5°-10° range we are definitely in the right hand portion of this plot, i.e. a rocky surface will have a significantly higher CPR than an ice/regolith mixture. Acquiring observations of high CPR at beta angles larger than about 5° would validate the theoretical physics that predicts such behavior. Once validated, then this offers robust ice/non-ice discrimination by radar measurements.

Method: A key to a successful bistatic observations is the ability to distinguish the desired bistatic signal from the direct path and forward scatter signals (Figure 3).

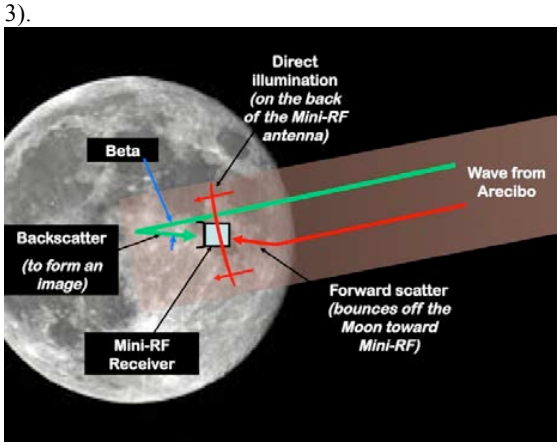

To this end the Mini-RF/AO team conducted a low-power (35 W transmitter) bistatic collect in April 2011. Analysis of data, by colleagues at Sandia National Laboratories (SNL), has shown that we were successful. Figure 4 shows some initial analysis of the data.

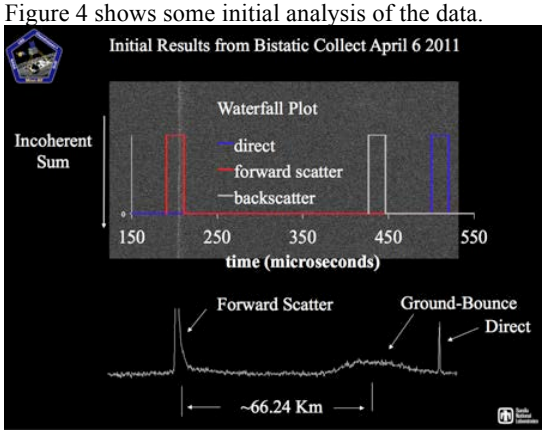

Figure 4. Initial analysis from the low-power bistatic test. The key point is that we are able to distinguish between the forward scatter, direct-path and bistatic signals.

Further analysis by SNL permitted the generation of images of both polarizations, together with some key derived products (Figure 5).

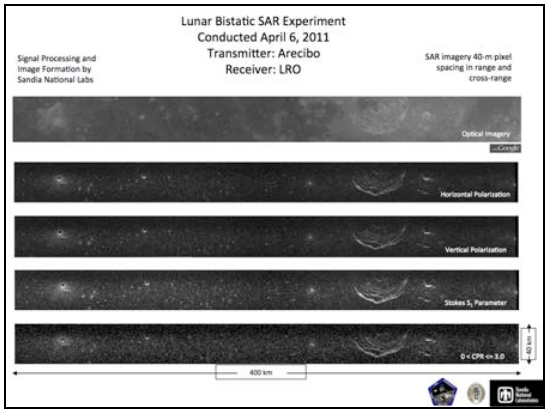

Figure 5. Low-power bistatic data images including both polarizations, S1 and CPR products. The top image is a Clementine mosaic of the same region.

Planned Observations: Mini-RF has instigated an Arecibo high-power bistatic campaign. This involves imaging both polar, and non-polar targets that have high monostatic CPR values. By acquiring non beta zero data of equatorial high-CPR regions (which we can safely assume have high CPR due to the presence of surface rocks) we can confirm the hypothesis that high CPR caused by rocks is reasonably invariant to the beta angle (red curve in Figure 1). The first high-power bistatic collect was undertaken on February 24th 2012.

The plan is to conduct multiple observations of polar craters that show enhanced monostatic CPR values in their interiors. To first order we will be looking to see if regions that have high CPR values in the monostatic data have high or low values in the bistatic data. If we find areas that become low only in the bistatic data then this provides strong supporting evidence that these are ice deposits. Initially we will attempt to acquire data in the β=~5-10° range. At these angles we expect there to be a clear high-low difference in CPR values for rocks versus ice.

Conclusions: Using Arecibo and Mini-RF we will collect the first ever planetary bistatic radar images at non β=0 angles. These data will provide a unique new piece of evidence to determine if the Moon's polar craters contain ice. We have a technically sound approach and have validated the concept by conducting the AO low-power test. Essentially we have now demonstrated a completely new instrument mode, capable of exciting and quite different science. This has not been done before for other planets, and will provide information on both polar ice and lunar surface roughness/dielectric constants.

References: [1] Spudis P. D. et al., GRL 2010. [2] Campbell B. et al., Nature, 2006 [3] Black et al., Icarus, 2001

SCIENCE AND PAYLOAD ACTIVITIES IN SUPPORT OF THE ESA LUNAR LANDER. J.D. Carpenter[1], R. Fisackerly, A. Pradier, B. Houdou, D. De Rosa, B. Gardini., [1] ESA-ESTEC, Keplerlaan 1, 2201AZ, Noordwijk, The Netherlands (E-mail: james.carpenter@esa.int).

Introduction: ESA's Human Space Flight and Operations directorate is continuing with preparations for its Lunar Lander project. The Lunar Lander is an unmanned precursor mission to future human exploration, whose purpose is to drive the development of key technologies and generate scientific knowledge that will position Europe as a participant in future exploration of the Moon and beyond.

The primary objective of the mission is to demonstrate soft precision landing with hazard avoidance. Once on the surface the mission provides an opportunity for the operation of a scientific payload which addresses the major unknowns for future exploration activities.

The mission targets a landing site close to the Luna r south pole in order to demonstrate precision landing and to make use of the favorable illumination available at key locations in this region. A detailed description of landing site identification and characterisation is provided in a parallel presentation [1].

The mission has been studied at Phase B1 level with Astrium (Bremen) as the prime contractor, since August 2010.

Figure 1. Artist's impression of the ESA Lunar Lander at the Lunar South Pole.

Scientific topics for investigation: The scientific topics that have been defined for the mission emphasise areas which will be of importance for the future of exploration but where significant unknowns remain. These include the integrated dusty plasma environment at the surface of the Moon and its effects on systems [e.g. 2]; lunar dust as a potential hazard to systems and human explorers [e.g. 3]; potential resources which can be utilized in the future including both volatiles (e.g. water) and those derived from minerals; and radiation as a potential hazard for human activities. Each of these topics is supported by an independent science Topical Team. These Topical Teams continuously review the science requirements and activities of the mission in the wider context of research into a scientific topic including other space platforms and research in terrestrial laboratories.

Model payload: In order to address these scientific topics and meet the associated requirements a model payload has been defined. This model payload is used to inform the mission study in advance of a formal selection in order to ensure that challenges associated with accommodating candidate experiments are properly accounted for. In addition the model payload provides a reference point for further investigations into optimal ways to address unknowns associated with the identified scientific topics. A list of instruments in the model payload is provided in Table 1.

The model payload includes a number of experiments for which design effort and further definition is required. In addition optimization of both scientific return and utilization of mission resources can be accomplished through increased integration of instruments with synergistic operations and scientific outputs. In order to address these issues a number of activities are ongoing to investigate packages of instruments. As well as detailing the scientific measurements to be made at the surface of the moon, these payload studies provide preliminary concepts for payloads, identify the major challenges for their development and ensure that the mission study properly accounts for the payload and its interfaces. The payloads under study are described below and are included in Table 1.

The Lunar Dust Analysis Package (L-DAP) is an instrument package to determine the microscopic properties of lunar dust including the size distribution of particles from tens nm – 100s µm, the shape and structure of grains, chemical and mineralogical composition of particles. The activity builds on significant experiment heritage obtained through the MECCA experiment package developed for NASA's Phoenix mission (originally defined as a human exploration precursor experiment) [4], the microscope developed for Beagle 2 [5] and MicroOmega on Exomars, the Raman-LIBS elegant breadboard developed in the frame of Exomars [6].

The Lunar Dust Environment and Plasma Package (L-DEPP) is a package to determine the charging, levitation and transport properties of lunar dust, in-situ on the Moon, and the associated properties of the local plasma environment and electric fields. Measurements include charges, velocities and trajectories of levitated dust particles, the temperature and density of the local plasma, electric surface potential, and observations of the radio spectrum (with an additional goal to prepare for future radiation astronomy activities). The L-DEPP study builds on extensive heritage in instrumentation for measurement of space plasmas and the associated environments, dust instrumentation and expertise in radio astronomy [e.g. 7 – 11].

The Lunar Volatile Resource Analysis Package (L-VRAP) is a package to measure the species of volatiles present close to the lunar surface, their abundance and distribution and demonstrate their extraction. The primary mechanism for performing such an analysis is expected to be mass spectroscopy, although additional complimentary measurements may be considered. The potential effects of contamination by the Lander may be critical and so quantifying the likely contamination and its effects are also being investigated. The system applied in the model payload is derived from the Gas Analysis Package on Beagle 2 [12] and the Ptolemy Instrument on Rosetta [13].

Summary: We report on the status of the ESA Lunar Lander mission, emphasizing related science and payload activities.

References: [1] De Rosa et al. (2012) LPSC [2] Horanyi and Stern (2011) PSS [3] Khan-Mayberry (2008) Acta Astronautica [4] Hecht et al. (2008) JGR, [5] Thomas et al. (2004) PSS [6] Courreges-Lacoste et al. (2007) Molecular and Biomolecular Spectroscopy [7] Srama et al. (2007) Dust in Planetary Systems [8] Grün et al (2009) Experimental Astronomy [9] Holback et al (2001) Ann. Geophys. [10] Eriksson (2007) Space Sci. Rev. [11] Rothkaehl et al (2008) Journal of Atmospheric and Solar-Terrestrial Physics [12] Wright et al (2000) LPSC [13] Todd et al (2007) Journal of Mass Spectroscopy.

Package	Instrument
Lunar Dust Analysis Package (L-DAP)	AFM
	Micro Raman-LIBS
	Microscope
	External Raman-LIBS
Lunar Dust Environment and Plasma Package (L-DEPP)	Dust Sensor
	Langmuir Probes
	Radio Antenna
	Ion/Electron Spectrometer
Lunar Volatile Resource Analysis Package (L-VRAP)	GCMS
	Ion trap mass spectrometer (TBD)
Other experiments not studied within packages	Panoramic stereo camera
	High resolution camera
	Robotic arm camera
	Radiation monitor
	Dust chemical reactivity
Other Payload	Mobile payload experiment

Table 1. Model payload applied in the Lunar Lander mission study prior to formal selection and experiment packages currently under investigation.

Lunar Dust Analysis Package (LDAP). S A Chalkley[1] , L.Richter[2],M.Goepel[2], M.Sovago[3], T.Pike[4], S.Yang[4], I. Hutchinson[5],R.Ingley [5] U Staufer[6] J.Rodenburg[7] Daniel Claus[7]
[1]SEA (UK) Ltd, Bristol, UK, simon.chalkley@sea.co.uk, [2]AKayser Threde (D), Munich (D), [3] TNO, Delft (NL), [4] Imperial College London UK, [5] Leicester University, UK, [6] Technical University Delft (NL) [7] Sheffield University, Sheffield, UK

Introduction: Lunar Dust is well known as a hazard for lunar exploration due to its invasive, fine microscopic structure and toxic properties. Gene Cernan (*the last man on the moon*) summarized it neatly ; "You have to live with it but you're continually fighting the dust problem both outside and inside the spacecraft[i]".
Conversely it also presents a potential resource which could be exploited if the characteristics and chemical composition is well known. Scientifically, the regolith provides an insight into the moon formation process and there are areas on the Moon which have never been explored before. For example the Lunar South Pole Aitken Basin is the oldest and largest on the moon, providing excavated deep crust which has not been found on the previous lunar landing missions

The SEA-led team has been designing a compact package, known as LDAP, which will provide key data on the lunar dust properties. The intention is for this package to be part of the payload suite deployed on the ESA Lunar Lander Mission in 2018. The LDAP has a centralised power and data electronics, as well as sample handling subsystem for the following set of internal instruments :

- Optical Microscope - with a 1μm resolution to provide context of the regolith samples
- Raman and LIBS spectrographic instrumentation – providing quantification of mineral and elemental composition information of the soil at close to grain scale. This includes the capability to detect (and measure abundance of) crystalline and adsorbed volatile phases, from their Raman signature. The LIBS equipment will also allow chemical identification of other ejecta in the vicinity of the Lander.
- Atomic (Magnetic) Force Microscope – providing nano-scale measurement of the fine particles and presence of nanophase Fe which is potentially toxic to humans
- Lenseless Microscope, a novel, low mass technology based on combining diffraction patterns to give high resolution 3D images of the sample.

This paper presents the technological challenges and trade offs arising from meeting the mission requirements. The issues associated with sample handling performed on a low mass budget are discussed, and the use of micro-machining and MEMS technology is covered. The paper also discusses the harsh environmental conditions at the Lunar South Pole and the impacts this has on the operation and survivability of an externally mounted package.

The expected performance of the whole package, including the use of LIBS under lunar vacuum conditions is also presented.

---

[i] Gene Cernan, Apollo 17 Debrief

EXPLORING THE FEASIBILITY OF DETERMINING LUNAR SOIL WATER CONTENTS WITH A COMBINED RAMAN/LIBS INSTRUMENT. A Colin[1], GR Davies[1], I Hutchinson[2], R Ingley[2], E Laan[3], R Motamedi[1], ARL Nichols[4], M Sovago[3], W van Westrenen[1], [1]VU University Amsterdam- the Netherlands, [2]University of Leicester- UK, [3]TNO Space- the Netherlands, [4]IFREE- Japan

Introduction: The recent detection of water on large areas of the lunar surface [1] has far-reaching consequences for the feasibility and design of future human exploration missions to the Moon. The data suggest that water is widely distributed across the lunar surface, shattering the long-held belief that water ice could only be present in permanently shadowed craters. Average water contents could amount to several tenths of percent in the top millimeter of lunar soil, with higher concentrations possible locally [1].

The presence of water at the lunar surface has potential implications for in situ resource utilization (ISRU) in future lunar exploration both as a resource in itself and also as a source for oxygen and hydrogen for fuel, through electrolysis. If water is present in significant quantities in the lunar soil then its extraction as a resource might be feasible.

Confirming and refining these findings by *in situ* measurements will be a top scientific priority of future lunar missions. Raman spectroscopy is dedicated to the molecular analysis and can provide mineralogical context analysis as well as water content assessment. LIBS permits identification of the elements present in the sample using their characteristic spectral lines, thus is suitable to measure water via H content. We are exploring whether in situ analyses using a combination of Raman and Laser Induced Breakdown Spectroscopy (LIBS) could be used to qualitatively and quantitatively detect water in the lunar soil.

As a first step, we have initiated a sensitivity study on analogue lunar surface materials to determine detection limits of water contents, using a combined Raman/LIBS instrument previously designed for the ExoMars mission (e.g. [2]). Three main activities will be undertaken in this project: (A) Minor modification of the VU University Amsterdam Mars simulation chamber to enable Raman and LIBS analyses under lunar surface pressures (B) Synthesis and characterisation of a range of lunar soil compositions, representative of the chemical variability found on the lunar surface, with different water contents. Bulk compositions will include those of low-titanium and high-titanium basalt end-members as identified by Apollo samples, as these span the likely range of volcanic rock compositions found at crater rims. (C) Sensitivity studies of water content measurements in these synthetic samples using the combined Raman/LIBS instrument. Fourier Transform Infrared spectroscopy analyses will be used as an independent check of water content. We intend to specifically quantify the effects of operating conditions, pressure, temperature, target composition and target grain size on measurement sensitivity for both Raman and LIBS.

This work is funded by the Netherlands Space Office (PI Preparatory Programme grant to WvW).

References: [1] Pieters CM, Goswami JN, Clark RN et al. (2009) Science 326, 568-572. [2] Laan EC, Ahlers B, van Westrenen W, et al. (2009) Proceedings of SPIE 7441, 744114.

ASTROBIOLOGY ON THE MOON. I. A. Crawford[1] [1]Department of Earth and Planetary Sciences, Birkbeck College London, Malet Street, London, WC1E 7HX, UK. i.crawford@bbk.ac.uk

Introduction: An ambitious programme of lunar exploration will reveal much of astrobiological interest (for reviews see [1,2,3,4] and references therein). Examples include:

(i) Better characterisation of the impact cratering rate in the Earth-Moon system, with implications for understanding the possible 'impact frustration' of the origin of life;

(ii) Records of the solar wind and galactic cosmic ray fluxes preserved in ancient regolith ('palaeoregolith') deposits, which may provide information on the evolution of the Sun and the changing galactic environment of the Solar System throughout its history;

(iii) Preservation of ancient meteorites blasted off Earth, Mars and Venus, which may preserve evidence of the early surface environments of these planets, as well as constraining models of lithopanspermia;

(iv) Preservation of samples of the Earth's early atmosphere not otherwise available;

(v) Preservation of cometary volatiles and organics, and/or radiation-driven prebiotic chemistry, in permanently shadowed polar craters; and

(vi) Preservation (or otherwise) of microorganisms and organics in the remains of spacecraft left on the lunar surface for up to fifty years [5], which will provide insights into planetary protection, panspermia, and the survival of life in the space environment.

Accessing the record: Focussed robotic missions to the lunar surface, such as ESA's proposed Lunar Lander [6] and the Lunar Beagle concept [7], will be able to address a number of these questions (especially those relating to the retention of volatiles and organics in cold polar regoliths). However, fully accessing thie lunar geological record of relevance to astrobiology will be greatly facilitated by the scientific infrastructure, on the spot decision making, enhanced surface mobility, and sample return capacity that would be provided by renewed human operations on the lunar surface. Specific architectural requirements will include:

(i) The ability to conduct 'sortie-class' expeditions to multiple localities;

(ii) Provision of surface mobility with a range of at least 100 km (ideally provided by a pressurized rover);

(iii) The means to detect and sample buried palaeoregolith deposits, with their potentially rich record of Solar System history [8,9]. For detection, ground penetrating radar may be a suitable technique; for access, unless suitable outcrops can be located, provision of a drilling capability to c. 100m depths may be required); and

(iv) Provision of adequate sample collection and return capacity (roughly estimated at several hundred kg per sortie).

These requirements are compatible with those proposed by the recently developed ISECG Global Exploration Roadmap [10]. It follows that a greatly improved understanding of the origin, history, and distribution of life in the Solar System would be a key scientific benefit of implementing this Roadmap.

Conclusion: The lunar geological record undoubtedly contains much of astrobiological interest, and properly accessing it will benefit from renewed human operations on the lunar surface. Moreover, such a programme of human lunar exploration will build up capabilities required for the later human exploration of Mars, which may also be expected to yield important astrobiological discoveries. Given that these astrobiological benefits are only a sub-set of all scientific reasons for wanting to explore the Moon, which include other areas of planetary science and astronomy not discussed here, the totality of the scientific case for a robust programme of lunar exploration, as envisaged by the Global Exploration Roadmap [10], appears to be overwhelming.

References: [1] Crawford I.A. (2006) *Internat. J. Astrobiology*, 5, 191-197. [2] Gronstal A. et al. (2007) *Astrobiology*, 7, 767-782. [3] Cockell C.S. (2010) *Earth, Moon Planets* 107, 3-10. [4] Crawford I.A. (2010) *Astrobiology,* 10, 577-587. [5] Glavin D.P. et al. (2010) *Earth, Moon Planets* 107, 87-93. [6] Carpenter J.D. et al. (2010) *Earth, Moon Planets* 107, 11-23. [7] Gibson E.K. et al. (2010) *Earth, Moon Planets* 107, 25-42. [8] Crawford I.A. et al. (2010) *Earth, Moon Planets* 107, 75-85. [9] Fagents S.A. et al. (2010) *Icarus*, 207, 595-604. [10]The Global Exploration Roadmap; http://www.nasa.gov/pdf/591067main_GER_2011_small_single.pdf .

CURRENT STATUS AND EXPECTED PERFORMANCE OF THE LUNAR LASER RANGING RETROREFLECTOR FOR THE 21ST CENTURY D. G. Currie[1], S. Dell'Agnello[2], G. O. Delle Monache[3] and K. Zacny[4]: [1]Department of Physics, University of Maryland, College Park, MD, currie@umd.edu, [2]Research Division, Laboratori Nazionali Frasdcati, Instituto Nazionali di Frascati, Via E. Fermi, 40 Frascati (Rome) I-00044, Italy, Simone Dell'Agenno@infn.infn.it, [3]Research Division, Laboratori Nazionali Frasdcati, Instituto Nazionali di Frascati, Via E. Fermi, 40 Frascati (Rome) I-00044, Italy, giovanni.dellemonache@lnf.infn.it and [4]Honeybee Robotics Spacecraft Mechanisms Corporation, 398 W Washington Blvd., Suite 200, Pasadena, CA 91103, zacny@honeybeerobotics.com

Introduction: The unique science results that have been obtained by Lunar Laser Ranging Program (LLRP) using the Apollo retroreflectors [1] and the science we expect to obtain with the Lunar Laser Ranging Retroreflector Array for the 21st Century (LLRRA-21) will be discussed. This includes the discovery of the liquid core of the moon and an evaluation of its size, shape and other properties. The liquid core has been recently confirmed by the reanalysis of Apollo seismology data by Renee Weber. The LLRP has also provided the best measurements for many of the other lunar properties, of the crust and the interior.

Current Challenge: While the Apollo retroreflector arrays are still in operation and continue to produce new state-of-the-art science results, the combination of the lunar librations and their design limit the range accuracy that may be obtained for each single photo-electron (SPE) return to ~20 mm. When the array of 100/300 Cube Corner Reflectors is tilted due to the librations, the return laser pulse is spread, reducing the accuracy of the SPE measurement.

Next Generation Lunar Retroreflector: The University of Maryland, who was the PI for the Apollo arrays, is developing a next generation lunar retroreflector (e.g., the Lunar Laser Ranging Retroreflector for the 21st Century or LLRRA-21) [2]. This holds promise for significant improvements in the understanding of the deep interior of the moon, that is, the liquid and solid core, the core mantel boundary and the inner mantle.

Deployment Issues: The magnitude of these improvements expected from the LLRRA-21 will depend critically on the method of robotic deployment. Three candidate methods of deployment: 1) On the lunar lander, 2) On the lunar surface and 3) Anchored one meter in the regolith [3]. The advantages, disadvantages and method of implementing these approaches will be reviewed. This will particularly address the implementations that can be supported by the Google Lunar X Prize flights of the next couple of years.

Thermal Behavior: The thermal behavior of the LLRRA-21 is critical to the ability for multiple ground stations to effectively conduct a ranging program over a full lunation cycle. To address this has required the developments of an extensive simulation using a sequence of programs, including IDL, Thermal Desktop and Code V.

Return Signal Level: The expected magnitude of the return signal from these optical/thermal simulations will be described in detail. The expected signal return will be similar to signal return that is currently being obtained from the Apollo 15 array. The design parameters required to obtain this performance will be described, with an illustration of the expected performance for the various conditions. With this information, we can evaluate the capability of various ground stations to conduct regular ranging programs.

Ground Station Capabilities: This will address the number of ground stations that can be expected to contribute and the frequency of observations what would be available for the science analysis. A brief discussion will address the required hardware upgrades for obtaining millimeter normal points.

Lifetime Issues: Finally, the lifetime issues related to the Apollo arrays and the design of the LLRRA-21 will be discussed. Apparently a dust deposit has significantly reduced the signal level that be obtained from the Apollo arrays. The designs to ameliorate these effects will be described.

Thermal Vacuum Testing: The package has been tested in the SCF, a unique facility developed at the INFN-LNF expressly for the evaluation of retroreflectors [4]. It provides optical and thermal sensing of the performance under solar simulation.

Acknowledgments: This work has been supported by the LUNAR team of the NASA Lunar Science Institute and by the INFN-LNF and ASI.

References: [1] Bender, P. L.; Currie, D. G.; Dicke, R. H. Science, Volume 182, Issue 4109, pp. 229-238 (1973) [2] Currie, D; Dell'Agnello, S.; Delle Monache, G. Acta Astronautica, v. 68, iss. 7-8, p. 667-680A [3] K. Zacny, D. Currie, et. al. Planetary and Space Science submitted January 2012 [4] Dell'Agnello, S.; Delle Monache, G. O.; Currie, D. G.; et. al Advances in Space Research, Vol. 47, Iss. 5, p. 822-842.

PETROGRAPHY AND AN AGE OF KREEP GABBRO-NORITIC CLASTS IN THE DHOFAR 1442 LUNAR METEORITE. S. I. Demidova[1], M. A. Nazarov[1], M. O. Anosova[1], Yu. A. Kostitsyn[1], F. Brandstätter[2], and Th. Ntaflos[3] [1]Vernadsky Institute of Geochemistry and Analytical Chemistry, Kosygin St. 19, Moscow 119991, Russia, demidova.si@yandex.ru; [2]Naturhistorisches Museum, A-1014 Vienna, Austria; [3]Department für Lithosphärenforschung, Universität Wien, Althanstrasse 14, 1090 Wien, Austria.

Introduction: Dhofar 1442 is a mingled lunar meteorite that contains abundant KREEP material. Some KREEP gabbro-noritic clasts possibly preserved their primary igneous texture. Here we report first data on petrography of the rocks and U-Pb ages of some of them. Recently we reported U-Pb ages of zircon fragments from the Dho 1442 meteorite [1]. The ages coincide with results recently published by Zhou et al. [2].

Methods: Chemical composition of the mineral phases was studied using the Cameca SX-100 microprobe (Vienna, Austria). Four zircon grains (8 analyses) were dated by the U-Th-Pb method using LA-ICPMS (Element 2) (Moscow, Russia) against the GJ and 91500 zircon standards. Zr content was used as the inner standard. The diameter of the laser beam was 30 μm. Obtained data were reduced using the Glitter and Isoplot softwares.

Results: Zircon grains were found in lithic clasts containing a KREEP component. These rocks are norites, gabbro-norites and gabbro having granoblastic to subophitic textures [1]. However four lithic fragments (0.5-3 mm in size) have possibly primary igneous textures (Fig. 1). They consist of coarse (50-200 μm in size) isometric pyroxene grains embedded into a fine-grained feldspathic matrix. Most pyroxenes (30-40% of the rocks) are coarsely exsolved and evenly distributed in the matrix. Similar pyroxenes are present in some rocks of the alkali suite [e.g., 4]. Some pyroxenes are present as poikilitic crystals. The matrix (60-70% of the rocks) has a subophitic to ophitic texture and consists mainly of subhedral to lath-shaped plagioclase and a minor amount of mesostasis represented by granophyre intergrowths, silica or a K,Si-rich glass. Occasionally K-rich feldspar forms bands in the plagioclase. Ilmenite, apatite and zircon are present as accessory minerals. Needle-shaped or subhedral ilmenites (~1-2%) occur often in a direct contact with zircon grains. Most zircons are small (up to 20 μm) subhedral or skeletal crystals (Fig. 2) but two of them are large angular grains (100-150 μm in long dimensions). One grain has poikilitic plagioclase inclusions (Fig. 3).

In mineral composition the rocks of possibly igneous origin are not distinguishable from other KREEP gabbro-noritic rocks of the meteorite [1] (Fig. 4). Pyroxenes of the rocks are restricted in MG# number within each clast, but differ from one lithic fragment to another one. They are mainly pigeonites ($En_{44-58}Wo_{5-13}$) and augites ($En_{38-41}Wo_{40-42}$), however orthopyroxenes ($En_{51-58}Wo_{3-5}$) are present also (Fig. 4). In contrast to pyroxenes plagioclases are rather variable in composition ($An_{76-92}Or_{0-5}$) (Fig. 5). K-rich feldspar is $An_{76-92}Or_{0-5}$.

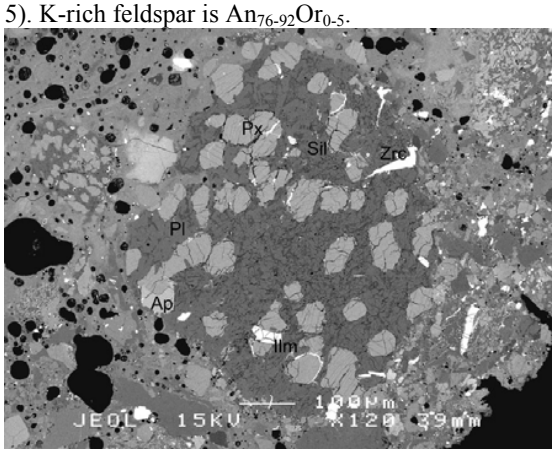

Fig. 1. BSE image of KREEP gabbro-noritic clast of possibly igneous origin.

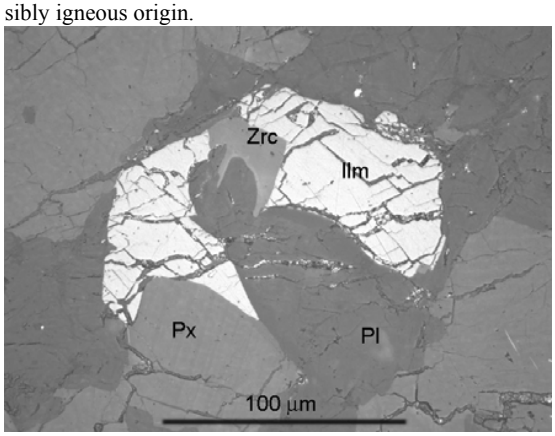

Fig. 2. Skeletal zircon crystal in a contact with ilmenite (reflected light).

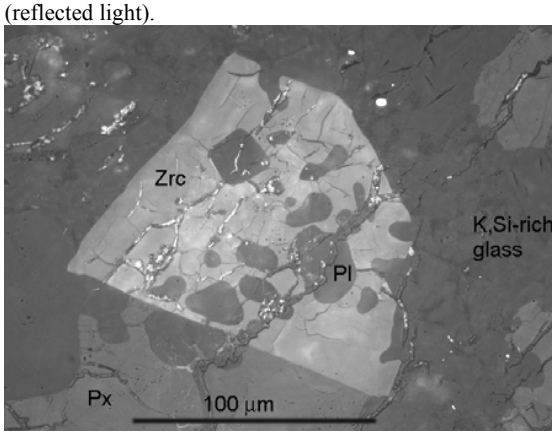

Fig. 3. Zircon grain with poikilitic plagioclase inclusions (reflected light).

Ilmenites contain 2.2-3.6 wt.% of MgO, 0.3-0.5 wt.% of Nb_2O_3 and up to 0.3 wt.% of ZrO_2. Zircons are characterized by a presence of 0.1-0.5 wt.% of Y_2O_3 and 1.2-1.7 wt.% of HfO_2, 8-45 ppm of Th and 24-69 ppm of U. Such minor element concentrations are common for zircons of KREEP mafic rocks [3].

U-Pb dating. Three zircon grains of a biggest clast and one zircon grain from a smaller one were dated. Small grain size of some zircons and the presence of abundant inclusions in one analyzed grain do not obstruct measurements because there is no radiogenic Pb in associated phases. All measured zircon grains have concordant or nearly concordant ages (discordance is up to 8%) of 3951±35 Ma. The value coincides well with the previously reported age of the "young" group [1,2] (Fig. 6).

Discussion. The Dho 1442 zircon ages are from 3.8 to 4.4 Ga [2] and suggest therefore a prolonged KREEP magmatism. A similar age range was established for Apollo 14 and NWA 4485 lunar meteorite zircon grains [5,6]. Two major age peaks are present in Dho 1442 meteorite: ~3.9 and ~4.3 Ga [1,2]. Mineral modes of the studied KREEP gabbro-noritic rocks and the low Th and U contents of their zircons are similar to those of the KREEP mafic rocks. It suggests that the ~3.95 Ga age may date a major event of the KREEP mafic magmatism.

The 4.3 Ga zircons occur as loose individual grains in the matrix [1,2] or in impact melt breccia clasts [2]. It assumes that their precursor rock was heavily crashed during impact processes. The 4.3 Ga event is recorded in zircons of Apollo 14 and 17 granophyres [3,5]. So we suggest that granophyric rocks are the best candidates for the "old" zircon group. Granophyric rocks and granitic glasses are clearly present in Dho 1442. Abundant Fe-rich pyroxene (Fig. 4) and silica fragments which are nearly absent in the lithic clasts occur in the matrix and probably represent also products of the granophyre destruction. Th and U contents of the "old" zircons are typical for zircons of the granophyres and higher (mainly 100-300 ppm of Th and 150-400 ppm of U) than those of the "young" group [3].

If it is true, than magmatism in the source region of Dho 1442 could change in composition from granophyric to KREEP gabbro-noritic during 4.3 – 3.9 Ga.

Acknowledgements: This study was supported by Austrian Academy of Sciences and by Russian Academy of Sciences (Program № 22).

[1] Demidova S. I. et al. (2012) *LPS XXXXIII,* Abstract #1090. [2] Zhou Q. et al. (2012) *LPS XXXXIII,* Abstract #1554. [3] Meyer C. et al. (1996) *Meteoritics & Planet. Sci., 31,* 370-387. [4] Marvin U. B. et al. (1991) *Proc. of Lunar and Planet. Sci., 21,* 119-135. [5] Nemchin A. A. et al. (2008) *Geochim. Cosmochim Acta, 72,* 668-689. [6] Arai T. et al. (2010) *LPS XXXXI,* Abstract #2379.

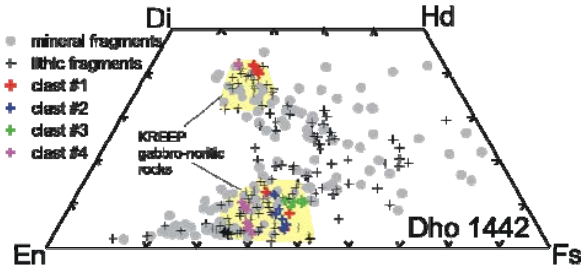

Fig. 4. Pyroxenes of Dho 1442. Clasts #1-4 are KREEP gabbro-noritic clast of possibly igneous origin.

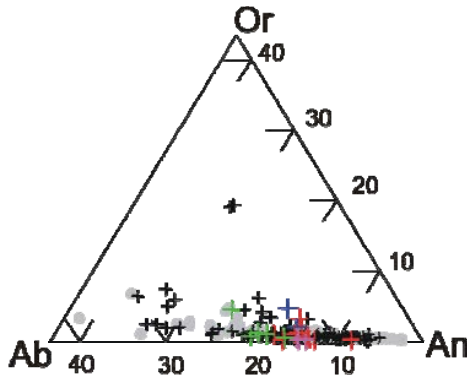

Fig. 5. Plagioclases of Dho 1442.

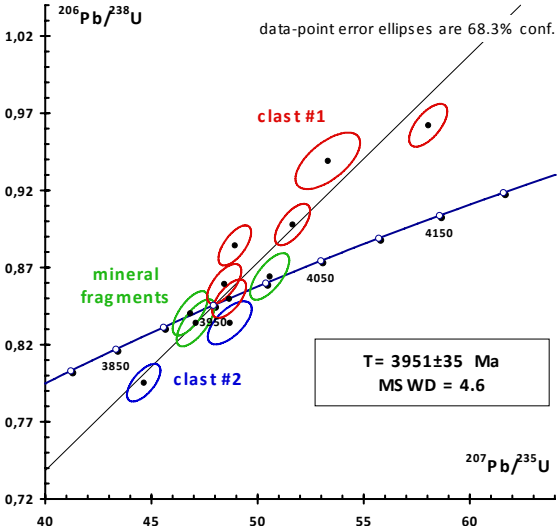

Fig. 6. Wetherill concordia plot with the data of "young" group of zircons from Dho 1442.

RAMAN LASER SPECTROMETER DEVELOPMENT FOR LUNAR APPLICATIONS. E. Diaz[1], C.Pérez[2], A.Moral[1], O. Álvarez[1], C.Tato[3], H.Thiele[4], M.Colombo[1], I. Hutchinson[5], R.Ingley[5], J.J.Thocaven[6], F. Rull[7], S. Maurice[6], J. Popp[8] , H.G.M.Edwards[8] on behalf of the RLS team.

[1] INTA-CAB, [2] INSA, [3] SENER, [4] Kayser-Threde, [5] University of Leicester, [6] CESR, [7] UVa, [8] IPC University of Jena, [9] University of Bradford.

Introduction: Raman Spectroscopy is a powerful tool for the structural and compositional analysis of a substance either in the solid, liquid or gas state. Raman spectroscopy can be used in macro or micro mode and at different distances from a fraction of millimeter up to hundred of meters.

The Raman Laser Spectrometer (RLS) is part of Pasteur payload inside ExoMars mission and it is being developed by an European Consortium composed by Spanish, French, German and UK partners. In its former configuration the RLS instrument consisted in the combination of both Raman and LIBS techniques analyzing at the same spot, in two operation modes: outside the rover linked to the robotic arm and inside the rover linked to the analytical laboratory. In the present configuration of the Exomars rover the instrument consist in an only Raman technique operating inside the analytical laboratory. An optical head connected by optical fibres with the laser and the spectrometer will analyze the crushed samples obtained by the drill system.

The aim of the work presented here is to provide a summary of its potential applications for Lunar science missions: science capabilities, alternatives for its combination with other techniques and engineering improvements to be developed to assess the lunar environmental conditions. For that the instrument current characteristics and performances, and its technological assessment program main results are presented and discussed

Instrument Functional description: The Raman Laser Spectrometer Instrument flight segment is composed by the following units (see Figure 1):

- SPU Spectrometer Unit, based on transmission optics, which includes active cooling for CCD temperature control by means of a TEC device.
- IOH, Internal Optical Head, which focuses the laser signal on to the sample by means of an autofocus system and collects the Raman signal to be analysed in the spectrometer.
- ICEU Instrument Control and Excitation Unit, including the power converter, the CCD readout electronics, the instrument processor and the excitation laser
- Others: Electrical and optical harness, software and the calibration target.

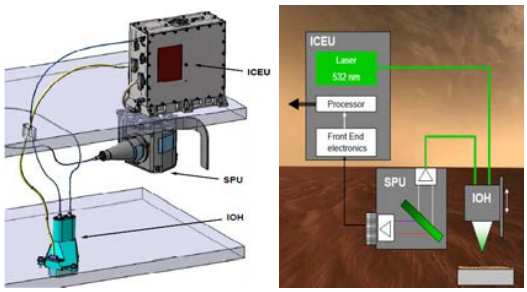

Figure 1. Left: RLS units in their present configuration inside the Exomars Pasteur payload. Right: RLS Functional scheme

The RLS working flow consists in the following main steps (see also Figure 1):

- the powdered sample is illuminated by means of the IOH optics, with the laser light coming (through the excitation fiber) from the laser located in the ICEU.
- The Raman signal obtained is properly filtered and delivered by the IOH (through the reception fiber) to the SPU.
- At the SPU the Raman signals are analysed by a transmission diffraction grating and registered in the CCD.
- The obtained image is sent to the ICEU FEE (Front End Electronics) and processed instrument processor electronics, previous prior to be sent to the Rover OBDH.

Instrument detection capabilities: The Raman spectra (number of peaks, positions and relative intensities) , are determined by the structural symmetry and elementary composition of the molecules. Therefore, by analysis of Raman spectral pattern and detailed peak positions, phase identification and chemical characterization of the samples can be made. In figure 2 a schematics of the Raman spectral positions arising from vibrations of the main molecular assemblages found in nature is depicted. The spectrometer is designed to covers all these vibrations and with enough spectral resolution allowing distinction between substances with similar structure and small chemical compositional differences. Moreover the spectrometer can be used for LIBS analysis in this Raman spectral range if a second pulsed laser is implemented. The use of LIBS in a reduced spectral range show limitations for elements identification. But these limitations can partially be

overcome provide the spectrometer is very luminous allowing the detection of secondary atomic emission picks.

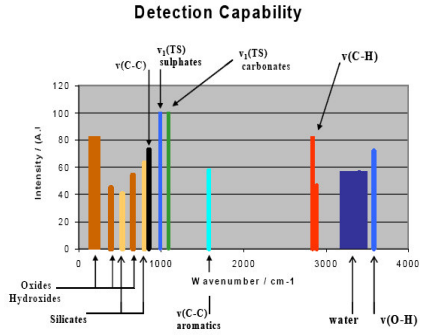

Figure 2. Raman detection capabilities of the present RLS configuration

RLS Instrument characteristics and performances: the RSL for Exomars has been developed under a modularity concept. It has been designed to provide its full performances in an operative thermal environment of between 0ºC and -40ºC (±10ºC of margin in both sides). Main characteristics and performances are as follows:

- Laser excitation wavelength: 532 nm
- Irradiance on sample: 0.8– 1.2 kW/cm2
- Spectral range: 150-3800 cm-1
- Spectral resolution: 6 cm-1 lower spectral wavenumbers; 8 cm-1 long spectral wavenumbers, and spectral accuracy < 1 cm-1
- Spot size: 50 microns, through an optical fiber of 50 microns core.
- Active focussing of Laser excitation signal onto the sample (powder) of ±1mm range and 2 µm resolution
- Mass ~ 2.4 kg and power consumption between 20W and 30 W (depending on the temperature range and operational mode).

Technological Readiness Status: along the past years RLS Team has performed in parallel a technology development program in order achieve a TRL5. The program was stated an executed following a bottom-top approach, i.e. starting for the validation from critical components, material and processes, and concluded with an end to end instrument breadboard. All the technological risk areas were identified at the early beginning. Components not available as space qualified devices or without enough space heritage or which have not been qualified for the same space environment (temperature, vibration, radiation, etc.) were included as technological risk devices. Validation at this level was performed in relevant environment.As well unit breadboards were developed and tested, and finally integrated in the instrument Breadboard (See Figure 3). At present the instrument has achived a TRL of 4.85, pending the conclusion of some ongoing tests that would provide, in case of success, a TRL above 5 in the following months.

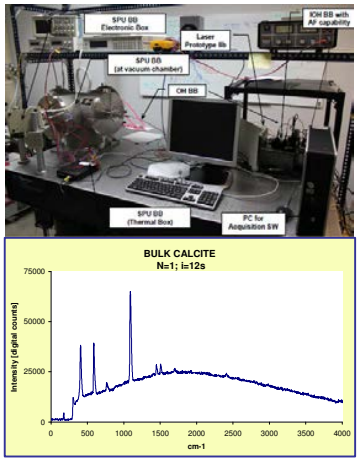

Figure 3. RLS breadboard and a typical Raman spectrum taken on calcite mineral

Improvements and Alternatives for Lunar applications: Raman Laser Spectrometer is a powerful tool for in situ planetary exploration, alone or in combination with other techniques and can support the Lunar science inside the coming missions. Among the potential alternatives of Raman spectroscopy use we consider the following: 1) Combination of Raman internal and external capabilities by means of recovering and external optical head on a robotic arm or moreover using remote Raman. In both cases the spectrometer would be shared by means of an optical switch in the spectrometer aperture. 2) Combination of Raman and LIBS. 3) Combination with IR microscope (Micromega, in Exomars). 4) Combination with X-ray diffraction instrument (XRD in ExoMars)

The technology preparations needs to consider the environmental differences between Mars and the Moon, namely thermal and radiation environment. Delta-validation should be taken into account for components susceptible to such conditions.

Acknowledments: This work was conducted under the auspices is Spanish MICINN (project AYA-2008-04529) , the Centre National d'Etudes Spatiales (CNES, Deutsches Zentrum für Luft- und Raumfahrt (DLR) and the UK funding agency (UKSA).

LUNAR SURFACE ANALOGY SIMULATION OF THE PROPOSED LANDINGS SITES OF TEAM PULI SPACE – HUNGARIAN GLXP TEAM. M. Deák[1] and T. Látos[2] [1]dmarton@elte.hu, Department of Physical Geography, Institute of Geography and Earth Sciences, Eötvös Loránd University, Hungary, Budapest 1117. Pázmány Péter sétány 1/a [2]Puli Space Technologies Ltd. 1161 Budapest, Csömöri út 161.

Introduction: The production one of the Google Lunar X Prize contestants, Team Puli Space's rover is at its first stage. The design of a spacecraft (in this case the Puli-1) must reflect the nature of its mission, so a rover should be built to be able to explore the area where it has descended. Team Puli Space, cooperating with the Hungarian Eötvös Loránd University of Science is now building a ground modeling table, reflecting the morphology of the proposed landing sites. This will be used for professional and educational purpose, participating in the Hungarian educational space probe program "Hunveyor".

Landing site candidates: At this stage of the mission, Team Puli Space has nine landing site candidates. These are all mare, or morphologically similar areas, where a relatively safe landing can be carried out (*Fig. 1*). The selection process included geological and future human exploration aspects too, so was for example Moretus (*Fig.1/9*) and Von Kármán (*Fig. 1/8*) chosen. At the bottom of Moretus's deep craters ice deposits are possible to exist, and Von Kármán is significant in the field of Helium-3 mining *[1]* – and also it would be the first lunar probe landing on the far side of the Moon.

For more information see: *[2]*.

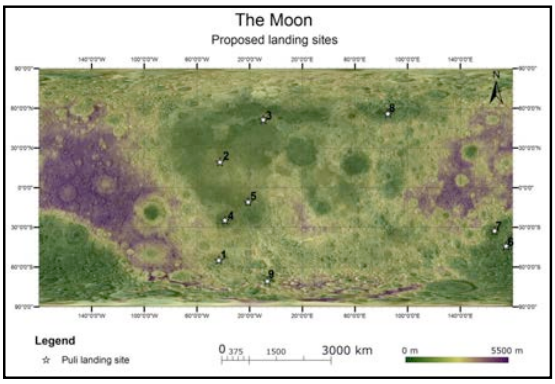

Figure 1: The map of the proposed landing sites of Team Puli Space
1: Schiller-crater, 2: Aristarchus, 3: Plato
4: Mare Humorum, 5: Mare Cognitum
6: Mare Humboldtianum 7: Thomson-crater
8: Von Kármán 9: Moretus

Morphology of the proposed landing sites: These areas are could be considered as "typical" mare areas. Their surface is relatively flat with a low crater density. The overall changes of altitude are low, and small craters having steep rims are scarce. A good example is the Plato (*Fig. 2*). Our planned descent method – after slowing from orbital speed – is the use of air bags, thus making a 3-4 km long "jumping" strip for the instrument. It is vital, that no obstacles or deep craters get into the way.

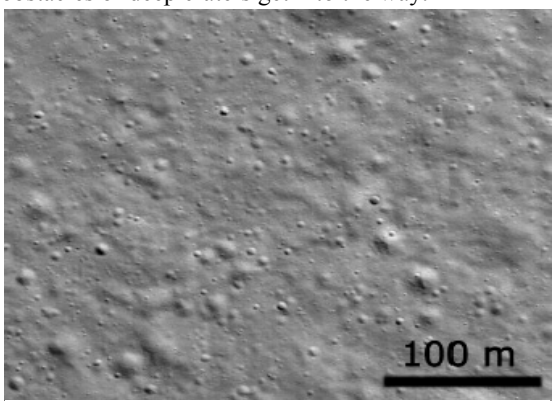

Figure 2: A sample of the Plato
LROC ID: M111659579LE

Ground modeling table: We planned a 32 m^2 ground modeling table to simulate this type of morphology. It consists of three (2+1) elements, each to test different aspects of lunar morphology (*Fig. 3*).

Segment 1. is made directly to reflect the mare

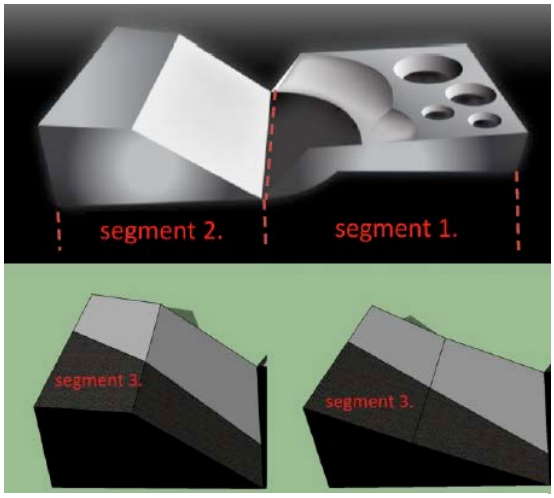

Figure 3: The three segments of the ground modeling table, and two different stages of Segment 3.

morphology. We used "typical" values to determine the size of the used craters, so we made them with the following radii: one with 2,5 m, one with 1 m, one with 0,75 m, one with 0,5 m and two with 0,3 m *[3]*. Creating bigger forms than these have relatively low steepness, so they can be simulated on Segment 2. According to earlier publications (for example *Anselmo et. al. 1976 [4]* and *Calinn et. al. 2011 [5]*) the depth-diameter ratio can be calculated with the

following: $d=0{,}68D^{0,44}$ so – in our experience – the steepness of a crater wall bigger than 3 m wouldn't affect greatly the movement capabilities of the rover. Following this ratio, a slope of a 3 m radius crater is 34 % steep, while one with 10 m radius is 23 % - and the slope of one with 20 m radius is only 15 %.

These values can be simulated on Segment 2, what is an adjustable slope, capable of simulating any values from 0 % to (a rather pointless) 200 %. The area of this segment is 3,4 m x 4 m (13,6 m^2).

Segment 3. (alternatively Segment 2+1) is a subsegment of Segment 2., what is also adjustable, so we can simulate quick changes in the morphology. The material covering the surface of this segment is variable with changeable plates, while on Segment 1 and 2 it is constant (see later). These plates can have different size of material from 0,2 mm to 50 mm, so we can test the movement capabilities of the rover on different slopes covered with different grain-sized material.

Lunar soil analogy: Many publications are written in this topic, but most of them are focusing on the engineering of new ones, and not on the analysis of natural or differently used material with approximately the same grain size distribution. The most common material used for this task is JSC-1 *[6]*, but the already produced amount is limited. We tried to find new analogies, considering different materials common in Hungary.

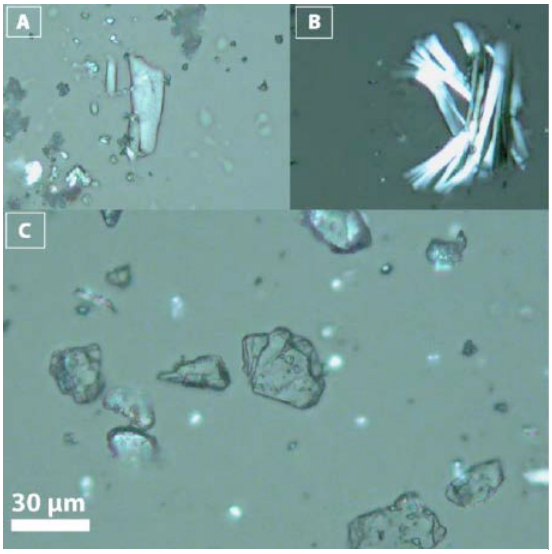

Figure 4: The images were captured by a ZEISS axioskop with partially crossed nicols A: Grinded limestone B: Grinded glass fiber C: Hydrated alumina

We analyzed grinded limestone used for cement production (*Fig. 4/A*), grinded glass fiber (*Fig. 4/B*) and hydrated alumina – $Al(OH)_3$ (*Fig. 4/C*). We analyzed the shape of the particles and the density of the material.

In our experience, the grinded glass-fiber turned out to be too dense and the particles were sticking too hard to each other. The grinded limestone showed better characteristics, but only when the particles distributed according to their size. With a small mixing – even by gravitational movement – they started to show similar attributes to the grinded glass fiber, rendering the sample useless to lunar soil simulation.

The mechanical properties of the hydrated alumina was – to our surprise – very similar to the one of the lunar soils. Detailed results are still to be made, but in general we can tell, that from this aspect it's very similar - so future analysis is planned.

Analogy area for the surface mission: We are also trying to find an area, where we can test the communicational and piloting software of the Puli-1. The terrain should reflect – if only roughly – the Lunar surface conditions.

Right now our primary candidate is a bauxite-mine in Gánt, Hungary (*Fig. 5*) which was already used by other Hunveyor teams as Lunar or Martian analogy.

Figure 5: Gánt, Hungary

References: [1] In: S. A Stern – Worlds Beyond; H. H. Schmitt (2002) *Return to the Moon!, 76-84.* **[2]** M. Deák (2011) *LPSC XLII. Abstract #1410* **[3]** Neukum, G.; Koenig, B.; Arkani-Hamed, J.; (1975) *The Moon vol. 12. pp. 201-2209.* **[4]** Anselmo, J. C.; Rehfuss, D. E.; Kincheloe, N. K.; Michael, D.; Wolfe, S. A. (1976) *LPI Conference 1976. 13-17 September* **[5]** Kalynn, J.; Johnson, C. L.; Osinski, G. R.; Barnouin, O. *LPSC XLII. Abstract #1514* **[6]** McKay, D. S.; Carter, J. L.; Boles, W. W.; Allen C. C.; Alton, J. H. (1994) *Engineering, Construction, and Operations in Space IV. pp. 857-866*

Acknowledgements: Special thanks to all members of Team Puli Space and Prof. Géza Zboray of to Dr. Géza Zboray of the Eötvös Loránd University, Department of Anatomy-, Cell- and Developmental Biology, for letting him use his laboratorial equipments.

LUNAR METEORITE Y-82192, HELIUM-3, AND THE LUNAR CRATER GIORDANO BRUNO. J. Fritz and V. A. Fernandes, Museum für Naturkunde, Leibniz Institut at Humboldt University, Berlin, Invalidenstr. 43, 10115 Berlin, Germany (joerg.fritz@mfn-berlin.de).

Introduction: The 145 lunar and 99 martian meteorites [1] revolutionized our understanding of the efficiency to deliver rock fragments from Mars and the Moon to Earth [i.e. 2,3]. The Moon has no atmosphere that decelerates particles and thus even 1) the smallest projectiles impact the lunar surface with cosmic velocities and 2) the smallest high speed ejecta can leave the gravity well of the Moon. Thus, lunar impact ejecta arriving on Earth are not limited to rock sized fragments, but include also dust. This lunar dust was not reported from the collection of interplanetary dust particles (IDP) and micrometeorites recovered on Earth. Likely, because differentiated mare and highland rocks are difficult to discriminate by routine XRF analyses from terrestrial materials in samples collected on Earth [4]. However, lunar dust might leave a geochemical fingerprint in the sedimentary record [5]. Relatively small amount of ~10 t of average lunar regolith contains a volume of ^{3}He equal to the annual global average of extraterrestrial ^{3}He introduced into marine sediments. Calculations suggest an average annual flux of lunar impact ejecta to Earth in the order of ~200 t [5]. Therefore, ages of lunar meteorite ejection events and ^{3}He-profiles of Earth's sediments are compared. It is discussed whether ejecta from the 22 km ∅ crater Giordano Bruno, the youngest lunar crater of its size [6], is represented by lunar meteorites recovered so far.

Giordano Bruno: According to urban legends formation of the Giordano Bruno crater was observed by medieval monks on June 18, 1178 A.D. [7]. However, formation of a 22 ∅ sized lunar crater would result in an intense storm of lunar meteorites onto Earth [8]. Such a spectacular meteor shower is not recorded in the historical chronicles around the world [8]. In addition, crater statistics attests a 1 - 10 Ma age for emplacement of the Giordano Bruno ejecta blanket onto the lunar surface [6].

Lunar meteorites are rock fragments impact-ejected from the Moon and subsequently delivered to Earth. The time of impact ejection can (besides problems related to a complex exposure history) be determined by measuring cosmogenic nuclides (see ref. Fig. 1). The ejection age is the sum of the space residence time (4π cosmic ray exposure age; CRE) and the terrestrial residence time. The CRE ages of lunar and martian meteorites revealed that during the last 20 Ma these meteorites were ejeceted by frequent and thus small impact events. This requires an efficient delivery of lunar and martian rock fragments to Earth [i.e. 3,9] by projectiles as small as ~30 m and 200 m that impact onto the Moon and Mars, respectively. The resulting craters are as small as 1 and 3 km ∅ on Moon and Mars, respectively, thus substantially smaller than Giordano Bruno. For comparison, a 22 km ∅ lunar crater would form, on average, every ~10 Ma [10].

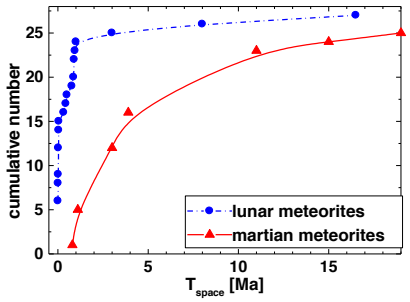

Figure 1: Cumulative space residence time of lunar and martian meteorites. Literature data for martian from references within [7] and lunar meteorites (see Figure 2).

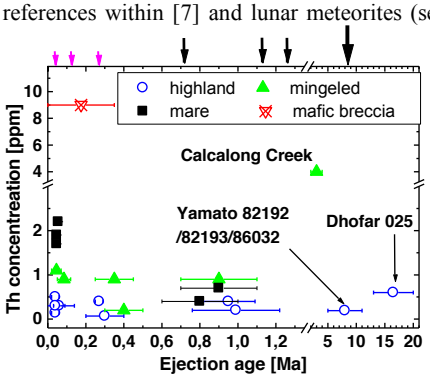

Figure 1: Compilation of ejection ages [11-14; 17-26] vs. Th concentrations [27] in lunar meteorites, with petrologic types indicated by symbols. Small pink arrows mark minor ^{3}He excursions, black arrows show excursions identified as spikes at 0.7, 1.1, and 1.3 Ma [15], and a major spike at 8.2 Ma [16] in the ^{3}He burial flux.

A cumulative plot of the meteorite space residence time (T_{Space}) shows the differences in the delivery of lunar and martian meteorites. A lunar impact delivers the majority of meteorites on quasi-geocentric orbits to Earth during the initial 0.5 to 1 Ma [10] (Figure 1). In contrast, a martian impact provides a 10 to 20 Ma lasting steady flux of meteorites that travel on heliocentric orbits to Earth. Note that, on average, the terrestrial age of meteorites is <0.5 Ma. Because of the high efficiency to deliver and recover lunar meteorites ejected from craters younger than 1 Ma, the similar number of lunar and martian meteorites show that the Giordano Bruno crater did NOT form during the last 1 Ma.

However, it is likely that some of the lunar meteorites that arrive on less efficient heliocentric orbits to Earth (T_{Space} >1 Ma) actually derived from the

largest crater that formed in the last 10 Ma. A compilation of petrology, Th concentration data, and ejection ages of lunar meteorites is presented in Fig. 1 to discriminate the different ejection events and to constrain the sampled source regions. The Giordano Bruno crater is situated in the Th poor lunar highlands on the northern limb of the Moon [6]. Thus, the Th rich mingled (basalts and highland rocks) breccia Calcalong Creek, ejected 2-4 Ma ago [11], presents a poor petrological match. The Th poor highland rock Dhofar 025 was ejected 14-20 Ma ago [12] and, thus, is barely in agreement with the formation age of 1 to 10 Ma as constrained by crater statistics [6]. Thus, the Th poor lunar highland rocks Yamato 82192/82193/86032 ejected 5 - 11 Ma ago [13,14] present the only lunar meteorites that match both the geochemical constraints on the source region and the temporal requirements discussed before.

Lunar ^{3}He in marine sediments: An efficient delivery of ^{3}He-rich lunar impact ejecta into Earth's sediments was proposed by [5] to resolve puzzling aspects related to the late Eocene projectile shower onto the Earth-Moon system. It was argued that a bombardment of the Moon by meter to hundred meter size projectiles provided a somehow steady flux of ^{3}He-rich lunar ejecta contributing to the extraterrestrial ^{3}He in Earth's sediments. An efficient delivery of ^{3}He rich lunar material to Earth's sediments implies a general spikiness of the terrestrial ^{3}He record. Random lunar impacts large enough (minimum size related to the temporal frequency of the ^{3}He spikes) should produce brief (~10ka) ^{3}He anomalies. Indeed, detailed ^{3}He profiles of the last 1.8 Ma report three brief spikes in the ^{3}He burial flux at ~0.714, ~1.137, and ~1.265 Ma ago [15] (Fig. 1). The lunar impact scenario argues that a relatively small amount of ^{3}He rich lunar ejecta (small compared to the total mass of IDPs arriving on Earth) substantially contributes to the volume of ^{3}He measured in Earth's sediments [5]. In contrast, a purely asteroidal or cometary origin of the ^{3}He rich particles in Earth's sediments (prevailing ^{3}He agents [15,16]) implies that the background flux of IDPs frequently increases by 3 to 5 times. Thus, assuming that 1) the three ^{3}He-spikes truly document brief and frequent spikes in the ^{3}He burial flux [15], and 2) the last 1.8 Ma are not characterised by a series of unusual events advocates the interpretation that lunar ejecta substantially contributed to the ^{3}He budget of Earth's sediments.

Is Giordano Bruno 8.2 Ma old? A nine-fold increase above background in the ^{3}He burial flux identified in 8.2±0.1 Ma old marine sediments was attributed to the collision forming the Veritas asteroid family [16]. Alternatively, this ^{3}He-spike could represent the ejecta from Giordano Bruno, thus providing the precise formation age for this lunar crater.

Testing the theory: The two scenarios can be discriminated by measuring Platinum Group Elements (PGE) and ^{3}He concentrations in these marine sediments. Both PGE and ^{3}He concentrations should increase for a ^{3}He-spike from "chondritic" IDP liberated by the break-up of the Veritas family [16]. In contrast ^{3}He rich and PGE poor lunar ejecta from Giordano Bruno crater would result in an increase in the ^{3}He concentrations but not in PGE concentrations. The inferred connection between Yamato 82192/82193/86032 and the Giordano Bruno crater can be tested by comparing geochemical data of these meteorites with orbital data from the lunar surface.

Relevance of testing the theory: Pinpointing source regions of lunar meteorites would provide samples from a well-constrained locality on the Moon distant to the Apollo and Luna landing sites. A precisely dated Giordano Bruno crater would present a landmark for the lunar crater production rate. The ejecta blanket is almost unaffected by secondary craters, as it is the youngest sizable lunar crater. Adittionally, it would present the most precisely dated ejecta blanket besides the small craters North Ray, South Ray and Cone. 3) With a simple telescope, the Giordano Bruno crater can be seen from all around the worl. Thus, Earth's sediments including the lunar ejecta qualify as a geo-/selenosite.

Acknowledgement: Financial support by the Helmholtz Alliance Planetary Evolution and Life (WP3200). Contribution of the ISSI Team on Lunar chronology.

Reference: [1] http://www.lpi.usra.edu/meteor/metbull.php. [2] Gladman B. (1997) *Icarus, 130*, 228-246. [3] Artemieva N.A. and Shuvalov V.V. (*2008) Solar Sys. Res., 42,* 329–334. [4] Rietmeijer F.J.M. (1998) Planetary Materials, Reviews in Mineralogy, *36*, 2-20. [5] Fritz J. et al. (2007) *Icarus*, *189*, 591–594. [6] Morota T. et al. (2009) *Meteoritic. & Planet. Sci., 44*, 1115-1120. [7] Calame O. and Mulholland J.D. (1978) *Science, 199, 875-877*. [8] Withers J. (2001) *Meteoritic. & Planet. Sci. 36*, 525-529. [9] Fritz J. et al. (2007) *Earth Planet. Sci. Let., 256*, 55–60. [10] Hartmann W. and Neukum G. (2001) *Spc. Sci. Rev., 96*, 165-194. [11] Nishiizumi K. et al. (1996) *Meteoritics & Planet. Sci., 31*, 893-896. [12] Nishiizumi K. and Caffee M.W. (2001) *Meteoritic. & Planet. Sci., 36*, Supp. A148. [13] Eugster O. (1989) *Science*, *245*, 1197-1202 [14] Lorenzetti S. et al. (2005) *Meteoritics & Planet. Sci., 40*, 315-327. [15] Patterson B. and Farley K.A. (1998) *Geochim. Chosmochim. Acta*, *62*, 3669–3682. [16] Farley K.A. et al. (2006) *Nature*, *439*, 295-297. [17] Nishiizumi K. et al. (2004) 35th LPSC Abst. #1130. [18] Nishiizumi K. et al. (1991) *Geochim. Cosmochim. Acta*, *55*, 3149-3155. [19] Nishiizumi K. and Caffee M.W. (2006) *Meteoritics & Planet. Sci., 41*, Supp., p.5368 [20] Nishiizumi K. et al. (2006) 37th LPSC Abst. # 2369. [21] Gnos E. et al. (2004) *Science 305*, 657-660. [22] Nishiizumi K. and Caffee M.W. (1996) 27th LPSC Abst. p.959. [23] Nishiizumi K. et al. (1999) 30th LPSC Abst. #1980. [24] Vogt S. et al. (1993) *Geochim. Cosmochim. Acta*, *57*, 3793-3799. [25] Nishiizumi K. et al. (2005) *Meteoritics & Planet. Sci., 40*, Supp. p.5270. [26] Nishiizumi K. and Caffee M.W. (2006) 37th LPSC Abst. #2101. [27] Korotev R. meteorites.wustl.edu/lunar/moon_meteorites.htm.

LUNAR IMPACTORS: A LOW-COST CUBESAT MISSION TO LUNAR MAGNETIC ANOMALIES (SWIRLS). I. Garrick-Bethell[1], R. Lin[2], H. Sanchez[3], and D. Hemingway[1]. [1]University of California, Santa Cruz (igarrick@ucsc.edu), [2]University of California, Berkeley. [3]NASA Ames Research Center.

Introduction: Lunar swirls are one of the most enigmatic geologic features in the solar system. Swirls are sinuous high-albedo features correlated with strong crustal magnetic fields (Fig. 1). Swirls are at the intersection of many disciplines, including the origins of lunar magnetism, space weathering, space plasma physics, dust lofting, and most recently, surface hydroxyl formation [1]. Therefore, a mission to swirls would benefit many in the planetary science community.

NASA Ames Research Center, UC Berkeley, and UC Santa Cruz have been designing a low-cost, low-mass mission to swirls that uses cubesat technology. Below we outline how this mission can cost-effectively make first of a kind measurements and inform a number of important problems in lunar science.

Multidisciplinary science at lunar swirls

Swirl formation: The two leading models for swirl formation are the solar wind deflection model [2], and the dust transport model [3]. Under the solar wind deflection model, the brightness of swirls is explained by the local magnetic field deflecting the solar wind (a darkening agent) from portions of the surface. Under the dust transport model, the brightness of swirls is explained by the accumulation of fine, bright dust, due to weak plasma-produced electric fields operating on charged dust lofted during terminator crossings. Measurements of the solar wind flux very near the surface, at bright and dark areas, would determine if the solar wind model is correct. Measurements of lofted dust very near the surface would help determine if dust lofting can contribute to swirl formation.

Lunar magnetism: The origin of lunar magnetism is still unknown, with interpretations suggesting either impact-produced plasma processes [4] or an ancient dynamo [5]. If crustal magnetic anomalies formed in a dynamo field, they should be homogenously magnetized with minimal short-wavelength variability in direction near the surface, except at the scale of small craters. Presently, magnetic field measurements at anomalies have only been taken above ~16 km in altitude, at best. Measurements of the magnetic field near the surface would help determine the strength and coherence of the underlying crustal magnetization, and thereby its formation mechanism. Such measurements would also help explain how the solar wind direction and flux is altered near the surface.

Lunar water: The M3 instrument on Chandrayaan has revealed that high lunar latitudes have higher abundances of hydroxyl molecules [6]. More recently, M3 data were used to show that lunar swirls have relatively low hydroxyl abundances relative to their surroundings [1]. Therefore, swirls are a natural laboratory for understanding water formation on the Moon, and likely on silicate bodies in general. Determining the swirl formation mechanism and quantifying the relevant processes should help elucidate how hydroxyl molecules and water form on the Moon's surface.

Space weathering: A long-standing question in space weathering is the relative importance of micrometeoroid impacts compared to the solar wind [7]. Under the solar wind deflection model for swirl formation, solar wind weathering at swirls is reduced, and the surface is kept brighter. However, because micrometeoroids are undeflected by the magnetic field and reach the surface, swirls may also be a natural laboratory for unraveling and quantifying the relative contributions of these two darkening agents. Improved knowledge of these processes would have applications to the spectral study of asteroids and Mercury.

Lunar dust: Dust lofting during terminator crossings has been inferred from a variety of measurements since the Surveyor missions [8], and may also be important in asteroid geology [9]. However, the amount of dust lofted above the lunar surface, if any, is not fully known. Measurements of the dust flux very near the surface, in particular during terminator crossings, would help constrain how much dust is lofted each day, and possibly the mechanisms behind dust lofting.

Plasma physics: The interaction of the solar wind with weak magnetic anomalies on the Moon presents interesting plasma physics phenomena, such as the development of a mini-magnetosphere [10]. The scale size of the magnetic anomalies ranges from below to above the solar wind proton gyrodiameter; thus, across the transition from kinetic to fluid behavior.

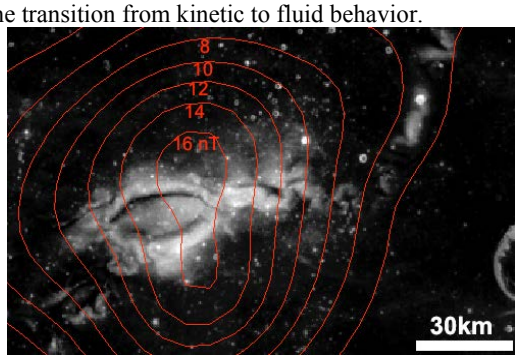

Fig. 1 – Reiner gamma swirl (Clementine 750 nm reflectance) and magnetic field contours at 18 km (Lunar Prospector).

A low-cost mission to lunar swirls

Mission objectives and concept: A mission to swirls that measures very near the surface:

1) Magnetic field strength and direction,
2) Solar wind flux and direction, and
3) Dust density,

would answer the key science questions above. A spacecraft on a very low-angle impact trajectory into the heart of a swirl could perform the necessary measurements at low altitude (Fig. 2), and transmit data in real-time to an orbiting spacecraft, up until the time of impact. Because many of the measurements can be made at high frequency, data from <50 m above the surface is possible, even though the spacecraft is traveling at >2 km/s. After impact, the probe's mission is over, but several probes can be launched to provide multiple transects at one swirl, or at several swirls.

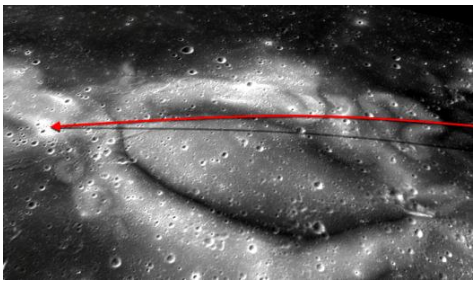

Fig. 2 – Low-angle impact trajectory over Reiner gamma swirl.

Spacecraft and payload: Ames has designed a small mother ship (<200 kg, Fig. 4) capable of orbiting the Moon and releasing two 3u cubesats on impact trajectories. Each of these cubesats is based on the CINEMA spacecraft (Fig. 3), an NSF-funded project built by UC Berkeley and Kyung Hee University (South Korea), and launching in June 2012. The CINEMA spacecraft carries two magnetometers (one inboard and one on a 0.9 m boom) and a particle detector (STEIN). Berkeley is currently designing a modified STEIN particle detector to measure the solar wind flux and direction at high cadence. In addition, Berkeley is designing a very high sensitivity dust detector.

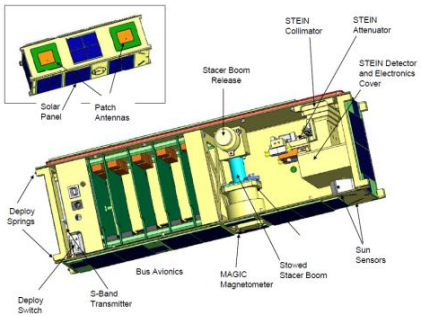

Fig. 3 – The NSF-funded 3u CINEMA cubesat, the basis of the impact probe, scheduled to launch in June 2012.

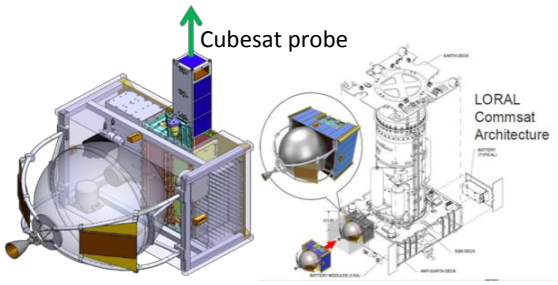

Fig. 4 – Left: Mother ship releasing a 3u cubesat probe. Right: Mothership piggybacking on a LORAL commsat launch.

Trajectory: Launching the spacecraft as a secondary payload greatly reduces the cost of the mission. Therefore, the trajectory to the Moon has been designed based on a drop-off in GTO by a commercial satellite launch (Fig. 5). Once at the Moon, the mother ship enters a highly elliptical orbit, and then conducts a burn to establish an impact trajectory. Then, the mother ship releases the probe, and performs a second burn to reestablish a stable orbit. The mothership flies over the impact site, collects data from the probe, and relays it to Earth. The total mission Δv is 1500 m/s.

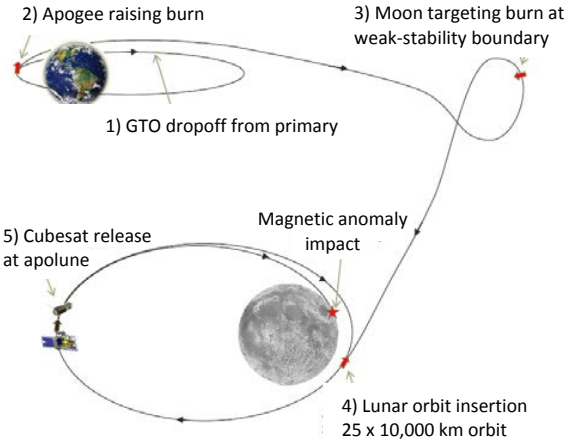

Fig. 5 – Spacecraft and probe trajectory to the Moon.

Conclusions: An impactor mission to lunar swirls could be accomplished for very low cost, while returning science that would benefit many planetary science disciplines. The mission would also demonstrate the first use of cubesats beyond low Earth orbit.

References: [1] Kramer, G. et al. (2011) *JGR* 116, E00G18. [2] Hood, L. L. and Schubert, G. (1980) *Science* 208, 49-51. [3] Garrick-Bethell, I. et al. (2011) *Icarus* 212, 480-292 [4] Hood, L. L. and Artemieva, N. A. (2008) *Icarus* 192, 485-502. [5] Garrick-Bethell, I. et al. (2009) *Science* 323, 356-359. [6] Pieters, C. M. et al. (2009) *Science*, 326, 568-572. [7] Hapke, B. (2001) *JGR* 106, 10039–10073. [8] Colwell, J. E., et al. (2007) *Rev. Geophys.* 45, RG2006. [9] Colwell, J. E. (2005) *Icarus* 175, 159–169. [10]. Kurata, et al. (2008) *GRL* 32, L24205.

LUNAR BASE FOR LIFE SCIENCES EXPERIMENTS.

Nandu Goswami[1], Pete Roma[2] , and Patrick DeBoever[3], Helmut Hinghofer-Szalkay[1]
[1] Medical University of Graz, Austria (Nandu.goswami@medunigraz.at), [2]Institutes for Behavior Resources, Baltimore, MD, USA, [3] Flemish Institute for Technological Research (VITO), Mol, Belgium, EU

.

Introduction: Understanding the development and interactions of physiological and behavioural adaptations is critical for mission planning in space exploration. Antarctica is probably the best Earth analog for Mars missions, but we lose fidelity in that there are no radiation effects and the infrastructure is already in place. Treating the Moon as a high-fidelity Mars analog would include the inherent physiological factors (hostile environment, microgravity, radiation) with the relative safety advantage of being closer to Earth than Mars (but still more dangerous/remote than Antarctica). We would, therefore, like to propose the analog environment of the moon for studying long-term effects of reduced g on life sciences experiments.

For the moon, we propose to study a) Physiological adaptations to the reduced g (eg. vestibular function, musculoskeletal changes, cardiopostural interactions, cerebral autoregulation); b) Changes and interrelationships between group cohesion (assessed by the Team Performance Task, TPT, which is currently being implemented in the 2012 winter-over at Concordia station, Antarctica) and neurobiological responses in standardized sessions; and c) Molecular mechanisms of these physiological and behavioural adaptations. Neurobiological concomitants of the TPT assay will be done by simultaneous measurements of cardiovascular function (heart rate, blood pressure, and heart rate variability), stress physiology (salivary cortisol and alpha-amylase), neurohormonal markers of social affiliation and stability (oxytocin and testosterone), and gene and protein expression changes in blood and saliva using -omics technologies. Application of the latter methods will permit formulation of a global picture of physiological and molecular changes as well as early biological effects associated with the multiple stressors and unique social dynamics experienced throughout the confinement period.

These studies would provide valuable insights on physiological adaptations, which occur at reduced g, behavioural, neurobiological, and -omics fingerprints that correlate with naturally occurring variations in-group cohesion over time in isolated, confined and extreme (ICE) environments. Understanding the biobehavioural mechanisms that mediate or contribute to compromised psychosocial function may guide the development of novel, effective, and operationally feasible techniques to enhance the development of countermeasures, crew selection and composition and training methods.

NORMALISATION OF CONTINUUM-REMOVED LUNAR SPECTRA. A. Grumpe[1], V. Zirin[1], F. Belkhir[1], C. Wöhler[1], [1]Image Analysis Group, TU Dortmund University, D–44227 Dortmund, Germany; {arne.grumpe | vladimir.zirin | fethi.belkhir | christian.woehler}@tu-dortmund.de

Introduction: A common technique of the analysing lunar spectra is unmixing of the observed reflectance spectra into standard reflectance spectra of compositional endmembers [1]. Other approaches explicitly rely on the depths and/or positions of the minima of absorption troughs in order to identify specific minerals in the lunar soil (cf. e.g. [2, 3]).

Since the surface reflectance depends on the illumination and viewing geometry [4], which is in turn governed by the small-scale topography of the lunar surface, a normalisation of reflectance spectra to a reference illumination and viewing geometry (commonly: 30° incidence angle, 0° emission angle, 30° phase angle [5]) is necessary, requiring high-resolution topographic data. However, the lateral resolution of available lunar digital elevation models (DEMs) is lower than the lateral resolution of recent hyperspectral imagery, and they might not be pixel-synchronous with the hyperspectral images due to uncertain selenolocation [6].

In this study, we present a framework for the normalisation of continuum-removed spectra with respect to illumination and viewing geometry. Especially, the phase angle dependence of the absorption wavelength and depth inferred from continuum-removed spectra is analysed.

Image registration and DEM construction: In order to improve the lateral resolution of existing DEMs, an extended photoclinometry and shape from shading algorithm is applied to the image data in combination with a DEM of lower lateral resolution (here: the GLD100 [7]) as proposed in [8]. Optionally, the lateral resolution may be further increased by applying the algorithm presented in [9] to the resulting DEM.

The construction of DEMs from multiple radiance images highly depends on the pixel synchronity of the images, while image sets with strongly varying illumination conditions are favourable for DEM construction [8]. We found that M^3 images acquired during different orbits show misregistrations of up to several kilometers. Therefore, an illumination-independent image registration method is required, where a complex transformation model has to be applied since translations, rotations, and perspective distortions are apparent.

Illumination independence is achieved by 3D reconstructions based on single images, which transform the radiance images into DEMs as proposed in [8]. In order to cope with the perspective distortions, images of features obtained from the constructed single-image DEMs, e.g. surface inclination angles or directional surface gradients, are derived and overlaid on the GLD100. The resulting 3D object is projected into the camera on the spacecraft, where the corresponding transformation is given by the camera position and orientation. These parameters are determined by minimising the Euclidean distances between corresponding control points in the images or by maximising the mutual information between the features across the images (cf. Fig. 1). Due to inaccuracies in the DEM and possibly non-constant spacecraft motion behaviour during image acquisition, the image registration can be refined by additionally applying a second-order polynomial transformation to the output of the 3D approach.

Normalisation of Spectral Data: After removal of the thermal emission component (cf. [10] or [11]), the observed reflectances are normalised to reference geometry based on the Hapke AMSA model [4] using the lunar parameters determined in [12] and the single-scattering albedo estimated pixel-wise using the DEM, and based on the empirical photometric function proposed by Hicks et al. [13]. Optionally, the distortion of the spectra due to small-scale topography can be compensated using the empirical method proposed in [11, 14]. This correction cannot be achieved with the phase angle dependent approach in

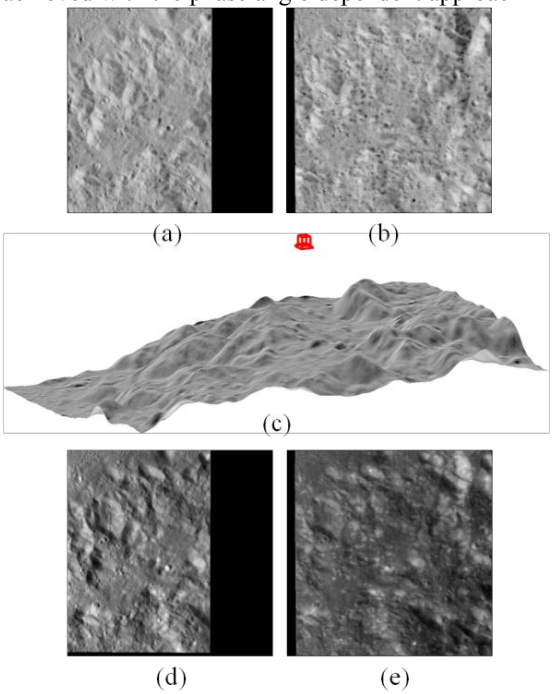

Fig. 1: Image Registration. Surface feature images (a) and (b) are extracted from single radiance images. (c) The feature image is overlaid on the DEM and projected into the camera. The extrinsic camera parameters are determined and used to register the reflectance images (d) and (e).

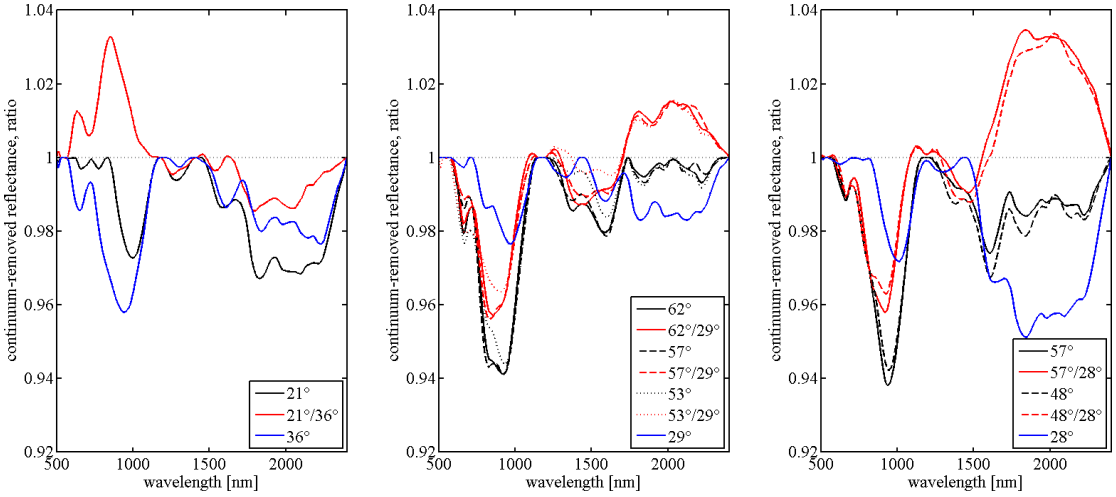

Fig. 2: Continuum-removed reflectance spectra and ratio spectra for the three test regions (left: 26–28°S, 116–118°E; centre: 17–19°S, 253–255°E; right: 15.6–17°N, 15–16.6°E). The numbers indicate phase angle values.

[13] as the phase angle is almost constant in the regarded images. The continuum of the spectrum is removed based on the convex hull approach [15]. For each of the three regarded test regions, four even (surface slope < 2°) subregions of 300 x 300 m^2 size were selected based on the constructed DEM.

For each test region, Fig. 2 shows the continuum-removed smoothed reflectance spectrum of one subregion and its ratio with respect to the spectrum acquired at the phase angle α_0 closest to 30°, for normalisation with the Hapke AMSA model [4].

Fig. 3 shows the shift $\Delta\lambda_{abs}$ of the absorption wavelength λ_{abs} of the absorption trough around 1000 nm and the relative variation δ/δ_0 of the band depth δ with changing phase angle α for the troughs around 1000 nm and 2000 nm. The relative band depth variations are computed as the ratios between the values of δ for the given phase angle α and for the phase angle α_0, respectively, where $\Delta\alpha = \alpha - \alpha_0$. The error bars denote the standard deviations over the subregions. The fitted curves are bias-free polynomials of 2nd order for $\Delta\lambda_{abs}$ and of 1st and 2nd order in the logarithmic scale for the depths of the absorption troughs at 1000 nm and 2000 nm, fitted to the averages over the subregions. For normalisation based on the Hapke AMSA model [4] with wavelength-independent (except for the single-scattering albedo) parameters, with increasing phase angle α the value of λ_{abs} becomes smaller, the depth of the 1000 nm trough increases, and the depth of the 2000 nm trough decreases. In contrast, the normalisation by Hicks et al. [13] based on wavelength-dependent parameters leads to a bimodal distribution of $\Delta\lambda_{abs}$ for $\Delta\alpha > 20°$, resulting in high fluctuations across the subregions, while both absorption depths decrease with increasing phase angle.

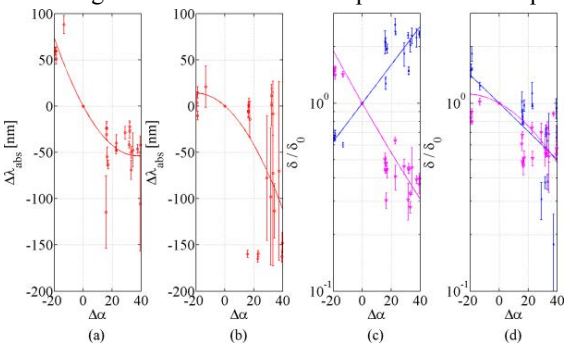

Fig. 3: Phase angle dependence of the variation $\Delta\lambda_{abs}$ of the absorption wavelength of the trough around 1000 nm (red) and the band depth ratio δ/δ_0 (blue: 1000 nm, magenta: 2000 nm trough) after normalisation using the Hapke AMSA model [4] ((a) and (c)) and the model by Hicks et al. [13] ((b) and (d)).

Conclusion: The observed absorption wavelength and band depth variations have been found to be phase angle dependent. Therefore, the normalisation of continuum-removed spectra can be refined either by applying an empirical correction to the extracted spectral features (cf. Fig. 3) or by performing a normalisation based on the Hapke AMSA model with appropriate wavelength dependent parameters.

References: [1] Mustard, J. F. and Pieters, C. M. (1988). *J. Geophys. Res. 94,* 13619-13634. [2] Matsunaga, T., et al. (2008) *Geophs. Res. Lett. 35*, L23201; [3] Bhatt, M., et al. (2011) *EPSC-DPS2011*, abstract #441; [4] Hapke, B. W. (2002) *Icarus 157*, 523–534. [5] Pieters, C. M. (1999) *Workshop New Views of the Moon 2*, 47. [6] Boardman, J. W., et al. (2011) *J. Geophys. Res. 116*, E00G14. [7] Scholten, F., et al. (2011) *LPSC XXXXII*, abstract #2046. [8] Grumpe, A. and Wöhler, C. (2011) *Proc. 7th IEEE Int. Symp. Image and Signal Processing and Analysis*, 609–614. [9] Grumpe, A. and Wöhler, C. (2012) *LPSC XXXXIII*, abstract #2597. [10] Clark, R. N., et al. (2011) *J. Geophys. Res. 116*, E00G16. [11] Wöhler, C. and Grumpe, A. (2012) *In: Innovations for Shape Analysis: Models and Algorithms. Rev. contrib. to Dagstuhl Seminar*, to appear. [12] Warell, J. (2004) *Icarus 167*, 271–286. [13] Hicks, M. D., et al. (2011) *J. Geophys. Res. 116*, E00G15. [14] Wöhler, C. and Grumpe, A. (2012) *LPSC XXXXIII*, abstract #1906. [15] Fu, Z., et al. (2007) *IEEE Trans. Geoscience and Remote Sensing 45(11)*, 3827–3844.

LUNAR THERMAL PROPERTIES OBSERVED BY THE DIVINER LUNAR RADIOMETER.

B. T. Greenhagen[1], D. A. Paige[2], and the Diviner Science Team, [1]Jet Propulsion Laboratory, California Institute of Technology, Pasadena, CA, USA; [2]University of California, Los Angeles, CA, USA.
Email: Benjamin.T.Greenhagen@jpl.nasa.gov

Introduction: The Diviner Lunar Radiometer is the first multispectral thermal instrument to globally map the surface of the Moon. This unprecedented and growing dataset is revealing the extreme nature of the lunar thermal environment, surface composition and thermophysical properties.

Diviner Lunar Radiometer: Launched onboard NASA's Lunar Reconaissance Orbiter in June 2009, the Diviner Lunar Radiometer is a nine channel pushbroom mapping radiometer designed to measure broadband reflected solar radiation and emitted thermal infrared radiation between 0.3 and 400 μm (Table 1) at spatial resolutions ranging from 0.2 to 1.3 km, depending on mission phase [1]. The two solar reflectance channels (ch. 1-2) are used to characterize the photometric properties of the lunar surface. The three shortest wavelength thermal infrared channels (ch. 3-5) were specifically designed to characterize the mid-infrared Christiansen Feature [2]. Diviner's longer wavelength thermal infrared channels (ch. 6-9) broadly span the thermal infrared and are used to characterize the lunar thermal environment, including thermophysical properties such as rock abundance and surface roughness. [1]

Table 1: Diviner Spectral Passbands

Ch.	Type	Start (μm)	End (μm)
1	Solar	0.35	2.8
2	Solar	0.35	2.8
3	8 μm	7.55	8.05
4	8 μm	8.10	8.40
5	8 μm	8.38	8.68
6	Thermal	13	23
7	Thermal	25	41
8	Thermal	50	100
9	Thermal	100	400

Coverage and Data Products: After almost three years of nearly continuous mapping, Diviner has now acquired observations over six complete diurnal cycles and three complete seasonal cycles. Diviner bulk daytime and nighttime observations have essentially global coverage; however, for any given area, two hours of local time coverage is typically 50% and 60% (Figure 1). Calibrated Diviner data (entire mission up through 12/15/11) and global maps (first year of 50 km mapping orbit) of visible brightness, brightness temperature, channel-integrated bolometric temperature, rock abundance, nighttime soil temperature, and silicate mineralogy are available from the PDS Geosciences Node [3,4].

Thermal Environment: The lunar thermal environment is extreme and complex, and posses challenges and opportunities for future landed missions. Surface temperatures in equatorial regions such as

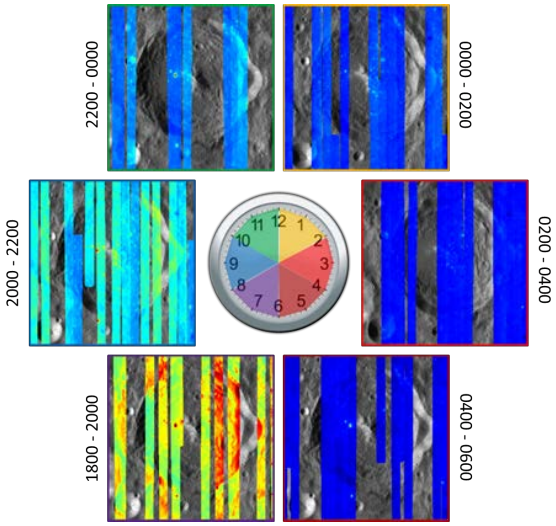

Figure 1: Example of Local Time Coverage. Diviner ch. 7 nighttime brightness temperature maps of Green Crater separated into 2 hour local time bins as indicated. Stretch 90K (blue) to 140K (red).

the Apollo landing sites are close to 400K at noon, and less then 100K at night, with annual average temperatures at depth of approximately 250K [5]. Diviner data have been used to identify areas with subsurface temperatures that are significantly hotter and colder than latitudinal averages. These thermally atypical regions extend the range of latitudes and the range of lunar environments that can be accessed, explored and sampled [6].

In the polar regions, Diviner observations place strong constraints on the thermal stability of polar volatiles. The lunar polar regions contain large areas within permanently shadowed craters with annual average temperatures of less than 50K (Figure 2). These regions are cold enough to permit the stability of near-surface water ice, as well as a range of more volatile and less volatile compounds. Frozen volatiles are thermally stable below the surface in many regions surrounding permanently shadowed areas within ~10 cm of the surface. [7]

Silicate Mineralogy: Diviner was designed to characterize the Christiansen Feature (CF) and constrain lunar silicate mineralogy (Figure 3) [2]. The CF is tied to the fundamental vibrational band and shifts to shorter wavelengths with increasing polymerization of the SiO_4 tetrahedra (e.g. quartz and plagioclase feldspar exhibit CFs at shorter wavelengths than less polymerized pyroxene and olivine) [e.g. 8]. Given the relatively restricted geochemistry of the lunar surface, Diviner measurements of CF position can be use to infer some geochemical abundances, including FeO [9].

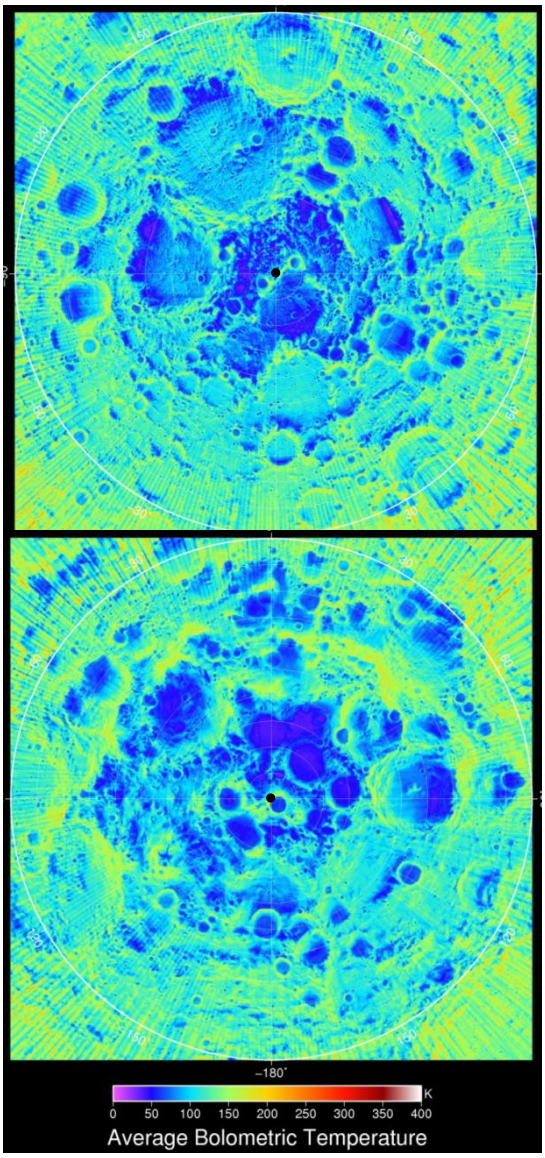

Figure 2: Polar Average Temperature. Maps of average bolometric termperature measured during Diviner's initial mapping phase for the North (top) and South (bottom) Poles. Outer latitude ring is 80°.

Diviner data have been used to identify areas with striking compositional diversity and have confirmed the presence of high silica minerals such as quartz or alkali feldspar for several lunar "red spots" and the Compton Belkovich anomaly on the lunar farside [10,2] and anomalous plagioclase compositions that were poorly sampled by Apollo [2,11]. Diviner compositional data data provide an important constraint on plagioclase abundance that can be used to infer the amount of country rock mixing [2,12]. These data are of critical importance for evaluating high value landing site targets in the SPA Basin and elsewhere.

Rock Abundance and Surface Roughness: Analyses of Diviner's dataset reveal the presence of significant regional and local variations in the thermophysical properties of the lunar regolith due to the presence of blocks and impact melt exposed by recent impacts, as well as regions of anomalously low thermal conductivity surrounding small, fresh impact craters (Figure 3). Both the presence of rocks in a predominately particulate surface and surface roughness induce variable temperatures or anisothermality within a given Diviner pixel. Anisothermality causes a wavelength difference in apparent brightness temperature. By using multispectral Diviner observations, it is possible to assess the magnitude of anisothermality and quantify the surface coverage of rocks, the temperature of the rock-free regolith, or the approximate RMS roughness of the surface. [6,13]

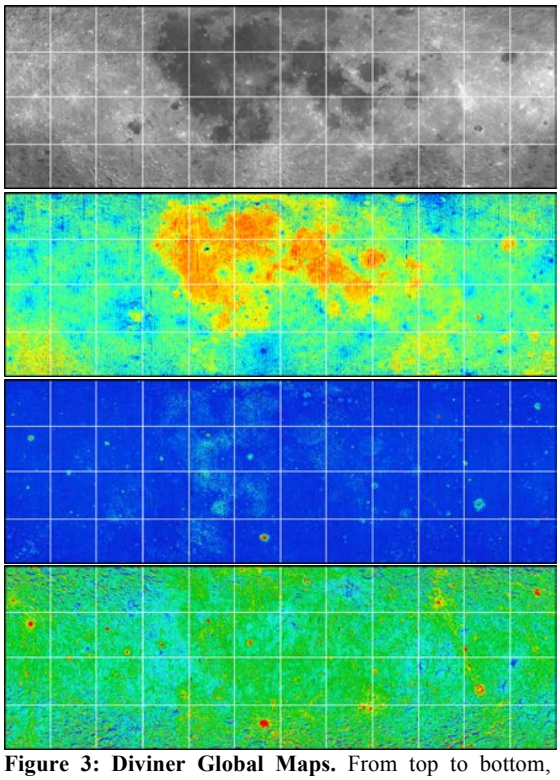

Figure 3: Diviner Global Maps. From top to bottom, Diviner maps of lambert albedo (stretched 0 to 0.25), silicate mineralogy (CF position, 7.8 to 8.55 μm), rock abundance (fractional coverage, 0 to 5%), and nighttime regolith temperature (70 to 120 K).

References: [1] Paige D.A. *et al*. (2010) *SSR*, *150*, 125. [2] Greenhagen B.T. *et al*. (2010) *Science*, *329*, 1507. [3] Paige D.A. *et al*. (2011) LPSC XLII, #2544. [4] Greenhagen B.T. *et al*. (2011) LPSC XLII, #2679. [5] Vasavada A.R. *et al*. (2012) *JGR*, submitted. [6] Bandfield J.L. *et al*. (2011) *JGR*, in press. [7] Paige D.A. *et al*. (2010) *Science*, *330*, 479. [8] Logan L.M. *et al*. (1973) *JGR*, *78*, 4983. [9] Alen C.C. *et al*. (2012) *JGR*, submitted. [10] Glotch T.D. *et al*. (2010) *Science*, *329*, 1510. [11] Donaldson Hanna K.L. *et al*. (2012) *LPS XLIII,* Abstract #1968. [12] Lucey P.G. and Greenhagen B.T. (2012) *LPS XLIII,* Abstract #1736. [13] Hayne P.O. *et al*. (2012) *LPS XLIII,* Abstract #2829.

SPHERICAL ROVER FOR LUNAR AND PLANETARY EXPLORATION. Jordi L. Gutiérrez[1] and Joshua Tristancho[2], [1]Departament de Física Aplicada, Escola d'Enginyeria de Telecomunicació i Aeroespacial de Castelldefels, Universitat Politècnica de Catalunya (jordi.gutierrez@upc.edu), [2]Escola d'Enginyeria de Telecomunicació i Aeroespacial de Castelldefels, Universitat Politècnica de Catalunya (joshua.tristancho@upc.edu).

Introduction: Historically, planetary and lunar rovers have been wheeled-driven. While this is usually seen as an advantage –due to the flight experience– in some cases, the unavoidable presence of gears and mobile parts can be a significant hazard to the mission. The abrasive lunar regolith has been the origin of substantial problems with the Apollo rovers.

Here we propose a completely different scheme: a spherical rover in which all the moving parts are protected from the environment by an external spherical shell.

Roving mechanism: The rover moves by displacing a mass from its equilibrium position. Once perturbed, the rover rotates to gain its equilibrium orientation. By perturbing this equilibrium the rover can move, and even climb slopes. There are two important figures of merit of these kind of rovers: the ratio between the counterweight mass and the total mass (μ), and the ratio betwen the position of the center of mass and the radius of the spherical shell (δ). Then, the maximum slope that can be climbed is

$$\beta_{max} = \sin^{-1}(\delta\mu) \qquad (1)$$

It must be noted that both δ and μ are less (or equal in the extreme, unfeasible, case) than 1, and that to obtain this expression we have assumed that the sphere does not slide. For typical cases, $\delta \approx 0.7$ and $\mu \approx 0.5$, which allows the rover to ascend slopes of less than 21 degrees. Our goal is to design the rover in such a way that it would be able to climb slopes up to 35 degrees, near the limit slope for regolith. This can be done, for example, by substitutind the dead counterweight mass with batteries and/or other massive components.

The rover can also steer by displacing the counterweight sideways of the translation path. In this way we can control the direction in an effectively manner.

By its simplicity, the propulsion mechanism is very robust, and hence it offers a high level of safety at a minimum cost.

There are several similar, indipendent designs in the literature, as can be seen in [1,2].

Open issues: There are still some open issues. The most important is related to the endurance, as the spherical shell is not very apt as a solar cell substrate. In any case, even if we had solar cells on the surface of the rover, they would be covered by regolith, and their efficiency would be severely dimisnished. To deal with this problem we are exploring the possibility of employing wireless power transmission [3,4]. In this case, the lander (mandatory for our rover design) would act as the energy provider; the energy could be relayed by laser means (with the problem again of the regolith covering the outer surface of the spherical shell) or by resonant inductive coils [3,4,5]. To do so witha good efficiency, it is essential that the resonant coils are alineated; this is not a problem, as the classical ball-plate problem has been satisfactory solved, and efficient algorithms are provided by [6].

There is also an issue with communications, that we have solved by using small antennas whith controlled phase shifts to modify the antenna pattern and make it more directive. The lander, provided witha high gain antenna, would then be used as a radio relay.

Thermal control will be provided by a completely passive system employing surface coatings (affected again by the regolith and its thermal properties) and by an interior shell of aerogel.

Applications: this kind of rovers can be used in several ways. The first one is as stand-alone exploration rovers, carrying experiments and cameras to points up to several hundreds of meters to the lander. Even if the lander is the main scientific vehicle, the landing procedures will perturb the state of the regolith near to the lander, thus modifying to some degree the scientific results. Having the possibility to move a few tens of meters (well beyond the reach of robotic arms) would ensure the access to pristine materials. They could laso act as scouts –or navigation aids– for larger, more advanced rovers. These rovers, probably wheel-driven, or leg-drive, have a typical speed much lower than spherical rovers, and safety issues would preclude its use on rough environments, like inside craters, where these small rovers could extend the mission's operational capabilities. In all cases, the algorithms [6] used to align the coils in the case of using resonant inductive coupling would easilly allow to point the experiments carried on the spherical rover if necessary.

References:

[1] Bruhn, F. et al. (2008) *Acta Astronautica, 63,* 618–631. [2] Armour, R. H., and Vincent, J. F. V. (2006) *J. Bionic Eng., 3,* 195–208. [3] Kurs, A. et al.. (2007) *Sci.,* 317, 83–86. [4] Bou, E. (2010), *In Space Wireless Power Transmission Systems*, Degree Thesis, Universitat Politècnica de Catalunya. [5] Sedwik, R. J. (2012), *Ann. Phys*., *327*, 407–420 [6] Mukherjee, R. et al., *J. Dyn. Sys*., *124*, 502–511

OPPORTUNITIES FOR LUNAR SCIENCE ABOARD GOOGLE LUNAR X PRIZE SPACECRAFT.
Alexandra Hall. Snr Director, Google Lunar X PRIZE, X PRIZE Foundation, 5510 Lincoln Blvd, Playa Vista, CA 90094, USA. Alex.hall@xprize.org

Introduction: The Google Lunar X PRIZE, launched in 2007, has a $20million prize purse to be awarded to the first privately funded team to land a robotic spacecraft on the surface of the Moon, move 500 meters and send back images and data. A second prize of $5million is available, as are $5millon of bonus prizes including water detection and imaging lunar heritage sites. With 26 teams competing, many from Europe, and some teams projecting launch dates in 2014 and 2015, there are opportunities for scientists to partner with teams to carry small science payloads.

Over the past 12 months, a number of discussions and meetings have taken place (in conjuction with the NASA Lunar Science Institute and others) to determine what sorts of small science payloads may be appropriate. A session at the 43rd Lunar and Planetary Science Conference recently held in Texas, further developed these ideas, which include seismometers, retroreflectors, dosimeters, and different imaging systems.

At the European Lunar Science Symposium, the author will introduce the current thinking on possible lunar science opportunities, introduce the European teams (many will be present) and our European Outreach Manager, and be seeking further feedback and ideas from the scientists present. We hope to inspire some productive collaborations.

THE MOON AS A TOUCHSTONE FOR SOLAR SYSTEM SCIENCE: LUNAR SCIENTIFIC FRONTIERS AND GOALS FOR FUTURE HUMAN AND ROBOTIC EXPLORATION. James W. Head, Department of Geological Sciences, Brown University, Providence, RI 02912 (james_head@brown.edu).

Lessons From Lunar Exploration: Ten things we have learned about the Moon from past and recent missions and analyses provide a fundamental scientific legacy and have set the stage for our thinking about the early evolution of the Earth and other planetary bodies and provided an important set of goals for future human and robotic exploration: **1) The Moon formed from the impact of a Mars-sized object into early Earth:** How does this process, and its immediate aftermath, set the Moon on an evolutionary path that is the same as, or different than, other planetary bodies? **2) The early Moon was characterized by a global-scale magma ocean:** Near-global melting caused by accretional energy produced an anorthositic highland crust, a "primary crust". Is the evolution of the lunar "primary crust" unique? How do primary crusts on planets with different compositions and interior structures form and evolve? **3) The Moon initially differentiated into chemical layers, including a crust and mantle, which set the stage for further evolution:** What is the nature of late-stage crustal differentation processes and how do they contribute to the character of lower planetary crusts? **4) The chemical and thermal nature of these stratified layers may have led to net negative buoyancy, large-scale overturn, and significant vertical mixing:** Is this predicted early overturn unique to the Moon or applicable to other planets, including Earth? **5) The Moon is stratified into mechanical layers; the lithosphere, the outer thermal boundary layer, thickened and became less heterogeneous with time:** What controlled the initial thickness, variability and rates of thickening on the Moon and other planets? What are the major mechanisms of lithospheric heat transfer (e.g., conduction, convection, advection, plate recycling) in space and time on each planetary body? **6) Tectonically, the Moon is a one-plate planet, characterized by a globally continuous lithosphere:** How does the evolution of the global state of stress in the lithosphere, recorded in the sequence of tectonic features, and the thickness of the lithosphere with time, as recorded in its flexural response to loads and in the gravity field, vary from body to body? **7) Lunar volcanism records processes of mantle melting in space and time, and the volcanic record reflects the general thermal evolution of the Moon, including the state and magnitude of stress in the lithosphere:** The unique ability to link lunar samples to specific deposits significantly enhances our understanding of these processes: for example, recent results implicate water in the formation of volatile-rich pyroclastic eruptions. How does the volcanic record of the planets differ,and why? **8) The Moon is a fundamental laboratory for the study of impact cratering processes, particularly at the complex crater to multi-ring basin scale:** The ability to combine studies of lunar impact breccias and melts with crater and basin deposits considerably enhances this understanding. How can this understandig be applied to other planets? **9) The Moon is a template for the record of the distribution and history of impactors in the inner solar system:** The lunar cratering record, in conjunction with the unique chronology afforded by returned and dated samples, can inform us about a) the reality of a Late Heavy Bombardment, b) the changing size-frequency distribution of impactor populations with time, c) the potential non-linear nature of the bombardment record in the last half of solar system history, and d) the likelihood of species-terminating future impact events on Earth. **10) Volatiles play a more important role in lunar evolution than previously thought:** Recent reports of detection of water and water-related species: a) as coatings on surface minerals, b) in buried near-polar deposits, and c) in mantle derived melts, all provide exciting insight into a range of water-related processes during different times in lunar history, including accretion, differentiation, cometary impact, and interaction with the solar wind.

Role of the Moon in Future Planetary Exploration: In what context does this integrated comparative planetology perspective place the Moon? Some see the Moon as a *cornerstone*: this metaphor implies that the Moon is of extreme importance because all other stones will be set in reference to it, thus determining the position of the entire structure. The Moon as a *keystone* implies a central cohesive source of support and stability for ideas about the formation and evolution of planets. Still others see the Moon as a *Blarney stone*: those who have "kissed the stone" have been imparted with an excessive skill in flattery about the Moon. It can be argued that the lessons from comparative planetology place the Moon where it belongs, as one member of a family of Solar System objects, each of which provides insight into fundamental lessons of planetary evolution. As such, an appropriate metaphor for the Moon might be a *touchstone*, which refers to any physical or intellectual measure by which the validity or merit of a concept can be tested.

The Renaissance of Lunar Exploration and What it Means for the Future: At the advent of the atomic age, Albert Einstein is reported to have said: "Everything has changed but our way of thinking", a thought that might be applied to our current understanding of the Moon and its role in Solar System exploration. Following the foundation of dozens of robotic and human missions to the Moon by the United States and the So-

viet Union, recently ESA, Japan, China, India and the United States have launched comprehensive missions to the Moon, and each, as well as Russia, has plans for continuing lunar exploration. The onslaught of new data is monumental, and the data are just barely starting to be ingested, digested and analyzed. Nonetheless, the future is clear. We are on the verge of a renaissance in our study and understanding of the Moon. We are acquiring extremely high spatial and spectral resolution data across a wide wavelength range. This has changed everything, and fundamental changes in our way of thinking will surely follow: The distribution of rocks from the lunar sample collection can now be mapped globally. New minerals and rock types are being discovered. The provenance of recognized rock types can be studied and established using new very high spatial and spectral resolution data. The mineralogy and context of individual large boulders and clusters of boulders can be mapped, and then placed in their geological contexts. Models of crustal stratigraphy can be tested and depth of sampling of craters can be assessed. Refined models of crustal stratigraphy and evolution can be constructed. New avenues of communications are being opened between planetary scientists utilizing approaches such as mineralogy, petrology, geochemistry, geology, spectroscopy, geophysics, etc. The lunar renaissance is propelled not just by the new data, but by the fundamental foundation and interpretative context provided by information collected by dozens of previous missions, including lunar samples collected by Astronauts during the six geological expeditions of the Apollo Lunar Exploration Program, and the Soviet robotic sample return missions (Luna 16, 20, and 24), and analyzed in sophisticated laboratories on Earth. Collectively, these data have provided a basic framework that is unequalled on any planetary body other than the Earth. For Earth, this framework provides unique insight into the formative years of Earth history, a record virtually destroyed by the dynamic nature of planet Earth.

Lessons for Future Lunar Exploration: The basic framework of the lunar renaissance will crisply define the questions to be addressed by a range of new lunar robotic missions including multiple geophyscical stations and networks, multiple farside and nearside sample return, and long-range rover missions providing interpolation, extrapolation and integration between and among Apollo, Luna, Lunokhod and future sample return sites. Opportunities for human and robotic partnerships abound, ranging from human-tended science stations orbiting the Moon, to telerobotic, low latency operations of scientific assets on the lunar farside from human science stations at L2. When humans inevitably return to explore the surface of the Moon in the coming decades, the lunar renaissance will have provided both compelling reasons for human exploration and detailed locations at which humans can optimize their exploration skills. Careful planning in the next few years can encourage and nurture the types of science and engineering synergism that made Apollo such a success, and provide a new legacy of fundamental insight into the origin and evolution of the Solar System and the formative years of our own Home Planet, Earth.

Dating the Moon with Crater Size-Frequency Distribution Measurements. H. Hiesinger[1], G. Neukum[2], R. Jaumann[3], J. W. Head[4], C. H. van der Bogert[1], F. Thiessen[1], J. H. Pasckert[1], [1]Institut für Planetologie, Westfälische Wilhelms-Universität Münster, Wilhelm-Klemm-Str. 10, 48149 Münster, Germany, Hiesinger@uni-muenster.de; [2]Freie Universität Berlin; [3]DLR-Institut für Planetenforschung; [4]Dept. of Geological Sciences, Brown University

Introduction: The chronology of geologic units on the lunar surface is based on radiometric ages determined from Apollo and Luna landing site samples, regional stratigraphic relationships, and crater degradation and size-frequency distribution measurements (CSFDs) [e.g., 1]. Accurate age estimates, for example of mare basalts, are necessary to place constraints on the duration and flux of lunar volcanism and the petrogenesis of lunar mare basalts and their relationship to the thermal evolution of the Moon [1, 2]. In addition, crater counts on ejecta blankets allow us to date individual craters, such as the stratigraphically important Copernicus crater. CSFDs on light plains enable us to test hypotheses of their origin. In particular, we can test the hypotheses that they were formed by a special type of highland volcanism [e.g., 3], by the impacts of either the Imbrium or the Orientale events [e.g., 4], or by the impacts of local/regional craters [e.g., 5]. New data from the international armada of lunar spacecraft provide the mineralogical, geochemical, morphological, topographic and age data that will further refine our understanding of the absolute stratigraphy of geologic units on the Moon.

Data and Methods: For our age determinations, we used Lunar Orbiter, Lunar Reconnaissance Orbiter Narrow Angle (NAC) and Wide Angle Camera (WAC), and Kaguya Terrain Camera (TC) images. The well-established technique of CSFD measurements is described elsewhere [e.g., 6-9]. To obtain the relative or absolute age of a photogeological unit, one must (1) measure the surface area of the unit, and (2) measure the diameters of each primary impact crater within this unit. The cumulative crater density of a geologic unit at a fixed reference diameter is directly related to the time the unit has been exposed to the meteorite flux and therefore gives a relative age of this unit. To obtain absolute model ages from CSFD measurements one has to link the radiometric ages from the returned samples to crater counts of the landing sites to establish the lunar cratering chronology [e.g., 8, 10-13].

Results: *Mare basalts:* We have dated basalts in Oceanus Procellarum, Imbrium, Serenitatis, Tranquillitatis, Humboldtianum, Australe, Humorum, Nubium, Cognitum, Nectaris, Frigoris, and numerous smaller occurrences within impact craters and sinus and lacus areas, most of which are of late Imbrian age [1]. Our results confirm and extend the general distribution of ages of mare basalt volcanism and further underline the predominance of older mare basalt ages in the eastern and southern nearside and in patches of maria peripheral to the larger maria, in contrast to the younger basalt ages on the western nearside, i.e., in Oceanus Procellarum.

Craters: Our new counts for North Ray, Tycho, and Copernicus craters fit, and thus support, the lunar chronology of [14] at young ages [15]. Our data are also generally consistent with a constant impact rate, although with only three data points we cannot exclude small episodic variations in the cratering rate. Variations in impact rate caused by cometary showers were suggested to occur periodically, for example, due to perturbation of the Oort cloud by galactic tides, the passage of the Solar System near a molecular cloud, or an unseen star [e.g., 16]. However, *Bailer-Jones* [17] systematically re-investigated the available data and found no periodicity, similar to results of [18-19].

Light plains: The ages of light plains vary by 360 Ma, making it unlikely they formed by a single event. However, nine units formed in a relatively close interval of 3.70-3.79 Ga. The oldest age of which post-dates the impacts of Imbrium and Orientale, which formed around 3.91 and 3.84 Ga, respectively [12] However, in the stratigraphy of [20], Orientale is 3.72-3.85 Ga old and Imbrium is 3.77-3.85 Ga old. Thus, it is possible that these nine units are associated with one or both of these impacts.

Conclusions: On the basis of our CSFDs we find that (1) in the investigated basins lunar volcanism was active for almost 3 b.y., starting at about 3.9-4.0 b.y. ago and ceasing at ~1.2 b.y. ago, (2) most basalts erupted during the late Imbrian Period at about 3.6-3.8 b.y. ago, (3) significantly fewer basalts were emplaced during the Eratosthenian Period, (4) basalts of possible Copernican age were only found in limited areas in Oceanus Procellarum, (5) our derived model ages of the ejecta blankets of Tycho, Copernicus, and North Ray agree well with radiometric and exposure ages of the Apollo 16, 17, and 12 landing sites, respectively; (6) our new crater counts for the Copernicus ejecta blanket better fit the lunar chronology than previous counts; (7) the new counts are generally consistent with a constant impact rate over the last 3 Ga; small variations can not be resolved in our data and require further investigations, (8) ages derived for light plains within the South Pole-Aitken basin show a wide range and cannot be solely linked to either the Orientale or the Imbrium impact, (9) a volcanic origin of at least some of the light plains cannot be excluded.

References: [1] Hiesinger et al., 2011. [2] Whitten et al., 2011. [3] Neukum, G., 1975. [4] Chao et al., 1973. [5] Oberbeck et al., 1974. [6] Hartmann, 1966. [7] Crater Analysis Techniques Working Group, 1979. [8] Neukum, 1983. [9] Hiesinger et al., 2000. [10] BVSP, 1981. [11] Strom and Neukum, 1988. [12] Neukum and Ivanov, 1994. [13] Stöffler and Ryder, 2001. [14] Neukum et al., 2001. [15] Hiesinger et al., 2012. [16] Gardner et al., 2011. [17] Bailer-Jones, 2011. [18] Grieve, 1991. [19] Jetsu and Pelt, 2000. [20] Stöffler and Ryder, 2001.

PHYSICS AND PHYSIOLOGY: THE HYDROSTATIC INDIFFERENCE CONCEPT

Helmut Hinghofer-Szalkay, Nandu Goswami
Institute of Physiology, Medical University of Graz, Austria (helmut.hinghofer@medunigraz.at)

.

Introduction and rationale: A body that is allowed to float freely in a given gravitational field is referred to as 'weightless', no hydrostatic pressure gradients exist within it. Interfering external forces create relative acceleration, and inertial forces ensue in the opposite direction. When a person stands upright, free fall (footward) is counteracted by the ground that generates headward acceleration and an 'eyeballs down' inertial force (+Gz). That force triggers relative movement between organs and tissues that differ in density, until further deformation is impeded by anatomical anchoring (e.g. in the inner ear graviceptors). Further, hydrostatic pressure gradients occur throughout fluid-filled spaces, such as in the arterial and venous system, respectively.

On Earth, there is a pressure gradient of 1 kPa (7,5 mmHg) per meter height difference in a given (open) vascular system. For instance, arterial blood pressure differs by ≈130 mmHg between brain and lower legs (depending on body length), putting the brain in disadvantage in terms of perfusion pressure when a person stands upright. In fact, an important aspect of proper cardiovascular functioning is how exactly arterial and venous pressures change with any given postural change.

A common concept here is to identify the location at which pressure stays unchanged when a person moves from one position (e.g., supine) to another (e.g., upright). This point would then serve as a natural reference for cardiovascular adaptations that become necessary when postural changes occur, and has become known as 'hydrostatic indifference point' (HIP). An HIP is not defined by a certain anatomical location; rather, it depends on the system (arterial, venous) and exact postural change considered (because blood volume distribution, fluid column extension, vascular biomechanics and neurohormonal status all shift with body position). In humans changing between supine and upright, the arterial HIP resides at heart level while the venous HIP is found below the diaphragm, roughly at liver level (Gauer & Thron 1965). Interestingly, pressure receptors are located outside the referring hydrostatic zones, which means that postural changes are able to trigger appropriate cardiovascular reflex effects (Hinghofer-Szalkay 2011).

Where are the HIPs located when the inertial force has different magnitude – such as on the surface of the moon, where gravity is only 1/6 of Earth level? This has not yet been investigated. Even more important, however, is the fact that hydrostatic gradients will be accordingly decreased (to 1/6 Earth level), meaning that (*ceteris paribus*) brain perfusion is much less jeopardized when standing upright on the moon. Orthostatic problems are certainly not to be expected from that perspective.

The real question, of course, is just how much moon gravity is sufficient as a countermeasure against cardiovascular deconditioning; nobody knows for sure. Simulation of 1/6 G on Earth (i.e., head-up tilt to ≈10°) is probably hampered by the fact that the full effect of 9.81 ms^{-1} is still present, even if not acting in the z axis (this argument applies to all bed rest models of weightlessness simulation, however).

Conclusion: Effects of moon gravity on the human cardiovascular system can be expected to be proportionally weaker than on Earth, where hydrostatic pressure gradients can cause orthostatic problems and loss of consciousness. At the same time, cardiovascular training is an important everyday countermeasure: frequent orthostatic challenges are salient to keep circulatory regulation and blood pressure in a physiological range. It is unknown to what degree the physical circumstances on the moon will suffice to keep the regulation of blood pressure and arterial perfusion at a resilience level that would allow astronauts to successfully cope with the higher gravitational stress upon their return to Earth.

References:

Gauer OH, Thron HL. Postural changes in the circulation. In: Handbook of Physiology - Circulation III, 1965; Ch 67, pp 2409-39 (Am Physiol Soc, Bethesda, MD)

Hinghofer-Szalkay H. Gravity, the hydrostatic indifference concept and the cardiovascular system. Eur J Appl Physiol 2011; 111: 163-74

DUSTY PLASMA PHYSICS ON THE LUNAR SURFACE. M. Horanyi (Colorado Center for Lunar Dust and Atmospheric Studies, LASP and Department of Physics, University of Colorado, Boulder, Colorado, 80309-0392, USA, horanyi@colorado.edu), S. Robertson, X. Wang, A. Collette, A. Dove, J. Szalay, A. Shu, T. Munsat, S. Kempf. D. Brain, Z. Sternovsky, E. Gruen, and the CCLDAS Team, (Colorado Center for Lunar Dust and Atmospheric Studies)

Introduction: The lunar surface is an excellent laboratory to study dusty plasma processes that are relevant to all airless objects throughout the solar system. The solar wind and UV radiation lead to charging of exposed surfaces, and the formation of plasma sheaths above them. Near-surface intense electric fields are thought to be capable of mobilizing and transporting small charged dust particles. Remote sensing and in situ observations indicating dust transport on the Moon date back to the Apollo era and remain highly controversial. Dust transport on airless bodies can significantly alter our interpretation of spectral identification of asteroids, the small-scale surface features of Mercury, and the Martian moons Phobos and Deimos. Understanding the behavior of dust laden plasma sheaths is of interest in basic plasma and planetary sciences, and holds the key to efficient dust hazard mitigation for the long-term use of optical and mechanical equipment for robotic and human exploration.

Small-scale Laboratory Experiments: This presentation will describe a series of laboratory experiments investigating the properties of photoelectron sheaths, and the emergence of intense electric fields near boundaries of lit and dark surfaces, and also regions shielded and exposed to the solar wind plasma flow. Our progress in the analysis and interpretation of the laboratory observations using simple analytic models and complex plasma simulation tools indicates that these models can be used to predict the expected properties of the lunar near-surface environment with increasing confidence.

Large-scale Laboratory Experiments: The focus of the CCLDAS experimental work includes the development of a hypervelocity dust accelerator to study the effects of dust impacts on surface in space. The typical size of the accelerated dust grain is in the range of $0.1 < r < 2$ μm and their velocity is in the range of $1 < v <$ 100 km/s. We will describe the assortment of diagnostic tools to enable the observation of the production of secondary ejecta particles, neutral gas, plasma, and EM radiation over a wide range of frequencies.

Dusty Plasma Landing Package (DPLP): The presentation will conclude with a list of science goals and measurement requirements for a set of surface experiments that were developed through our computer simulation studies, and laboratory experiments.

How do results from a commercial finite element thermal transfer code compare with analytical methods and surface brightness temperature observations from the Lunar Diviner Radiometer on Lunar Reconnaissance Orbiter? E. Ingram[1], I. R. Thomas[1], and N. E. Bowles[1] emily.ingram@queens.ox.ac.uk, Atmospheric, Oceanic and Planetary Physics, Clarendon Laboratory, Parks Road, Oxford OX1 3PU, UK

Introduction: Other the past few years, several increasingly sophisticated thermal transfer models have been developed to simulate the surface temperature in shadowed lunar craters. Recent results from the Lunar Diviner Radiometer experiment on NASA's Lunar Reconnaissance Orbiter allowing a direct experimental comparison for the first time (e.g. [1]). At the same time as these 'bespoke' techniques have been developing, there have been improvements in the performance and availability of commercially available finite element codes that, in principle, can be used to carry out similar simulations. To test this, we present a comparison of different methods for computing the surface temperature distributions within shadowed craters on airless bodies such as the Moon.

Methodology: The initial aim of this work was to test the capability of commercially available finite element software, in this case 'Autodesk Simulation Multi-physics 2012' with previously published models such as those described in [2], [3] and[4].

The model described by [2] was used to calculate the maximum temperature of the shaded side of a bowl shaped crater, allowing specific temperatures to be compared with an identically shaped crater calculated using finite element code (Figure 1). A comparison of these techniques is in progress.

At the same time, the more complex model described by [4] is being implemented using their standard test case of an idealised, truncated cone based on the aspect ratio and latitude of Peary crater (88.6°N 33.0°E, 74km diameter). This model includes subtler effects including double shielding from the Sun at high latitudes so will provide a significantly more robust test of the commercial model.

Once the results from the multi-purpose finite element code have been validated, attempts will be made to incorporate topographic data measured by the LOLA instrument on NASA's Lunar Reconnaissance Orbiter [5] into the commercial code to allow comparison against both LRO Diviner brightness temperature data and the output from more sophisticated models such as those described in [1].

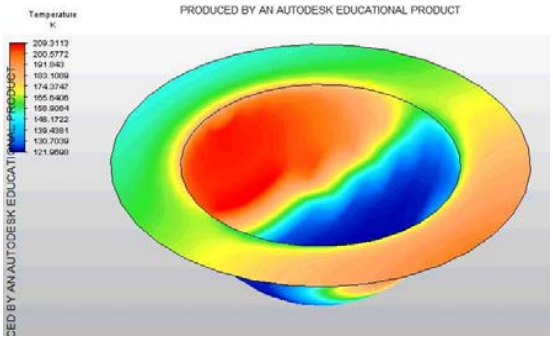

Figure 1. Temperature distribution for an idealised crater calculated using a commercial finite element code that includes radiative transfer (provisional, using different depth/diameter ratio and angle to the Sun)

References: [1] Paige D.A., Siegler M.A., Zhang J.A. *et al.* (2010) *Vol 330 No 6003*, 479-482. [2] Ingersoll A.P., Svitek T. and Murray B.C. (1992) *Icarus 100* 40-47 [3] Vasavada A.R., Paige D.A., Wood S.E. (1999), *Icarus 141* 179-193 [4] Carruba V. and Coradini A. (1999) *Icarus 142* 402-413 [5] Smith D.E., Zuber M.T., Neumann G.A. *et al.* (2009) *Geophysical Research Letters 37* L18204

A DEDICATED SMALL LUNAR EXPLORATION ORBITER (S-LEO)

R. Jaumann[1,2], H. Hoffmann[1], H. Hiesinger[3], F. Claasen[4], T. Spohn[1], U. Mall[5], J. Helbert[1], N. Kappelmann[6], K. Werner[6], R. Wimmer-Schweingruber[7], R. Srama[8], J. Oberst[1], M. Werner[9], G. Neukum[2], S. van Gasselt[2], N. Schmitz[1], K. Eichentopf[1], T. Knigge[10], U. Kummer[10], M. Langemann[10]

[1]German Aerospace Center (DLR) Berlin, Institute of Planetary Research, Berlin, Germany (ralf.jaumann@dlr.de), [2]Institute of Geological Sciences, Freie Universität, Berlin, Germany, [3]Westfälische Wilhelms-Universität, Münster, Germany, [4]DLR, Raumfahrtmanagement, Bonn, Germany, [5]Max-Planck-Institut für Sonnensystemforschung, Katlenburg-Lindau, Germany, [6]Universität Tübingen, Institut für Astronomie und Astrophysik, Tübingen, Germany, [7]Christian-Albrechts-Universität, Institut für experimentelle und angewandte Physik, Kiel, Germany, [8]Max-Planck-Institut für Kernphysik Heidelberg, Heidelberg, Germany, [9]DLR, Institut für Hochfrequenztechnik und Radarsysteme, Wessling, Germany, [10]EADS, Astrium, Friedrichshafen, Germany.

The Moon gives witness to more than 4.5 Ga of Solar System history. The Moon is our closest companion and can easily be reached from Earth at any time, even with a relatively modest financial budget. Consequently, the Moon was the first logical step in the exploration of our Solar System before we pursued more distant targets such as Mars and beyond. The vast amount of knowledge gained from the Apollo and other lunar missions of the late 1960s and early 1970s demonstrates how valuable the Moon is for the understanding of our planetary system (e.g. [1], [2]). Even today, the Moon remains an extremely interesting target scientifically and technologically. New data have helped to address some of our questions about the Earth-Moon system, but many remain unanswered and new questions arose. In particular, the discovery of water at the lunar poles, water and hydroxyl-bearing surface materials, other volatiles, as well as the discovery of young volcanism have changed our view of the Moon. Therefore, returning to the Moon is the critical stepping-stone to further exploring our immediate planetary neighborhood. Here, we present scientific and technological arguments for a Small Lunar Explorations Orbiter (S-LEO) dedicated to investigate so far unsolved questions and processes. Numerous space-faring nations have realized and identified the unique opportunities related to lunar exploration and have planned missions to the Moon within the next few years. Among these missions, S-LEO will be unique, because of its unprecedented spatial and spectral resolutions. S-LEO will significantly improve our understanding of the lunar environment in terms of composition, surface ages, mineralogy, physical properties, and volatile and regolith processes. S-LEO will carry an entire suite of innovative, complementary technologies, including high-resolution camera systems, spectrometers that cover previously unexplored parts of the electromagnetic spectrum over a broad range of wavelengths, and a communication system to be able to interact with landed equipment also on the farside. The S-LEO concept is technologically challenging but feasible, and will gather unique, integrated, interdisciplinary datasets and will provide an unprecedented new context for all other international lunar missions. The most visible mission goals of S-LEO will be the identification and mapping of lunar volatiles and the investigation of their origin and evolution with high spatial as well as spectral resolution on a global scale. Spectral mapping in the X-ray, ultraviolet and mid-infrared domains will provide insight into mineralogical and thermal properties that have remained unexplored in these wavelength ranges and which will provide the mineralogical context for volatile processes. The determination of the dust distribution in the lunar orbit will provide information about processes between the lunar surface and exosphere supported by direct observations of lunar flashes. Measuring of the radiation environment will finally complete the exosphere investigations. Combined observations based on simultaneous instrument adjustment and correlated data processing will provide an integrated geological, geochemical and geophysical database.

Thus, S-LEO is featuring a set of unique scientific capabilities w.r.t. other planned missions including: (1) dedicated observation of volatiles (mainly H_2O and OH), their formation and evolution in direct context with the geological and mineralogical surface and with high spectral and spatial resolution (< 1 m/px); (2) besides the VIS-NIR spectral range so far uncovered wavelengths in the ultraviolet (0.2 – 0.4 µm) and mid-infrared (7 - 14 µm) will be mapped to provide mineralogical context for volatile processes (e.g. sources of oxygen); (3) monitoring of dust and radiation in the lunar environment and their interaction with the surface; and (4) monitoring of present-day meteoroitic impacts.

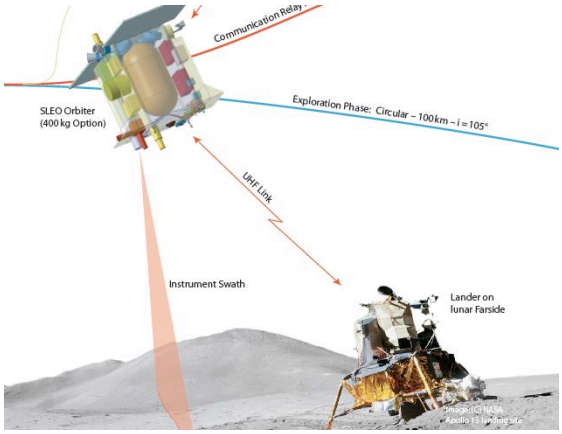

References:

[1] H. Hiesinger, J.W. Head, New Views of Lunar Geoscience: An Introduction and Overview, In: New Views of the Moon (B.L. Jolliff et al. eds.) Rev. Min. Geochem., 60, 1-81 (2006). [2] R. Jaumann, The Moon, In: Encyclopedia of Astrobiology, M. Gargaud et al. (eds.), Vol. 2, Springer, 280-282 (2011)

ADVANCEMENTS IN LUNAR SCIENCE FROM STUDIES OF LUNAR METEORITES. K. H. Joy[1, 2]
[1]Center for Lunar Science and Exploration, The Lunar and Planetary Institute - USRA, 3600 Bay Area Blvd., Houston, Texas 77058 (joy@lpi.usra.edu), USA. [2] School of Earth, Atmospheric and Environmental Sciences, University of Manchester, Oxford Road, Manchester M13 9PL, UK

Sampling the Moon: Manned and unmanned missions to the Moon have returned ~382 kg of lunar rocks and soils [1]. These were all collected from within and around the nearside Procellarum KREEP Terrane, or from equatorial latitudes on the eastern limb (Fig. 1). Therefore, interpretations of the Moon's geological past have been derived from a geographically restricted dataset on the lunar nearside. Lunar meteorites, in contrast, are sourced from random localities on the surface, and, thus, provide a better understanding of the geological history of the Moon, even though their precise provenance is unknown.

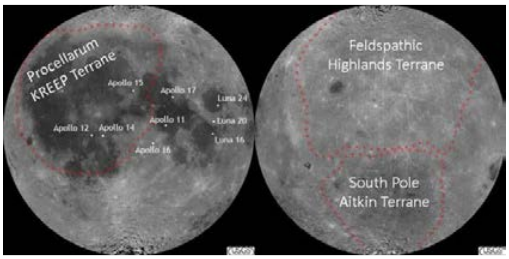

Figure 1. Location of the Apollo and Luna sample return landing sites. Also shown are the main lunar geochemical crustal terranes as defined by [2]. Overlain on a Clementine mission albedo map of the Moon.

Lunar meteorites: To date there have been ~154 individual (named) lunar meteorites collected on Earth. These form, through compositional, mineralogical or isotopic similarities, ~72 landing-paired stones where the material originated from ~51 source impact craters on the Moon [3]. Radiogenic isotope studies indicate that the majority of known lunar meteorites have been launched from the Moon in the last 10 million years [4], and all have been launched in the last 20 million [5] from small craters only a few kilometres or less in diameter [6].

Scientific significance: Studies of lunar meteorites have helped to advance lunar science by challenging the paradigms and hypothesis developed from studies of Apollo and Luna samples [7]. Examples of these advances include:

Understanding the formation of the ancient primary crust. Feldspathic lunar meteorites (*e.g.,* see Fig. 2) provided the first samples from the Feldspathic Highlands Terrane on the farside of the Moon (Fig. 1), offering new perspectives to the compositional diversity of the lunar primary crust [8-13], and the history of its formation. The diversity of anothositic material in lunar meteorites indicate that it is probable that the crust did not form in a simplistic single floatation magma ocean event, and that more complex geological processes (multiple magma oceans, serial magmatism?) were responsible for its formation [9, 14-15].

Figure 2. Scanned thick section of feldspathic regolith breccia lunar meteorite Dar al Gani (DaG) 400 [13]. Many small rock fragments (clasts) of impact melt breccias and anorthositic lithologies are consolidated together in a fine grained matrix.

Understanding the diversity and timing of mantle melting and secondary crust formation. Mare basalts sampled by the Apollo and Luna missions are typically bimodal in composition between high-Ti (typically >10 wt% TiO_2) and low-Ti (1-6 wt% TiO_2) types. However, basaltic lunar meteorites are compositionally more diverse than Apollo and Luna samples, with many very-low-Ti (VLT <1 wt% TiO_2: *e.g.,* Figure 3) and intermediate TiO_2 (6-10 wt% TiO_2) hand specimens and small rock fragments [16] offering new insights to the heterogeneity of the lunar mantle [17].

Basaltic lunar meteorites also represent the youngest [18-19] and the oldest [20] sampled mare basalt lava flows, providing insights to secular mantle melting events, the role of KREEP (late-stage products of the lunar differentiation event) in mantle melting, and heat flow in the lunar interior.

Figure 3. Scanned thin section of crystalline basaltic meteorite Miller Range (MIL) 05035,34 [17]. The meteorite has a bulk VLT composition and is KREEP-poor compared with most Apollo and Luna mare basalts [17].

Understanding the global compositional diversity of the lunar surface. Rock and mineral fragments within regolith breccia samples have revealed new types of lunar lithologies [21] and the existence of new minerals [22], demonstrating the complexities of lunar geological processes.

The bulk composition of regolith breccia meteorites (consolidated lunar soils) have been used to help calibrate remote sensing geochemical datasets, providing a more accurate global perspective of the compositional diversity of the lunar surface [23-24].

Understanding the impact bombardment history of the Moon and the inner Solar System. A few lunar meteorite stones, and many individual rock fragments in brecciated samples (*e.g.,* Fig. 2) were formed in impact cratering episodes [13]. Radiometric age dating of these samples reveals the timing of impacts on the Moon [25-27], and provides a vital window to studying the lunar cratering history in regions distal to the Imbrium basin-forming event (this record dominates the impact history of Apollo samples). Unraveling this archive is critical to addressing if there was a spike in impact bombardment in the inner Solar System at ~3.9 Ga (referred to as the lunar cataclysm hypothesis [7]), and if there have been more recent spikes in the impact record, related to the initiation, proliferation and retardation of life here on Earth.

Future perspectives: With the discovery of new lunar meteorites in hot and cold desert environments here on Earth, we gain a renewed understanding of the geological and impact history of the Moon [7].

References: [1] Vaniman D. et al. (1991) Chapter 2. *Lunar sourcebook: A user's guide to the Moon*. (ISBN 0-521-33444-6). [2] Jolliff B. L. (2000) *J.Geophys. Res*. 105, 4197–4216. [3] Korotev R. L. (2012) http://meteorites.wustl.edu/lunar/ [4] Korotev R. L. (2005) *Chemie der Erde* 65, 297–346. [5] Head J.W. III. Et al. (2002) *Science*. 298, 1752–1756. [6] Nishiizumi K., and Caffee M. W. (2001) 64th Meteoritical Society Meeting, Abstract #5411.

[7] NRC (2007) The Scientific Context for the Exploration of the Moon. ISBN: 0-309-10920-5. [8] Palme H. et al. (1991) *Geochim. Cosmochim. Acta*. 55, 3105–3122. [9] Korotev R. L. et al. (2003) 67, 4895–4923. [10] Korotev R. L. et al. (2009) *Meteoritics & Planet. Sci*., 44, 1287–1322. [11] Takeda H. et al (2006) *Earth Planet. Sci. Lett*. 247, 171–184. [12] Arai T. et al. (2008). *Earth, Planets, Space*. 60, 433–444. [13] Joy K. H. et al. (2010) Meteorit. *Meteoritics & Planet. Sci*., 45, 917– 946. [14] Longhi J. (2003) *J. Geophys. Res*. 108, 5083, doi:10.1029/2002JE001941. [15] Gross J. et al. (2012) *LPS XLIII*, Abstract #2306. [16] Robinson K. L. et al. (2012) *Meteoritics & Planet. Sci.,* doi: 10.1111/j.1945-5100.2012.01344.x. [17] Joy K. H. et al. (2008) *Geochim. Cosmochim. Acta* 72, 3822–3844. [18] Fernandes V. A. et al. (2003) *Meteoritics & Planet. Sci.,* 38, 555–564.[19] Borg L. E. et al. (2004) *Nature* 432, 209–211. [20] Terada K. et al. (2007) *Nature* 450, 849–853. [21] Gross J. and Treiman A. H. (2011) *J. Geophys. Res*. 116, E10009, 9 doi:10.1029/2011JE003858. [22] Anand M. et al. (2004) *PNAS* 101, 6847-6851. [23] Warren P.H. (2005) *Meteoritics & Planet. Sci.,* 40, 335–511. [24] Prettyman T. H. et al. (2006) *J. Geophys. Res*. – *Planets*. 111, E12007, doi:10.1029/2005JE002656. [25] Cohen B. A. et al. (2000) *Science*. 290, 1754–1756. [26] Cohen B. A. et al. (2005) *Meteoritics & Planet. Sci.,* 40, 755-777. [27] Nyquist L. et al. (2006) *Geochim. Cosmochim. Acta*. 70, 5990-6015.

SUMMARY OF KAGUYA SCIENCE. M. Kato, H. Ootake, and Kaguya Science Team, Japan Aerospace Exploration Agency (3-1-1 Yoshinodai, Sagamihara Chuo, Kanagawa 2525210 Japan, and e-mail; kato@planeta.sci.isas.jaxa.jp and ootake.hisashi@.jaxa.jp).

Introduction: The Kaguya spacecraft was launched on September 14, 2007 from the Tanegashima Space Center TNSC, and inserted into lunar polar orbit on October 4. After deployment of two expandable antenna for radar sounder and mast for magnetic field measurement, and checking performance of scientific instruments, science observations were carried out for twenty one months of nominal and extended mission periods. On June 11, 2009 the main orbiter impacted on the lunar surface of 65.5S/80.4E, crater rim of Gill-B, and its mission was terminated. The Kaguya team continues to archive data amounting to ten terabytes to release to public and studying the lunar science theme previously allocated in the beginning of the mission[1,2].

Science Instruments: Scientific instruments onboard Kaguya and their abbreviations are summarized in Table 1. Their detailed specifications are referred in Ref.2. The instruments are categorized into six purposes and plural ones are complementally employed using their merits. The XRS and the CPS received critical radiation damages on sensors resulting in failure to get useful data. Other instruments were very healthy and succeed to acquire lunar data with high quality and quantity never collected so far.

Table 1. Science Instruments and Abbreviations

X-ray Spectrometer	XRS
Gamma-ray Spectrometer	GRS
Charged Particle Spectrometer	CPS
Multi-band Imager	MI
Spectral Profiler	SP
Terrain Camera	TC
Lunar Radar Sounder	LRS
Lunar Altimeter	LALT
Relay Satellite Transponder	RSAT
VLBI Radio Source	VRAD
Lunar Magnetometer	LMAG
Plasma Angle Composition Experiment	PACE
Radio Source	RS
Upper Atmosphere Imager	UPI
High Difinition Television System	HDTV

Science Targets: Lunar studies have advanced with the integration of scientific data from various categories. The targets of science of the Moon are as follows:

- Chemical constituents of the Moon
- Interior structure of the Moon
- Dichotomy of nearside and farside of the Moon
- Differentiation in the magma ocean
- Origin of the lunar magnetic field
- Lunar tectonics.

These science targets will be integrated to study the origin and evolution of the Moon.

Targets of sciences on the Moon and from the Moon are established by observations of solar wind by PACE and terrestrial plasmasphere by UPI.

Science Summary; The Kaguya science team has archived the Kaguya data and has made them available to the public[3] through JAXA/ISAS's science data providing system DARTS (http://darts.isas.jaxa.jp); the team is involved in various studies in which the data are used. Although data analysis and science study are ongoing, the major scientific achievements to date are summarized as follows:

1) Identification of ubiquitous pure anorthosite in outcrops of central peaks of large craters by MI and SP. 2) Identification of olivine on the crater rim of large crater basins by SP. 3) Discovery of multiple reflectors of radio waves under large mares and ocean in the nearside by LRS. 4) Use of RSAT for confirmation of free-air gravity anomaly in the whole Moon and identification of farside anomalies that are different from nearside mass concentration anomalies. 5) Confirmation of lunar global topography by LALT. 6) Re-estimation of crustal thickness by Kaguya data of gravity and topography. 7) Re-estimation of the formation ages of nearside and farside mares by crater counting using high resolution images of TC. 8) Confirmation of magnetic anomalies and mini magnetosphere by LMAG and PACE. 9) Reconfirmation of global distribution of radio-active elements K, U and Th by GRS. 10) Discovery of SW proton reflection from the lunar surface, SW entry into lunar wake, and interaction with the Moon by PACE. 11) Confirmation of the polar illumination rate by LALT topographic data. 12) Remarkable improvement of gravitational field of the Moon by RSAT farside and VRAD precise measurements.

The Kaguya mission followed the Clementine and Lunar Prospector science- oriented precursor missions, and has played a significant role as a frontier mission. The Chinese orbiters Chang'E-1 and -2, the Indian orbiter Chandrayaan-1, and the US LRO/LCROSS mission dedicated to landing site investigation for human exploration were sent to the Moon after the Kaguya launch. Cross-referencing of the data acquired by these missions and international collaborative studies are indispensable in advancing the science of the Moon, on the Moon, and from the Moon.

References: [1] Kato, M., Sasaki, S., and Takizawa, Y. (2008) *Adv. Space Res.* **42**, 294-300. [2] Kato, M., Sasaki, S., and Takizawa, Y, Space Sci. Rev.**154** (2010) 3-19. [3] Hoshino, H. et al. (2010) Space Sci. Rev. **154** (2010) 317-342.

LUNAR RADIATION ENVIRONMENT. A. Keating[1,2] and P.Goncalves[2], [1]European Space Agency, TEC-QEC, Keplerlaan 1, 2200AG Noordwijk, The Netherlands, keating@lip.pt ; [2]LIP-Laboratory of Instrumentation and Experimental Particle Physics, Av Elias Garcia, 1000-149 Lisbon Portugal, patricia@lip.pt.

Introduction: Radiation at the moon and planetary surfaces is dominated by four distinct populations: low energy Solar Wind Particles (SWPs), high energy Galactic Cosmic Rays (GCRs), sporadic high energy particles released during Solar Energetic Proton (SEP) events and secondary (albedo) radiation. For planetary surfaces the expected fluxes of primary particles, for isotropic distributions of incident particles, are decreased by 50%, since they are shielded below the horizon. On the other hand SEP and GCR particles impacting on the planetary surfaces interact with nuclei in the regolith and surface materials and secondary radiation is produced via processes including neutron capture, inelastic scattering and high energy spallation. The products of these reactions can include neutrons, gamma rays and various nuclear fragments. Given the higher energies attained by GCR, these induce most of the secondary particle production in planetary environments. The precise composition and spectra of secondary emission is a function of the energy of the incident particles and the properties of the local regolith but the dominant products are neutrons. An important factor conditioning the neutron albedo radiation from planetary surfaces is the presence of water in the soils in sufficient quantity to absorb a significant amount of the neutron albedo. Tab 1, describes the contribution of the different radiation sources for the radiation environment on the Moon.

Radiation source	Moon
GCR Protons, heavier elements	reach surface
GCR Secondaries mostly neutrons	In soil (upward)
SEP	Reach surface
SEP Secondaries	In soil (upward) – but less important that GCR induced, given low SEP energy
Low Energy Solar Wind Particles	reach surface

Tab. 1 - Contribution of the different radiation sources for the radiation environment on the Moon

Lunar missions suffer from the exposure to the various sources of radiation listed above, both during the cruise phase and for the case of landings on the Lunar surface[1-4]. Fig. 1 depicts Medium energy neutron counts showing the two polar dips which indicate water ice.

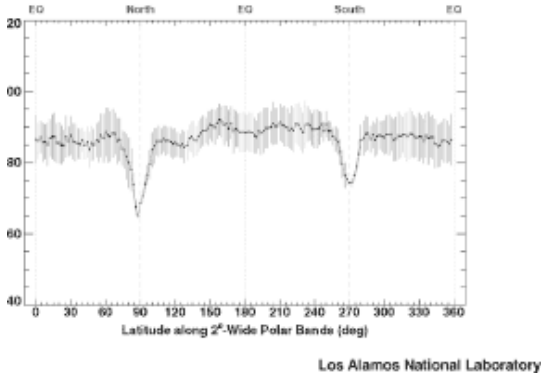

Fig. 1- Medium energy neutron counts (LP data) showing the two polar dips which indicate water ice[5]

A Lunar Lander mission would be specially suited to perform measurements of the radiation environment on the surface of the moon, enabling to assess the radiation exposure risks not only for manned missions, but also for the systems, components and materials of spacecraft and of future Lunar facilities. Such knowledge would enable to perform further validations of the Lunar environment models and would be fundamental for establishing radiation hazard mitigation strategies.

References:

[1] J.H. Adams, M. Bhattacharya, Z.W. Lin, G. Pendleton, J.W. Watts, The ionizing radiation environment on the moon. Adv. Space Res. 40, 338–341 (2007)

[2] R.K. Tripathi, J.W. Wilson, F.F. Badavi, G. De Angelis, A characterization of the moon radiation environment for radiation analysis, Advances in Space Research 37 (2006) 1749–1758

[3] Clowdsley, M.S., De Angelis, G., Badavi, F.F., et al. Surface environments for exploration, in: El-Genk, M. (Ed.), Proceedings of the SpacTechnology and Application International Forum (STAIF-2003) 'Expanding the Frontiers of Science', AIP Conference Proceedings, New York, pp. 1034–1045, 2003

[4]G. De Angelis, F.F.Badavi, J.M. Clem, S.R. Blattnig, M.S. Clowdsley, J.E. Nealy, R.K. Tripathi, and J.W. Wilsond Modeling of the Lunar Radiation Environment, Nuclear Physics B (Proc. Suppl.) 166 (2007) 169–183

[5]Lunar Prospector web site: http://lunar.arc.nasa.gov/results/neures.htm

COMPOSITIONAL MAPPING OF THE LUNAR SURFACE WITH A DUST DETECTOR. S. Kempf[1,2], M. Horanyi[1,2], Z. Sternovsky[1,2], R. Srama[3], and E. Grün[1], ([1]LASP and Department of Physics, U. of Colorado at Boulder, USA; [2]Colorado Center for Lunar Dust and Atmospheric Studies, U. of Colorado, Boulder, USA; [3]Institute of Space Systems, University of Stuttgart, Stuttgart, Germany).

Introduction: The moon is wrapped into a dust envelope produced by hypervelocity impacts of micrometeoroids or interstellar grains. A more or less constant flux of fast projectiles strikes the lunar surface, produces secondary material and a fraction of it leaves the surface forming the dust envelope. The ejecta particles populating the dust envelop carry precious information about the composition of lunar surface, the properties of the regolith, as well as about the impactor flux itself. Furthermore, measurements of the dynamic properties of the ejectas provide a deep insight into the lunar dust production mechanism.

Upcomming exploration of the Lunar dust environment: In 2013, the Lunar Dust EXperiment (LDEX) on the LADEE spacecraft will measure the spatial distribution and grain sizes of the lunar dust exosphere [1]. LDEX is an impact ionization detector, capable of measuring the mass of dust grains in excess of 1.7×10^{-16} kg (radius $r\gtrsim0.3$ μm), in a 50 km altitude periapsis orbit about the Moon. Furthermore, the detector will for the first time verify the presence of nano-sized dust lofted over the terminator regions by plasma effects. However, the LDEX dust detector lacks the ability to characterize the composition of the lunar dust fines.

Lunar dust detector with chemical analysis capability: So far, the methods used to analyse the surfaces of airless bodies are IR and gamma-ray spectroscopy. Compositional mapping is based on the fact that such bodies are always wrapped in a dust exophere produced by high velocity impacts of meteoroids. A dust detector with chemical analysis capability in orbit around the body is able to map the surface composition by determining the composition of the surface ejecta [2, 3]. The major advantage of this technique is that the in-situ analysis of the surface material is very sensitive and is capable to determine even trace amounts of chemical species. Here we will introduce a lightweight linear impact mass spectrometer capable to characterise the composition of the surface ejecta and which is sensitive enough to verify the presence of water ice on the Lunar surface.

References:

[1] Horanyi et al., COSPAR 2010, 38, p. 478. [2] Kempf et al. (2009), *European Planetary Science Congress*, pp. 472–473. [3] Postberg et al. (2011) *Planet. Space Sci., 59,* 1815-1825.

Analysis of Crater Lara and Immediate Neighborhood as Potential Science Landing Targets. S. Khan[1]
[1]Team Synergy Moon, sean_con@gmx.de

Introduction: The proposed Landing site of the mission of the GLXP team Team Synergy Moon is the Taurus Littorw Region, investigated during the Apollo 17 mission. In this study, we investigate the potential of the region as a possible landing target.

The Taurus Littrow region is a valley located in the Taurus Mountain range, and is ornamented by a number of craters and rilles. The mountain range is formed on Mare Serenitatis , near the connection to Mare Tranquilitatis. The Taurus system is a ring of mountains, in a southern direction from the Littrow Crater, which is a heavily worn impact crater. The whole system is located in Lunar nearside.

Geology: The Apollo 17 mission returned sampled from that area, improving our understnading about the region, in addition to telescope based observation.

Formation. Radioactive dating of of the samples indicate the edge of the mountains, as well as Serenitatis to be 3.8 to 3.9 Billion years. The impact Breccia found in the surface indicate a imapct origin of the system. [1]

Surface Properties. Apollo 17 EVA discovered the presence of orange glass beads, which indicates the presence of Extrusive Volcanic activities. However, the albedo of the material is relatively low, despite the age. [1]

In the southern uplands, the surface is composed of lighter colored magma.

Formations. Besides the mountain ring system consisting of Northen Massif, Bowen Apollo, and Southern Massif, the region contains, among other things, the crater Lara, and the rille Scarpe.

Potential Science Objectives: The fact that the location was chosen as the Apollo 17 landing site already suggests the potential of it as a science landing site. Besides, since we already have a wealth of data from apollo, the prospect of revisiting the site is worth investigating. The GLXP mission of Team Synergy Moon involves traversing the lunar surface using robotic rover and possibly micro-rovers. The Mission profile will probably not extend 10 kilometers in range from landing point. We assume the location of the Apollo 17 Lunar Descent Module (A17 LDM) as the point of reference (PR)

The regional map. The Taurus Littorw valley is not circular, elongated along an axis pointing towards Serenitatis. [1] The southern exits are partially blocked by subsequent crater formations, the principle exit being the one to the west, also partially blocked by low mountains. The Orbital Gravity Data suggests the presense of multiple underlaying basins. [1]

General slope. The immediate idea at this point is finding the large scale sturcture and anomalies of the system, which however, does not fall in the scope of TSM mission. Other more specialized missions (e.g. Grail) are intended for this purpose already.

Dynamics. The crater Lara appears to be a young crater, as the A17 EVA station 3 sample indicates (around 100 million years) [1], The lava drapes over a scrape, possibly a fault. Since tectonic activity in moon does not occur, the driving force behind such fault formation may well be thermal deformation of crust. The thermal activity on the surface can be observed using static sensors inserted into ground.

The Mare basin deposit consists of particles with mean radius 40µm, consisting volcanic glass [1]. On lunar surface, transport of microparticles is well known [2] [3]. The target valley is a almost closed system with a exit to a vast low laying basin. It is possible to monitor the dust transport in the closed system relatively well by monitoring the exits. The exits lie within the reachable range of a rover. Static sensors / microrobots dropped from a rover can perform the task of monitoring the exits.

The final topic of interest is erosion. There exits very young Tracks left by A17 EVA, and photographed by Lunar Reconnaissance Orbiter Camera, from the camera (and from theoretical models) considerable erosion is not to expect. The massif foothills consists of masswasteing deposits [1], which are rather young as well. However, since these targets lie within rovers reach, investigation of erosion may be undertaken.

Conclusion: There exists possibilities of science return with limited resource and instruments as assumed by the mission profile of Team Synergy Moon. As the team continues to investigate, further possibilities and possible targets continue to appear.

References:

[1] Wolfe E. W. et al. (1981, digital version 2004) The Geologic Investigation of the Taurus-Littrow Valley: Apollo 17 Landing Site, Apollo 17 Lunar Surface Journal, GSPP 1080. [2] Garrick-Bethell I. et al. (2011) Icarus 212 480–492 [3] Sternovsky Z and Robertson S. (2002) JGR, 107, NO. E11, 5105, doi:10.1029/2002JE001897

ORIENTED SYMPLECTIC INCLUSIONS IN LUNAR OLIVINE: AN EVIDENCE FOR H_2O IN LUNAR MAGMAS?

N.R. Khisina[1], R. Wirth[2], R. Abart[3], D. Rhede[2] and W. Heinrich[2], [1]Vernadsky Institute of Geochemistry and Analytical Chemistry of RAS, Kosygin st 19, Moscow 119991 Russia, khisina@gmail.com, [2]Helmholtz Centre Potsdam, GFZ German Research Centre for Geosciences, Telegrafenberg, D-14473 Potsdam, Germany, [3]University of Vienna, Althanstrasse 14, UZA 2, 2B325, A-1090 Wien, Austria

Introduction: Oriented Cr,Ca-rich symplectitic inclusions in lunar olivines are known as diopside-chromite vermicular intergrowths in interiors of olivine grains [1, 2]. Firstly Cr,Ca-symplectites have been studied in lunar olivines from lunar rocks delivered by Apollo missions [1, 2]. Later, oriented symplectitic inclusions consisting of Ca-clinopyroxene and magnetite/Al-spinel were observed in terrestrial olivine [3]. The available optical, EMPA and TEM data published during the last ten years show that spinel-pyroxene symplectites are rather typical for olivine from martian meteorites [4-6]. The origin of the spinel-pyroxene symplectites is still debated. More than 30 years ago oriented lamellae very enriched in Ca and Cr have been found in Mg-rich olivine grains probably associated with a cumulate rock later disintegrated under impact from lunar regolith delivered by the soviet Luna-24 lunar mission. Here we report the results of FE-EMPA and FFIB/TEM study of one of these olivine grains and discuss a possible mechanism of symplectite formation by a dehydrogenation-oxidation reaction.

Results: The lamellae consist of worm-like intergrowth of $FeCr_2O_4$ chromite (Chr) and $CaMgSiO_4$ diopside (Di), with a Chr:Di molar ratio as 1:2, and display the following orientation relationship: $(100)_{Ol}$ // $(111)_{Chr}$ // $(100)_{Di}$; $[010]_{Ol}$ // $[211]_{Chr}$ // $[001]_{Di}$;; $[001]_{Ol}$ // $[011]_{Chr}$ // $[010]_{Di}$. The lamella/olivine interface is parallel to (100) olivine. The linear extension and the orientation relationship between the symplectic inclusions and olivine matrix might suggest that they have been nucleated on OH-bearing deformation defects in the olivine host. Concentration profile measurements for Ca and Cr as well as local mass balance calculations led to conclusion that symplectic inclusions have been formed by a solid state reaction in olivine without adding of Ca and Cr from the outside of olivine. Symplectite formation was a diffusion-controlled process and proceeded by cation exchange between olivine host and growing symplectic inclusion such as Ca+Cr (olivine) ↔ 2Mg (lamellae) exchange and $Cr^{2+} \rightarrow Cr^{3+}$ oxidation process. Symplectic lamellae have been formed by a replacement of olivine for the two-phase assemblage without a change in volume.
The chromite-diopside intergrowth attained a "cellular" microstructure formed by a single-stage process implying that (a) the exsolution of the calcium-chromium rich lamellae from the olivine and (b) phase separation at the symplectitic reaction front were contemporaneous. The time scales estimated from the calcium diffusion profile indicate a short lived thermal event affected the oxidation.

Discussion: The symplectites in olivine from lunar, terrestrial and martian rocks are very similar with respect to their morphology, texture, crystallographic orientation in the olivine host and phase constituents. These features are, however, inconsistent with the well known features of "dry" olivine oxidation. Our data suggest that the oxidation during symplectite formation process was carried out by a dehydrogenation of OH-bearing symplectite precursor such as hydrous olivine $MgH_2SiO_4 \cdot 3(MgFe)_2SiO_4$:

$$Cr^{2+} + 2OH^-_{(structure)} = Cr^{3+} + 1/2H_{2(gas)} + O^{2-}_{(structure)}.$$

The dehydrogenation-oxidation model of symplectite formation is valid for terrestrial and martian olivine as far as (i) terrestrial and martian olivine contain up to several hundred ppm (10) and (ii) hydrous olivine lamellae suggested as a precursor for symplectite were observed in terrestrial mantle olivine [7]. How much reliable would be the dehydrogenation-oxidation model for symplectite in lunar sample? A presence of water in the lunar mantle is now provided by the data on H_2O content up to 70 ppm H_2O in lunar green picritic glasses [8-9], OH content detected in lunar apatite [10, 11] and the recent data on OH measured as 20-35 ppm H_2O in lunar olivine associated with the late-stage KREEP-rich mesostases in lunar Apollo basalts [12]. The dehydrogenation of olivine, if this would be a case of symplectite appearance in lunar olivine understudy, might suggest that lunar olivine of high deep origin would contain some water (OH^-), and this would give additional argument for a presence of water on the Moon.

References: [1] Gooley R. et al. (1974) *GCA, 38*, 1329-1339. [2] Bell P.M. et al. (1975) *Proc. LPS VI*, 231-248. [3] Moseley D. (1984) *Am. Miner., 69*, 139-153. [4] Greshake A. et al. (1998) *LPS XXIX*, Abstract #1069. [5] Greshake A. et al. (2000) *LPS XXXI*, Abstract #1150. [6] Mikouchi T. et al. (2000) *Meteoritics & Planet. Sci., 35*, 937-942. [7] Khisina N.R. and Wirth R. (2002) *PCM, 29*, 98-111. [8] Saal A.E. et al. (2008) *Nature, 454*, 192-195. [9] Hauri E.H. et al. (2009) *LPS XXXX*, Abstract #2344. [10] Boyce J.W. et al. (2010) *Nature*, 466, 466-469.[11] McCubbin F.M. et al. (2010) *Am. Miner., 95*, 1142-1150. [12] Liu Y. et al. (2012) *LPS XXXXIII*, Abstract #1866.

Ultra-Long-Wavelength Radio Observations on the moon; probing the Lunar environment and the cosmological Dark Ages .

M. Klein Wolt[1,2] and A. Aminaei[1] and J.R. Schrader[3] and P. Zarka[4] and A. J. Boonstra[5] and H. Falcke[1]

[1]Department of Astrophysics Radboud University Nijmegen, Heijendaalseweg 135, 6525 AJ Nijmegen, The Netherlands, M.KleinWolt@astro.ru.nl [2]Science & Technology, Olof Palmestraat 14, 2616 LR Delft, The Netherlands, [3]Netherlands Institute for Space Research (SRON), Sorbonnelaan 2, 3584 CA, Utrecht, The Netherlands, [4]Laboratoire d'Études Spatiales et d'Instrumentation en Astrophysique (LESIA) Observatoire de Paris, Bât. 16, bureau 213 5, Place Jules Janssen 92195 Meudon Cedex France, [5]Netherlands Institute for Radio Astronomy (Astron), Oude Hoogeveensedijk 4, 7991 PD, Dwingeloo, The Netherlands

We present the scientific and technical aspects of Lunar radio observations using a tripole antenna and a sensitive digital receiver in a broad spectral range (10 kHz-100MHz). This experiment, referred to as the Lunar Radio eXplorer (LRX), is a dedicated instrument selected for the ESA Lunar Lander mission (expected launch in 2018) as part of the Lunar Dust Environment and Plasma Package (L-DEPP). A Phase-A study on the LRX is currently performed under the supervision of the Radboud University Nijmegen. The Lunar Lander will essentially be a path-finder mission and address key questions to prepare for future lunar human and science missions. In addition, the LRX will open up the virtually last unexplored frequency regime below 10 MHz which is inaccessible from the earth due to a cut-off in the earth's atmosphere and the interference from man-made radio signals. We present an overview of the key science cases the LRX will address: the study of Lunar environment, Solar and Planetary science and radio astronomy and cosmology.

In the study of the Lunar environment, the LRX antenna will be used to monitor the lunar exosphere and its interaction with the Earths magnetosphere and solar wind plasma. The moon is known for having a weak ionosphere that can be mapped in detail through in-situ measurements of known and stable radio sources as they move across the lunar sky and set below the horizon. One of the LRX's major goals, and essential for future scientific exploration of the moon, will be to measure the lunar radio background noise and to determine the limit of lunar radio observations. In addition, acting as a ground penetrating radar, the LRX would also provide significant information about the moon surface and subsurfaces.

The LRX antenna on the moon will be able to address a multitude of radio astronomy science cases. For example, radio bursts from ultra-high energy cosmic rays hitting the moon surface will be studied, essentially using the moon as cosmic ray detector, and the LRX aims to study solar flares and CMEs as well as observations of radio emission from planets such as Jupiter and Saturn. This will provide present-day information on the current rotation periods of these planets. More importantly, placing the antenna at the Lunar south (north) pole would not only allow to observe the dark and sun-lit side of the moon simultaneously, but also provide shielding from man-made RFI while the earth is below the horizon. This will provide the stable observing conditions that are required to look for the global radio signal from atomic hydrogen produced in the early phase of the universe, before the first stars and galaxies formed; i.e. to measure the signal from the so-called "dark ages".

Finally, based on our experience with the LOFAR (Low Frequency Array) and AERA (Auger Engineering Radio Array) experiments, we review the technical details of the LRX experiment towards the future plan for a large lunar radio interferometer.

AN ACTIVE X-RAY SPECTROMETER (AXS) FOR THE ROVER OF THE JAPANESE SELENE-2 MISSION FOR CHEMICAL IN-SITU CHARACTERIZATION OF LUNAR MATERIAL. G. Klingelhöfer[1], J. Brückner[2], K. J. Kim[3], Y. Amano[4], B. Bernhardt[5], M. Blumers[1], W. V. Boynton[6], T. J. Fagan[4], D. Hamara[6], N. Hasebe[4], G. Ju[7], P. Lechner[8], L. F. Lim[9], T. Ohta[4], E. Shibamura[10], and R. D. Starr[9, 11]; [1]Inst. of Inorg. Chem. & Analyt. Chemistry, J. Gutenberg-Univ., Staudinger Weg 9, 55128 Mainz, Germany, klingel@mail.uni-mainz.de, [2]Max-Planck-Inst. F. Chemistry, Mainz, Germany, [3]Geol. Res. Div., Korea Inst. of Geosci. & Min. Res., Daejeon, South Korea, [4]Res. Inst. Sci. & Engin., Waseda University, Japan, [5]Von Hoerner & Sulger GmbH, Schwetzingen, Germany, [6]Lunar & Planet. Lab., Univ. of Arizona, USA, [7]Korea Aerospace Research Institute, [8]PN Sensor GmbH, Munich, Germany, [9]NASA GSFC, MD, USA, [10]Saitama Prefectural University, Japan, [11]Catholic Univ. of America, DC, USA.

Introduction: The Japanese space agency JAXA is planning and preparing their next mission to the moon, SELENE-2. It will be the first lunar landing mission of Japan involving an orbiter, a lander, and a rover. The launch is scheduled for the years of about 2015/2016. One of the main mission objectives is the geophysical and geochemical characterization of the lunar surface and subsurface [1, 2]. A specific instrument should provide data for the chemical in-situ characterization of the lunar surface material

One candidate for the scientific payload of the SELENE-2 rover is an Active X-ray Spectrometer (AXS) for in-situ x-ray fluorescence measurements. The AXS can measure the major elements: Mg, Al, Si, Ca, Ti, and Fe, the minor elements, Na, K, P, S, Cl, Cr, and Mn and the trace element Ni, all depending on their concentrations. The AXS is a "derivative" of the Alpha Particle X-Ray spectrometer (APXS). The APXS was and is part of the scientific payload of several planetary missions like lunar NASA landers Surveyor 5 to 7 (precursor instrument) [3], NASA Mars Pathfinder Rover Sojourner [4], two NASA Mars Exploration Rovers (MER) [5], and ESA Rosetta comet lander Philae [6].

Principle: The basic modification of the AXS compared to the APXS is the replacement of the radioactive sources by a switchable x-ray generator. The APXS takes advantage of the alpha decay of Cm-244 and the subsequent x-ray emission of the daughter product Pu-240. Hence, we have two modes: particle induced x-ray emission (PIXE) for low-Z elements (low atomic weight) and x-ray fluorescence (XRF) for high-Z elements. The used excitation source requires careful handling of the APXS with respect to radiation safety requirements. Avoiding radioactivity and using a switchable x-ray generator can support applications, where only temporary radiation protection is preferred.

For the AXS, the x-ray generator uses a pyroelectric crystal to generate energetic electrons that produce x-rays in a target material [7]. This permits the sole application of XRF compared to the two modes of APXS. Measurements of low-Z elements need a vacuum set-up of the AXS and longer integration times compared to APXS. The newly conceived AXS is a very small, light-weight, and low-power instrument, which is favorable for space applications on planetary bodies with no or a thin atmosphere.

The design of the AXS will also take advantage of improvements in x-ray detector technology. Newly developed large-area silicon drift detectors (SDD) with superior energy resolution compared to previous detectors provide shorter integration times and higher sensitivity.

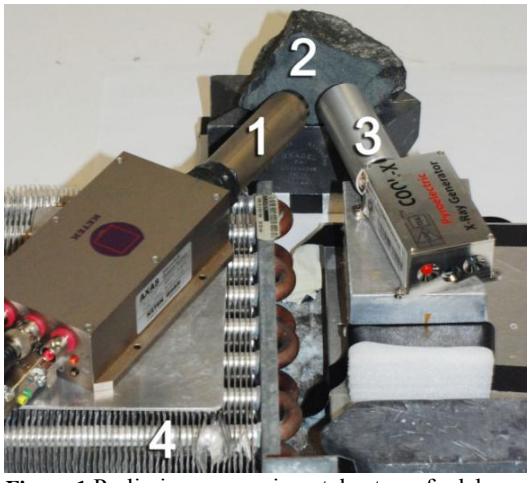

Figure 1 Preliminary experimental setup of a laboratory AXS: measurement of a polished basalt rock surface, see label {2}. X-ray detector {1} with electronics box (KETEC, Germany) sitting on a cooling device {4}; x-ray generator {3} (type COOL-X, Amptek, USA) with an aluminum collimator tube.

Experimental Setup: To evaluate the AXS concept a preliminary set-up was used and in-situ measurements were performed. X-rays, which are produced by a generator, are bombarding the surface layer of a rock. Characteristic x-rays are excited in the surface layer. A fraction of these x-rays are emitted by the rock surface and counted by a large-area SDD detector (Fig. 1).

An analytical x-ray acquisition System AXAS-SDD (KETEC, Germany) with a detector surface area of 100 mm^2, a beryllium window, and a zircon collimator was used. The electronic box of the x-ray detector was cooled by a recirculating cooler, additionally, to obtain a sufficiently good energy resolution. The data acquisition was done with a small multi-channel analyzer (Amptek Pocket MCA8000A).

A miniature x-ray generator with pyroelectric crystal (COOL-X, Amptek Inc.) provided 8-keV x-rays. The crystal consists of lithiumtantalate ($LiTaO_3$) to generate electrons that produce x-rays in the target foil (copper). The hermetically sealed package has a 250-µm thin beryllium window, which allows the x-rays to be transmitted [8]. When the pyroelectric crystal is thermally cycled, x-rays of specific energy are produced: During heating Cu-K_α (8.05 keV), Cu-K_β (8.90 keV), and during cooling Ta-L_α (8.14 keV), Ta-L_β (9.02 keV), and Ta-L_γ (10.90 keV) plus a Bremsstrahlung continuum. To avoid stray radiation from the x-ray generator a collimating aluminum tube was applied to the housing of the COOL-X element.

Generators Thermal Cycles: When activated the x-ray generator was thermally cycled between a heating phase (duration ca. 18 sec) and cooling phase (ca. 86 sec). The x-ray flux varied throughout the cycle and peaked during the last seconds of each phase [9]. Figure 2 exhibits the x-ray emission spectra during the thermal cyles.

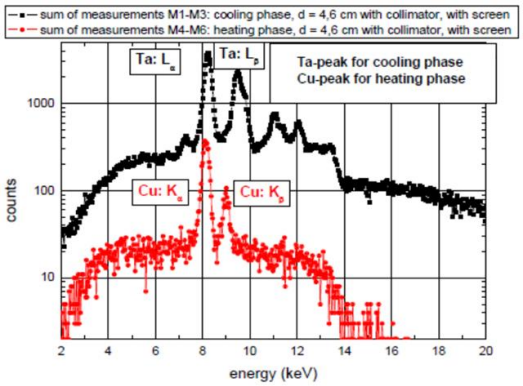

Figure 2 X-ray emission spectrum of x-ray generator (Amptek COOL-X) during heating (black) and cooling phase (red).

Analysis of Lunar Material: The determination of the chemical composition of regolith and rocks at the selected landing site is of great importance to the exploration of the Moon. It reveals the geochemistry of the landing site, characterizes its geology, and provides the necessary data to compare it with previous and future landing sites.

As the Moon is an atmosphere-less body, the mechanical and thermal effects (melting) of impacts by micro-meteorites, small and large asteroids can be studied. The combined effects of irradiation by light and bombardment by cosmic-ray particles produce "space weathering" of rock surfaces [10]. Provided a grinding tool is onboard the rover, the comparison of natural and abraded surfaces by the analysis of the AXS can provide profound insight in the effect of space weathering.

Previously collected samples from the Moon are thought to come from the crust. None seems to have come from the mantle. Spectroscopic data from the Japanese lunar satellite Kaguya show evidence that the mantle of the Moon may be exposed on certain areas of its surface [11]. The AXS analysis can support the search for the rare mantle material.

Summary: The new concept of the AXS comprises a switchable x-ray generator based on a special pyroelectric effect and a high-resolution SDD detector. Such a device provides an on-demand x-ray-spectrometer, small in volume, light-weight, and low power. A space-proof version is in planning for the Japanese lunar SELENE-2 rover mission. Depending on the mission scenario either quick in-situ elemental checks or long integrations for in-depth analysis can be performed.

Outlook: A switchable, compact x-ray spectrometer would be very useful for human exploration of the lunar surface. Whenever, an elemental analysis of resource material is needed, the AXS could serve as a handy, everyday device. Demonstration of the capabilities of the AXS could be done during the upcoming ESA Lunar Lander mission, as no geochemical data exist of the surface material of the lunar South Pole.

References: [1] Matsumoto K. et al. (2008) *ILEWG/LEAG/SRR-2008*. [2] Tanaka S. et al. (2008) NLSI Lunar Sic. Conf. #2044. [3] Patterson J. H. et al. (1969), *J. Geophys. Res., 74*, (25), 6120. [4] Rieder R. et al. (1997) *J. Geophys. Res.*, 102 (E2), 4027. [5] Rieder R. et al. (2003) *J. Geophys. Res., 108* (E12), 8066. [6] Klingelhöfer G. et al. (2007) *Space Sci. Rev., 128*, 383. [7] Brownridge J. and Raboy S. (1999) *J. Appl. Phys., 86*, 640. [8] Amptek COOL-X specifications. [9] Schmanke D. et al. (2012) *43rd LPSC*, #2831. [10] Lucey P. et al. (2006) *Rev. Min. Geochem., 60*, 83. [11] Yamamoto S. et al. (2010) *Nature Geosci., 3*, 533.

DEEP MOONQUAKE FOCAL MECHANISMS: RECOVERY AND IMPLICATIONS. M. Knapmeyer[1] and R. C. Weber[2], [1]DLR Institute of Planetary Research (martin.knapmeyer@dlr.de), [2]NASA Marshall Space Flight Center (renee.c.weber@nasa.gov).

Introduction: A defining characteristic of deep moonquakes is their tendency to occur with monthly (tidal) periodicity, prompting previous studies to infer that they are related to the buildup and release of tidal stress within the Moon [1–5]. In studies of tidal forcing, a key constraint is the focal mechanism: the fault parameters (strike, dip, and slip angles) describing the type of failure moonquakes represent. Knowledge of the failure plane allows us to resolve the tidal stress into its shear and normal components and evaluate the state of stress at the observed moonquake occurrence times.

The quality of the lunar seismic data and the limited source/receiver geometries of the Apollo seismic network prohibit the determination of deep moonquake fault parameters using first-motion polarities, as is typically done in terrestrial seismology [6]. Without being able to resolve tidal stress into shear and normal components on a known failure plane, we can examine only gross qualities of the tidal stress tensor (such as principal stress directions or maximum shear stress) with respect to moonquake occurrence, so we cannot fully address the role of tidal stress in moonquake generation (using, for example, a Coulomb stress criterion as has been used to describe some types of earthquake failure [7]).

Approach: We will examine the extent to which shear (S) and compression (P) wave amplitude ratios can constrain moonquake fault geometry by determining whether, for a given cluster, there exists a focal mechanism that can produce a radiation pattern consistent with the amplitudes measured by the Apollo instruments (Figure 1). Amplitudes are read in the ray coordinate frame, directly from seismograms for which the P and S arrivals are clearly identifiable on all long-period channels of the four Apollo stations. We apply an empirical station correction to account for site effects at the four Apollo stations, and the differences between P- and S-wave attenuation in the lunar interior [8].

Instead of focusing on the best fitting solution only, we formulate the inverse problem using a falsification criterion: all source orientations that do not reproduce the observed S/P amplitude ratios within an error margin derived from the uncertainty of the amplitude readings are rejected. All others are accepted as possible solutions. The inversion is carried out using an exhaustive grid search on a regular grid with predefined step size, encompassing all possible combinations of strike

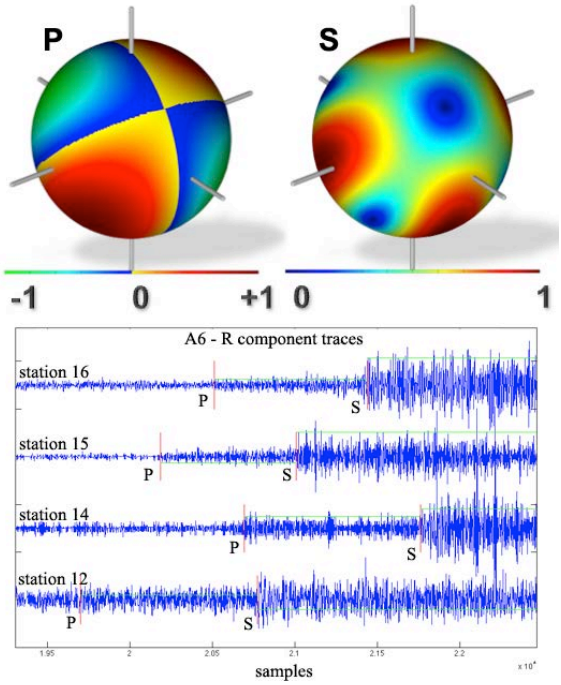

Figure 1: *For an arbitrary focal mechanism, the P and S amplitudes from a known moonquake cluster are projected on a sphere (top) and can be estimated at the Apollo station locations. These estimates are compared to the amplitudes read from actual Apollo seismograms (bottom).*

(clockwise from North), dip (relative to horizontal), and slip (direction of fault motion between strike and dip). To assess the sensitivity of the inversion to the uncertainty of the lunar interior structure, we will carry out repeated inversions with different velocity structures [e.g. 9-11].

Our data set consists of a total of 106 events from 25 deep moonquake clusters [12]. The largest contribution of 37 events originates from the most active cluster, A001, while other clusters are represented by one to nine events.

Results: Since the definition of a cluster implies that all events share the same source orientation, a comparison of the inversion results of all events from one cluster reduces ambiguities in the inversion. Using the method outlined above, we were able to reduce the fault plane parameter space for a given cluster on average by half (Figure 2).

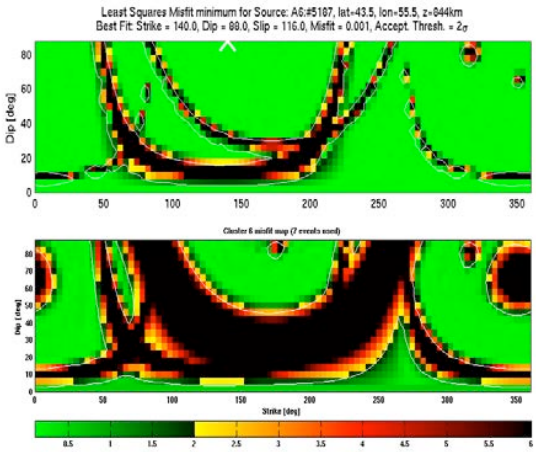

Figure 2: *Least-squares misfit between observed and calculated amplitudes on a regular grid of fault orientations (dip ranging from 0 – 90° and strike ranging from 0 – 360°) for a single A6 event (top) and the result averaged over all useable events from the A6 source region (bottom). The accepted regions (green) are selected by highlighting fault orientations which predict amplitudes within 2σ of the measured values.*

Once we obtain a suite of fault parameters for a given source, we can attempt to further constrain the focal mechanism by including analyses of tidal stresses. In an earlier study [13], we used the occurrence times of individual events from a given moonquake cluster to evaluate the tidal shear and normal stresses similarly resolved onto failure planes described by a regular grid of fault parameters. We imposed the failure criterion that a linear combination of shear and normal stress that best approximated a constant value indicated the most likely fault orientation. Combining the results of this grid search with our amplitude analysis further constrains the most likely focal mechanism for our set of clusters (Figure 3).

Future work: With the best-fit focal mechanism in hand for each cluster, we can create synthetic seismograms using a reflectivity approach [14], for comparison with the Apollo seismograms. This will possibly allow us to predict the times and amplitudes of reflected seismic phases from the Moon's deep layers, placing further constrains on the structure of the lunar interior.

References: [1] Toksöz et al., *Science* **196**, 979–981, 1977. [2] Lammlein, PEPI **14**, 224–273, 1977. [3] Cheng & Toksöz, *JGR* **83**, 845–853, 1978. [4] Goulty, *PEPI* **19**, 52–58, 1979. [5] Minshull & Goulty, *PEPI* **52**, 41–55, 1988. [6] Nakamura, *Proc. Lunar Planet Sci. Conf. 9th*, 3589–3607, 1978. [7] Smith & Sandwell, *JGR* **108**, 10.1029/2002JB002136, 2003 [8] Hardebeck and Shearer, *BSSA* **93**, 2434–2444, 2003. [9] Nakamura, *JRG* **88**, 677–686, 1983. [10] Lognonne et al., *EPSL* **211**, 27–44, 2003. [11] Khan and Mosegaard, *JGR* **107**, 10.1029/2001JE001658, 2002. [12] Nakamura, *JGR* **110**, 10.1029/2004JE002332, 2005. [13] Weber et al., *JGR* **114**, 10.1029/2008JE003286, 2009. [14] Friederich & Dalkolmo, *GJI* **122**, 365–374, 1995.

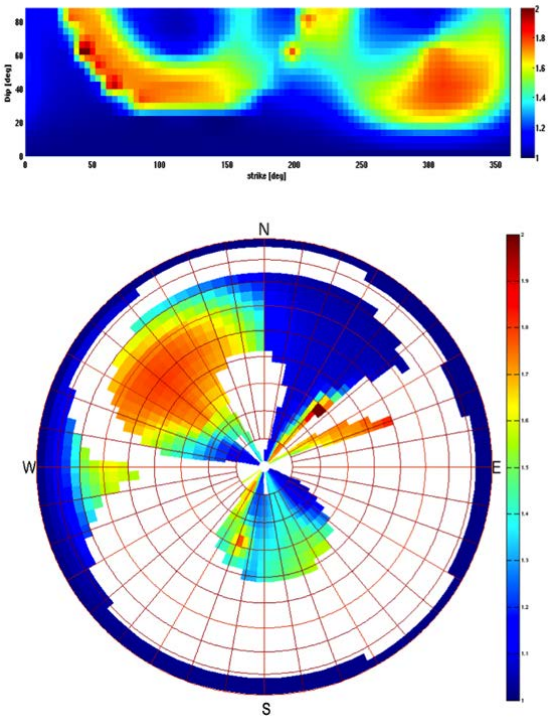

Figure 3: ***(top)*** *Variance in the tidal stress at A6 moonquake times mapped onto all possible fault plane orientations. The values are scaled so that the minimum variance is equal to one and the colorbar covers the range from minimum to twice the minimum (alternatively, the "half-width"). (**bottom**) Polar projection of the focal sphere showing mechanisms that are compatible with both the amplitude ratio and tidal stress constraints. Dip ranges from 90° (vertical) in the center to 0° (horizontal) at the rim. The white regions are those mechanisms that are excluded by the amplitude analysis (outside the 2σ accepted regions) and the color bar again shows the scaled variance values. Blue regions represent the best fitting fault orientations. In this case, A6 is likely represented either by a horizontal plane, or a plane that strikes ~25°E of North and dips ~40° from horizontal.*

LUNAR CRATERS WITH EXTERIOR IMPACT MELT DEPOSITS. S. D. Koeber[1], B. W. Denevi[2], J. D. Stopar[1], and M. S. Robinson[1], [1]Arizona State University, Tempe, AZ 85287; [2] John Hopkins University Applied Physics Laboratory, Laurel, MD 20723. Correspondence: skoeber@ser.asu.edu

Introduction: Fresh lunar craters displaying impact melt deposits (Fig. 1) provide superlative examples of pristine melt compared to Earth and Mars, which are subjected to post-formation erosion and weathering [1]. Therefore, lunar impact melt deposit morphology, volume, and distribution provides a better understanding of the impact process.

Fifty craters of Copernican age displaying external impact melt deposits were identified using Lunar Reconnaissance Orbiter - Narrow Angle Camera (NAC) (pixel scale: ~50 cm) and Wide Angle Camera (WAC) (pixel scale: ~100 m) images [2]. The crater diameters range from 2 km to 40 km and are globally distributed (Fig. 2).

Observations of Deposits: Exterior impact melt deposits were determined on the basis of their spatial association with craters, surface cooling fractures, and morphologic flow features such as lobate flows and channels [3]. The presence of boulders along the flow margins also assisted in identifying flows. Exterior melt flows usually begin near the crater rim flowing downslope away from the crater (Fig. 1).

Forty-seven of the fifty craters identified display exterior flows (the other three only had ponded deposits). The flows display a diverse range of morphologic features such as flow channels, compression ridges, multiple streamlines, superposed flow lobes, and smooth surfaces, and surface cooling fractures. Commonly, melt deposits of thin veneers and ponds of melt are observed.

Locating craters with exterior melt: Mapping the location of craters displaying exterior impact melt on a global WAC color map revealed that most of the craters exhibited bright rays in bands 1 (320 nm), 3 (415 nm), and 7 (690 nm) and on the optical maturity parameter (OMAT) map, created from multispectral Clementine images [4].

Results and Discussion: We found no correlation between the volume of exterior melt and the crater diameter [5]. Eighteen craters formed on the rim or inside of a preexisting larger crater. For example, a small crater (D=9km; 102.46°W, 13.31°S) located on the rim of Lowell crater (D=66km; 103.42°W, 12.9°S) produced an exterior flow 13.5 km in length. Perhaps, impacting into or on a rim of a larger crater facilitated interior melt being expelled during the impact process. The exterior melt deposits from these eighteen craters may indicate that melt distribution is not simply controlled by impact trajectory [6].

Efforts to locate craters exhibiting bright rays in the WAC color map with and without exterior impact melt deposits are ongoing. Currently, craters displaying exterior impact melt deposits are more numerous in the highlands regions versus the mare. Perhaps, craters with exterior impact melt deposits are easier to identify in highland regions because the contrast between the craters rays and surrounding material appears brighter in the global WAC color map. Craters with exterior impact melt located in the mare do exist.

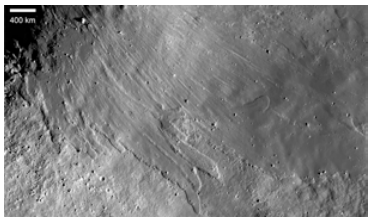

Figure 1: Exterior flows on outer rim of 13.5 km diameter crater, NAC M114925405

References: [1] Bray V. J. et al. (2010) *Geophys. Res., 37,* L21202. [2] Robinson, M., S. et al. *Space Sci. Rev.* 150, pp. 81-124, (2010). [3] Howard, K. A. et al. (1975) *J. Res. U.S. Geol. Surv.,* 3, pp.237-251. [4] Grier. A. J. (2001) *Geophys. Res.,* 106, pp. 32,847-32,862. [5] Denevi B.W. et al. (2012) *Icarus* (in review). [6] Bray V. J. et al. (2010) *LPS.XXXXI, Abstract#2371.*

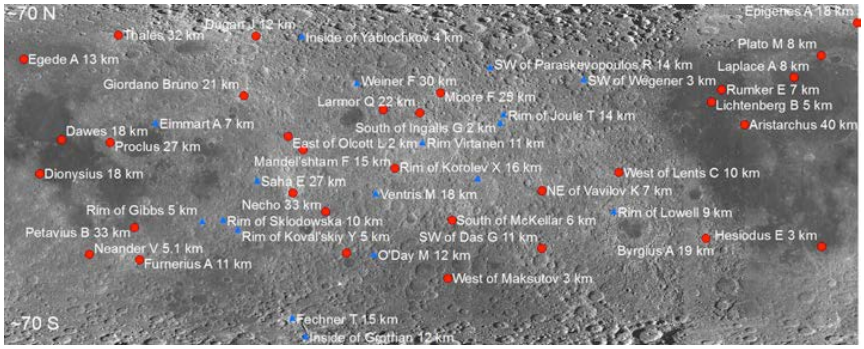

Figure 2: A WAC image denoting the fifty craters names and diameter sizes with exterior impact melt deposits. Blue triangles denote craters impacted on the rim or inside of a preexisting crater, the red circle denote the other craters.

USING THE MOON TO EXPLORE THE EVOLUTION OF THE ENTIRE SOLAR SYSTEM. D. A. Kring[1,2], [1]Center for Lunar Science and Exploration, USRA-LPI, 3600 Bay Area Blvd., Houston, TX 77058 (kring@lpi.usra.edu), [2]NASA Lunar Science Institute.

Introduction: The Moon is the best and most accessible place in the solar system to explore the fundamental principles of our origin. Among the most interesting concepts to be explored are the lunar cataclysm [e.g., 1-4] and impact-origin of life [e.g., 5,6] hypotheses (Fig. 1). The former suggests there was a severe period of bombardment several hundred million years after solar system formation, while the latter suggests that event is entangled with the origin and early evolution of life. Both concepts have implications for the rest of the solar system and planetary systems elsewhere.

The canonical lunar cataclysm is defined by ~15 basin-forming impacts that occurred during the Nectarian Period and Early Imbrian Epoch. Nearly 30 additional basins were produced during the pre-Nectarian on the Moon, but they were not sampled during Apollo. It is not yet clear if they were produced during the same cataclysmic surge of cratering events (Fig. 1); they are, thus, targets of future lunar missions [e.g., 7].

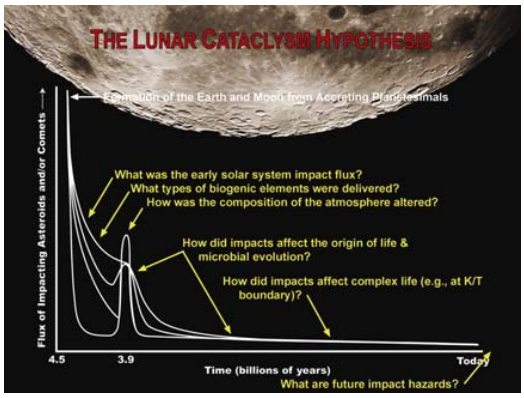

Fig. 1. Schematic diagram illustrating the potential flux of impactors to the Earth-Moon system and the questions that remain [6]. The greatest uncertainty, which is represented by several curves, lies in events between the formation of the Moon and the end of the basin-forming epoch ~3.8×10^9 yrs ago.

Sources of Impactors: Siderophile signatures of impactors are entrained in lunar impact melts and suggest the impactors were dominated by asteroids rather than comets ([8] and references therein). Recent analyses of Apollo 17 specimens [9,10] indicate a pre-Serenitatis impactor (>3.89 Ga) had affinities with ordinary chondrites, the Serenitatis impactor (~3.89 Ga) was a chondritic asteroid (but unlike any meteorites in our current collection from the asteroid belt), and that a post-Serenitatis (~3.75 Ga) impactor had affinities to enstatite chondrites or, marginally, ordinary chondrites. Interestingly, these data imply there were more ordinary chondrite planetesimals than those currently represented by the LL, L, and H groups of meteorites.

A completely independent assessment of the impactors can be derived from the size distribution of the lunar basins and smaller craters in the ancient cratered highlands of the Moon [11]. That analysis suggests asteroids dominated the flux and that the asteroid belt was sampled in a size-independent fashion. That latter observation implies resonances swept through the asteroid belt and that Jupiter's orbit shifted.

That same method was recently used to probe the crater size distribution further ([12]). That study discovered a shift in the size distribution of craters that implies a shift in the impact velocities of impacting asteroids. At some point between the formation of the South Pole-Aitken and Nectaris basins, impact velocities may have roughly doubled. This is consistent with a shift in the orbits of Jupiter and other outer solar system planets that has previously been implied [e.g., 13, 11] for the production of the Nectarian and Early Imbrian basins. It also implies, however, that some of the pre-Nectarian basins, including the South Pole-Aitken Basin, were produced independently through other collisional mechanisms.

A third independent assessment of the source of impactors can be derived from the lunar regolith. A recent study of Apollo 16 samples discovered the first mineralogic and lithologic remnants of projectiles during the latter phase of the basin-forming epoch ([14]]. Those results are also consistent with an asteroidal source for the impactors. Indeed, the relics are dominated by fragments of chondrules similar to those in chondritic meteorites.

The Inner Solar System Cataclysm: In addition to the lunar-derived insights above, evidence about early solar system bombardment is also being gleaned from asteroids, some of which confirms interpretations of lunar data and some of which provides other insights.

A recent analysis of impact melt breccias from the H-chondrite parent body indicate significant collisional activity 4.0-3.5 Ga [15], followed by a sharp decline in the flux of impacting debris. Impact ages in that same 4.0-3.5 Ga interval have been seen in a large number of samples from the HED parent body and in a smaller number of samples from the L and LL chondrite parent bodies [e.g., 16-18]. In addition, a major collision involving the IIE parent body occurred ~3.7-3.6 Ga [e.g., 18]. The large number of impact events among asteroids 4.0-3.5 Ga implies

the lunar cataclysm is really an inner solar system cataclysm [8].

In almost all cases, the samples being measured come from simple craters and the ejecta around simple craters. Thus, most of the impact events represented by the chondritic samples are smaller than those that produced the lunar basins. (A collision among planetesimals with the same energy needed to produce a lunar basin would completely disrupt the planetesimals.) Thus, collisional age spectra dominated by simple cratering events on chondritic bodies may be similar, but not identical, to the age spectra of basin-size events on the Moon. This is likely one reason chondritic ages range from 4.0-3.5 Ga, while the basin-forming epoch on the Moon ended 3.8-3.7 Ga. It also seems likely that the dynamical situation (asteroids are closer to the source of the impactors than the Moon) may produce subtle differences in the age spectra among asteroids and the Moon.

Flux of Asteroids to the Moon: If the lunar cataclysm occurred within 20 to 200 Myr, then the annualized mass flux to the Moon was ~3.5×10^{13} to ~3.5×10^{14} g/yr for a Nectarian and Early Imbrian event [19]. If the pre-Nectarian basins were also involved, then the annualized mass flux was 2.3×10^{14} to 2.3×10^{15} g/yr. Asteroids contain significant quantities of H_2O and other biogenic elements [20]. Recent data [9,10,14] imply chondritic projectiles, some with affinities to enstatite, ordinary, and carbonaceous chondrites. That implies ~6×10^{19} to ~1×10^{21} g of H_2O were delivered to the Moon during the Nectarian and Early Imbrian, and an additional ~3×10^{20} to ~7×10^{21} g of H_2O during the pre-Nectarian, although some of that mass would have been lost from the Moon as high-velocity ejecta. The mass flux to the Earth was at least 13 times greater. While substantial, the canonical cataclysm could not have delivered the entire inventory of Earth's water. A large fraction of Earth's water was delivered during the earlier accretional phase.

Preparing for Future Missions: It has become increasingly clear that the Moon is the best and most accessible source of information about early solar system processes. Geochemical and geological data are revealing how the Earth-Moon system evolved, how other inner solar system planets were affected by collisional events, and how the orbits of outer solar system planets shifted.

To further test the lunar cataclysm hypothesis and its implications for the entire solar system, we need to recover new impact samples from the lunar surface that have a well-understood geologic context and have properties suitable for complementary analyses of their ages and siderophile content. A series of landing site studies are underway and a leading candidate that has emerged is Schrödinger Basin [21]. This is the second youngest basin on the Moon. It also resides within the oldest and largest basin on the Moon, South Pole-Aitken Basin. Thus, samples within Schrödinger Basin may provide the ages of both basins and effectively bracket the duration of the entire basin-forming epoch.

If the age of samples of the South Pole-Aitken Basin indicate it is part of the lunar cataclysm, then that implies there were ~3 times more basin-forming impacts than in the canonical model. On the other hand, if the age of South Pole-Aitken Basin is much older (consistent with [12]), then pre-Nectarian basins with successively younger relative ages need to be sampled to determine when the cataclysm began. Candidate targets include the Nubium Basin (middle pre-Nectarian), Smythii Basin (slightly younger), and the Apollo Basin (the last of the pre-Nectarian Basins and also within the South Pole-Aitken Basin). The timing of the latter third of the basin-forming epoch and the nature of the projectiles involved will require better documented samples of impact melt or impact-metamorphosed samples from Nectaris, Serenitatis, Crisium, Schrödinger, and Orientale.

These types of sample return missions are best conducted with well-trained crew [22], although they can also be addressed with integrated human and robotic systems [23], including ops from the Earth-Moon L2 position [24].

References: [1] Turner G. et al. (1973) *Proc. Lunar Sci. Conf., 4th*, 1889–1914. [2] Tera F. et al. (1974) *EPSL, 22*, 1–21. [3] Cohen B. A. et al. (2000) *Science, 290*, 1754–1756. [4] Cohen B. A. et al. (2005) *Meteoritics & Planet. Sci., 40,* 755–777. [5] Kring D. A. (2000) *GSA Today*, *10(8)*, 1–7. [6] Kring D. A. (2003) *Astrobiology*, *3*, 133–152. [7] National Research Council (2007) *The Scientific Context for Exploration of the Moon*. [8] Kring D. A. and Cohen B. A. (2002) *JGR, 107*, doi: 10.1029/2001JE001529. [9] Puchtel I. S. et al. (2008) *GCA, 72*, 3022–3042. [10] Galenas M. G. et al. (2011) *LPS XXXXII,* Abstract #1413. [11] Strom R. G. et al. (2005) *Science, 309*, 1847–1850. [12] Marchi S. et al. (2012) *EPSL, 325-326,* 27–38. [13] Gomes R. et al. (2005) *Nature, 435*, 466. [14] Joy K. (2011) *LPS XXXXII,* Abstract #2103. [15] Swindle T. D. (2009) *Meteoritics & Planet. Sci., 44,* 747–762. [16] Bogard D. D. (1995) *Meteoritics, 30,* 244–268. [17] Swindle T. D. and Kring D. A. (2008) *Early Solar System Bombardment Workshop*, Abstract #3004. [18] Bogard D. D. (2011) *Chemie der Erde, 71*, 207–226. [19] Kring D. A. (2008) *NLSI Lunar Science Conference*, Abstract #2140. [20] Kring D. A. et al. (1996) *EPSL, 140*, 201–212. [21] O'Sullivan K. M. et al. (2011) *GSA Special Paper, 477*, 117–128. [22] Kring D. A. (2010) *Nördlingen Ries Crater Workshop*, Abstract #7036. [23] Kring D. A. and Rademacher J. (2007) *LPS XXXVIII*, Abstract #1595. [24] Norris S. C. (2011) *Human Exploration Community Workshop on the GER*.

ITALY AND THE GOOGLE LUNAR X PRIZE COMPETITION: THE AMALIA PROJECT STATE OF THE ART. A.E.Finzi[1], M.R.Lavagna[1], G.Capuano[2], G.Chiocchia[3], L.Schirone[4], P.Messidoro[5], A.Sacchetti[6]
[1]Politecnico di Milano (Via La Masa 34, 20156 Milano lavagna@aero.polimi.it), [2] Technosystem Development SpA (Pozzuoli, Napoli-Italia), [3]Politecnico di Torino (Cso Duca degli Abruzzi 24, Torino), [4]Università "La Sapienza"(Ple Aldo Moro 5, Roma) , [5]Thales Alenia Space –Italia (Strada Antica di Collegno 253, Torino), [6] OHB-CGS SpA (Via Gallarate 150, 20151 Milano)

Introduction: The XPrize Foundation together with Google, proposed in 2007 a very hard challenge to privates: to send a robot on the Moon surface within December 31, 2015 which is asked to cover at least 500 m reporting through both videos and images its walk on the surface. The whole mission must be privately funded at 90%.

Currently twenty-six official teams are competing for the prize, coming from all over the world both national and international.

Italy is answering to this call with the AMALIA mission (Ascensio Machinae Ad Lunam Italica Arte): the team, completely Italian, is composed of major Italian Aerospace Engineering Universities and national space industries: Politecnico di Milano, Politecnico di Torino, Università di Roma "La Sapienza", Università di Napoli "Federico II", for the academic participation and Thales Alenia Space-Italia SpA, Compagnia Generale per lo Spazio SpA and TechnoSystem Development SpA for the industrial side.

These entities have already an impressive track record in contributing to and developing space exploration and planetary missions for the Italian and the European Space Agencies.

The AMALIA mission baseline sees a lander vehicle releasing a wheeled rover on the Moon surface; the lander vehicle plays the cargo role for the Earth-Moon transfer too.

The vehicles design is driven by the mass minimization to limit launch costs: therefore miniaturized hardware components are exploited; redundancy is applied only where strictly needed to contain the mission critics.

The launcher is almost selected, having in mind the technical constraints satisfaction together with the costs limitation goals.

Chemical propulsion currently represents the design solution to control both the transfer trajectory and the landing phase with a specific thrusting profile to cope with fuel mass minimization and thruster throttling limitations. The selected landing site is equatorial.

A four wheels rover with specifically designed suspensions will be released on the surface; navigation will be accomplished by merging classic and visual odometry supported by three cameras mounted on a mast; those cameras will also supply data required to answer challenge official requirements. On board autonomy is limited, leaving the authority to the Ground. A prototype of the vehicle is currently under development.

Deeper details on the Team Italia technical work so far, sponsorship recruitment and AMALIA mission peculiarities are offered.

THE MOON AS A SCIENCE PLATFORM. J. Lazio[1,2] for the Lunar University Network for Astrophysics Research, [1]Jet Propulsion Laboratory, California Institute of Technology, 4800 Oak Grove Dr., M/S 138-308, Pasadena, CA 91109 USA; Joseph.Lazio@jpl.nasa.gov, [2]NASA Lunar Science Institute, NASA/Ames Research Center.

Introduction: For over four decades, the Moon has been recognized as a unique platform for conducting science observations. In the past decade, the focus on the Moon has sharpened considerably, motivated in part by a series of astrophysical discoveries and improved understandings.

Prime Science: In this presentation, I shall summarize some of the key science that exploits the surface of the Moon; similar considerations have been explored by Jester & Falcke [1].

Probing Cosmic Dawn and the Dark Ages. What were the first objects to light up the Universe? Following the formation of the cosmic microwave background (CMB), the Universe entered a largely neutral state. Ground- and space-based telescopes now make it clear, however, that within 1 billion years after the Big Bang, stellar assemblies likely to serve as the precursors to today's galaxies had assembled. Determining the nature of and epoch of formation for the first luminous sources will be the focus of multi-wavelength observations for this decade, and potentially beyond. The dominant baryonic component of the neutral intergalactic medium (IGM), and the raw material for star formation, is hydrogen. The temperature evolution of the IGM, in response to the first luminous objects, can be tracked via the hyperfine spin-flip (21 cm) transition of neutral hydrogen. There is potentially even a signal prior to the formation of the first stars due to the different cooling rates of the IGM and the CMB.

The Universal expansion redshifts the 21 cm line to much longer wavelengths, to a portion of the radio spectrum used extensively by both civil and military transmitters and for which ionospheric absorption becomes important. The far side of the Moon is shielded from terrestrial emissions and represents a unique location in the inner solar system for observing the redshifted 21 cm line during and before Cosmic Dawn. Internationally, a series of concepts for telescopes to exploit the shielded radio zone on and above the far side of the Moon are being developed [2,3].

The Sun and Particle Acceleration. High-energy particle acceleration occurs in diverse astrophysical environments including the Sun and other stars, supernovae, black holes, and quasars. A fundamental problem is in understanding the mechanisms and sites of this acceleration, in particular the roles of shock waves and magnetic reconnection. Within the inner heliosphere—an interval of 1–10 solar radii ($R_\odot$) from the Sun—solar flares and coronal mass ejections (CMEs) are efficient particle accelerators.

Low frequency observations are an excellent remote diagnostic because electrons accelerated by these structures can produce intense radio bursts. The intensities of these bursts make them easy to detect, as well as providing information about the acceleration regions.

Lacking a dense ionosphere, a radio telescope sited on the Moon could observe to much lower frequencies, and therefore much closer to the Earth, than are accessible from the ground [4]. In addition to providing information about particle acceleration in the inner heliosphere, such a telescope could also serve as part of an "early warning system" for humans in spacecraft.

Extrasolar planets. Within the past decade, the census of extrasolar planets has grown from a few to many hundreds. While there are continuing efforts to find more planets, there is also growing interest in characterizing the known planets.

All of the "magnetic" planets in the solar system (Earth, Jupiter, Saturn, Uranus, and Neptune) generate planetary-scale magnetic fields as the result of internal dynamo currents within the planet. The solar wind incident on these planetary magnetospheres is an energy source to the planetary magnetospheres, and the magnetosphere-solar wind interaction produces energetic (keV) electrons that then propagate along magnetic field lines into auroral regions, where electron cyclotron masers are produced. In the case of the Earth, its magnetic field may be partially responsible for its habitability.

A lunar-based radio telescope would be an ideal instrument for searching for magnetically-generated emissions from nearby extrasolar planets. It potentially could observe at frequencies below those accessible from the ground, and, if located on the far side, would be shielded from intense terrestrial emissions.

Acknowledgements: The LUNAR consortium is funded by the NASA Lunar Science Institute to investigate concepts for astrophysical observatories on the Moon. Part of this research was carried out at the Jet Propulsion Laboratory, California Institute of Technology, under a contract with the National Aeronautics and Space Administration.

References:

[1] Jester S. and Falcke H. (2009) New Astron. Rev., 53, 1–26. [2] Burns J. O. et al. (2012) *Adv. Space Res.*, *49*, 433–450. [3] Mimoun D. et al. (2011) *Exp. Astron.*, in press. [4] Lazio T. J. W. et al. (2011) Adv. Space Res., 48, 1942–1957.

IS IT INTERSTELLAR MATTER ON THE MOON? V.V. Shevchenko, Y. Lu. Sternberg State Astronomical Institute, Lomonosov Moscow State University, Moscow, 119992, Russia (vladislav_shevch@mail.ru)

Introduction: Neutron flux measurements of the Moon's south pole region from the Lunar Exploration Neutron Detector (LEND) on the *Lunar Reconnaissance Orbiter (LRO)* spacecraft were used for hydrogen mapping of the lunar south pole area. The final value corresponds to a water (as ice) content of ~4% by weight [1]. Independent estimates of the water content were receved by *LCROSS*/*Centaur* mission for region of impact site in crater Cabeus [2]. The maximum total water vapor and water ice within the instrument field of view was 155 kilograms. Given the estimated total excavated mass of regolith that reached sunlight, and hence was observable, the concentration of water ice in the regolith at the *LCROSS*/*Centaur* impact site is estimated to be 5.6 % by mass. Authors of work [2] noted: "In addition to water, spectral bands of a number of other volatile compounds were observed, including light hydrocarbons, sulfur-bearing species, and carbon dioxide (H_2S/H_2O, NH_3/H_2O, SO_2/H_2O, and CO/H_2O). Of interest is the indication from this preliminary analyses that some volatiles other than water are considerably more abundant (some by orders of magnitude) than the ratios found in comets, in the interstellar medium, or predicted from gas-gas reactions in the protoplanetary disk".

Where comet matter from: The nature of diffuse albedo anomalies on the lunar surface that look like "swirls" is one of most interesting mystery in current lunar studies. There are two main classes of hypothesises of the swirl origin: formation of the swirls in the regions antipodal to large impact basins (1), and formation of the swirls in result of cometary impacts (2). The first hypothesis proposes that swirls represent regions whose higher albedo have been preserved due to deflection of the solar wind ion bombardment by strong crustal fields. The most likely magnetization mechanism was proposed by Hood [3], in which the ionized vapor cloud produced in a hypervelocity basin-forming impact expands around the Moon and concentrates the pre-existing ambient magnetic field at the basin antipode. For example, the data obtained by the *Lunar Prospector* showed that swirl features are associated with magnetic anomalies and they lie on regions antipodal to the Imbrium, Serenitatis, and Crisium basins. However, any swirl markings are absent on regions antipodal to Humorum, Hertzprung, Mare Moscovience and Humboldtianum basins in spate of similar age and diameter of them. There are some isolated anomalies at Reiner Gamma, Rima Sirsalis, Descartes, and Airy [4]. Isolated anomalies within the Nectarian-aged Moscoviense basins have a weak magnetization. Fig. 1 shows fragments of swirl in Mare Moscovience region. This image is the Clementine color composite mosaic comprised of three of the five Clementine UVVIS multispectral bands (415nm, 750nm, 1000nm) [5].

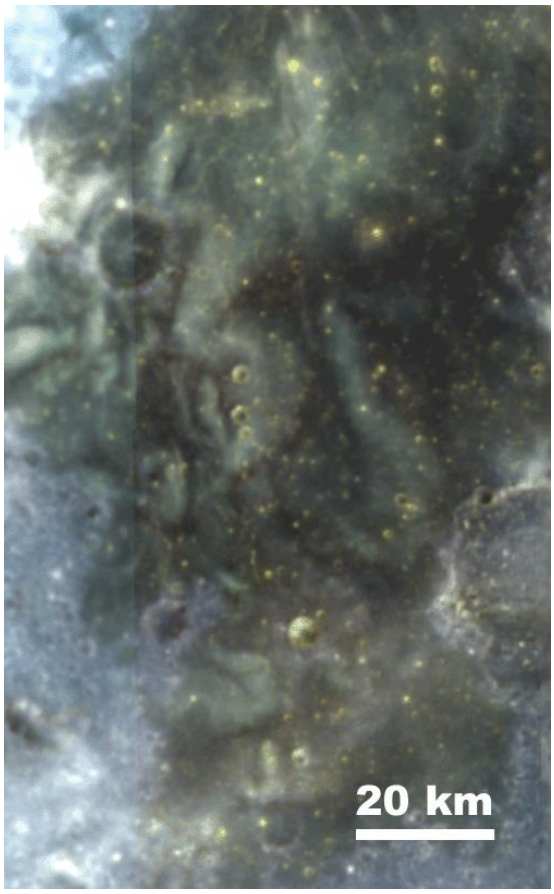

Fig 1

The second hypothesis does not suggest correlation between the swirl locations and the regions antipodal to basins. Gold and Soter suggested a mechanism of a local magnetic field origin on the Moon in result of cometary impact [6]. The local shock produced by collision of the main mass of a comet nucleus with the Moon will indeed occur just when the ambient solar wind fields have been strongly enhanced, as the large partially ionized cometary coma is compressed against the lunar surface. Schultz and Srnka [7], Bell and Hawke [8], Shevchenko [9], Pinet at al. [10] considered that swirl patterns on the lunar surface could be related to the imprint of recent cometary impacts. In order to investigate the features of the swirl distribution along lunar surface there were identified and mapped swirl locations within regions where they were observed. The areas of all identified swirl fragments were measured and statis-

tical analysis of the distribution was performed (Fig 2).

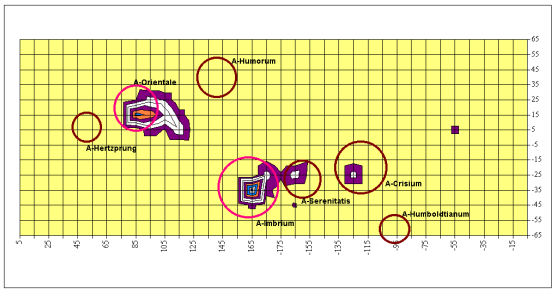

Fig 2

The more strong correlation is observed for youngest large basins: Orientale and Imbrium. The swirls are absent in region antipodal to youngest (more younger than Imbrium basin) but small (320 km) Schrodinger basin. The Reiner Gamma formation is most obvious example of that the correlation mentioned above is not statistically strong and do not exclude the swirl origin associated with external reason, such as cometary impact. So, the most convincing model for the swirls origin seems to be lunar surface contact with the gas/dust coma of comets passing by or falling onto the Moon [10]. It's possible to show that the most probable scenario for origin of the water ice polar deposits is the falls of young comets onto the Moon during comet showers. Characterized by their low average density and large nuclei as well as in the considerable mass of the matter they brought even several falls of such young comets could provide for the revealed ice concentration on the lunar pole.

Comet matter on the Moon: In particular the comet Hale-Bopp has become a sufficiently convincing confirmation of the existence of the bodies with gigantic nuclei. Thus its parameters can serve as the first interaction data for the quantitative assessment of the lunar ice with a comet origin. The lowest limit of the nucleus substance density can be less than 0.1 g/cm^3 if this comet nucleus rotation period is 11.47 hours [11]. The fall of a body with a density of 0.1 g/cm^3 and an impact velocity of 40 km/s (these parameters are similar to those of the Hale-Bopp comet) results in a collision with the same physical parameters as a solid body with a density of 1.0 g/cm^3 and a collision velocity of 10.5 km/s does [12]. According to the other model the initial temperature of the vapour collision formed cloud will be about 6300^{o}C. The most probable thermal velocity of the atoms will be about 5.5 km/s. This means that the dissipating part of the cloud mass will be 0.9 of its total mass taking into account the parabolic velocity for the Moon of 2.4 km/s. Nucleus diameter of the Hale-Bopp comet was estimated to be about 40 km. Consequently after a similar body with a density of 0.1 g/cm^3 falls on the lunar surface a vapour cloud with a mass of about 3.4x10^{18}g is formed. The water melting, surface, and crush-up energies are neglected. According to the above given assessment the mass of the volatile compounds which stay in the lunar environment will be 3.4x10^{17}g. Assuming that these substances, distributed equally above the lunar surface, will further cool and deposit in the regolith upper layer, the assessed mass will be about 10^{10} g per a square kilometer.

Whence the comet came into inner part of Solar System: The Hale-Bopp comet is a similar potential impactor. In that time Szab´o et al. [13] detected comet Hale–Bopp at 30.7 AU, which is the most distant detection of a comet so far. It's position between Kuiper Belt and Oort Cloud. Oort Cloud comets are currently believed to have formed in the Sun's protoplanetary disk and to have been ejected to large heliocentric orbits by the giant planets. Detailed models of this process fail to reproduce all of the available observational constraints, however. In particular, the Oort Cloud appears to be substantially more populous than the models predict. Levison et al. presented numerical simulations that show that the Sun captured comets from other stars while it was in its birth cluster [14]. The results imply that a substantial fraction of the Oort Cloud comets, perhaps exceeding 90%, are from the protoplanetary disks of other stars!

Conclusions: It's know that other stars have circumstellar clouds of dust or icy bodies that may be analogous to the Kuiper Belt in the Solar System. So, we can propose that a particles of a dust may be brought on the Moon by giant comet from other star system!

Acknowledgments: Author is grateful to NASA LEND Science Team, I.G.Mitrofanov, PI, and NASA LCROSS Science Team, Colaprete A., PI. This research is supported by RFBR grant 11-02-90440-Ukr_f_a.

References: [1] Mitrofanov I.G. et al. (2010) *Science, 330*, 483-486. [2] Colaprete A. et al. (2010) *Science, 330*, 463-468. [3] Hood L.L. and Williams C.R. (1989) *LPSC 19*, 99-113. [4] Richmond, N. C. and Hood, L. L. (2008) *JGR, 113*, E02010. [5] http://www.lpi.usra.edu/lunar/tools/clementine. [6] Gold T. and Soter S. (1976) *Planet. and Space Scie. 24*, 45-54. [7] Schultz P. H. and L. J. Srnka (1980) *Nature*, *284*, 22-26. [8] Bell J.F. and Hawke B.R. (1987) *Publ. Astron. Soc. Pac., 99*, 862-867. [9] Shevchenko V.V. (1999) *LPS XXX*, Abstract # 1317. [10] Pinet P.C. et al. (2000) *JGR, 105*, 9457-9475. [11] Meech K.J. (1997) *Preprint IfA-97-38*, 16. [12] O'Keef J.D. and Ahrens T.J. (1982) *JGR, 87*, 6668-6680. [13] Szab´o Gy.M. et al. (2011) *Astron. & Astroph. manuscript no. hb, April 25*. [14] Levison H.F. et al. (2010) *Science. Published Online June 10, 2010*.

CORRELATIONS BETWEEN IRON DISTRIBUTION AND MORPHOLOGICAL EVOLUTION OF MARE MOSCOVIENSE. Lu Yangxiaoyi, Moscow State University, Sternberg Astronomical Institute, Universitetsky pr. 13, 119234, Moscow, Russia, luyangxiaoyi@gmail.com

Introduction: The Moscoviense basin is the most prominent mare basalt filled multi-ring impact formation on the lunar farside highlands. Mare basalt of Mare Moscoviense is divided into a few individual basalt flows. Haruyama et al. reported mare volcanism at the Moscoviense basin until 2.57 Ga [1]. Morota et al. determined the thickness and age of individual basalt units of Mare Moscoviense. In the work it was concluded that the magma production in the upper mantle beneath Mare Moscoviense is from 3 to 10 times lower than that of the nearside mantle [2]. Investigation of spectral anomalies in global data acquired with the Moon Mineralogy Mapper (M3) has revealed a new, unique, and unexpected spinel-rich lithology on the central nearside [3]. Then spinel-rich rock was discovered at the Moscoviense region using spectral image data by Moon Mineralogy Mapper (M3) [4]. However, in work [5] was shown that olivine-rich rocks observed at ring structures of the Moscoviense basin too. Those olivine rich rocks suggested that they are probably upper mantle materials excavated by impact. So, iron-rich surface rocks is a very important indicators of evolution of the Moon.

Topographic data for Moscoviense basin: We used data from the Chang'E-1 satellite that was successfully launched on October 24, 2007 from the Chinese Xichang Satellite Launch Center, and after a one year primary mission and nearly a half year extended mission it impacted the Moon. One of the principal scientific instruments on the board of spacecraft was a laser altimeter (LAM) used to measure the distance between the orbiter and the lunar surface. In result of the Chang'E-1 mission global model of the Moon's topography has been constructed [6]. This model, referenced to a mean radius of 1738 km, has an absolute vertical accuracy of approximately 31 m and a spatial resolution of 0.25^{o} (corresponding to approximately 7.5 km on the lunar surface). Based on the elevation spacing (1.4 km along-track and 7 km across-track), all the elevations were binned and interpolated to form a 0.25°×0.25° grid. According to these data we selected for analysis most low area that characterized height about – 4 km referenced to a sphere with a radius of 1738 km. It was used topographic profile across the Moscoviense basin placed along track of orbit 0256 (along meridian with longitude 149^{o} E) [6]. The spectral images for this area were constracted using the Clementine spacecraft data [7]. Fig. 1 represents spectral image of the Moscoviense basin constracted from 3 spectral units (415 nm, 750 nm and 950 nm).

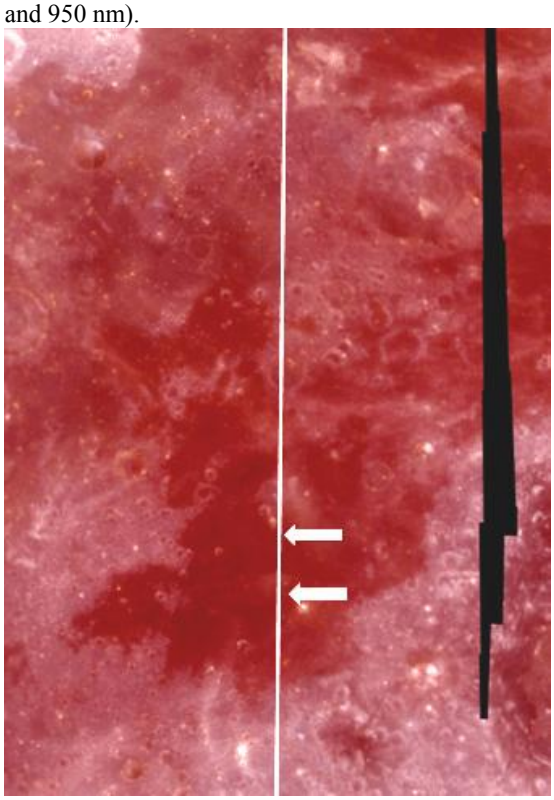

Figure 1. Spectral image of the Southern part of Mare Moscoviense [7]. White line shows track of the orbit 0256 of the Chang'E-1 satellite on the lunar surface. White arrows show area with height about - 4 km referenced to a sphere with a radius of 1738 km.

Spectral analysis of the depression: Using spectral imaging of the lunar surface from the Clementine spacecraft [7], we can obtain the remote evaluation of iron in the surface layer of the area. In this case we have used the method developed by Lucey et al. [8] and successfully applied by Shkuratov et al. [9] and Pinet et al. [10] to the remote analysis of the composition and maturity of the surface layer of the Moon. From spectral measuring (images in 750 nm and 950 nm were used) it follows that FeO content in the surface layer of the depression area increases to 19% and more. Fig. 2 represents diagram of the FeO distribution along track of the orbit 0256 of the Chang'E-1 satellite. The values of R_{750} и R_{950} were measured on the spectral images from the Clementine lunar probe [7]. The value of FeO for regions with height about – 2 km is not more 17 – 18%. Moreover, central part of the depression (lat. 25.6^{o}) characterized height about – 4 km referenced to a

sphere with a radius of 1738 km.

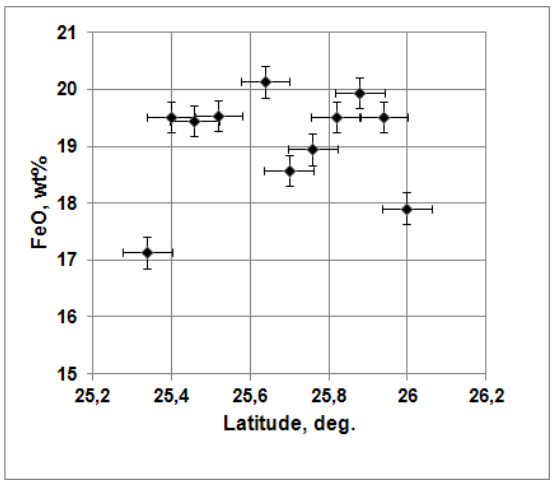

Figure 2. Diagram of the FeO distribution inside depression area. The horizontal axis is lunar latitude, where one degree corresponds to 30.3 km.

Discussion: Recent investigations of the Moscoviense basin show that formation is an very interesting place on the Moon [11]. The Moon Mineralogy Mapper (M3) team identified unusual mineralogical exposures [4]. Other studies of the Moscoviense basin have identified several unusual features of this farside formation. It is one of the few farside formation that has abundant mare deposits. Moreover, number of works are consider the Moscoviense basin as having the thinnest crust on the entire Moon [12]. Morota et al. [13] proposed that thickness equal ~ 600 m is the lower limit of the total thickness of mare basalts in Mare Moscoviense (SELENE (Kaguya) data). They presumed that the total thickness is less than 1 km, because the crater density of the flooded craters is roughly as high as the density of large craters in the highland unit of Moscoviense basin, suggesting that most large post-Moscoviense basin craters survive the subsequent mare flooding. The age of Moscoviense basin is estimated to be ~4.1 Ga. According to the stratigraphy of Neukum & Ivanov [14], this is classified as a Nectarian system, which is consistent with the classification of Wilhelms [15]. Morota et al. [13] consider that oldest unit of mare basalts in Mare Moscoviense is observed in the southern part and have a model age of 3.9 Ga. The mare basalt of this unit is thicker than 100 m. According to cumulative crater size-frequency distributions obtained in [13] the depression area above mentioned is most young basaltic flow which has age of 2.6 Ga. In [13] the depression area is named as the eastern mare unit. Haruyama et al. [1] reported that the layer of mare basalt in this unit is extremely unusual. Its thickness is ~ 40 m only (Fig. 3).

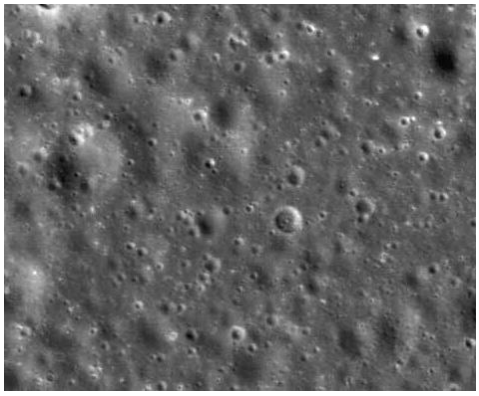

Figure 3. Morphological type of the depression area surface. A least features observed in the image have size 2 – 3 m. LROC image M105901516L [16].

On the other hand, it was proposed model of larger mantle pluge. Kaguya crustal thickness models show that the Mos-coviense basin has an extremely large (both in width and height) mantle plug, larger than other basins of the same type [12]. Moreover, height of the mantle plug of the Moscoviense basin is much higher than that of other basins. The extremely large mantle plug (i.e. extremely large excavation) is therefore probable to explain by upper mantle materials excavated in result of impact. Ishihara et al. [17] propose a double impact formation hypothesis for the Moscoviense basin. This hypothesis easily explains the mantle plug size, the exposure of olivine rich material probably excavated from upper mantle by basin forming impact and other features of the Moscoviense basin. In any case we can consider that we observe iron-rich basalts from upper mantle in area of depression.

References: [1] Haruyama, J. et al. (2009) *Science, 323*, 905–908. [2] Morota, T. et al. (2009) *GRL, 36*, L21202. [3] Pieters et al., *Current Science*, 2009. [4] Pieters, C.M. et al. (2010) *LPS XLI*, #1854. [5] Yamamoto, S. et al. (2010) *Nature Geoscience, 3*, 533-536. [6] Huang, Q. et al. (2010) *LPS XLI*, #1265. [7] LPI Clementine Mapping Project (2011). [8] Lucey P. G. et al. (2000) *JGR, 105*, 20.377–20.386. [9] Shkuratov Yu.G. et al. (1999) *Icarus, 137*, 222–234. [10] Pinet P.C. et al. (2000) *JGR, 105*, (E4), 9457-947. [11] Thaisen K.G. et al. (2011) *LPS XLII*, #2574. [12] Ishihara Y. et al. (2009) *GRL, 36*, L1920. [13] Morota T. et al. (2009) *LPS XL*, #1280. [14] Neukum, G. & Ivanov, B.A. (1994) in *Hazards Due to Comet and Asteroids*, p.359-416. [15] Wilhelms, D.E. (1987) *The geologic history of the Moon, USGS*, 1348pp. [16] http://wms.lroc.asu.edu/lroc. [17] Ishihara Y. et al. (2011) *LPS XLII*, #1124.

SCIENTIFIC INVESTIGATIONS OF FUTURE RUSSIAN LUNAR LANDERS. I. G. Mitrofanov[1] and L. M. Zelenyi[1], [1]Institute for Space Research, Profsojuznaja 84/32, 117997 Moscow, Russia, imitrofa@space.ru.

Scientific goals will be presented for future Russian Lander of Luna-Resource and Luna-Glob missions. Investigations will be described for addressing these goals, and selected scientific instruments will be reviewed, which correspond to these investigations.

LUNAR RESERVOIR OF VARIOUS ELEMENTS BY POROUS FILTER OF REGOLITH SOILS.

Y. Miura,
Yamaguchi University (Yoshida 1677-1, Yamaguchi, 753-8612, Japan), and University of Al. I. Cuza (Dept. of Geology Sci., Boulevard Carol I no. 20 A, 700505-Iaşi, România) , California Institute of Technology (JPL, Pasadena, CA 91109-8099, USA). **E-mail:** yasmiura@yamaguchi-u.ac.jp, moonyas@hotmail.com

Introduction: Big unsolved problem of the lunar interior elements and molecules including light gasses-fluids and heavy rare-earth-elements (REE) is considered to be originated from "stable Earth-type process" (with stable atmosphere and/or sea-water) [1, 2] or from "dynamic impacts sources by meteoroids or planetary collision" [3-8]. However little study on the Moon has been reported clearly on role from surface materials of lunar regolith soils. The main purpose of the paper is to discuss new proposed model of the lunar interior reservoir (as Moon-type natural resources) of various elements and molecules through porous regolith soils on the Moon (possibly for Asteroids and planets of Mercury, Venus and Mars) [7, 8].

Porous regolith soils on the Moon: Hardness for impact extra-lunar materials can be discussed by porosity and density data of the six lunar rocks (four highland and two Mare), various six chondritic meteorites and Apollo lunar regolith soils as follows [1, 7 and 8] (Fig.1 and Table 1).

1) Porosity and density data of lunar regolith soils (high porosity and low density) are completely different with those of the lunar rocks and various meteorites (low porosity and high density), which indicates multiple impact fragmental regolith soils.
2) Drilled core samples of the regolith soils reveal bulk estimated values from 15cm to 60cm [1] with decreased porosity and increased density, though porous regolith soils are still the same.
3) The lunar breccias show the same or higher porosity of various chondritic meteorites, but the same density of common chondrites and achondrites.
4) The lunar highland crystalline rock (15418 anorthosite) is similar with CO carbonaceous chondrite.
5) The lunar Mare basalts reveal the lowest porosity (some similar achondrite) and highest density (similar H and L chondrites).

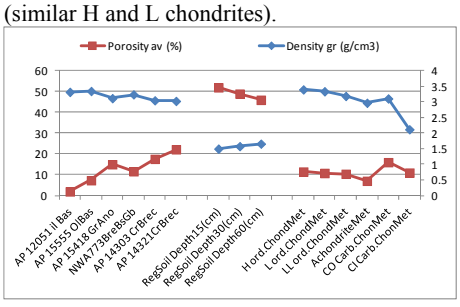

Fig. 1. Porosity and density data of six lunar rocks, six chondritic meteorites and lunar regolith core soils [1].

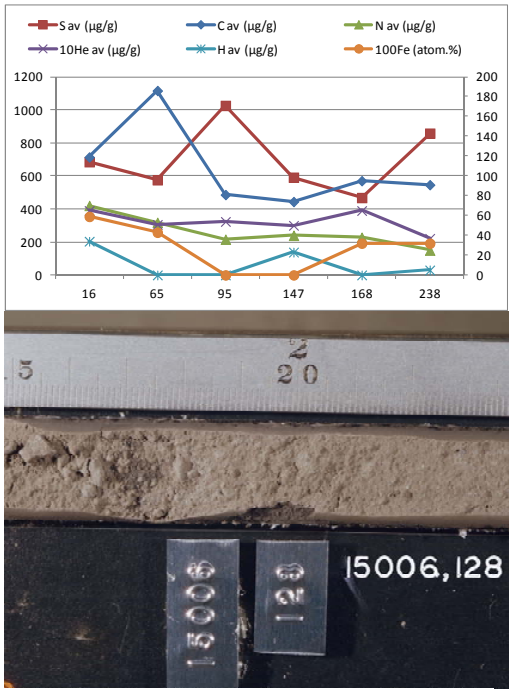

Fig.2. Depth profiles of light elements and Fe contents of the Apollo drilled cores 15001-15006 [1, 9 and 10]. Photo is drilled regolith soils (Fe-bearing pale brown) of 15006,128 sample [1, 10].

Lunar depth profiles of various elements: Depth profiles of the Apollo drilled core samples (15001-15006) are obtained from 16cm to 238cm in depth as follows [1, 9-14] (Fig. 2 and Table 1).

1) All bulk contents of S, C, N, He, H and Fe elements are obtained irregularly to deeper sites
2) Solar wind source of H, He and N elements and meteoritic Fe sources are the richest in shallow sample 16 cm in depth, but molecular elements of C and S (as CO_2 and SO_2 etc.) are the richest in relatively deeper sites of 65cm and 95cm in depth, respectively.
3) Evidence of penetration to deeper sites through porous regolith soils during impacts is proved by two peaks of depth profiles of the six elements with lower second peaks, where heavy elements C, S and Fe are relatively deeper sites of the second rich peaks (168cm to 238cm) which are produced by direct shallow penetration (by smaller extra-lunar collisions), and/or larger mixing on larger impacts on porous regolith with gravitational deposition.

Carbon and Fe contents of the lunar surface: Bulk carbon contents of the Apollo lunar surface samples are discussed by 32 samples of 7Apollo12, 13Apollo15, 5Apollo16 and 7Apollo17 as follows (Fig.3 and Table 1) [7, 9-14]:

1) Carbon contents are largely changed at every Apollo landing sites, but the highest and lowest contents are Apollo 17th and 12th sites, respectively.

2) Iron contents are not directly related with carbon contents, but the lowest content is obtained at the Apollo 16th site which is from the highland rocks.

3) Carbon contents of the surface rocks are not uniform with continuous collisions, but easily decreased (due to airless lunar circumstances).

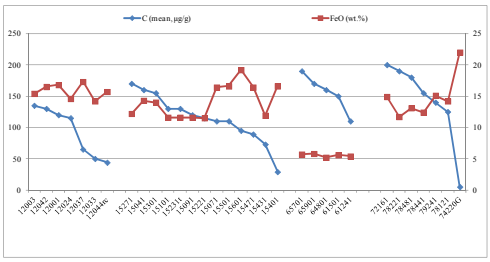

Fig. 3. Carbon and iron contents of 32 Apollo surface samples of Apollo 12th, 15th , 16th and 17th [7, 9-14].

Rare-earth elements of regolith soils: Rare-earth elements (REE) are enriched in lunar regolith soils and breccias compared with Mare basalts [15, 16] (*cf.* Fig.4 and Table 1) as follows.

1) Regarding with REE, Y is rich in regolith soils, but Ce is largely enriched in the impact breccias.

2) Carbon, REE (Y, Ce and Eu) and Ca contents are enriched in the regolith soils and breccias.

3) Carbon contents are related with Eu (and Ca) contents in the lunar impact breccias. This is strongly supported that "lunar crust layering" are not global magma ocean model, but "impact-related layering" [5-7] with increased the REE (including Eu) and Ca (combined with impact-carbon) [15, 16].

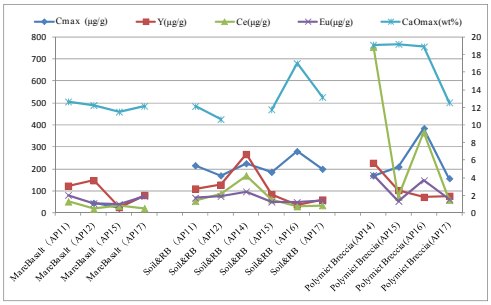

Fig.4. Carbon, the REE (Y, Ce and Eu) and Ca contents of the Apollo Mare basalts, regolith soils and impact breccias [1, 7 and 11-16].

Table 1. Characteristics of the Apollo regolith soils.

1) *Void-rich texture:* The highest porosity50%.
2) *Drilled cores:* Two enriched peaks (C, Fe, S).
3) *Surface samples:* Bulk carbon decreases.
4) *Enriched REE*: Enriched carbon, Ca and REE
5) *Gas filter:* Interior reservoir for gas and fluid .

Regoliths filter to form interior reservoirs: The present results can be applied to interior fluid-gas reservoir of various elements, including carbon-bearing light gasses-fluids with some water molecules in closed interior. This model of "regolith filtering" is clearly useful to airless and waterless Moon (also airless Mercury and Asteroids, and waterless Mars and Venus) in Table 1 [3-7, 17].

Summary: The results are summarized as follows: 1) Big unsolved problem of the lunar interior light elements and molecules including heavy rare-earth-elements (REE) can be explained by "regolith filtering" from "dynamic impacts sources by meteoroids or planetary collision". 2) Lunar regolith soils reveal very high porosity (ca.50%) to transport light gas and molecule during impact collision. 3) The Apollo drilled cores reveals two enriched peaks of relatively heavy C, S and Fe in deeper sites which are produced by direct shallow penetration, and/or larger mixing on larger impacts on soils.

4) Carbon contents with irregular decreases at every Apollo surface samples are enriched with Ca and REE elements, which support impact layering of the lunar crust in this study. 5) The present results are applied to interior fluid-gas reservoir of carbon-bearing light gasses-fluids by the "regolith filtering" which is applied to Moon, Asteroids and the Earth-type planets.

Acknowledgements: Author thanks to Prof. S. Sasaki, Dr. T. TANOSAKI and Emer. Prof. T. Kato.

References: [1] Heiken G., Vaniman D. and French B., *Lunar source book* (Cambridge Univ. Press) (1991), 27-45. [2] Taylor S. R., *Planetary Science: A Lunar Perspective* (LPI) (1982), 1-439. [3] Miura Y. (2007): *LPS XXXVIII* (LPI, USA), abstract # 1277 [4] Miura Y. [5] Miura Y. (2010): *LPS XXXXII*, Abstract #2462. [6] Miura Y. (2011): *LPS XXXXII*, Abstract #2817. [7] Miura Y. (2012): *LPSCXXXXIII, abstract#2920.#1203.* [8] Miura Y. (2012): *NETS-2012* (LPI), abstract #3100. [9] Graf J.G. (1993): *Lunar Soils Grain Size Catalog.* NASA Refer. Publication 1265. [10] *Lunar Science & Exploration* (2011): *Apollo Image Atlas*, http://www.lpi.usra.edu/resources/apollo/ (LPI, USA).[11] Smith J. et al. (1973): *Proc. 4th Lunar Sci. Conf., Geochim. Cosmochim. Acta*, 2, 1651-1656. [12] Moore C. *et al.* (1971): *Proc.2nd Lunar Sci. Conf.*, 2, (MIT Press) 1343-1350. [13] Moore C. *et al.* (1973): *Proc. 4th Lunar Sci. Conf., Geochim. Cosmochii. Acta*, 2, 1613-1623. [14] Moore C. *et al.* (1974): *Proc.5th Lunar Sci. Conf., Geochim. Cosmochim. Acta*, 2, 1897-1906. [15] Miura Y. (2011): *Proc. 33rd Solar System Sci. Sympo*. (ISAS, Japan), pp.5 (in Japanese). [16] Miura Y. (2011): *LEAG-2011* (LPI, USA), abstract #2001.[17] Miura Y. (2011): *2011 Vexag Int. Workshop* (Washington D.C.), Abstracts #23, #24.

NEW MODEL OF LUNAR CRUST WITH IMPACT-RELATED AGGREGATES AND PROCESSES.

Y. Miura, Yamaguchi University (Yoshida 1677-1, Yamaguchi, 753-8612, Japan), Univ. of Al.I.Cuza (Dept. of Geology Sci., Bld. Carol I no. 20 A, 700505-Iaşi, România), and California Institute of Technology (JPL, Pasadena, CA 91109-8099, USA). **E-mail:** yasmiura@yamaguchi-u.ac.jp, moonyas@hotmail.com

Introduction: Previous model of lunar crust formation is based on global differentiation in the Moon itself [1, 2 and 3]. When major original rock compositions on the Moon are considered to be transported from primordial planets including Earth (triggered by planetary collision of giant impact process), the following lunar processes of magmatic ocean, impact differentiation and impact-related mega-regolith soils are fairely explained. The main purpose of the paper is to discuss new proposed model of lunar crust with major impact process aggregates with carbon (C) and meteoritic iron (Fe) and nickel (Ni) contents reported in the previous studies [4-8, 10-14], together with the Rare-earth-elements (REE) data [14, 15].

Primordial block-aggregates from planets: Although previous lunar layering model is based on initial lunar interior differentiation to form light anorthositic crust and heavy basaltic mantle estimated from the Apollo sampling samples [1], but light crust components of the present Moon can be considered to be transported as the remnants of planetary collision (known as giant impact [1, 2]) which initial layering has been formed at each planet (including primordial Earth). This transported crust component by collision impact process can be also produced high-temperature materials (mantle-related layers) and low-temperature materials (crust-related layers) as listed in Table 1.

Incomplete layering on the Moon: Little "continuous" heat sources on the Moon is considered to produce "incomplete layers" of impact-related aggregated blocks originated from collided shallow interior of the Earth-type planets. In fact,
a) non-cycles of three materials states (vapor-liquid-solid, called as VLS) on the solid Moon, and b) bulk density of the Moon (3340kg/m^3) is very lower than Earth (5515 kg/m^3**)** which is the similar with those of Asteroids of Vesta (3340 kg/m^3) and Massalia (3260 kg/m^3), and c) diameter of the Moon (from planetary blocks) are considerably larger than the Asteroids (from cosmic dust or planetesimal). This indicates that bulk mafic silicate compositions are similar but block-aggregates are different from smaller Asteroids and larger planets (Table 1).

Table 1. Two steps of lunar source and crust formation .

Formation step	Impact source and layering
a) Planeraty surfaces (Primordial Earth)	Separation by planetary collision (*i.e.* giant impact)
b) Incomplete layering (Irregular surface)	Few continuous heat sources (non-cycles of state changes) [4]

Evidences of anomalous lunar minerals: The Apollo lunar rocks reveal anomalous lunar minerals compared with the Earth-type minerals with slow magmatic evolution as follows [10-13]: a) Number of lunar minerals without hydro-alteration are less than a few % than that of terrestrial minerals [1, 5]. b) Major lunar crustal minerals of plagioclase shows i) a few vacant sites in Ca-rich plagioclase with carbon element [10,13], ii) higher amounts of foreign Mg and/or Fe mixed with olivine/pyroxene minerals [6, 8, 14], and iii) few micro-lamellar textures with slow-cooling formation [11]. c) Impact breccias and regolith soils contain significant amounts of carbon, chlorine and rare-earth elements (REE) [6, 8 and 14].

Impact evidence with higher porosity: Porosity of the lunar rock samples indicates impact effects. In fact, a) older lunar rocks and breccias (15418, 14321 and 14303) show *higher porosities* (ca. 2 to 9 times) with lower density than those of younger basalts (15555 and 12051) [9]. b) Older breccias (14321 and 14303) reveal highest porosity than other type of rocks. c) Old lunar anorthosite (15418) reveals higher porosity than Mare basalts (15555 and 12051) as shown in Fig. 1.

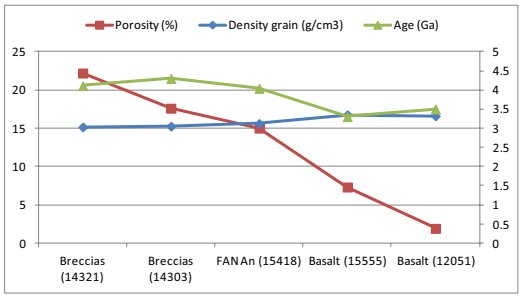

Fig. 1. Lunar data of density, porosity and age in the pristine Apollo Mare basalt (15555 and 12051) and highland anorthosite (15418) and breccias (14321 and 14303) [1, 2, and 6-9]. The diagram suggests that primordial lunar rocks of breccias and anorthosite reveal high porosity by impact effects

Impact indicators by Fe-Ni-Co and carbon: Significant amounts of iron-meteoritic components (Fe, Ni and Co) and carbon contents are considered to be indicator of dynamic impact process on the lunar samples [1-9] as follows (Fig. 2):
a) The oldest FAN breccias (67016) have *higher* values of Fe, Ni, Co and C contents than younger crystalline FAN sample (67075) [8, 9 and 15], which indicates first *pristine* FAN sample reveals

dynamic impact block-aggregates (Fig. 2).
b) The oldest Mg-suite-type samples (76535 and 15455) [16] reveal higher values of carbon and Co contents than younger 14321 breccias.
c) The oldest samples (67016 and 15455) reveal the highest carbon content which indicates dynamic *mixing* process at the block aggregates (Fig.2).

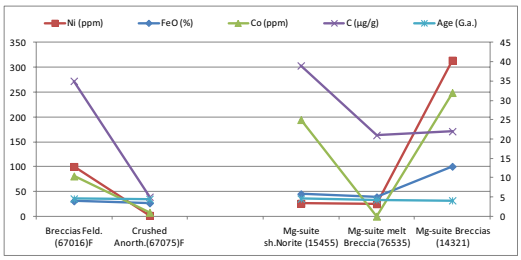

Fig. 2. Five values of FeO, Ni, Co and C contents and age of two AP16 highland (FAN) and three AP14,15 and 17 evolved (Mg-suite) lunar samples [1, 16] to show dynamic impact remnants.

The oldest lunar highland crust rock: Present new model of lunar highland crust is considered to be impact block-aggregates from planetary collision, which is supported by the following data:
a) The oldest lunar highland sample (67016) reveals higher values of impact indicators (Fe, Ni, Co and C) than younger old highland sample (67075).
b) Both oldest lunar samples (67016 highland anorthosite and 15455 Mg-suite norite) reveal the highest values of carbon and Co contents related with impact effects.
c) There is "no clear relation" with rock age data and impact signature (Fe, Ni, Co and C), which suggest few "continuous destroy process with age" on homogenous or heterogeneous lunar surface crystalline rocks formed by magmatic melting on the Moon previously reported.

Rare-earth elements of the soils and breccias: Rare-earth elements (REE) are enriched in lunar regolith soils and breccias compared with the Mare basalts [14, 15] (*cf.* Fig. and Table in [15]). In fact, carbon contents are related with Eu (and Ca) contents in the lunar impact breccias. This result strongly indicates that "lunar crust layering" [1, 2] are not "global magma ocean model", but "impact-related layering" [8, 15] with increased Ca and the REE (including Eu) and Ca (including carbon) [15].

Summary: The results in this study are summarized as follows:
a) Present new model of lunar crust formation is proposed by dynamic transportation and mixture process from primordial planets including Earth triggered by planetary collision of giant impact process, which can be explained the following lunar processes of magmatic ocean with impact melting and differentiation and impact-related mega-regolith soils on the Moon.
b) Little "continuous" heat source on the dry solid Moon with same density values of solid Asteroids produces incomplete layers of larger impact-related aggregated blocks originated from collided Earth-type planets.
c) The lunar rocks reveal anomalous lunar minerals of poor variety without hydro-alteration, Ca-plagioclases with limited compositional ranges, and impact-related mixtures of Fe, Mg, carbon, chlorine and rare-earth elements (REE) including Eu.
d) Older lunar rocks and breccias (15418, 14321 and 14303) show *higher porosities* than those of younger basalts (15555 and 12051). Old lunar anorthosite (15418) reveals higher porosity than younger Mare basalts (15555 and 12051).
e) The oldest FAN breccias (67016) have *higher* values of Fe, Ni, Co and C contents than younger crystalline FAN sample (67075). The oldest samples (67016 and 15455) reveal the highest carbon contents which indicates dynamic *mixing* process at the block aggregates and first *pristine* FAN sample.
f) The oldest lunar highland sample (67016) and Mg-suite norite (15455) reveal higher values of impact indicators (Fe, Ni, Co and C) than younger old highland sample (67075).
g) "Few clear relation" with rock age data and impact signature (Fe, Ni, Co and C) suggest few "continuous destroy process with age" on lunar surface rocks formed by magmatic melting previously reported.

Acknowledgements: Author thanks to Emer. Prof. T. Kato and Dr T. Tanosaki for carbon data and discussion.

References: [1] Heiken G., D. and French B., *Lunar source boo*k (Cambridge Univ. Press) (1991), 27- 120. [2] Taylor S. R., *Planetary Science: A Lunar Perspective* (LPI) (1982), 1-439. [3] French B. and Short N., *Shock Metamorphism of Natural Materials* (Mono Book Co., USA), 1-555. [4] Miura Y. (2007): *LPSCXXXVIII* (LPI), abstract #1277. [5] Miura Y. (1987): *Applied Physics Soc.* (Tokyo), Spec. Issue 1-6. [6] Miura Y. (2011): *Proc. 33rd Solar System Sci. Sympo*. (ISAS, Japan), pp.5 (in Japanese). [7] Miura Y. (2012): *NETS-2012* (Houston), abstract #3100. [8] Miura Y. (2012): *LPSCXXXXIII* , abstract#1203, #2920. [9] Macke R. et al. (2011), *LPSCXXXXII*, abstract #1986. [10] Miura Y. (2010): *LPSXXXXI* (LPI), abstract #2462. [11] Miura Y. and Tomisaka T. (1978): *Am. Mineral.*, 63, 584-590. [12] Miura Y. (2006) *LPSXXXVII* (LPI,USA), abstract # 2441. [13] Miura Y. (2007): *LPS XXXVIII* (LPI, USA), abstract # 1277. [14] Miura Y. (2011): *LEAG-2011* (LPI, USA), abstract #2001. [15] Miura Y. (2012): European Lunar Symposium-2012 (Berlin) (submitted in this volume). [16] Lunar Sci. Exploration (2011): Website data base, http://www.lpi.usra.edu/lunar/ (LPI, USA).

The Lunar Volatile Resources Analysis Package. A. D. Morse[1], S. J. Barber[1], K. R. Dewar[1], J. M. Pillinger[1], S. Sheridan[1], I. P. Wright[1], E. K. Gibson[2], J. A. Merrifield[3], C. J. Howe[4], L. J. Waugh[5] and C. T. Pillinger[1], [1]Planetary & Space Sciences, The Open University, Walton Hall, Milton Keynes. MK7 6AA UK. (a.d.morse@open.ac.uk), [2]Astromaterials Research Office, NASA Johnson Space Center, Houston, TX 77058, USA, [3]Fluid Gravity Engineering, 1 West Street, Emsworth, PO10 7DX, UK, [4]RAL Space, Didcot, Oxfordshire, OX11 0QX, UK, [5]EADS Astrium Ltd., Gunnels Wood Rd., Stevenage SG1 2AS, UK.

Introduction: The presence and abundance of lunar volatiles is an important consideration for ISRU (In Situ Resource Utilisation) since this is likely to be a part of a strategy for supporting long term human exploration of the moon. The Lunar Volatile Resources Analysis Package (L-VRAP) is part of the provisional payload for the ESA European Lander [1] and aims to measure the abundance and chemical/isotopic composition of volatiles from regolith samples and the lunar exosphere.

L-VRAP Concept: The Package concept is based on instruments flown for other lander missions (e.g. GAP[2], TEGA[3], and Ptolemy[4]). Regolith samples are loaded into one of 24 ovens on a carousel whereupon the volatiles are extracted by either pyrolysis or combustion to temperatures of least 800°C. The abundance and chemical composition is determined by an ion trap mass spectrometer. The volatiles are then chemically processed to be suitable for isotopic analysis by a magnetic sector mass spectrometer. L-VRAP also contains reference gases of known chemical and isotopic composition to enable precise isotopic measurements. The CAD layout is shown in figures 1 and 2.

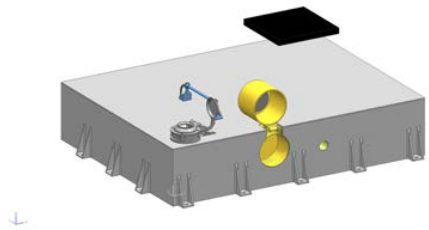

Figure 1. L-VRAP CAD model showing enclosure. Enclosure dimensions 460 mm × 350 mm, ht 97 mm

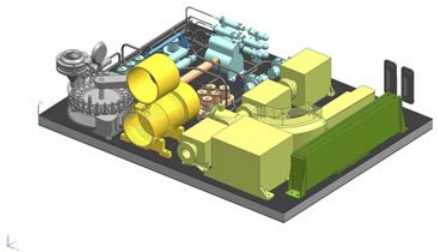

Figure 2 CAD model if the internal layout of L-VRAP. Subsystem details are listed opposite.

Solid Sample Inlet.
24 resistively heated ovens mounted on carousel
Sample size 50-100mg
Imager to estimate sample volume
Tapping station to seal sample

Chemical Processing System.
Valves and manifolds to control gases
Reagents and reactors to process volatiles
Reference gases H, C, N, O & noble gases
Reference gas mixture for ion trap MS

Ion Trap Mass Spectrometer.
Ring electrode r_0 = 8mm, 1MHz RF
Mass range 10 – 150 amu
Unit mass resolution
Electron multiplier detector
Frequency 1 mass spectrum/second

Magnetic Sector Mass Spectrometer.
6cm radius 90° magnetic sector
Mass range 2 – 150 amu
Mass resolution M/ΔM = 65
Triple Faraday cup detectors for C, N, O isotopes
Double Faraday cup detector for D/H isotopes
Electron multiplier detector for noble gases
Isotopic precision ±0.1‰ μmol samples, ±1‰ nmol samples.

Sample collection: The Lunar Lander includes a robotic arm capable of scooping samples from up to 3.5m from the lander centre and to a nominal depth of 10cm. A timeline has been developed to analyse volatiles at various depths and locations as well as their variation over time and changing illumination conditions. The possible inclusion of a mobile payload element with a mole would allow a much larger range of samples to be acquired.

Exosphere samples: In addition to analysing volatiles released from regolith samples, L-VRAP can directly analyse the tenuous lunar exosphere by opening the mass spectrometers to the lunar environment. The ion trap MS can rapidly monitor the full mass range to detect transient events (e.g. during changes of illumination) whereas the magnetic sector MS has greater sensitivity can detect the less abundant volatiles. The housing for the Ion Trap MS also includes a material which passively traps the exosphere. Hence the exosphere can be collected over a long time scale during darkness.

Contamination: An important consideration for this study is the effects of contamination from the Lander. The landing sequence will use about 1000

kg of propellant, with a large fraction directed onto the landing site. Initial modeling indicates that uncontaminated samples will be accessible by the robotic arm at depths of several centimeters. Knowledge of the contamination composition and distribution will allow the identification of surface volatiles, either by subtracting the contamination or by identifying protected areas such as surface shielded by small rocks.

References: [1] Carpenter J. D. et al. (2012) *LPSC XLIII*, Abstract#1990. [2] Hoffmann J. H. et al. (2008) *J.Am.Soc.Mass Spectrom*. 19, 1377-1383. [3] Stewart et al. (2003) *J. Geophys Res*. Abstracts 5, 09489. [4] Morse A. D. et al. (2009) *In: Rosetta: ESA's mission to the origin of the solar system, 19.6*, 669–686.

TO THE MOON ON A SHOESTRING. EUROLUNA'S ENTRY IN THE X PRIZE COMPETITION. Tor Foss Mortensen[1] and Søren Rasmussen[2]. [1] Langtved Data A/S, Sct. Hansgade 13, 4100 Ringsted, Denmark, [2]Euroluna AG, Svitzerland.

Abstract: The Euroluna Team is one of the around 30 teams competing in the Google Lunar X PRIZE competition.

The Euroluna Team was formed in 2007, and the first flight hardware was acquired in 2010.

General. This paper will describe the current plans of the Euroluna missions. Missions are low cost and include two Earth orbiters and one Lunar Lander.

The Euroluna missions are based on as much Commercial Off the Shelf components as possible and on keeping the overall mass of the orbiters and landers in the 1 to 5 kg range.

Components and printed circuit boards are based on the Cubesat family and an ion thruster is used for propulsion. For landing on the Moon a special design is under development.

Special software of own design is used for simulat ion of trajectories and energy consumption.

Challenges with low isp thrusters. The special considerations relating to the design of the trajectory and landing procedure are discussed. Ephemerides from the Jet Propulsion Lab are used for navigation.

The Authors:

Tor Foss Mortensen, MSEE, BC.

Søren Rasmussen, MSCE.

References:

[1] Jet Propulsion Lab, http://ssd.jpl.nasa.gov/?horizons

[2] Keith R. Symon, (1960) Mechanics, Addison Wesley.

[3] James R. Wertz and Wiley J. Larsen (editors), Space Mission Analysis and Design, Third Edition, Space Technology Library.

Development status of the Lunar Laser Ranging Experiment for SELENE-2 H. Noda[1], H. Kunimori[2], H. Araki[1], T. Fuse[2], H. Hanada[1], M. Katayama[3], T. Otsubo[4], S. Sasaki[1], S. Tazawa[1], S. Tsuruta[1], K. Funazaki[5], H. Taniguchi[5], K. Murata[5], [1]National Astronomical Observatory of Japan (2-12 Hoshigaoka, Mizusawa, Oshu, Iwate, Japan. noda@miz.nao.ac.jp), [2]National Institute of Information and Communications Technology (NICT) (Koganei, Tokyo, Japan), [4]National Astronomical Observatory of Japan (Mitaka, Tokyo, Japan), [4]Hitotsubashi University (Kunitachi, Tokyo, Japan), [5]Iwate University (Morioka, Iwate, Japan).

Introduction: We present the development status of the Lunar Laser Ranging experiment proposed to Japanese SELENE-2 lunar landing mission. The Lunar Laser Ranging measures the distance between laser link stations on the Earth and retroreflectors on the Moon, by detecting the time of flight of photons of high-powered laser emitted from the ground station. Since the Earth-Moon distance contains information of lunar orbit, lunar solid tides, and lunar orientation and rotation, we can estimate the inner structure of the Moon through orientation, rotation and tide.

Retroreflector: Retroreflectors put by the Apollo and Luna missions in 1970's (Apollo 11, 14, 15, Lunakhod rover 1 and 2) are arrays of many small Corner Cube Prisms (CCP) (3.8 cm diameter for Apollo). Because of the tilt of these arrays from the Earth direction due to the optical libration, the returned laser pulse is broaden, causing the main range error of more than 1.5 cm ([1]). Therefore retroreflectors with larger single aperture are necessary for more accurate ranging. Meanwhile, the beam width of retroreflector is inversely proportional to the fourth power of aperture. Therefore as the aperture becomes larger, the beam width becomes smaller so that the divergence of the reflected beam cannot cancel the velocity aberration of 3.5 - 7 micro radians ([2]). To cancel the velocity aberration, a large retroreflector needs small amount of offset angle between the reflecting planes (called Dihedral Angle Offset or DAO) to spoil the return beam pattern. The DAO must be optimized to be less than 1 second of arc with 0.1 seconds of arc accuracy for collect more photons [2,3].

We propose a large single retroreflector of hollow-type with 15 cm aperture. Larger aperture up to 20 cm might be favorable if more mass is permitted for payloads. Assuming the ground station as 1.5 m diameter telescope with relatively high energy laser (about 100 mJ, 10 Hz repetition rate), enough photoelectrons can be detected within 10 minutes to achieve less than 1 cm of range uncertainty.

As for the mirror material, some ceramic products (ZPF: zero expansion stiffness ceramics or SiC: silicon carbide) are under consideration. The thermal quality of the material can be evaluated by the coefficient of the thermal expansion (CTE) and the thermal conductivity (TC). The ratio TC/CTE is a good measure of the thermal stability of materials. The TC/CTE ratio for ZPF (~250) is more than five times as large as that of the SiC (~50) or Zerodure (~30), therefore ZPF seems to be the most favorable material for the retroreflector. The method to fasten three planes each other must be developed. Also, realization of such small DAO as 0.1 seconds of arc is challenging with current technology, therefore the development of fabrication method is important.

The reflectivity of each plane of the retroreflector must be as high as possible, because the light must be reflected three times in the retroreflector. In case of bare aluminum coat, the reflectivity at 550 nm is 91.6% and the total reflectivity for a retroreflector becomes as low as 76.9%. On the other hand, the reflectivity of the silver is 97.9% at the same wavelength and the total value for the retroreflector will be kept high as 93.8%. Though silver has the highest reflectivity among metals, it is susceptible to corrosion, resulting much lower reflectivity with tarnishing. Therefore a method for generating durable silver coating on a ceramic mirror which can survive in space as well as on the Earth must be developed in the near future.

References: [1] Murphy T. et al. (2008) *PAPS*, 120, 20-37. [2] Otsubo T. et al. (2010) *Adv. Space Res.*, 45, 733-740. [3] Otsubo T. et al. (2011) *Earth Planet Space*, 63**,** e13-e16.

A New Disintegrative Capture Theory for the Origin of the Moon. Peter D. Noerdlinger[1]
[1]Technology Advancements, Inc, 1222 Oakleaf Circle, Boulder, CO 80304 USA. pdnoerd@gmail.com

Introduction:

Prior to the discovery that the Moon has an Oxygen isotope ratio very close to that of the Earth and very small iron core, a number of researchers [1-5] worked out details of possible capture. Based on geology, capture is still favored by Harrison Schmitt [6]. The smallness of the actual lunar iron core led to abandonment of whole capture theories, as there is no obvious way to get rid of most of an original lunar iron core ~32% by mass. Previous disintegrative capture theories all involving disintegration *during* capture were abandoned. Our disintegrative theory puts the disintegration *after* the capture. The proto-Moon was captured into a descending orbit, initially eccentric, but soon circularized by tidal forces. The origin of the proto-Moon (PM) before capture is at the L4 Lagrange point [7], but the impactor Theia had the mass of Mars. Our PM has mass ~1/39 that of Earth or about 4 times less than the BG giant impactor. Capture occurs just inside the co-rotation radius, so that the PM descends towards Earth. The outer layers of the PM are stripped to form a disk of rock particles. All the rock is in that disk or else has struck Earth by the time the PM remnant reaches 2.243 Earth radii (RE), after which the iron core descends to ~2.23 (RE), then disintegrating into an iron ring. The core, having driven the rock disk outside the Roche limit, tidally coaxes the ring of rock to form into a single Moon at about 3.5 Earth radii before itself breaking into a ring of iron droplets. The newly formed Moon then tidally drives the iron ring and any portion of the stripped rock that lay within the orbit of the disintegrating PM, down to the surface of the Earth, producing the "Late Veneer" [8]. The inner rock disk and iron ring particles arrive at the Earth's equator at LEO speed ~ 8 km s^{-1} and zero angle of incidence. This contrasts to the Giant Impact (GI) case, where Theia's core enters at near-normal incidence and descends rapidly to join the Earth's core, thus having no discernable contribution to the Late Veneer. In the present theory, as contrasted to the GI case, the lunar material is never vaporized. The last parcels of rock to tear free from the PM's core might be driven out and hit the Moon on the nearside, so as to form the first maria at the same time, within ~ a few days, as the PM core plasters the Earth's surface with core material and rock. The magnetization of Troctolite 76535 [9] originated in the PM, which had a large enough iron core to support a dynamo.

Fig 1. Orbit Entering Capture Phase

The successive circles are the Earth surface, the Roche limit and the co-rotation (synchronous) radius counting outwards. Earlier orbital motion resembles Figs. (4) and (5) of BG.

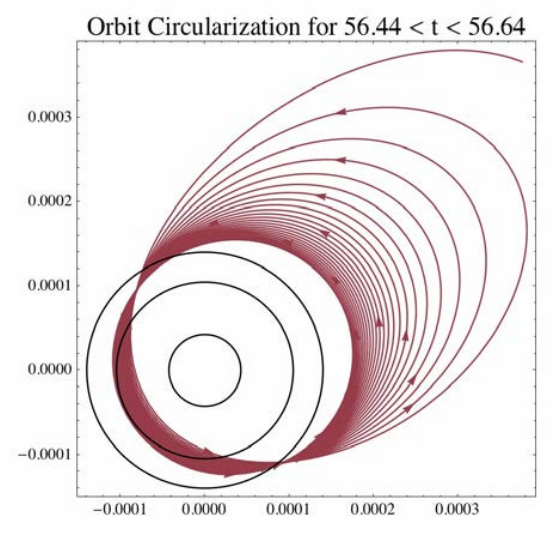

Fig 2. Orbit History (up to capture phase)

The vertical broken line is the final transition to within the co-orbital (synchronous) radius. The time scale is after Ref. [7].

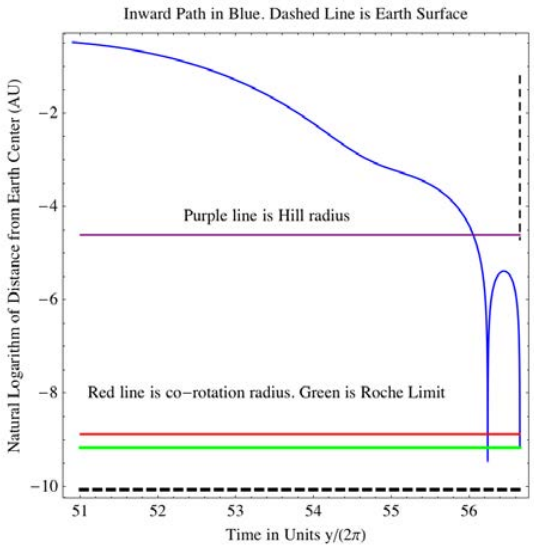

References:

[1] Gerstenkorn, H. 1969, *Icarus* **11**, 189-207.
[2] Singer, S. F. 1968. *Geophys. J. RAS* **15**, 205-226.
[3] Öpik, E, J., 1972, *Irish Astron. J.* **10**, 190
[4] Conway, B. 1982, *Icarus* **51**, 610-622
[5] Malcuit, R. J. et al 1989 Proc. 19th LPS Conf. 581 – 591

[6] Schmitt, H. 2006, in *Solar System Update* (Ed: Blondel, P., Mason, J.), Springer-Verlag, Berlin
[7] Belbruno, E., Gott, J.R. 2005, *A. J.* **129**, 1724-1745. (BG)
[8] O'Neill, H. S. C. 1991, *GCA* **55**, 1159–1172
[9] Garrick-Bethell, I., et al 2009, *Science* **323**, 356-359

MOVIDA: An instrument for the characterization of lunar dust charging and levitation process and measurement of volatiles. E. Palomba[1], A. Longobardo[1], A. Bearzotti[2] , E. Zampetti[2], S. Pantalei[2], B. Saggin[3] [1]IAPS-INAF, via Fosso del Cavaliere 100, 00133 Rome, Italy (Ernesto.palomba@ifsi-roma.inaf.it), [2]IMM-CNR, via Fosso del Cavaliere 100, 00133 Rome, Italy, [3]Politecnico di Milano, Piazza L. da Vinci 32, 20133 Milano, Italy.

Introduction: The MOVIDA (Moon Volatile Investigator and Dust Analyser) instrument here presented is being developed by a consortium of institutes, leaded by IAPS-INAF, which plans to characterise the lunar environment and potential in situ resources to identify their implications for future human exploration. MOVIDA main scientific objectives are:

- measure the properties of lunar dust and the processes of charging and levitation;
- identify potential resources, which might be exploited in future exploration missions, such as water or organic rich material

Working principle: MOVIDA is devoted to the measurement of the lunar dust and to the characterisation of the dust charging and levitation processes. It will measure the dust grain mass and charge allowing, possibly, the discrimination of the grain size. A miniaturised and built-in heater will allow to perform heating cycles to measure volatiles (water and organics) possibly present in grain dusty material.

MOVIDA is based on an array of micro-oscillators whose detecting part is made up of piezoelectric crystals with a conductive electrode that act as a collector of micron and sub-micron size particles.

Piezoelectric crystal microbalances are one of the most widely used chemical sensors in gas/particle sensing for Space and in environmental and biological applications. They are also commonly used in the laboratory to control the thickness of materials deposited like thin films. These sensors convert mass changes into fundamental resonance frequency variations. They have been widely applied in Space to monitor dust flux and volatile outgassing [1, 2].

Microbalances are made up of a piezoelectric foil with metallic electrodes deposited on both sides.

The fundamental transduction equation according to Sauerbrey equation [3] is:

$$\Delta f \propto \frac{f_0^2}{A}\Delta m$$

which states that the change in resonance frequency Δf of a thin quartz crystal is proportional to the additional mass Δm deposited on it, f_0 being the resonance frequency of the uncovered quartz and A the sensitive area. The main innovation introduced by MOVIDA consists in the development of a new generation of microbalances able to attract charged dust grain by means of a variable Electric Field (EF), generated locally by the instrument itself. The application of this EF will break the equilibrium between the Electric and the Gravity Fields on the Moon (as explained by the Levitation model), allowing the electrically charged dust grains to be attracted toward the microbalance. In principle, by varying the local EF it is possible to attract grain with different size and electric charge. The electronics will be designed to optimize the configuration of a capacitors cascade in order to measure the electric charge accumulated onto the sensor (using the capacitors discharge principle). A built-in heater will allow to perform μThermogravimetric analysis (TGA). This special design of a built-in heater dramatically reduces the total mass and the power required to perform thermal cycles. The TGA measures the change in mass of a sample as a function of temperature and time. The technique can characterize materials that exhibit weight loss or gain due to kinetic processes, mainly: decomposition, oxidation or dehydration.

Technical characteristics: MOVIDA requires low mass, low size and is low power-consuming. Its technical characteristics are summarized in Table 1.

Mass	<500g
Volume	< 300 cm^3 (main electronics & sensing system included)
Average data rate	0.5 kbps
Average required power	< 2 W

Table 1: MOVIDA technical characteristics

MOVIDA Current status: The technical concepts of MOVIDA benefit of developments already performed for a project that was recently selected by ESA and is currently under study for the proposed Cosmic Vision M-Class mission Marco Polo, Marco PoloR [4] and L-Class mission JUICE [5]. The instrument, called VISTA (Volatile InSitu Thermogravimetry Analyser), is a miniaturised thermogravimetry analyser that will perform measurements of the volatile compounds (water and organics) adsorbed onto the asteroid regolith. The VISTA study is presently funded by Italian Space Agency and INAF. One of the main goals of the study is to perform a feasibility analysis (including laboratory measurements) to increase the VISTA TRL to a level of 5.

The evaluation of mass, volume and vata given here have been extrapolated from the VISTA instrument considering the new improvements.

Anticipated impact in the field: The study and characterization of the lunar dust charging and levitation has significant implications both from the sci-

entific point of view and for enabling future long-duration human lunar missions. During the Apollo missions it was noted that lunar dust (with diameter less than 20 μm) easily entered the cabin after astronauts Extra Vehicular Activity: this dust created several problems both to crew safety and instrumentation [6]. Measurement of water and organic rich materials is extremely important to understand what kind of resources can be available to humans on the Moon and what kind of processes act to originate and/or destroy Lunar volatiles.

Anticipated risks: The technology of MOVIDA is mature and has been demonstrated on different planetary missions. The new improvements, consisting in measuring electric charge by capacitor discharge and in capturing charged particle by means of a controlled Electric Field, are demonstrated in their basic principles. Their performances should be evaluated experimentally.

References: [1] Wood B.E. *et al.* (1996), *Proc. SPIE* 2864, 187-194. [2] Palomba E. *et al.* (2002), *Adv. Spa. Res.*, 29, 8, 1155-1158; [3] Sauerbrey G. (1959), *Z. Phys.*, 155, 206-222; [4] Barucci M.A. *et al*. (2011), *EPSC abstract*, 496; [5] Gowen R.A. *et al*. (2011), *Adv. Spa. Res.*, 48, 4, 725-742; [6] Taylor L. A. *et al.* (2005) *1st Space Explor. Conf., AIAA*.

Thermodynamic aspects of lunar regolith processing for SWIP evolution - Experiments and theory.

S. Parzinger, M. Spinnler and T. Sattelmayer
Technische Universität München – Lehrstuhl für Thermodynamik, Boltzmannstr. 15, 85747 Garching

Introduction: This work represents the thermodynamic part of the project LUISE (Lunar In-Situ Experiment). The goal of this project is the thermal processing of lunar regolith, as an effective way to extract solar wind implanted particles (SWIP). Since the thermal conductivity of powders in general is very low under vacuum conditions (about 5 – 20 mW/(m K)), heating a larger amount of lunar regolith on the moon is a difficult task. The goal of the present work was to create a basic understanding of the thermodynamic processes occurring during the heating of lunar regolith from vacuum up to atmospheric conditions.

For the experimental determination of the effective thermal conductivity of JSC-1A, the hot-plate technique was used under atmospheric and vacuum conditions. Besides, a cavity receiver breadboard design was used for further investigations under vacuum conditions. In general, the heat transfer in a porous media is described by three combining mechanisms: heat transfer through the fluid and point contact, through the contact area and due to radiation. To ensure that radiation is in the optical thick regime the probe thickness was chosen larger than 10 mm. This is an important issue especially for vacuum conditions, where radiation is the dominant mechanism. The experimental results are in good agreement with the known theory of Zehner, Bauer and Schlünder. Those results were used for the development of a numerical simulation model. In this model, the outgassing of the SWIPs and its increasing influence on the effective thermal conductivity of the lunar regolith is implemented. The higher conductivity is caused by the increasing number of gas molecules.

With this experimental results and the developed model, a first prediction of the influence of outgassing SWIP on the heating process of lunar regolith is possible. First simulations show that the processing time to reach temperatures of up to 1000 °C can be reduced by a factor of 10.

QUALITATIVE ESTIMATION OF THE SENSITIVITY OF THE STELLAR COORDINATES TO THE DEFORMABILITY OF THE LUNAR BODY WHEN SIMULATION OBSERVATIONS IN THE JAPANESE PROJECT ILOM.

N. Petrova[1,2] and H. Hanada[3], [1] Kazan Federal University, 18, Kremljevskaja str., Kazan, 420008, Russia, e-mail: nk_petrova@mail.ru; [2] Kazan State Power Engineering University, 51, Krasnoselskaja str., Kazan, 420066, Russia; [3] National Astronomical Observatory, 2-12 Hoshigaoka, Mizusawa, Iwate 023-0861, Japan, e-mail: hanada@miz.nao.ac.jp

Introduction: In the next decade in many countries a series of space experiments is planned to observe the lunar physical libration with tools mounted on lunar surface. The Japanese project ILOM (In situ Lunar Orientation Measurement) is planned to be realized as one of kinds of observations of lunar rotation at the second stage of SELENE-2 mission [1]. One of the important elements of the project is placing of a small optical telescope on the lunar surface with the purpose to detect the lunar physical libration with high accuracy 0.001 arc sec.

It is known numerical and analytical approaches exist in the theory of physical libration of the Moon, they complement each other: a numerical approach has higher accuracy and is used for direct processing of observations, the analytical approach is less accuracy , but is more flexible in simulating observations and their subsequent interpretation. Accordingly, the analytical theory of lunar physical libration is used in the current study to model the observation process of the ILOM-project in order to identify the sensitivity of stellar tracks to the parameters of the gravitational field of the Moon, the coefficients of elasticity and the dissipation of the lunar body, the characteristics of the lunar core. Stage of the study aimed at determining the sensitivity of stellar tracks for the deformability of the lunar body is presented in this report.

Analytical theory for the case of deformable Moon: The analytical theory of lunar libration [2], [3] is used for the imitation of the observations. The theory gives dependence on the time and Stokes coefficients (till the fourth order) in the form of Poisson series. The expansion of Petrova's analytical theory in the case of a deformable Moon is made on the basis of complements, calculated by Chapront et al. [4] to the Moon's libration theory [5] concerning tidal effects. Moon's theory also takes into account a rigid body. Chapront et al. have developed the theory, considering the effects of perturbation due to the deformation of the Moon by the Earth, the Sun and lunar rotation (tidal perturbations).

These perturbations in the case of an anelastic model with constant time delay are represented in the semi-analytical form. The series were obtained for the Love number k_2 = 0.02992. Chapront et al. used the dynamical model DE245, therefore the series of Petrova's theory is reduced to the semi-analytical form, using Stokes coefficients of the same gravity field model. We are interested only in a qualitative manifestation of the effects of elasticity in selenographic coordinates of the stars, but not in the accuracy of the coordinates. of stars in the observations. Therefore, we believe that the simple joining of the two types of series to be warranted.

Calculation libration angles for a rigid and deformable Moon The problem is solved by the following algorithm:

1. A fictitious star with ecliptical coordinates of the Northern pole of the Moon is taken.

2. Its selenographic coordinates x^o, y^o are calculated on the basis of the extended libration theory for the period of 1 year. The coordinates are considered as "observed" coordinates.

3. These coordinates are introduced into equations of the inverse problem of libration [6]. The equations are solved by the gradient method. The angles of libration for a rigid Moon $\rho^c(t)$, $\tau^c(t)$, $\sigma^c(t)$ are taken as the first approximation to start the iterative process. Solution of the inverse problem gives us the libration angles for a deformable Moon $\rho^o(t)$, $\tau^o(t)$, $\sigma^o(t)$, which we call as an "observed" libration .

4. The residuals: $\Delta\tau(t) = \tau^o(t) - \tau^c(t)$, $\Delta\rho(t) = \rho^o(t) - \rho^c(t)$, $\Delta I\sigma(t) = I(\sigma^o(t) - \sigma^c(t))$ are analysed.

It's shown that longitudinal libration is not sensitive any variation of coordinates and can not be revealed from observations of polar stars.

Analysis of residuals: We carry out the Fast Fourier Transform on the residuals. Obtained spectra for libration angles are shown on Fig. 1. Numerical values of frequencies, respective periods and amplitudes are given in Table 1. In order to identify the obtained frequencies with the origin frequencies of libration theory, we calculate $\Delta\rho$ and $\Delta\sigma$ in analytical form using the software Poisson Series Processor. The terms, whose amplitudes are greater than 0.001", are presented in Table 2.

Comparing respective parameters from both tables allows giving some comments to future spectral analysis of residuals, which will be directed on definition of parameters characterising the lunar elasticity, in particular, of the Love number k_2.

We dare to suggest that the components with the periods of 25.29 days and 29.5 days (Table 1) are result of blend of the harmonics, whose periods are

close to the lunar rotation period ~27.3 days: *F, l*-2*F, l*-2*D, l.* Analysis of blends is a complicated problem of spectral analysis, nevertheless the improvement of k_2 will cause the total decrease of residuals in this region. Strong harmonic 2*F* with the period of 13.62 days is very useful for the analysis: there are no other harmonics in its vicinity. Weak component with the period of 9.077days corresponds to the (*l*-2*F*)-term. It may be also interesting for analysis, although its amplitude is on the verge of accuracy; however, our simulation reveals this component.

In comparison with a rigid model the tidal model causes not just periodical variations, but the constant small shifts in libration angles (– 0,0117″ in $\Delta\rho$ and -0.2619″ in $\Delta\sigma$), as evidenced by analytical representation of the residual spectra (Table 2). Improving the k2 will cause decreasing these shifts too.

Thus, several components sensitive to the parameter k_2 are revealed from examination of residual spectra.

The effectiveness of simulation could be improved, if we compared tidal models with different values of k_2. For this purpose it is desirable to improve the analytical theory, supplementing it by the partial derivatives of libration angles with respect to k_2. This idea was realized by Eckhardt [7] for elastic model- "solution 514", his partial derivatives contain a few terms in comparison with solution of Chapront et al. [4].

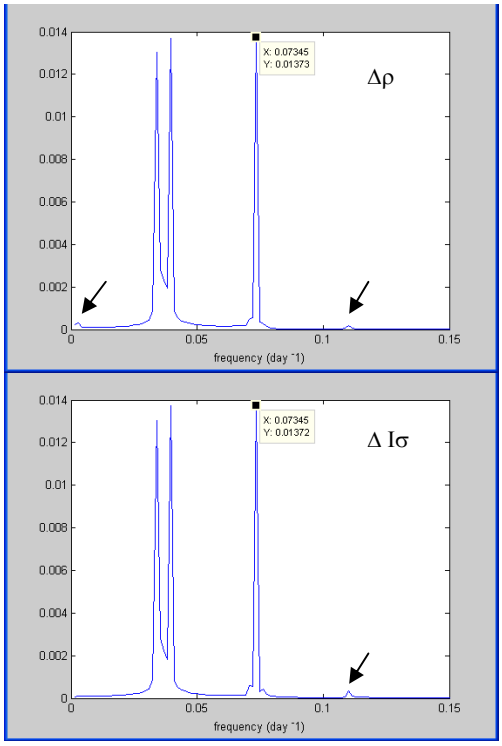

Fig. 1 Spectrum of residuals of $\Delta\rho(t)$ and $\Delta I\sigma(t)$. The unity of ordinate is arc sec

Table 1. Frequencies and amplitudes revealed by Fourier transformation of simulated residuals in ρ and $I\sigma$

Frequency (revolution per day)	Period T (day)	Δρ (arc sec)	ΔIσ (arc sec)
0.11020	9,077	0.0002	0.0003
0.07345	13.62	0.0137	0.0137
0.03955	25.29	0.0137	0.0137
0.03390	29.5	0.0130	0.0130
0.00283	353.9	0.0003	0

Table 2. Parameters of the analytical series calculated for the residuals in libration angles ρ and $I\sigma$

Delaunay arguments l F l' D	Frequency (revolution per day)	Period T (day)	Δρ(arc sec)		ΔIσ(arc sec)	
			Cos	Sin	Cos	Sin
0 0 0 0	-	-	0.0117	-	-0.2619	-
0 1 0 0	0.03675	27.2122	-0.0040	-0.0240	0.0238	-0.0040
0 2 0 0	0.07350	13.6061	0.0064	-0.0002	-0.0006	0.0063
1 -2 0 0	-0.03720	-26.8783	-0.0241	0.0204	0.0187	0.0241
1 0 0 -2	-0.03143	31.8119	0.0010			-0.0010
1 0 0 0	0.03629	27.5546	0.0351	0.0074	-0.0073	0.0351
1 2 0 -2	0.04206	23.7746	-0.0010			-0.0010
1 2 0 0	0.10979	9.1085				0.0002
2 -2 0 0	-0.00091	-1095.17	0.0004	0.0002		
2 0 0 0	0.07258	13.7773	0.0003		-0.0001	0.0010

References: [1] Hanada H, Araki H., Tazawa S. et al. Development of a digital zenith telescope for advanced astrometry. Science China **(**Physics, Mechanics & Astronomy). Vol.54, (2011) (in press) [2] Petrova N. Analytical extension of Lunar libration tables. Earth, Moon and Planets, Vol. 73, No 1, p. 71-99, 1996. [3] Gusev A., Petrova N. Rotation, physical libration and internal structure of the Moon. The Book. Kazan university press. 208 p., 2008 (in Russian). [4] Chapront J., Chapront –Touzé M., Francou G. Complements to Moon's Lunar libration theory. Cel. Mech. & Dyn. Astron., v.73, pp 317-328, 1999. [5] Moons, M.: 1982, 'Analytical theory of libration of the Moon', *Celest. Mech. & Dyn. Astr.*, **26**, 131. [6] Petrova N., Abdulmyanov T., Hanada H. (2012) 43-rd LPSC, 1027. [7] Eckhardt D.H. Theory of the libration of the Moon. The Moon and the Planets, 25, pp. 3 – 50, 1981.

A MINIATURISED XRD/XRF INSTRUMENT FOR THE IN SITU ANALYSIS OF LUNAR SOILS/ROCKS. L. Marinangeli[1] , L. Pompilio[1] , I.B. Hutchinson[2], G. Adami[3] and A. Stevoli[3], [1]IRSPS-Universita' G. d'Annunzio, via dei Vestini 31, 66013 Chieti, Italy e-mail: luciam@irsps.unich.it [2]Space Research Center, University of Leicester, United Kingdom [3]Thales Alenia Space - Italia, Milan.

Introduction: The knowledge of the surface composition is crucial for the identification of potential resources and for the understanding of the surface/crustal evolution. An ultra-miniaturised (mass 1.5 kg; volume ~22x6x12 cm^3) X-rays diffractometer/fluorescence instrument (MARS-XRD) has been developed for the the mineralogical and chemical characterization of Martian soils/rocks and included in the ExoMars-Pasteur payload [1,2] (Figure 1). The simultaneous acquisition of in-situ chemical and petrological information trough a similar instrument would give significant improvement to lunar robotic missions, as well. The complete characterization of lunar soils/rocks would indeed help us unraveling many doubtful points regarding the mantle composition, crustal evolution and resource potential of the Moon. Based on the ExoMars experience, we propose a similar instrument for the chemical and mineralogical analysis of the lunar rocks. The proposed instrument is an innovative and advanced concept which gather the experience achieved in Europe for the miniaturisation of the design.

Main objectives: The capability of simultaneously acquiring X-rays diffraction (XRD) and fluorescence (XRF) measurements would allow us to disclose the mineralogy and chemistry of lunar soils/rocks.

Unraveling the composition of surface materials is crucial in order to identify processes occurring at the surface and at the crustal interior. As an example, the identification of the mineral paragenesis of igneous rocks provide information on the type of crustal differentiation and volcanic processes in terms of temperature, pressure and volatile content, together with crucial information to model the mantle characteristics (i.e. viscosity) at the time of the rock formation. This is the only way to get information on the past interior conditions which can be coupled to planned geophysical investigations.

The identification of the iron-bearing minerals (i.e., oxides) can help in understanding the magnetic field at the time of rock formation. A detailed mineralogical characterization of the surface sample is required to reconstruct the variation of the interior dynamics of the planet.

Furthermore, determination of chemical composition extended to trace elements (i.e., Rb, Sr) will provide more detailed information about magmatic and crustal differentiation of the lunar samples collected during the mission.

Working principle: The instrument is based on an innovative concept which combines X-ray diffraction and fluorescence techniques to simultaneously measure the mineralogy and chemistry of soils/rocks.

X-rays diffraction is a well-established analytical technique for the identification of minerals, as well as other crystalline materials. XRD is the most common routine tool for mineral identification of unknown substances using a very small volume of sample. Almost all we know about the location of atoms, their sizes and their bonding in crystal structures has been largely derived from X-rays diffraction studies. XRD is particularly useful to determine the degree of crystallinity in samples, possible deviations of the minerals from their ideal compositions (presence of element substitutions and solid solutions), the structural state of the minerals (which can be used to deduce temperatures and/or pressures of formation), and the degree of hydration for minerals that contain water in their structure.

X-rays fluorescence spectroscopy is used in most research laboratories to study the chemistry of inorganic substances. Through irradiation with X-rays, the sample generates an X-rays emission spectrum that is characteristic for each element in the sample. The XRF spectrum is characterized by spectral lines centered at wavelengths which are diagnostic of each chemical element.

The combination of XRD and XRF techniques provides a complete mineralogical characterization of the rock sample with one instrument. The proposed instrument consists of a radioisotope as source of X-rays, a collimator and a CCD-based detection system. The instrument follows a fixed reflection geometry to fulfill the diffraction principle.

The instrument takes advantage of the use of a radioactive source (55Fe and 241Am isotopes has been fully tested at the breadboard level) to reduce the power consumption compared to the more common X-ray tube. However, given the status of the art for cold-cathode X-ray carbon nanotube, this option may be also investigated.

Operations: A full measurement cycle consists of data acquisition and integration in several hours. XRF and XRD measurements are acquired simultaneously and the separation of the two types of information is achieved via software. The instrument is able to analyze samples spanning from fine powders to pristine surfaces with clean and smooth cut. In the latter case, the rover should be equipped with an appropriate tool for sample preparation (i.e., the

Rock Abrasion Tool onboard MERs). The instrument should be as close as possible to the sample surface during the integration time.

Testing instrument capabilities: A number of measurements have been acquired on terrestrial analogues of Martian soils/rocks and compared with measurements acquired using commercial instruments in order to test detection limits and accuracy.

Further testing is planned with lunar analogues and samples, such as mare regolith and basalts, and various glass types as well.

References: [1] Marinangeli et al. (2007) *LPS XXXVIII,* Abstract #1322. [2] Marinangeli et al. (2011) *EPSC-DPS.,* Abstract #1232.

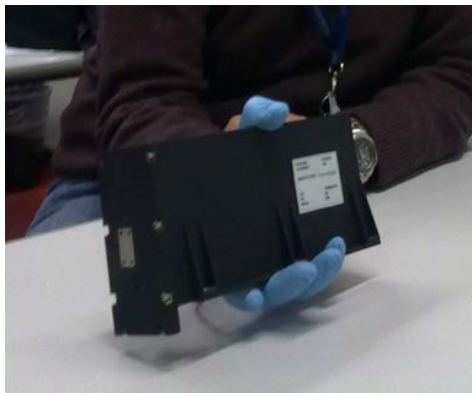

Figure 1. MARS-XRD Structural and Thermal Model (STM) developed at TASI-Milan.

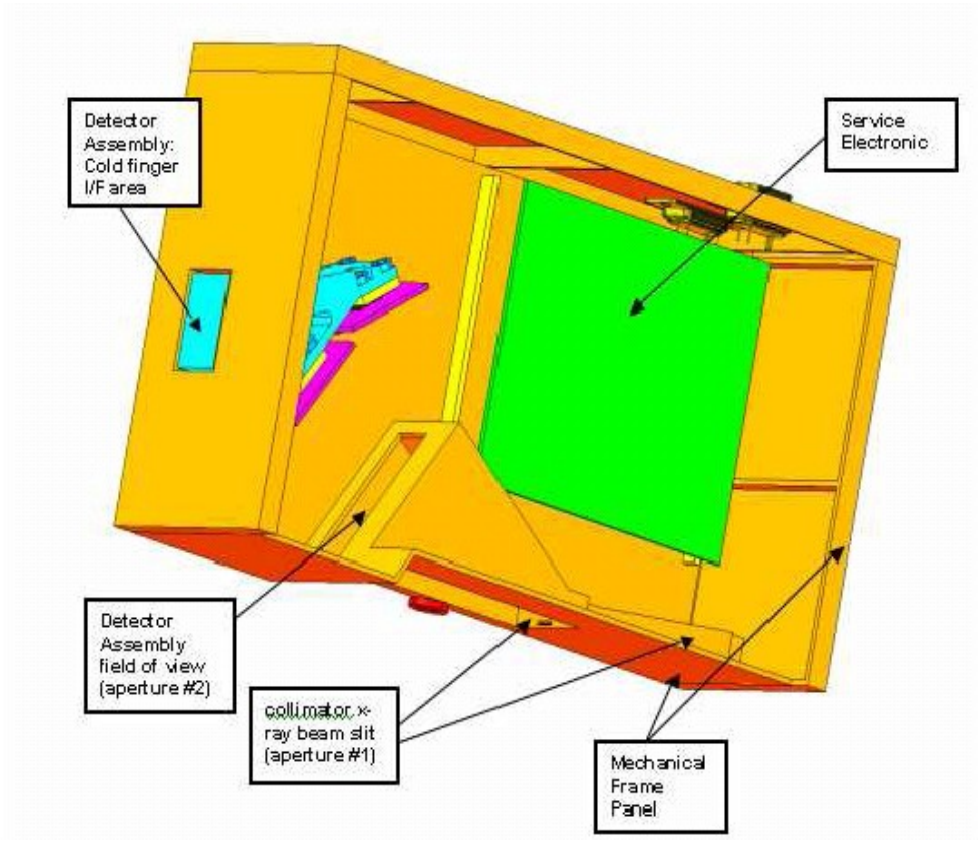

Figure 2. Drawing of the MARS-XRD instrument with the description of the different subsystems.

CHEMICAL COMPOSITION OF LUNAR REGOLITH IN CRATERS WITH COLD TRAPS AT THE LUNAR POLES. S. G. Pugacheva and V. V. Shevchenko, Sternberg Astronomical Institute of the Lomonosov Moscow State University, 13 Universitetsky pr., 119992 Moscow, Russia, pugach@sai.msu.ru.

Introduction: Introduction: The article presents the results of integrated study of the craters at lunar South and North Poles with high content of hydrogen in the soil matter. The surface of the craters that are situated in the area of the lunar Poles is not exposed to the direct sun light and has extremely low temperature (below 90 K), which remains for billions of years.

The estimated values of photometric parameters in visible and infrared spectral ranges show that the illumination conditions of pole craters create prerequisites for formation of considerable water ice fields in the cold traps of the craters. Measurement made by KA Lunar Prospector (LP) and Lunar Reconnaissance Orbiter (LRO) proves high content of hydrogen in the lunar soil [1, 2, 3 and 4].

The main target of research is to determine any indirect indicator of the hydrogen presence in the soil of the Moon's regolith. We have analyzed the ultimate chemical composition of thorium, ferric oxide and hydrogen contents in the soil matter from 11 craters with the cold traps.

There were selected the craters at South Pole: Cabeus (85.28°S, -41.81°W, D=100.58 km), Shackleton (89.63°S, 132.32°E, D=21 km), Faustini (81.18°S, 85.02°E, D=42.48 km), Shoemaker (88.03°S, 39.85°E, D=48.33 km), Haworth (87.2°S, -7.49°W, D=51.42 km), and craters located near the North Pole: Peary (88.57°N, 25.73°E, D=85.15 km); Rozhdestvenskiy (85.49°N, -158.44W, D=180 km); Whipple (89.14°N, 119.92°E, D=14.53 km); Hermite (87.08°N, -91.31°W, D=104.64 km), Byrd (85.38°N, 12.05°E, D=91.92 km); Lenard (85.17°N, -109.32°W, D=45.24).

We calculated the histogram demonstrated the height distribution in the craters with cold drapes. The modes of the height distribution in the Cabeus, Shackleton, Faustini, Shoemaker and Haworth craters are -4.5, -0.70, -2.7, -3.5, -3.5 km, respectively. Modes of the height distribution of the craters of North Pole are equal Peary (-2.6 km), Rozhdestvenskiy (-5.0 km), Whipple (-1.9 km), Hermite (-3.5 km), Byrd (-1.3 km), Lenard (-2.5 km).

Regarding the altitudinal level the crater Cabeus and crater Rozhdestvenskiy are situated significantly lower than other craters with "cold traps".

The abundances of the chemical elements: In order to make estimation of the chemical composition elements of the soil matter in the cold traps were used the measurements of Th, FeO and H contents by a spectrometer on KA LP [1]. The measurements of the ultimate soil composition have the spatial resolution of 0.5° x 0.5° that approximately coincides with a tetragon with 15 km side. The histograms of the elements distribution of the soil chemical composition of the craters with cold traps and table of statistical parameters will be represented in our article.

The most difference of thorium and hydrogen contents is observed in soil matter of craters. The concentration of FeO ferric oxide in the craters is approximately the same. Probably the low content of thorium in the area of the Cabeus and Rozhdestvenskiy craters is resulted from high irregularity of the surface micro-relief. In our articles published in 2003, we resumed a regression dependency between thorium content in the lunar soil samples and degree of irregularity of the surface micro-relief [5, 6, 7].

The histograms in Figure 1, 2 show the distribution of the hydrogen content in the craters, plotted using the data from LP catalogue. According to figures the general distributions of hydrogen in craters Cabeus and Roshdestvenskiy are of polymodal nature and can be divided into two marginal distributions that have form close to normal distribution. In this case, the first mode in crater Cabeus means 125 ppm, and the second mode of the hydrogen distribution is 170 ppm. The second mode of the hydrogen distribution matches with the northern shadowed border of Cabeus formation. The hydrogen distribution of the Roshdestvenskiy crater has also two modes, 115 ppm and 140 ppm. High content of hydrogen observes in craters Peary (155 ppm) and Whipple (150 ppm).

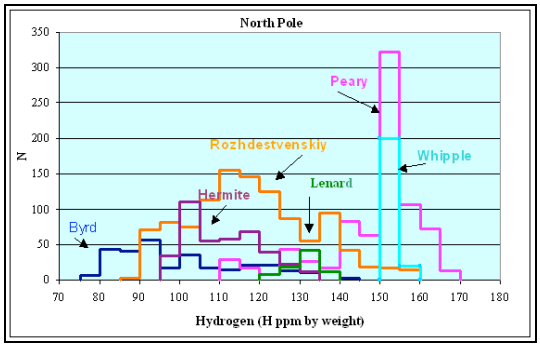

Fig. 1. The hydrogen distributions in the surface layer at the lunar craters near the North Pole.

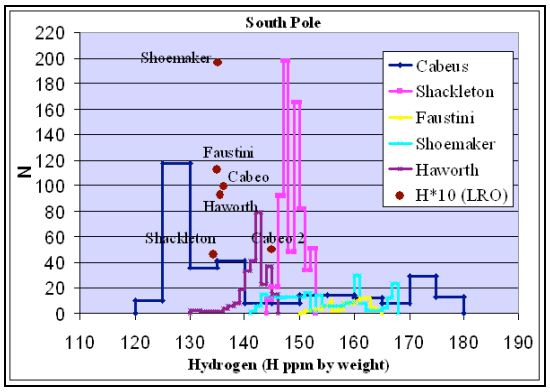

Fig. 2. The hydrogen distributions in the surface layer at the lunar craters near the South Pole. Brown circles show values of the hydrogen content measured by KA LRO.

The hydrogen measurement gaps between two spectrometers might be caused by time of lunar day and migration of hydrogen molecules into lower and cold surface areas under influence of the sunlight. As per one of the hypothesis, the water and hydroxyl may be the components of volcanic rock minerals of phosphates group.

Conclusions: The analysis of the results obtained confirms that the continental areas of the lunar Poles are not homogenous. The variety of basalt types is resulted from the depth and melting temperature of any substance in accretion process. The changes in basalts composition are contributed with the meteoroid- and comet impacts that cause the substance melting and formation of various breccias. Probably, the regolith of the “cold traps" has higher porosity and irregularity microstructure that can create conditions to accumulation of H_2O in the subsurface. Possible, this type to surfaces (oxhide) is the relic type of porous surface, which was formed under influence of a continental ice.

References: [1] Lawrence, D. J. et al., (2002) *J. Geophys. Res., Ser. E,* vol. 107, no. 12, p. 5130. [2] Ivatury V., Mcclanahan T.P. (2009) *LPS XXXX,* Abstract #1134. [3] Litvak, M.L., Mitrofanov, I.G., et al. (2011) *LPS XXXXII,* Abstract #1765. [4] Mitrofanov I. G., Litvak, M.L., et al. (2011) *LPS XXXXII,* Abstract #1787. [5] Shevchenko V. V. et al. (2003) *Proceedings of the International Lunar Conference,* 511-513. [6] Pugacheva S. G. and Shevchenko V. V. (2003) *LPS XXXI,* Abstract #1112. [7] Pugacheva S. G., Shevchenko V. V. (2003) *LPS XXXI,* Abstract #1112.

SIDEROPHILE ELEMENTS IN THE MOON: METAL-SILICATE PARTITIONING AND IMPLICATIONS FOR LUNAR CORE FORMATION. N. Rai and W. van Westrenen, Faculty of Earth and Life Sciences, VU University Amsterdam, The Netherlands (n.rai@vu.nl).

Introduction: The popular paradigm for the formation of the Earth-Moon system considers the Moon to be a byproduct of a giant impact between a Mars-sized planetesimal and the proto-Earth. Material ejected from this massive collision and mainly originating from the impactor, accreted in orbit around the Earth to form the Moon. This high-energy process resulting in extensive melting on the Earth and Moon, would have lead to planetary-scale differentiation on the young Moon. As on Earth, such differentiation could have led to the formation of a metallic core on the Moon. Most models for the interior of the Moon include a relatively small iron-rich core, having a radius between 200 and 450 km [1,2]. A recent study [3] based on the reanalysis of Apollo lunar seismograms using advanced array-processing methods to search for the presence of reflected and converted seismic energy from the core, suggests the presence of a solid inner and fluid outer core, overlain by a partially molten silicate layer in the lower mantle. The precise composition, formation conditions, and thermal evolution through time of the lunar core are not well constrained at present.

Core-mantle differentiation in planetary bodies leads to majority of the siderophile elements being strongly partitioned into the iron-rich metallic core. Since the degree of extraction of these elements into metallic phases is governed according to their metal/silicate partition coefficients (D) and the pressure-temperature-composition conditions during core formation, abundances of these elements in the silicate Moon can in principle be used to constrain lunar core formation conditions and composition [2,4,5]. Here we re-examine whether a consistent set of lunar core formation conditions can be obtained to match observed siderophile element depletions in the silicate Moon based on recent improvements in our understanding of siderophile element partitioning.

Approach: Estimates of siderophile element abundances in the lunar mantle have previously been used to argue for the presence of a small metallic core (0.1-5.5 wt%) [2,4,5], but recent improved approaches developed to constrain terrestrial core formation models (including better thermodynamic models and the ability to model changing conditions through time) have not been applied to the Moon to date. Figure 1 shows observed levels of bulk lunar silicate depletion for siderophile elements, based on values from [5,6,7]. We combine recently published metal-silicate partitioning data for Ni, Co, Cr, Mn, Ga, P, Pb, W and V with literature data [8-19] and characterize the dependence of the partition coefficients(D) on temperature, pressure, oxygen fugacity

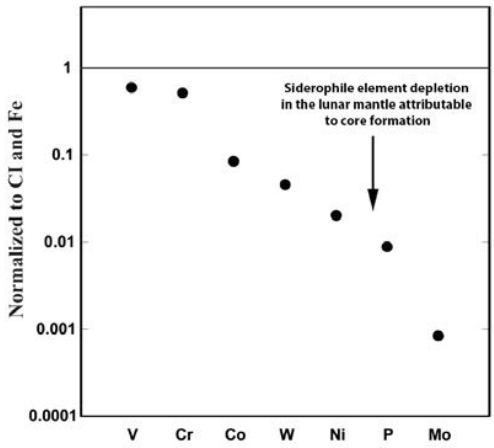

Figure 1. Estimated siderophile element depletion in the lunar mantle,based on refs. [5,6,7].

and silicate melt structure and composition to derive equations of the following form:

$$\log D = \alpha + \beta(\Delta IW) + \delta(1/T) + \varepsilon(P/T) + \chi(nbo/t) \quad (1)$$

Trace elements in metal alloys are known to strongly interact with major components such as Fe, Si, C and S, causing metal-silicate partitioning experiments performed under different compositional conditions to produce scattered results. Using a thermodynamic approach [13], all metal-silicate partitioning data used in this modelling work were corrected to a common reference point which is the effective value for a trace component mixing in pure metallic element in the liquid state. All partitioning data was parameterized according to Equation (1). For each element, only statistically valid regression coefficients were considered to model the conditions of lunar core formation Our parametrizations are based on partitioning data obtained at pressures between 1 atm and 6 GPa, covering the range of pressures in the Moon. There is a hot and ongoing debate about the question whether metal-silicate partition coefficients show different behaviour at low pressure (< 5 GPa) compared to pressures above 5 GPa [20-22]. By using data obtained at pressures that are relevant to the Moon only (P < 6 GPa) our results will be directly applicable to the Moon regardless of the final outcome of this debate. Using these parameterizations and the proposed bulk Moon composition of [4], we model core formation in the Moon.

Results: Pressure-temperature solution domains that would produce metal-silicate partition coefficients required to match the observed depletion of these elements in the lunar mantle were calculated for each element at changing conditions of oxygen

fugacity according to the following relation derived from Equation (1):

$$P = (T/\varepsilon)*[\log D - \alpha - \beta(\Delta IW) - \chi(nbo/t) - \delta(1/T)] \quad (2)$$

Figure 2 shows the resulting overlap in P-T solution space for Ni, Co W, P, and Mo in the pressure range of 3.5 - 4 GPa and temperature between 2100-2200 K at IW-1.5 and nbo/t =2.8, assuming a pure Fe core.

However, under these conditions, we did not find

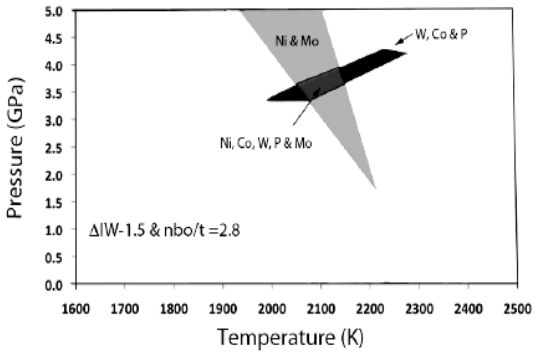

Figure 2: Overlap in the solution spaces for Ni, Co, W, P and Mo in the pressure range 3.5 - 4 GPa and between 2100-2200 K at IW-1.5 and nbo/t =2.8, assuming pure Fe metal.

any overlap between the solution spaces of the weakly siderophile elements V and Cr with those for Ni, Co, W, P and Mo. Both V and Cr show lithophile behavior at these oxidation conditions (Figure 3). At the more reducing conditions where V and Cr become siderophile enough to account for their observed mantle depletion, other elements such as Ni, Co, W, P and Mo become much more depleted than observed.

Discussion: Preliminary results suggest that when using the proposed bulk Moon composition of [4] and siderophile element abundances from [5,6,7], metal-silicate partitioning data for Ni, Co, W, P and Mo are consistent with the Moon possessing a small pure iron metallic core, with metal-silicate equilibration pressures close to the pressure at the current core-mantle boundary. As the pressure of equilibration obtained from analyses like these is generally taken as the approximate pressure at the bottom of a silicate magma ocean, this result would suggest the Moon was fully molten at the time of core formation.

Outlook: Geophysical models of the Moon [3, 24] support the presence of up to 6 weight% of a lighter alloying element such as sulphur in the lunar core and recent analyses of lunar melt inclusions [23] indicate that realistic lunar interior evolution models should also consider the constraints imposed

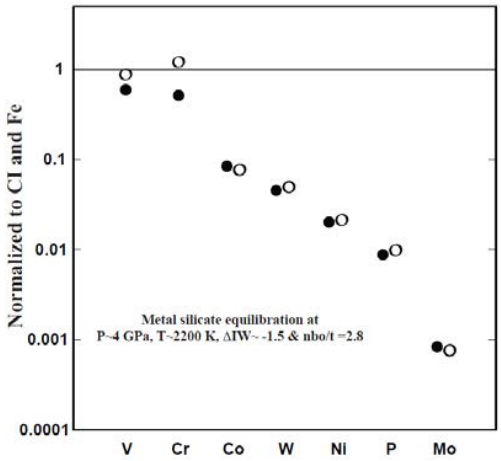

Figure 3: Solid symbols show the estimated element depletion in the lunar mantle. Depletion in Ni, Co, W, P and Mo can be accounted for by metal-silicate equilibration at P~4 GPa, T~2200 K, ΔIW~-1.5 and nbo/t = 2.8. Under these conditions V and Cr remain lithophile (open symbols).

by the presence of H_2O. Future work will include incorporation of the effects of light elements in the metal and the presence of water in the silicate on our results.

References: [1] Weiczorek et al. (2006) *Rev. Mineral. Geochem., 60*, 221-364 [2] Righter and Drake (1996) *Icarus*, *124*, 513-529 [3] Weber et al. (2011) *Science*, *331*, 309-312 [4] O'Neill (1991) *GCA*, *55*, 1135-1157 [5] Walter et al. (2000) In *Origin of the Earth and Moon*, U of A Press, Tucson, 265–289 [6] Newsom and Bessera (1990) *LPSC XXI,* 875–876 [7] Newsom and Runcorn (1991) *LPSC XXII,* 973–974 [8] Thibault & Walter (1995) *GCA*, *59*, 991-1002 [9] Li &Agee, (1996) *GCA*, *65*, 1821-1832 [10] Walter &Thibault (1996) *Science*, *270*, 1186-1189 [11] Jana & Walker (1997) *EPSL*, *150*, 463-472 [12] Chabot and Agee (2003) *GCA*, *67*, 2077-2091 [13] Wade and Wood, (2005) *EPSL*, *236*, 78-95 [14] Kegler et al., (2008) *EPSL*, *268*, 28-40 [15] Wood et al., (2008) *GCA*, *72*, 1415-1426 [16] Corgne et al. (2009) *GCA*, *72*, 574-589 [17] Cottrell et al. (2009) *EPSL*, *281*, 275-287 [18] Mann et al. (2009) *GCA*, *73*, 7360-7386 [19] Siebert et al. (2011) *GCA*, *75*, 1451–1489[20] Righter et al. (2011) *EPSL*, *304*, 158-167 [21] Palme et al. (2011) *EPSL*, *312*, 516-518 [22] Sanloup et al. (2011) *EPSL, 306*, 118-122 [23] Hauri et al. (2011) *Science, 333,* 213-215 [24] Garcia et al. (2011) *EPSL, 188*, 96-113.

PHOTOGEOLOGICAL STUDY OF CENTRAL UPLIFTS IN SOME LUNAR IMPACT CRATERS.

D. Rommel[1] and C. Koeberl[1,2], [1]Department of Lithospheric Research, University of Vienna, Althanstrasse 14, 1090 Vienna, Austria; [2]Natural History Museum, Burgring 7, 1010 Vienna, Austria (e-mail: daniela.rommel@univie.ac.at, christian.koeberl@univie.ac.at).

Introduction: The exact mechanism of the formation of central uplifts in impact structures is still debated. On the one hand, exposed terrestrial craters are mostly eroded, covered, or buried, which makes them difficult to reach for detailed studies; on the other hand, a large number of craters on other planetary bodies are well preserved, but again difficult to investigate in detail. Nevertheless, terrestrial craters have been studied, e.g., through international large scale drilling projects. Such work included, for example, investigations of the physical properties of the rocks, and the determination of shock attenuation in the central uplift by combining petrographic studies with numerical modeling. Work on the Bosumtwi impact crater, Ghana, has shown that brittle deformation played an important role in the formation of the central uplift in such a medium-sized impact structure [1, 2]. Extraterrestrial impact craters can be studied by, for example, high resolution camera systems or spectrometers for structural, thermophysical, or mineralogical studies. It is difficult to compare detailed terrestrial field work, and laboratory studies, with remote sensing investigations on other planets.

The aim of this work is to use photogeological studies to search for signs of similar brittle deformation in central uplifts of craters on the Moon. This was done by searching for evidence of coherent blocks, possibly in the form of distinct layering, in central peaks. An indication would be if there is a common dip direction in layered and tilted deposits in these central uplifts. We have results for four craters, with a diameter of 40-100 km and a central peak of 10-20 km diameter, with some first observations six more craters to obtain preliminaryinterpretations.

Uplift Formation: Many parameters, such as lithology, temperature, density, and other solid/elastic properties influence the extent, shape, and size of a central uplift, as well as shock levels attained in the rock. In complex impact structures, the original position and distribution of shocked rocks is typically modified when the rebound of the crater floor leads to the formation of a central uplift. Thus two processes act during the modification stage: downward-directed gravitational collapse of the inner rim and uplift of the transient crater floor. The initially steep walls of the transient crater collapsed under gravitational forces, forming characteristic terraces.

Concerning the development of the central uplift, the formation is thought to occur by displacements along faults as a brittle component in the case of moderately sized impact structures, whereas in the case of larger impact structures central uplifts involve fluidization and/or large differential movements of target blocks. To see if similar processes can be detected in lunar craters, we performed some initial photogeological analysis to search for layering or bedding in central peak formations.

Methods; Theophilus Crater: For detailed photogeological analysis we used high resolution photograpic images from the Narrow Angle Camera (NAC) of the Lunar Reconnaissance Orbiter spacecraft. The processing of the individual orbital stripes was carried out by using the Integrated System for Imagers and Spectrometers (ISIS), a specialized image processing package from the U.S. Geological Survey. The resolution for some of the images is up to 0.4 m/px and is used here for our interpretations and conclusions.

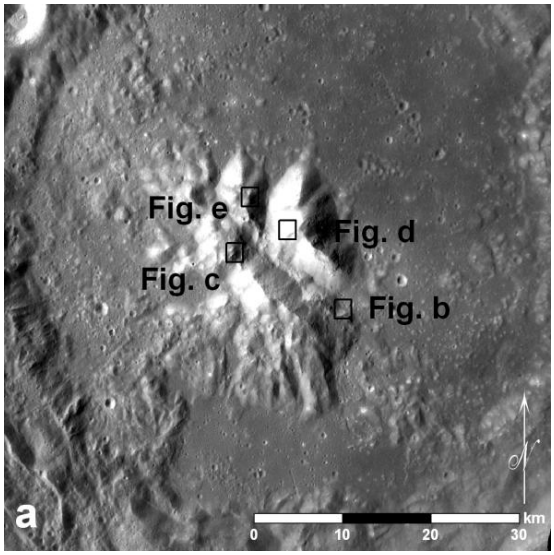

Fig. 1a. LROC WAC image M119679316ME of the central peak of the crater Theophilus (lat. -11.4, lon. 26.2). The boxes shows the close-up views of the research areas discussed in Figures b, c, d and e.

One of the craters studied here is the complex impact structure Theophilus, located (-11.4°S, 26.4°E) north-west of Nectaris, with a diameter of ~100 km, with a central peak extent of 15-20 km, and ~1.5 km in height (Fig. 1a), and an Eratosthenian age [3]. Initial investigations of Theophilus date back to the early 19th century, and later observations with the 40-inch Yerkes refractor were used to analyze its structural layout and composition. It was even postulated that the central peaks were covered in snow and ice [4, 5]. Recent studies include high spatial and spectral resolution data from the Moon Mineralogy Mapper (M^3) instrument onboard the Indian Chandrayan-1 spacecraft and indicate that the main lithol-

ogies are dominated by anorthosite, but that on top of most of the central peaks there are some outcrops of a rock rich in low-Fe / Mg-spinel [6].

Results: In our photogeological investigations we found several different locations where rock packages of 10 to 50 m thickness seem to crop out (and are not entirely covered by regolith), and for those we attempted to measured strike and dip. Their average dip direction is in the range of ~145-200° SW-NE/SO-NW (Fig. 1b, c, d and e). Also, we observed almost vertically dipping rock packages (Fig. 1b, the red ? symbol), with the same orientation of SW-NE, suggesting a general steep collapse of the blocks that constitute the central uplifts.

Interpretations: The presence of visible compact blocks preserving layers is considered in this work as evidence that during of the impact process the target, at least at the depth from which the central uplift material came from, was not completely fluidized or melted. A model of acoustic fluidization, which has been advocated for central uplift formation, would not be expected to result in such large-scale blocks as those that were observed. Naturally it is difficult to generalize from just one crater; thus we will try to find similar outcrops at other central peaks of lunar craters.

Conclusion: On the central peak of Theophilus we noted evidence for layering in large blocks. Lunar craters have a rather simple target lithology; at terrestrial craters, this can be much more complicated, and the presence of water also will cause a difference in the melting and deformation processes in that it will be more difficult to preserve blocks as large as those seen at Theophilus.

Acknowledgments: We thank J. Plescia for invaluable help with the ISIS program and the images.

References:

[1] Ferriere, L., Koeberl, C., Ivanov, B., and Reimold, W.U. (2008) Science 322, 1678–1681.

[2] Koeberl, C. (2009) Lunar Reconnaissance Orbiter Science Targeting Meeting, Abstract #6030.

[3] Wilhelms, D. E. (1987) The geologic history of the Moon, U.S. Geol.Surv.Prof.Pap. 1348, 302 pp.

[4] Pickering, W. H. (1917) The snow peaks of Theophilus, Popular Astronomy, Vol. XXV, No.3, 148-155.

[5] Bolton, S. (1905) Theophilus, MmBAA, Vol XIII, 149-154.

[6] Dhingra, D., Pieters, C.M., Boardman, J.W., Head, J.W., Isaacson, P.J. and Taylor, L.A. (2011) Geophysical Research Letters 38, L11201

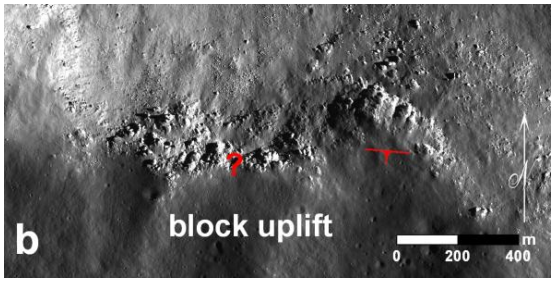

Fig. 1b. Blocky uplift, red symbol indicates dipdirection, red ? may indicate a vertical dip (LROC NAC image M116140939).

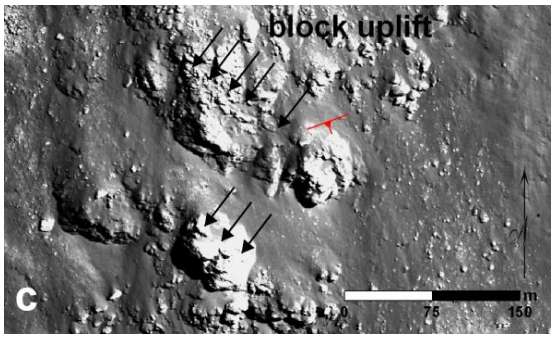

Fig. 1c. Black arrows indicate solid blocks with layering, partially exposed, partially covered by debris flows of regolith or impact-melt. Previous studies suggest the presence of Mg-spinel/plagioclase on top of the peaks [6] (LROC NAC image M116140939).

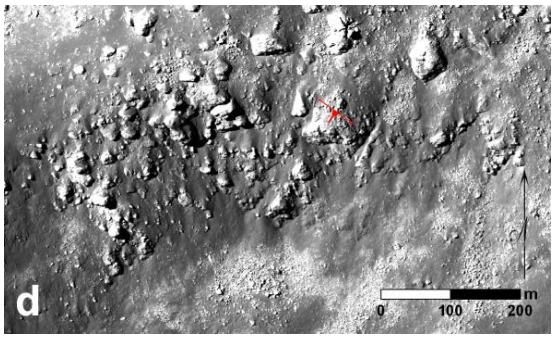

Fig. 1d. Partially exposed solid blocks, partly covered by debris flows of regolith or impact-melt. Red symbol indicates dipdirection (LROC NAC image M152702349).

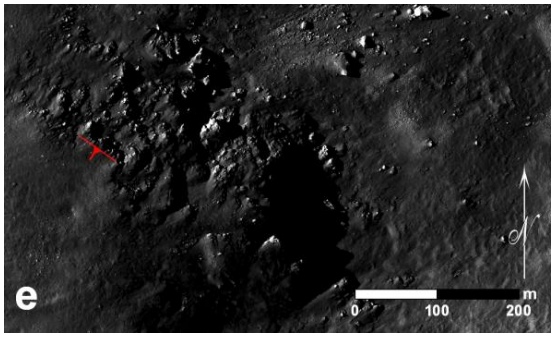

Fig. 1e. Brittle blocks, close to a small impact crater. Red symbol indicates dipdirection (LROC NAC image M168035080).

MINERALOGICAL AND GEOCHEMICAL CHARACTERIZATION OF THE MOON SURFACE USING COMBINED RAMAN-LIBS TECHNIQUES. F. Rull[1], A. Vegas[2]. [1]Centro de Astrobiologia, Unidad Asociada UVA-CSIC. Ed.INDITI P.203 Parque Tecnologico de Boecillo, E47151 Boecillo (Valladolid) (Spain). [2]TCP Sistemas e Ingenieria, C/ Fernández Caro, 7 E28027 Madrid (Spain) (Corresponding Author F. Rull, rull@fmc.uva.es, Tf. +34983140501)

Introduction: Mineral phase identification combined with chemical composition using Raman and LIBS spectroscopic techniques respectively constitutes a very powerful tool for surface analysis on Earth and in planetary exploration. Used at stand-off distances these techniques show particular advantages when placed on rovers or landers compared with contact techniques because they simplify the operation mode and allow to reach targets usually unreachable to the robotic arms.

In this paper a prototype of combined Raman-LIBS instrument is presented and the surface science capable to be performed at the Moon is stressed on the basis of the results obtained in laboratory and field conditions in representative Lunar-like mineral samples. In order to be consistent with the potential operation mode of the Lunar Lander for the nex ESA mission to the Moon, these spectra were performed in contact mode using the Raman part and in remote mode up to 15 meters using both the Raman and LIBS techniques coupled to a small telescope. The instrument used is basically the Raman instrument under development for ExoMars mission with some modifications.

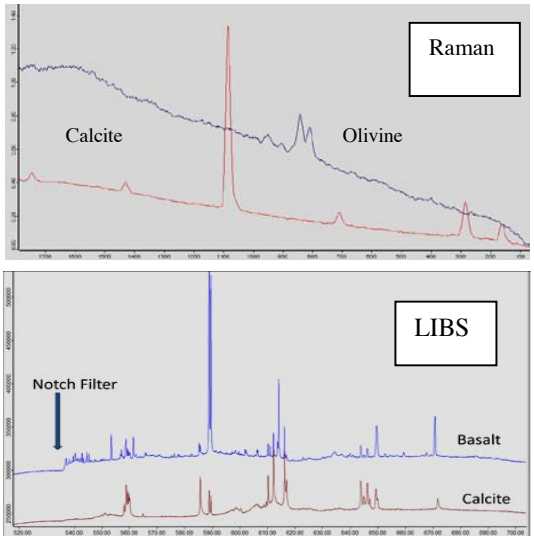

Figure 1. Raman and LIBS spectra of basalt and calcite obtained at 15 meters distance. From Raman the olivine mineral phase is shown.

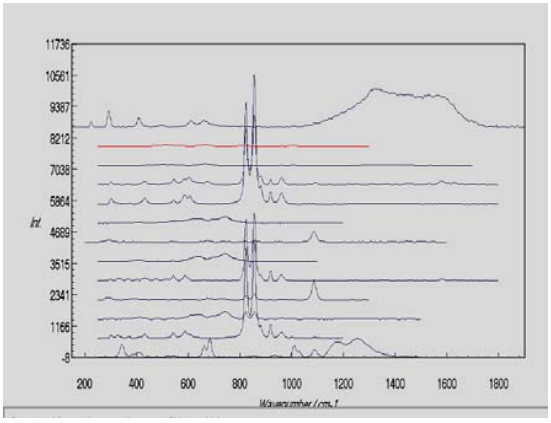

Figure 2. Raman spectrum of a basalt sample taken in contact mode using the Raman instrument for Exomars. The Raman optical head is attached to a robotic arm and spectra are obtained in automatic mode without any sample preparation.

Conclusions

The results obtained show that the combined instrument is a powerful tool for supplying detailed mineralogical and geochemical information of sample surfaces at the sub-millimetre scale in the range from contact to 20 meters and in consequence constitutes a potential candidate for enabling future exploration of the Moon surface. These results also show that mineral identification is very precise using Raman in contact mode while surface geochemistry is quite well adapted to the remote LIBS operation.

SEARCHING FOR WATER ICE PERMAFROST: LEND RESULTS FROM LRO. A. B. Sanin, I. G. Mitrofanov, M. L. Litvak and A. V. Malakhov, Space Research Institute, Profsoyuznaya street 84/32, Moscow, Russia, 117997, sanin@mx.iki.rssi.ru.

Introduction: We use data gathered by the Lunar Exploration Neutron Detector (LEND) collimated sensors during more than one year of the mapping phase of NASA's Lunar Reconnaissance Orbiter (LRO) mission to make estimations of the epithermal neutron flux from the lunar circumpolar regions. Results of testing for water ice permafrost in Permanently Shadowed Regions and in sunlit areas will be presented.

MIMOS IIA – A TOOL FOR CHEMICAL AND MINERALOGICAL CHARACTERIZATION OF LUNAR DUST AND REGOLITH AND IN SITU REOURCE UTILISATION. C. Schröder[1], G. Klingelhöfer[2], R.V. Morris[3], M. Blumers[2], B. Bernhardt[4], J. Brückner[5], and P. Lechner[6], [1]University of Bayreuth and Eberhard Karls University Tübingen, Siwartstr. 10, 72076 Tübingen, Germany, christian.schroeder@ifg.uni-tuebingen.de, [2]Institute of Inorgnic Chemistry and Analytical Chemistry, Johannes Gutenberg-University, Staudinger Weg 9, 55128 Mainz, Germany, klingel@mail.uni-mainz.de, [3]NASA Johnson Space Center, Houston, TX, USA, [4]Von Hoerner & Sulger GmbH, Schwetzingen, Germany, [5]Max-Planck-Institute for Chemistry, Mainz, Germany, [6]PN Sensor GmbH, Munich, Germany.

Introduction: MIMOS IIa is a combined Mössbauer and X-ray Fluorescence (XRF) spectrometer, which enables the simultaneous characteriazation of Fe-bearing mineralogy, Fe oxidation states and chemical composition of lunar dust and regolith [1,2]. We proposed this instrument in response to the Request for Information for ESA's First Lunar Lander in 2009. The subsequently defined model payload for the phase B1 study included an X-ray spectrometer to determine the elemental composition of lunar dust and the chemistry of potential resources. Here we will briefly describe the instrument and show how MIMOS IIa will meet and exceed those requirements.

Instrument Description: MIMOS IIa is an advanced version of the highly successful Mars Exploration Rover (MER) Mössbauer spectrometers [3]. It consists of (i) a sensorhead (Fig. 1) housing the Mössbauer drive, the detector system and amplifiers, and the radition source, and (ii) an electronics board holding the data acquisition and instrument control unit (CPU + FPGA), voltage converters, and electrical and data interfaces to the spacecraft.

Dimensions, mass, power consumption, data rate. The sensorhead has a volume of 50 × 53.5 × 94 mm³, the electronics board of 100 × 160 × 20 mm³. The whole system including connecting cables weighs less than 500 g. Power consumption is 4 W during data acquisition and can be turned off completely if the instrument is not in operation. Data product size per analysis is 512 kBytes (4 Mbit).

Detector system and analysis time. One weakness of the MER instruments was the long data acquisition time of 8 hrs with a fresh radiation source and mutliples thereof upon its decay [4]. MIMOS IIa uses Si Drift Detectors (SDDs) [5] instead of Si PIN diodes. Their better energy resolution leads to an improved signal-to-noise ratio and effectively reduces the required measurement time by an order of magnitude. Furthermore, they allow high resolution XRF spectroscopy down to ~1 keV, i.e. detection of elements with Z > Na, in parallel to Mössbauer measurements.

Radiation source. The decay of the radioactive isotope ^{57}Co in Rh matrix source provides the 14.4 keV γ-rays used for Mössbauer spectroscopy, and 122 keV and 136 keV γ-rays as well as 6.4 keV Fe and 20.1 keV

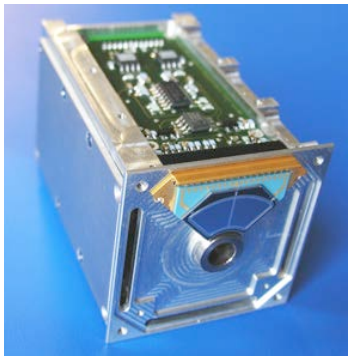

Figure 1. MIMOS IIa sensorhead with one of four SDD elements installed and detector amplification electronics exposed.

Rh K_α X-rays. It is therefore also an effecvtive excitation source for XRF spextroscopy. Compared to X-ray tubes used in commercial handheld XRF spectrometers, the radioactive isotope has the advantage of zero power consumption. The halflife of ^{57}Co is 270 days which is comparable to the complete projected mission time of ESA's First Lunar Lander (17-29 days transfer time plus 6-8 months surface operations). For comparison, only the transfer time to Mars is on the order of one source halflife, and MER Opportunity is still operating 8 years (or ~11 haflifes) after landing.

Flight heritage and Technology Readiness Level. MIMOS IIa combines the flight heritage of the miniaturized Mössbauer Spectrometer MIMOS II (e.g. MER [3], Beagle 2 [6], Phobos-Grunt [7]) and the experience with SDDs to obtain XRF spectra with the Alpha Particle X-ray spectrometer (APXS; e.g. MER [8], Rosetta [9]). In 2008, a copy of the MER Mössbauer spectrometers was used as process monitor and prospecting tool in a NASA-led field test on Mauna Kea, Hawaii, to test in situ resource utilization (ISRU) hardware concepts for oxygen production from lunar regolith [10]. A prototype MIMOS IIa was used in a similar ISRU field test on Maun Kea in 2010 [11,12]. MIMOS IIa has been assessed as TRL 5 following

ESA's ExoMars Payload Design Review in November 2008.

Analysis of Lunar Dust, Regolith and Potential Resources: Knowledge of the chemical and mineralogical composition is fundamental for understanding the properties of lunar dust, regolith and potential resources. MIMOS IIa can quantitatively determine the composition for elements with Z > Na, identify Fe-bearing mineral phases and quantify the distribution of Fe between the mineral phases. It provides complementary information to other mineralogical techniques such as X-ray diffraction and Raman-LIBS, e.g. the quantification of Fe oxidation states or information on nanocrystalline and amorphous material, such as nanophase Fe(0) particles and glass.

Characterisation of lunar dust and regolith. The information provided by MIMOS IIa allows to differentiate between the major consitutuents of the lunar surface - i.e. maria, highlands or KREEP material - and to distinguishit between volcanic-ash regolith and impact-derived regolith [13].

The Fe(0) content of surface fines is a measure of maturity, i.e. exposure time [13]. Measurement of the Fe(0) content of freshly exposed fines at the beginning and end of the Lunar Lander mission can help to constrain micrometeoroid flux at the landing site.

To understand the possible electrostatic mobilization of lunar dust, it is important to know the dielectric properties of its mineral constituents, for example by determining the abundance of insulating glass versus conductive Fe metal.

In Situ Resource Utilisation. Oxygen can be extracted from lunar regolith, whereby the yield is directly proportional to FeO content [14,15]. FeO is reduced by hydrogen to form Fe metal and water. The hydrogen source may be residual hydrogen in the tanks of a lunar lander. The water can be split electrochemically into oxygen and hydrogen. While the oxygen is consumed, the hydrogen is fed back into the reaction. Several such hardware concepts were evaluated during two field tests on Mauna Kea, Hawaii, in 2008 [10] and 2010 [11,12]. MIMOS IIa worked successfully as both a process monitor and a prospecting tool. As process monitor, Fe oxidation states were determined before and after reductive treatment, and oxygen yield was calculated. As prospecting tool MIMOS IIa was mounted on a feedstock collecting rover. Feedstock would be selected for high FeO content and analysed for mineral content. The latter determines the optimum temperature during reduction: Ilmenite is reduced at 900°C, olivine at 1000°C and all other FeO-bearing phases at 1100°C.

Figure 2. MIMOS IIa prototype installed as prospecting tool on the NORCAT rover during the 2010 lunar ISRU field test on Mauna kea, Hawaii [11].

Summary: MIMOS IIa is a combined Mössbauer and XRF spectrometer within the volume, mass, power and data volume constraints of a single instrument. It provides chemical and mineralogical information fundamental for the understanding of the properties and behavior of lunar dust, regolith and potential resources. It is derived from separate precursor instruments, each with extensive flight heritage. It has a certified TRL ≥ 5. A prototype has been successfully implemented in lunar ISRU field test campaigns.

References: [1] Blumers M. et al. (2010) *Nucl. Instr. and Meth. A, 624,* 277-281. [2] Schröder C. et al. (2011) *Geochemistry: Exploration, Environment, Analysis, 11,* 129-143. [3] Klingelhöfer G. et al. (2003) *JGR, 108*(E12), 8067. [4] Schröder C. et al. (2008) *Hyperfine Interactions, 182,* 149-156. [5] Lechner P. et al. (1996) *Nucl. Instr. and Meth. A, 377,* 346–351. [6] Pullan D. et al. (2003) ESA SP-1240. [7] Rodionov D. et al. (2010) *Solar System Research, 44,* 362-370. [8] Rieder R. et al. (2003) *JGR, 108*(E12), 8066. [9] Klingelhöfer G. et al. (2007) *Space Science Reviews, 128,* 383–396. [10] Morris R.V. et al. (2009) Lunar Base Symposium, Abstract #A5-5. [11] Klingelhöfer G. et al. (2011) *LPS XLII,* Abstract #2810. [12] Ten Kate I. et al. (2012) *Journal of Aerospace Engineering,* in press. [13] Morris R.V. et al. (1998) *Hyperfine Interactions, 117,* 405-432. [14] Allen C.C. et al. (1994) *JGR, 99*(E11), 23173-23185. [15] Allen C.C. et al. (1994) *JGR, 101*(E11), 26085-26095.

THE MOLTEN SALT ELECTROLYTIC WINNING OF OXYGEN AND METAL FROM LUNAR REGOLITH. C. Schwandt[1,2], J. A. Hamilton[2], D. J. Fray[1], and I. A. Crawford[3], [1]Department of Materials Science and Metallurgy, University of Cambridge, Cambridge, UK, [2]Green Metals Ltd, London, UK, [3]Department of Earth and Planetary Sciences, Birkbeck College, University of London, London, UK (cs254@cam.ac.uk, jah@greenmetals.co.uk, djf25@cam.ac.uk, i.crawford@ucl.ac.uk).

Abstract: The present article provides a summary and assessment of the various techniques that have been, and still are, considered for the extraction of oxygen from lunar source materials. Classical approaches are based on chemical reduction with hydrogen and methane, vapour phase pyrolysis or aqueous acid treatment. While all these methods have been demonstrated successfully in the laboratory, they also exhibit major drawbacks. A particular issue is that these methods only provide high yields of oxygen when the feedstock is rich in iron oxide. Another classical approach is based on the electrolysis of molten regolith. This does not require a specific feedstock, but the operating temperature is very high and there are a number of processing issues.

The main emphasis of this article is on a novel electro-deoxidation process that has been derived from the FFC-Cambridge process for the direct molten salt electrolytic conversion of metal oxides into the corresponding metals and alloys [1]. This method relies on the electrolysis of lunar materials such as ilmenite or regolith in the solid state in such a way that the oxygen from the oxide cathode is extracted in its ionic form, transported through the molten salt electrolyte, and then liberated in its molecular form at a suitable anode. The method has been validated in the laboratory, and has the additional advantage that a metal product is generated concurrently with the oxygen. In order for this to become possible, it was necessary to identify a material that may be used long-term as an oxygen-evolving anode in the molten salt. This is a key advance that is also of immense importance to the successful industrialisation of the FFC process for terrestrial applications [2]. Future targets are to develop the process such that the use of a powder oxide precursor becomes possible, so the cumbersome preparation of sintered oxide bodies is avoided, and a liquid cathode is formed in-situ, so the continuous winning of the metal product is achieved.

The recent discovery of water ice on the moon is highlighted but it is also pointed out that the mining, melting and electrolysis of the water ice would face tremendous challenges owing to its most inconvenient location in extremely cold and permanently shadowed lunar areas. The notion therefore is that the research on, and the development of, alternative ISRU processes for the extraction of oxygen from lunar materials continues to be an area of major relevance.

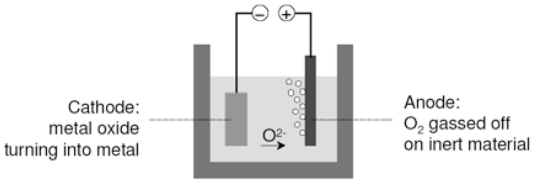

Figure 1. Schematic of the molten salt electro-deoxidation cell for the winning of oxygen and metal from lunar materials.

Figure 2. Laboratory rig for the electro-deoxidation of lunar materials.

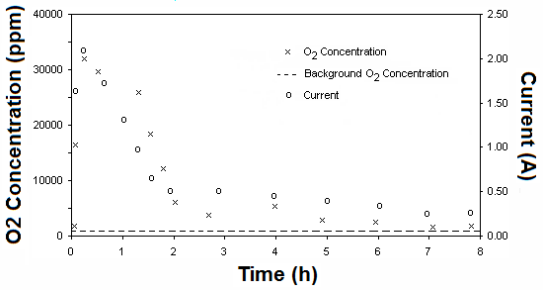

Figure 3. Data recorded during a typical electro-deoxidation experiment of lunar materials.

References: [1] Chen G. Z., Fray D. J., and Farthing T. W. (2000) Nature, 407, 361–364. [2] Schwandt C., Doughty G. R., and Fray D. J. (2010) Key Eng. Mat., 436, 13–25.

A MOON ROVER PLATFORM FOR SCIENTIFIC EXPERIMENTS FROM SELENOKHOD – THE RUSSIAN GOOGLE LUNAR X PRIZE TEAM.

E. V. Brodin[1], N. N. Dzis-Voynarovskiy[1], N. V. Golikov[1], A. B. Khalezov[1], S. V. Kuzhelevskiy[1], V. L. Kushmantsev[1], S. V. Maltsev[1], M. I. Malenkov[2], S. V. Romanov[1], D. A. Ruppel[1], S. Y. Sedykh, S. A. Smirnov[1], I. A. Sobolev[1], A. Yu. Shaenko[1] and T. A. Shahverdyan.

[1]Selenokhod LLC, 141700, 7 Zavodskaya str., Dolgoprudny, Moscow Region, Russia, selenokhod@selenokhod.com,

[2]Saint Petersburg State Polytechnical University, 195251, 29 Polytechnicheskaya str., St.Petersburg, Russia, postbox@stu.neva.ru.

On September 13, 2007 Google and X PRIZE Foundation announced Google Lunar X PRIZE (GLXP). The winner of the GLXP will be the team whose mobile robot (rover) will make a successful landing on the Moon, pass at least 500 meters and transmit high definition video and images to Earth.

The only Russian participant of the competition is Selenokhod. The project began in late 2008. Preliminary design of the rover has been done and received positive reviews from Space Research Institute of Russian Academy of Sciences. Creation of a test article for movement tests is in progress. First movement tests will start in the beginning of July.

The platform of a mini-rover being developed by Selenokhod is perfectly suitable for deployment from landing scientific lunar missions, like Russian Luna-Glob Lunar lander mission. A mini-rover could serve as an auxiliary instrument used to create a “long base” for some of the core scientific instruments of the lander. Reconnaissance and gathering regolith samples can be other options.

Selenokhod rover is intended to be a platform for various scientific instruments. The presentation will focus on some of the key technical requirements to be met to create a fully operational mini-rover for real-world lunar missions.

Selenokhod is considering options of deploying a mission on the Moon with Russian scientific community. This work is planned to be completed by November, 2012.

Lunar Dust Lifting Experiment (LDLE) for the ESA Lunar Lander: NASA/GRC-rover campaign in desert of Nevada

E. Seran[1], M. Godefroy[1],
N. Renno[2], T. Kremic[3], P.-Y. Meslin[4]

[1] LATMOS, [4] IRAP, France
[2] SPRL, [3] NASA GRC, US

In the framework of developing electric field instruments for the LDLE package we propose to organise a campaign of observations in desert of Nevada using a NASA/GRC rover. This campaign will address some critical issues which are encountered in the operations of electric field instruments on the deck of a planetary probe. The main objectives of this campaign are:
- Accommodation tests of electric field instruments on the rover;
- Estimations of the electric perturbations induced by the rover with different electrical grounding conditions;
- Estimations of electric perturbations generated by solar panels, conducting surfaces, masts, etc.
- Tests of the "space" versions of the electric field instruments and their masts;
- Comparison of electric field measurements onboard the rover with "static" measurements in different conditions of dust activity.
This campaign will provide us with a solid knowledge of the performances of our LDLE package. It shall also validate the design of electric field instruments, their supports and implementation.

DEVELOPMENT OF THE BIGGEST AND THE LEAST TERRESTRIAL PLANETS: EVIDENCE FROM COMPARATIVE STUDY OF THE EARTH AND THE MOON. E. V. Sharkov, IGEM RAS, Staromonetny per., 35, Moscow 119017, Russia; e-mail: sharkov@igem.ru

Introduction: Like all terrestrial planets, Earth and Moon have close inner structure (consist of iron cores and silicate envelopes) and developed at the close scenario [1 and references herein]. Geological processes on the both planetary bodies became after solidification of their global magmatic oceans which occurred from bottom to top and resulted in appearance the primordial sialic crust on the Earth and anorthositic - on the Moon.

Evolution of the Earth: The further tectonomagmatic development of the Earth began from eruptions of high-Mg magmas, derived from depleted mantle sources; such magmas predominated in Archean (komatiite-basaltic series) and especially in the early Paleoproterozoic (2.5-2.35 Ga), when magmas of the siliceous high-Mg series (SHMS) were common. At the range c. 2.35-2.0 Ga high-Mg magmas in the global scale were gradually replaced by geochemical-enriched magmas (Fe-Ti picrites and basalts of OIB type), common for Phanerozoic within-plate settings. At ~2.0 Ga it was followed by irreversible transition of the Early Precambrian plume-tectonics to modern plate tectonics which was accompanied by appearance of zones of oceanic spreading with thin newly-formed basaltic crust. Ancient sialic crust became to involve in descending flows in subduction zones and "buried" in the deep mantle be incorporated in "slab cementeries", revealed by seismic tomography [3].

Evolution of the Moon: Magmatic activity on the Moon began c. 4.4-4.35 Ga from the magnesian suite, which was rather close to the terrestrial SHMS on its geochemistry and isotopy [2]. Such activity lasted till ~4.2 Ga and via "alkaline" series (KREEP) was gradually changed by basaltic volcanism of newly-formed large maria depressions with thinned crust, appeared at 3.9-3.8 Ga. Such volcanism (including low- and high-Ti varieties, close in essence to terrestrial plume-related magmatism) lasted till ~3 Ga [4]. So, evolution of the Moon's tectonomagmatic processes was rather similar to the terrestrial one in the Paleoproterozoic. Such closeness evidently suggests that maria were not a result of heavy bombardment and very likely appeared above extended plume heads [1]. So, the Moon, as compared to the Earth, evolved more quick and by shorter scenario: there are no here granite-greenstone terranes and only tectonomagmatic processes, typical for the terrestrial early and middle Paleoproterozoic, occurred here. Maria with their powerful basaltic volcanism and thinned crust remind of terrestrial oceans; the latter also has begun as a result of plume activity how example of the Red Sea evidences.

Discussion and conclusions. The main feature of evolution of the Earth and the Moon is existence of irreversible change in geological and petrological processes at the middle stages their development. Their second stages were characterized by appearance of mantle derived magmas enriched in Fe, Ti, Nb, Ta and other incompatible elements in contrast to depleted magmas of the first stage. From this follows that such material was preserved in the deepest parts of the planetary bodies and was involved in tectonomagmatic processes only after long periods.

We suggest that such situation could be possible only the case when the bodies initially had heterogeneous structure and heated inward, while their outer shells cooled. Only such model can explain the fact that the primordial core material was conserved for about 2 b.y. into the Earth and ~0.4 b.y. into the Moon and only later was involved in tectonomagmatic processes. The fact that the magnetic field strength of the Earth and Moon attained a maximum at the crucial boundaries (~2.35 Ga and 3.9 Ga, respectively) [5,6] suggests that their cores had completely melted by that time which finally resulted in reorganization of their endogenic activity. The differences in evolution of tectonic and magmatic processes on the Earth and the Moon are probably related to different size of these planetary bodies.

Thus, the Earth and the Moon were developed at the same scenario, but more rapid and short-cut in case of the Moon, where situation evolved close to processes in the terrestrial Paleoproterozoic. Both planetary bodies experience irreversible change of tectonomagmatic processes at middle stages of their existence. The same transition suffered Venus and Mars, where ancient thick ("continental"?) crust, survived on uplifted terras, were replaced in considerable degree by secondary basaltic crust of vast young lowland plains. So, practically all terrestrial planets likely evolved as independent bodied by analogous way; situation on Mercury is not clear yet.

References:

[1] Sharkov E.V. and Bogatikov, O.A. (2010) *Geotectonics*, 44(2), 83-101. [2] Snyder, G.A. et al. *JGR,* 100, 9365–9388. [3] van der Hilst R.D. and Li C. (2010) *JGR*, 115, B07308, doi: 10.1029/2009JB006882. [4] Hiesinger H. and Head III J. W. (2006) *Rev. Mineral. Geochem*., 60, 1–81. [5] Rancorn S.K. (1983) *Nature,* 304(5927), 589–596. [6] Reddy S.M. and Evans D.A.D. (2009) *Geol. Soc. London, Spec. Publ*., 323, 1-26.

A mole deployed mass spectrometer for in-situ sub-surface volatile characterisation. S.Sheridan[1], M.W. Bardwell[1], A. D. Morse[1], S.J.Barber[1], T. Zoest[2] and I. P. Wright[1]. [1]Planetary & Space Sciences, The Open University, Walton Hall, Milton Keynes. MK7 6AA UK. (s.sheridan@open.ac.uk), [2]DLR Institute for Space Systems, Bremen, Germany.

Introduction: In recent years observational studies of the moon using orbital spacecraft and investigations carried out on returned samples have inferred the presence of a significant reservoir of volatile compounds, particularly water. It seems very likely that these volatile compounds will be concentrated at the poles and other locations, such as at depth, where low temperatures exist to provide cryogenic traps. However, the full inventory of these species, their concentration and their sources are unknown. Of particular interest is whether, or not, the abundances are sufficient to allow extraction and recovery as consumables for ISRU (In Situ Resource Utilisation) for use in the long term exploration of both the Moon itself and further out into the solar system.

Scientific aims: To address some of these issues a lander platform with a volatile analysis instrument is required that is specifically designed for identification and quantification of volatiles. The Lunar Volatile Resources Analysis Package is part of the provisional payload for the ESA European Lander [1] and aims to measure the chemical abundance, chemical and isotopic composition of volatiles from regolith samples and the lunar exosphere [2]. It is important to understand, and limit where possible the contamination of the lunar surface by external volatiles in order that measurements are scientifically meaningful. A landing sequence will contaminate the locality of the lander with rocket propellant by-products. Therefore, to allow meaningful scientific return careful considerations must be given to the sampling campaign, i.e. sampling from below or outside of the contamination zone. To this end, it is considered that the use of a sub-surface penetrating mole offers the possibility of accessing material from within the contamination layer and then at increasing depth into pristine sub-surface material.

Instrument concept: We are currently studying the design of a volatile analysis instrument and its associated delivery system that offers the opportunity of accessing material outside of the reach of conventional sampling arms. The design uses the heritage gained from the Ptolemy Mass Spectrometer [3] and the Beagle 2 sub-surface penetrating mole device [4]. The purpose of the study is to produce a prototype integrated package consisting of a mole deployment device and an integrated mass spectrometer instrument to enable in-situ characterization of the water and volatile content of the lunar regolith at increasing depth. The design takes into consideration the harsh physical conditions imposed on instrument payload by the penetration mechanism and consists of a miniature ion trap mass spectrometer, an ion detector and a low power field effect ion source. The fully integrated instrument will measure the abundance and chemical composition of volatiles released from regolith as the mole penetrator is driven to increasing depth. A CAD model of the mass spectrometer is shown in Figure 1 and instrument parameter and resources are shown in Table 2.

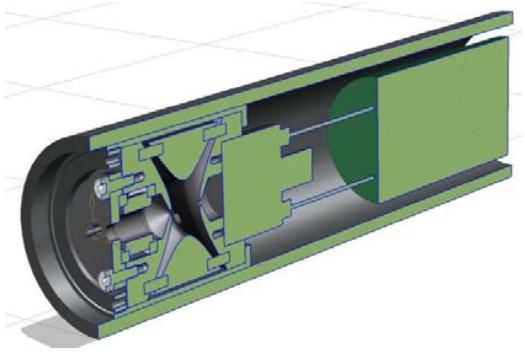

Figure 1 CAD model of the integrated mass spectrometer housed inside a 32 mm diameter sub-surface penetrating mole device.

Table 1 The mass spectrometer instrument parameters and resources

Parameter	Value
m/z range	10-150 amu
Mass resolution	Unit resolution [>18 at m/z 18; >200 at m/z 200]
Size	Cylinder (30 × 70 mm) [r_{0} = 5 mm]
RF frequency	1-2 MHz [during mass scan]
Power	< 3 W
Mass	300 g

Summary: An instrumented ground penetrating mole with an integrated miniature mass spectrometer would have applications for sub-surface volatile detection and characterization at other airless solar system bodies such as asteroids, comets and planetary moons.

References: [1] Carpenter J. D. et al. (2012) LPSC XLIII, Abstract#1990. [2] Morse A. D. et al. (2012) LPSC XLIII, Abstract#2320. [3] Morse A. D. et al. (2009) In: Rosetta: ESA's mission to the origin of the solar system, 19.6, 669–686. [4] Richter, H.E. et al. (2002) Planet. Space Sci. 50, 903–913.

ESTIMATE OF THE LUNAR SURFACE AGE: DISCUSSION AND RESULTS. A.A.Barenbaum[1] and M.I.Shpekin[2] , 1- Oil and Gas Research Institute RAS <azary@mail.ru> , 2 - Kazan Federal University <Michael.Shpekin@ksu.ru>

The facts and calculations suggest that the galactic comet nuclei are inevitably disintegrated in the atmospheres of Earth and Venus . This raises the powerful hypersonic jet [16], which does not create a crater, and the whole enormous kinetic energy of the comet is directed to the rocks heating up under the surface. Subsequently, this energy is released in different tectonic and volcanic processes [17]. Typical manifestations of these processes [18] in a "thin" lithosphere is the formation of seamounts on Earth, and shield volcanoes on Venus, while a powerful layer of the lithosphere - the so called phenomenon of "modern lifts".

The lift height was different. On most of the Pacific coast, it was the first hundreds of meters, on the Siberian platform 200-1000 m, in South Africa 300-400 m in the west and 900-1200 m in the east. The fastest growth occurred in mountainous terrain. Thus, the Arabian platform increased the height of 2 km, the Alps - up to 3 km, and the Himalayas - up to 6 km. The rise of asthenosphere is observed under most of the mountains . The lift leads to the uplift of crustal blocks in diameter ~ n· (10-100) km to a height of up to ~ 1 km in distance between the elevations greater than their diameter on a number of flat sections. In some places the rise of the asthenosphere was accompanied by modern intense outpourings of magma [19].

Similar processes occur on Mars. Calculations show that even 100 times less dense than Earth, its atmo-sphere leads to two important physical effects. On the one hand, it causes severe ablation of the galactic nuclei of comets, which reduces the diameter of a crater and shifts the distribution in Fig. 1, b relative to the Moon. And on the other hand, part of the energy goes into heating of comets asthenosphere under the southern hemisphere of Mars, which explains its uplifting at 2-4 km relatively flat and poorly cratered northern hemisphere. Huge volcanoes of Mars, with clear indexes of recent activity are probably the channels of excess heat from the asthenosphere of the planet.

Volcanic and tectonic processes have occurred on the Moon last 5 million years albeit on a smaller scale. They continue today.

Modern volcanotectonic processes on the Moon. Evidence of processes such as sloping "waterlogged" lava craters, craters broken by faults, etc. are marked by many researchers. The very same volcanic activity has been established on the Moon in1958 N.A. Kozyrev [20]. He found a release of pulverized volcanic ash and gas in the Alphonsus crater with a diameter of 120 km on the visible side of the Moon. Spectral analysis showed the presence in the ejection of molecules C2,CN,etc. Another, even more compelling example of volcanic processes is a volcano [5], discovered at the bottom of the Tsiolkovsky crater on the far side of the Moon by the pictures of the "Apollo 17" crew. Crater with a diameter of 180 km is characterized by a complicated structure and the central peak, typical for craters of cometary origin. Volcano height of 102 m is located almost in the center of the crater on a small flat oval elevated of plume nature diameter 24-26 km. On high-resolution images lava flows are visible, indicating an almost contemporary eruption of the volcano (Fig. 3).

Estimates made on the basis of images photogrammetry showed that the height of the volcano is about 102 meters. Diameter at the base of the volcanic cone is 1,760 meters. Slopes of the volcano have an inclination toward the bottom of the crater about 7°-8°. Emissions of the material are observed only in one direction, and this trend points to the central peak of the Tsiolkovsky crater. Other characteristics are listed in Table 1 [5], [21].

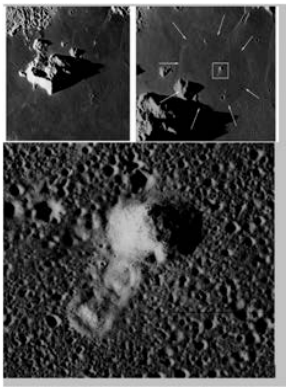

Table 1. Characteristics of the plume and the volcano at the Tsiolkovsky crater bottom

Plume	
Diameter	24 – 26 km
Longitude of center	129 33 E
Latitude of center	-19 27 S
Distance from central peak	32 km
Volcano	
Longitude	129 52 E
Latitude	-19 36 S
Base diameter	1760 m
Cone hight	102 m
Throat diameter	50-70 m
Cone inclination	7-8 degrees
Material ejection	2 × 1 km
Distance from central peak	36 km

Fig.2 Above left: central part of Tsiolkovsky crater bottom
Above right: studied site to the East from central peak

Fig.3 Below: Volcano and its vicinity in the rays of sunset
This territory is noted by white rectangular on Fig.2

(AS17-M-2798. Credit:NASA/JSC/Arizona State University)

At closer look at the top of the cone, small craters are visible . This is probably the vent through which volcanic material is done, now resembling a frozen lava. The diameter of the central crater is about 50-70 meters. Volcanic cone contains no small impact craters, indicating its modern age. Of the same say the reflective properties of the volcano, which are noticeably lighter than the surrounding terrain, because had not been yet covered with dark lunar dust. These facts speak in favor of recent, and perhaps even modern activity of the volcano.

It is significant that the volcano is located in the center of the low rise of the plume origin. The combination of these structures on the Earth is typical of shallow magma chamber, resulting in the crash site of galactic comets [22]. Probably, this camera has

arisen and exists today under the bottom of the Tsiolkovsky crater.

Summary and conclusions.

• The time of formation of the main topographic structures on the Moon - its continents and seas, as well as all the planets are not uniquely associated with the age of rocks composing these structures.

• The main factor that determined the modern look of the Moon, Mars and Mercury was the bombardment of the solar system by galactic comets between 5.0÷0.6 million years ago.

• Multiple galactic comets falling sharply increased flow on the Moon and planets, tectonic and volcanic processes that continue to this day.

• An example of these processes is discovery at the Tsiolkovsky crater, apparently, an active volcano 102 meters high, crowning a low plume base diameter of 24-26 km.

In this regard it should be emphasized that the question of the formation of geodynamic pockets under large impact craters still have not been studied theoretically [23].

References: [15] Barenbaum A.A, Gladenkov, Yr.B., Yasamanov, N.A. (2002) Stratigraphy. Geological Correlation. V.10. № 2. p.3-14. (in Russian). [16] Barenbaum A.A., Shuvalov V.V. (2007) Physics extreme states of matter-2007, Ed. Fortov V.E. etc., Chernogolovka: IPCP. p.139-140. (in Russian). [17] Barenbaum A.A., Hain V.E., Yasamanov N.A. (2004) Vestnik MGU. Ser.4. Geology. № 3. p.3-16. [18] Barenbaum A.A. (2008) Materials XIV Intern. Conference. Petrozavodsk, Karelian Science Center RAS, P.1, p.43-47 (in Russian). [19] Artyushkov E.V. (1994) *Doklady Akad. Nauk,* **336**, №5, p.680-683 (in Russian). [20]Kozyrev, N.A. (1959) Priroda. № 3. p.84-87. (in Russian). [21]Shpekin, M.I., Barenbaum A.A. (2011) Proceedings of the conference VNKSF-17. Ekaterinburg. p.476-477. (in Russian). [22] Barenbaum A.A. (2010a) Proceedings of XLIII meeting on the Tectonics: Tectonics and Geodynamics of the fold belts and Phanerozoic platforms. V.1. Moscow. PH GEOS. p.38-42. (in Russian). [23] Barenbaum A.A. (2010b) Zababakhin readings: Proceedings of the X Intern. Conference. Snezhinsk. PH VNIITF. p.13. (in Russian).

ESTIMATE OF THE LUNAR SURFACE AGE: INTRODUCTION AND DISCUSSION.

A.A.Barenbaum[1] and M.I.Shpekin[2], 1- Oil and Gas Research Institute RAS <azary@mail.ru>, 2 - Kazan Federal University <Michael.Shpekin@ksu.ru>

Preface. Most part of the lunar surface relief was formed during the last 5 million years. The conclusion was received on the basis of detail analysis of large craters of the Moon, Earth, Mars and Mercury. Fall of the galactic comets 5.0÷0.6 million years ago and the tectonomagmatic processes induced by the comets played major role in shaping of the Moon topography.

Processes of tectonics and volcanism are occurring on the Moon today also. An example is the volcano found in the Tsiolkovsky crater on the far side of the Moon. The volcano has a height of 102 m and is located almost in the bottom center of the crater with a diameter of 180 km on a low oval elevation of plume nature 24-26 km in size.

Introduction. It is believed that the relief of the lunar surface, as well as Mercury and Mars formed more than 3 billion years ago as a result of falls on these celestial bodies planetesimals remained after solar system formation in the interplanetary space [1]. This opinion justify the data on the crater, as well as measurements of the isotopic age of lunar rocks samples delivered to Earth, testifying to their formation more than 3 billion years ago [2].

The spacecraft planetary exploration, made in recent years, however, cast doubt on such an ancient age of the surface topography, in particular, the Moon and Mars. At the poles of the celestial bodies the large masses of frozen water were discovered and recently dry riverbeds can be seen on Mars [3]. These and many other facts do not find a convincing explanation within the framework of existing concepts.

We suggest another interpretation of the observed facts. It is based on an analysis from the standpoint of galaxycentric paradigm [4], the distribution of comet craters on planets and the discovery of modern volcano [5] in one of them - Tsiolkovsky crater on the Moon. Our studies show that most of the surface of the Moon, Mars and Mercury are completely saturated by such craters. Since their formation is associated with ejection of rocks from depths of ~ 3 km or more, the old age of the lunar rocks samples brought to Earth says in first place about the time of solidification of the material, but not the actual age of the formation of the lunar surface.

The arguments and evidence that the lunar surface is hardly more than 5 million years, and the process of its formation continues today are given below.

General characteristics of the Moon relief. The main topographical features of the Moon, Mars and Mercury surface are covered with large craters uplifted areas - "continents" and cratered to a much less extent, lower parts - "the sea ". It is significant that the continents tend to be the southern hemisphere of the celestial bodies and the sea is mainly located in its northern hemisphere.

There is also an important specificity in the morphology and distribution of craters. According to [6], two distinct populations of craters - diameter D<15 km and D>15 km stand out on the Moon. The first are the most numerous in the seas, and the second - on the continent. The depth H of the first is approximately equal to 1/ 5 of their diameter, while the craters of the second type are smaller. The first type of craters has a simple structure and is best described by the dependence $H = 0.196D^{1.01}$, whereas the latter are more complicated, have central hills and gentle slopes. In the diameter range $11 \le D \le 400$ km of these craters are followed depen-ding on $H = 1.044D^{0.301}$. Thus, with the impinging appearance of craters the rocks from the depths of ~ 3 ÷7 km may be disposed on the surface.

The transition between the types of craters on the curve H(D) is not monotonic, forming a region of overlap. The same applies to craters on Mars and Mercury [7].

The distributions of craters by diameter are peculiar, as well as their density on the continents and seas (Fig. 1-a). For craters with D ~ 100 km, their density on the continents is 100 times higher than in the seas, and at D ~ 10 km, this difference is reduced to 10. Significant differences in the cratering degree in different planets appear only for D> 400 km, where the density of craters on the Moon 4-10 times higher than on Mars.

The craters distribution on the Moon, Mars and Mercury are similar in configuration and are close in numerical parameters. Moreover, the distribution of marine crater diameter should be inversely quadratic dependence, while the continental craters are subjected to an exponential law. Since the last ones are much more numerous, the exponential distribution of craters by diameter is characteristic of these planets in general (Figure 1-b).

Bending curves in Fig. 1-a for the continent at D = 60 ÷ 100 km and line graphs for the seas associate with two [8] or even three [9] bombing of space bodies of different ages, partially destroying the traces of earlier falls. Modeling the crater distribution by means of special sizing of crating bodies [8], however, was inconclusive [7].

It is more difficult to explain [11] similarity in the distribution of craters in so much different celestial bodies like the Moon, Mars and Mercury, differing in the geological history, the

force of gravity on the surface and the distance from the asteroid belt and the Sun. The basic idea, that was involved in, is associated with the possibility of complete saturation of large craters, at least the

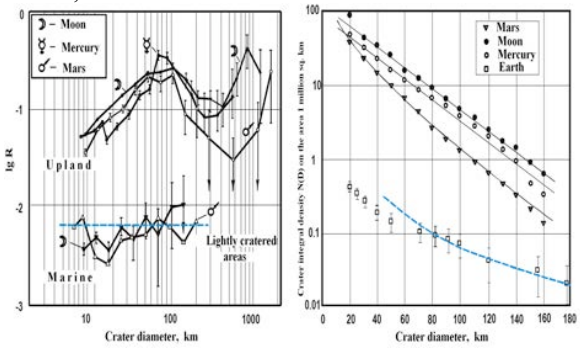

a **b**

Fig. 1. Density distribution of craters by diameter: **a)** the differential D(ΔN) with a step ΔD=D÷√2D a double logarithmic scale [8] and **b)** the integral N (> D) in a logarithmic scale [4], constructed according to[10]. The dotted line in the figure corresponds inversely quadratic dependence on D.

surface of the continents [8],[12], [13],[14]. This point was not managed to resolve. Currently accepted view is [7] that planets are far from the state of saturation by the large craters.

A new approach to the problem. According to Barenbaum [4], the Sun in its motion in the Galaxy once every 20-37 million years crosses the jet streams of material flowing from the center of our star system. In moments of these intersections duration ~ 2 ÷ 5 million years the solar system is exposed to intense bombardment by galactic comets. In the Earth's geological history, all these times are marked as the era of global natural catastrophes. These events are the straton boundaries of modern geochronological scale.

Last bombardment by galactic comets occurred in the period 5.0÷0.6 million years ago at the boundary of the Neogene and Quarter [15]. Today, these comets are absolutely unavailable for detection from the Earth by means of astronomy. Therefore, we judge the properties of these objects by the consequences of their fal-ling on our and other planets, as well as the results of their collision with the bodies of the asteroid belt [4].

Available data suggest that the masses of the nuclei of galactic comets vary in the range from 10^{12} to 10^{17} g, and their kinetic energy is from 10^{20} to 10^{25} J. The matter density of the comet is close to 1.0 g/cm^3. It is composed of 80-90% water ice and ~ of 10-15% the carbon components.

Chemical elements heavier than carbon and oxygen have the space prevalence, but their content is not more than one percent [4]. The galactic comets falls are characterized as "comet showers" when during a bombardment ~ 10^4÷ 10^7 such bodies could fall on the Earth. In contrast to large asteroids and comets of solar system these comets are characterized by an exponential distribution of mass and energy, which causes the same distribution of the crater diameters created by them (Fig. 1-b).

The number of the falling comets at the same time is so great that full saturation of the surface by craters is reached even during one bomb period. The theoretical value of the "marginal" density of the crating for the Moon, Mars and Mercury is ≈ 100 craters with a diameter ≥ D 10 km area of 1 million km^2 [4]. Because of the ecliptic obliquity at the angle of 62 ° to the galactic plane in which the comets move, their latest bombing came mainly to the southern hemisphere of the planets. Therefore, the complete saturation of the craters tends only to that hemisphere of the Moon and Mars. Data in Fig. 1-b confirm this conclusion.

There is another important fact that should be noted in discussing the data of Fig. 1-b. This is the absence of craters on Earth, created by galactic comets. All the large craters on Earth are formed downs asteroids. The distribution of these craters by diameter in region D≥70 km, slightly prone to observational selection, good to be a power by inversely quadratic dependence.

References: [1]Hiesinger H., Head J.W. III, Wolf U., Jaumann R., Neukum G. (2010) J. Geophys. Res. V.115, E03003, doi: 10.1029/2009JE 003380. [2]Hays J.F., Walker J. (1975) Cosmochemistry Moon and planets. Ed. Vinogradov, A.P., Moscow. Nauka. p.274-282. (in Russian). [3]Wikipedia. http://ru.wikipedia. org/wiki/ Mars_ (planet). [4] Barenbaum A.A. (2010) Galaxycentric paradigm in geology and astronomy. Moscow: BH "LIBROKOM". 544 p. (in Russian). [5]Shpekin M.I. (2009) Intern. Conf.: Astronomy and World. Heritage: Across Time and Continents. Kazan. Russia. p. 219-221. [6]Pike R.J. (1977) Impact and explosion cratering Eds. Roddy D., Pepin R., Merrill R., Pergamon Press. NewWork. p.489-509. [7]Meloche, G. (1994) Formation of impact craters. Geological process. Moscow. Mir. 336 p. [8]Voronov, A., Strom, R.G., Garkis, M. (1986) Satellites of Jupiter. Moscow: Mir, Part 2. p.5-48. [9]Urey, G. (1975) The Moon. Eds. Runcorn S. and Urey H. Moscow. Mir. p.287-302. [10]Kazimirov, D.A., Sitnikov, B.D., Poroshkova, G.A. and others (1980) Preprint GIN-GAISH. [11]Marov, M.Yr. (1981) Solar system Planet. Moscow: Nauka. 256 p. (in Russian). [12]Gault D.E. (1970) Radio Sci ences. V.5. p.273-291. [13] Basilevsky A.T. (1973) Space Researches V.**11** (4), p. 612-622. [14]Woronov A. (1977) J. Geophys. Res. V.82. p.2447-2456. [15] Barenbaum A.A, Gladenkov, Yr.B., Yasamanov, N.A. (2002) Stratigraphy. Geological Correlation. V.10. № 2. p.3-14.

SOME ASTRONOMICAL ASPECTS OF THE STUDY OF LUNAR REGOLITH.

M.P. Sinitsyn, Moscow State University, Sternberg Astronomical Institute, 13 Universitetsky prospect, Moscow 119992, Russia (msinitsyn.sai@gmail.com).

Introduction: Modern research methods provides extensive new information about the lunar regolith. Upcoming space missions as well as the construction of a lunar base in future will provide many times more data for further analysis. What are the astronomical scientific results can be derived from a detailed study of the regolith? In what areas of the lunar surface should first pay attention to the process of systematic excavation of the regolith for research?

Possible changes in isotopic composition and flow of solar wind in the process of evolution.

In one percent of solar wind particles, corresponding to heavier than hydrogen and helium isotopes of elements are present noble gases such as neon and argon. These isotopes are deposited and permanently retained in the regolith.

If we compare the ratio of some isotopes in the regolith [6], relating to different epochs of the same isotope ratios in modern solar wind [11], one can imagine how the composition of the solar wind changed over time. Studies isotope os $^{4}_{2}He/^{3}_{2}He, ^{22}_{10}Ne/^{21}_{10}Ne, ^{36}_{18}Ar/^{38}_{18}Ar$ in the regolith of different ages show that there is almost complete compliance these ratios with similar ratios in the solar wind.

However, revealed that the isotopic ratios of nitrogen $^{15}_{7}N/^{14}_{7}N$ in the regolith is growing by about 15% every billion years [6]. The only plausible explanation for this fact is the change in the ratio of nitrogen isotopes in the solar wind. This result, obtained in the studies of lunar samples brought back by Apollo spacecraft, still remains unexplained. It is possible that this ratio indicates a change in the solar wind flow over time. It should be noted also that the isotope ratios of some volatiles, in particular xenon in the regolith vary considerably over time, which may indicate that the flow of the ancient solar wind (~ 3.5-4 billion years old) was 2-3 times higher. Changes in the depth of penetration of solar wind into minerals give the opportunity to explore the variation of SW proton energy. It is assumed also that the ancient solar wind was more energetic.

Recovering the history of changes in GCR over the past 200 million years

The accumulation of the regolith is approximately 1 mm per million years. This means that over 200 million years, a layer of regolith is about 20 cm. This period is small enough so that the upper layer of regolith has not undergone a complete mixing with the earlier layers. Therefore, in this case, the uppermost layer, contain information about changing the flow of galactic rays and solar wind during this last period. The most suitable objects to study the recent events taking place around the solar system, are the impact and magmatic melts.

Images of melts of different nature were obtained using LROC with almost the entire surface of the Moon. In Fig.1 shows the impact cracked blocked melt, which is very handy for the extraction of its vertical sample.

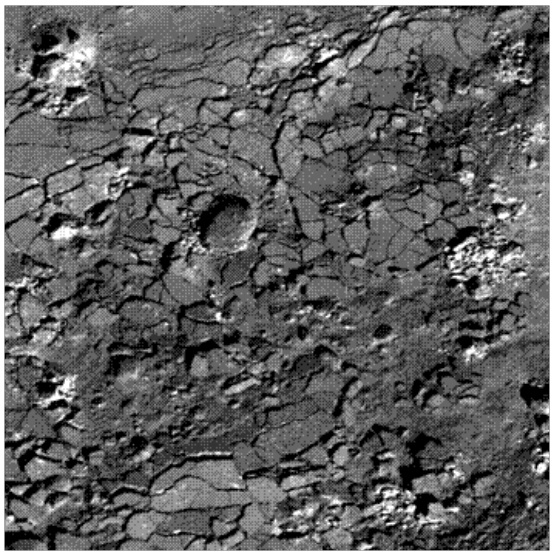

Fig.1 Blocked impact melt on Giordano Bruno crater floor(LROC).

The melt is convenient because at the time of formation of all the previous information is erased and the age of the next records does not exceed the age of impact or volcanic formation.

As evidence of possible changes in the flux of GCR or SW can point to hydrogen anomalies observed in very immature impact craters [7].

Recovering the history of the evolution of the Solar System through the records in the regolith over a period of up to 4 billion years

To recover almost the entire history of the evolution of track records and deposits of volatiles in the regolith must have a strong correlation between age and depth of entries in the regolith. Therefore, introduced the concept paleoregolita. This regolith, which was exhibited at the surface only once and was preserved for various reasons[1,2,3,4]. The existence of a palaeoregolith has been brilliantly confirmed by images LROC (fig.1). In the picture are layers of volcanic magma at each other. Between them are clearly visible layers of the regolith that formed between eruptions. This is the palaeoregolith. Systematically extracting and studying regolith and palaeoregolith we can trace the whole process of rotation of the Solar System around the galactic center. It

is possible to identify the composition of stellar matter sleeves, through which passed the Solar System, as well as the composition of the gas and dust clouds in its path[3]. Exploring the regolith, we can very accurately detect an epoch in which the surface of the Moon fell out the most active cometary material [9].

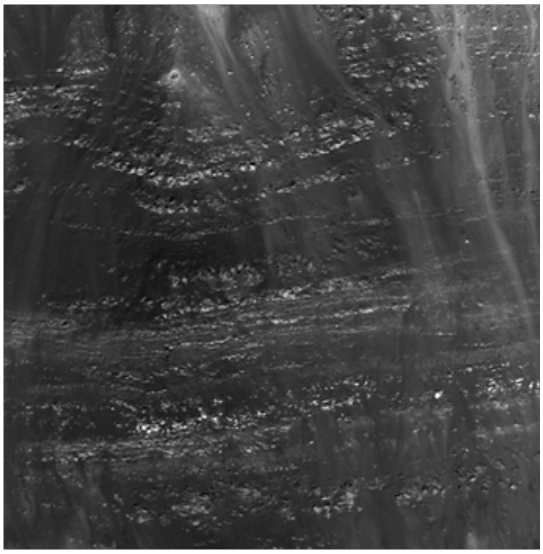

Fig. 2 The real location the palaeoregolith on the slopes of Euler crater (LROC).

Understanding the complexity of the extraction of regolith from the slopes of craters, we propose to consider some other possible locations of its occurrence, as follows: terraces of some craters, tectonic and volcanic extended objects, modern preserved palaeoregolith layers (fig.3).

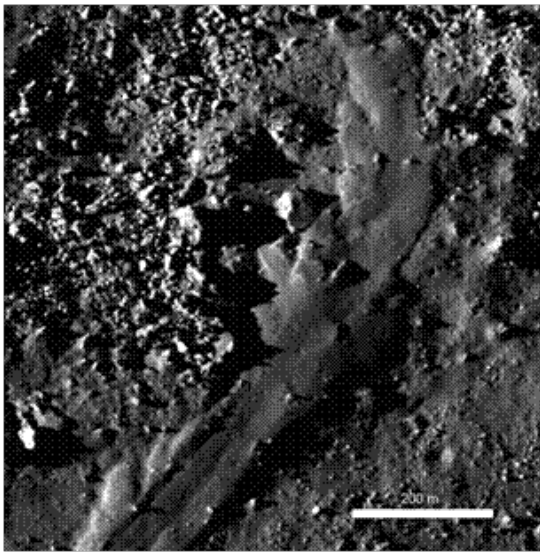

Fig. 3 *Formation preserved regolith under impact melt flow on edges of any craters rims (LROC).*

Conclusions:

As a result of the LRO camera obtained many images, which show the location of impact melts and the sites of occurrence of palaeoregolith. Also clearly visible craters in which palaeoregolith can potentially placed. For extensive information on the astronomical time scale of several billion years, require a systematic excavation of the regolith (preferably in the form of a vertical core) in the field of its most hermetic deposition. Also, it is possible to explore the deepest extraction of the regolith (up to 4 meters), in which the mixing is not too much. Excavation and study of samples of impact melt may be much easier due to the occurrence of the surface and the absence of mixing.

References:

[1] Crawford I.A. et al. (2010) Earth, Moon & Planets107,75-85 [2] Crawford I. A.et al.(2009) LROSTM, Abstract #6007 [3] Crawford I.A. et al. (2010) Vol.5, EPSC2010-735 [4] Crawford I.A. et al.(2007) LPSC XXXVIII, Abstract #1323 [5] Grozaz G. et al.(1977) Phil. Trans.R.Soc. 285, 587-592 [6] Heiken G.H. et al. (1991) Lunar Sourcebook,LPI, 354-356 [7] Sinitsyn M.P.(2012) LPSC XLIII, Abstract #1659 [8] Sinitsyn M.P. (2011) LPSC XLII, Abstract #[9] Shevchenko V.V. (2012) LPSC XLIII, Abstract #1275 [10] Takayuki Ono et al. (2009) Science 323, [11] Wiens R.C. et al. (2004) EPSL 222, 697-712.

LUNAR X-RAY SPECTROSCOPY WITH A NEW GENERATION OF SWEPT CHARGE DEVCES ON THE CHANDRAYAAN-2 CLASS INSTRUMENT. P. H. Smith[1], J.P.D.Gow[1], N.J.Murray[1], R.Burgon[1], A.D.Holland[1], M.Anand[2], P.Pool[3], P.Sreekumar[4], S.Narendranath[4].
[1]e2v centre for electronic imaging, Open University, Walton Hall, Milton Keynes, MK7 6AA, UK,
[2]Planetary and Space Science, Open University, Walton Hall, Milton Keynes, MK7 6AA, UK
[3]e2v technologies plc, 106 Waterhouse Lane, Chelmsford, CM1 2QU, UK,
[4]ISRO Satellite Centre (ISAC), PB No. 1795, Vimanapura Post, Banglore – 560 017, India

Introduction: The Chandrayaan-2 Large Area Soft-X-ray Spectrometer (CLASS) [1] is due to be launched by the Indian Space Research Organisation (ISRO) in 2014. CLASS will map the elemental composition of the lunar surface by measuring the X-ray fluorescence stimulated by solar X-rays. The aim is to perform a global study on the diversity and distribution of lunar lithologies, providing a map of elemental abundances of the lunar crust, focusing on the major crustal provinces and mare diversity [1] .

The CLASS instrument will use an array of e2v technologies CCD236 swept charge devices (SCD), a new generation of SCD X-ray detector. The CCD236 is a large area (20 x 20 mm^2) soft X-ray detector optimized at 0.5 keV to 10 keV [2], and benefits from improvements in design to allow for increased detector area, a reduction in split X-ray events and improvements towards radiation hardness. It will effectively increase the detection area from 24cm^2 used on C1XS [3] to 64cm^2 for CLASS but with the same electronic requirements [1].

Chandrayaan-2 is planned to orbit the Moon from a 200 km altitude orbit [1] for 1 year during a period of high solar activity, thus increasing its chances of encountering higher energy and frequency of solar flares interacting with the lunar surface. This may enable mapping of heavier elements such as Ti, Mg and Fe during such high-energy events, but may also result in an increased proton damage to the detectors during the mission.

Based on the flightpath of Chandrayaan-1, an end of life proton fluence can be estimated, giving a prediction for the SCD performance at the end of the mission. Sufficient shielding on the detectors will be required for the mission duration to decrease the degradation of resolution caused by radiation damage but without reducing the detected fluorescence.

In this presentation, we will provide an overview of the CLASS instrument, the CCD236 detectors, optimisation of the energy resolution and the planned radiation damage study.

References:

[1] Radhakrishna V, *et al.*, (2001) 42nd Lunar and Planetary Science Conference, The Chandrayaan-2 Large Area Soft X-ray Spectrometer (CLASS), p 1708.
[2] Holland A. and Pool P., (2008) Proc. SPIE 7021, A new family of swept charge devices (SCDs) for X-ray spectroscopy applications.
[3] Goswami J. N, *et al.*, (2008) Acta Astronautica, Chandrayaan-1 mission to the Moon, Vol. 63, p 1215-20.

IN SEARCH OF SHADE IN PERSISTENTLY ILLUMINATED REGIONS NEAR THE LUNAR POLES. E. J. Speyerer[1] M. S. Robinson[1], S. J. Lawrence[1], K. Burns[1], J. D. Stopar[1], [1]School of Earth and Space Exploration, Arizona State University, Tempe, AZ, USA (espeyerer@ser.asu.edu).

Introduction: The Moon's slightly tilted spin axis (1.54° at its current state) relative to the ecliptic normal provides a unique lighting environment near the lunar poles [1]. Topographic highs (e.g., crater rims and elevated massifs) remain persistently illuminated for the entire precessional cycle (18.6 years). Meanwhile, some crater floors and topographic depressions remain in shadow throughout the same cycle. These two types of areas are key sites for future human and robotic explorers. Using images acquired by the Lunar Reconnaissance Orbiter (LRO) Narrow Angle Camera (NAC), we identify the occurrences of these two environments coexisting in small, localized areas.

Previous Studies: Many studies have focused on identifying and delimiting these two environments (persistently illuminated and permanently shadowed) using both topographic and image based datasets. Most recently, from altimetric data from Laser Altimeter (LALT) and Lunar Orbiter Laser Altimeter (LOLA) onboard the Kaguya and LRO spacecraft, researchers have simulated the lighting conditions of the polar regions and identified discrete points in the elevation models that receive the most illumination, and quantify the surface area near the pole in permanent shadow.

Recent work [5] using images acquired by the LRO Wide Angle Camera (WAC) revealed a highly illuminated region (0.93 km^2) on the rim of Shackleton crater that remains persistently illuminated for 94% of the year and recedes into shadow for a maximum period of only 62 hours. Such a location is ideal for future exploration and long duration habitats due to its persistent access to solar energy, benign thermal conditions, and proximity to large permanently shadowed regions (PSRs), like the floor of Shackleton crater.

Impact of Small Scale Topography: While many studies have focused on delimiting these regions, small scale topography in these persistently illuminated regions can cause local regions to remain out of direct sunlight all year. For example, due to the extreme lighting geometry, a meter tall boulder on the surface can cast a shadow for 37 m. Likewise, the interior of a small crater can remain in shadow due to its slightly raised rim. Using NAC derived illumination mosaics compiled from images acquired over the entire mission, we identify small, potentially permanently shadowed regions in these highly illuminated areas.

NAC Illumination Analysis: During a majority of orbits (~every 2 hours), the WAC acquires a 104 km wide image across the pole that is used to create illumination maps of the region [5]. In contrast, the spatial coverage of NAC images acquired during a polar pass is limited due to the narrower field of view (5.7° combined). However, since the start of the mission, the NACs have acquired over 21,000 image pairs within 5° of the both poles over a full range of lighting conditions, thus providing the means to investigate lighting conditions at the meter scale.

In a search for shadowed areas in or adjacent to persistently illuminated regions, we map projected a subset of NAC images covering the rim of Shackleton crater. The mapped images were converted into binary images to represent their illumination state (0=shadowed, 1=illuminated). Binary images were stacked in map space and the percent each mapped pixel was illuminated was calculated. Since the NAC does not image the same surface during every orbit, we cannot provide meaningful estimates for the amount of time a feature is illuminated at this scale, but we can identify potential PSRs that have remained shadowed in all images acquired to date. Figure 1 highlights a collection of craters located in persistently illuminated regions that have a majority of their interior remaining in shadow.

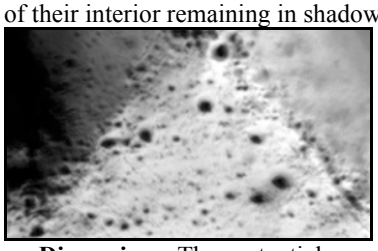

Figure 1- NAC illumination map of a region on the rim of Shackleton crater. (image is 3.75 km wide)

Discussion: The potential presence of permanently shadowed features in the persistently illuminated regions has major implications for future exploration of the lunar poles. There have been numerous mission proposals [e.g., 6,7] to explore large PSRs with landers, rovers, and standoff instruments. These large PSRs generally have steep slopes and, by definition, no easy access to direct solar energy making it difficult for vehicles to traverse and survive for long periods. However, small PSRs found in these persistently illuminated regions are more easily accessible and a tall (several meters), but feasible, mast could collect solar energy to support operations [4,8]. Furthermore, a polar rover could explore a series of these small permanently shadowed regions with standoff instrumentation that would require substantially less power than needed to explore the larger and less accessible PSRs like Shackleton crater.

References: [1] Siegler et al. (2011) *JGR*, 116, E03010. [2] Noda et al. (2008) *GRL*, 35, L24203. [3] Bussey et al. (2010) *Icarus*, 207, 558-564. [4] Mazarico et al. (2010) *Icarus*, 211, 1066-1081. [5] Speyerer et al. (2012) *Icarus*, in revision. [6] Barlett et al. (2008) Int. Symp. on Artificial Intel. [7] Pedersen et al. (2008) Int. Symp. on Artificial Intel. [8] Bussey et al. (2011) LEAG Annual Meeting.

AUTOMATIC REGISTRATION OF ALTIMETRIC OBSERVATIONS TO STEREO DERIVED ELEVATION MODELS. E. J. Speyerer[1], K. Burns[1], and M. S. Robinson[1], [1]School of Earth and Space Exploration, Arizona State University, Tempe, AZ, USA (espeyerer@ser.asu.edu).

Introduction: Altimetric observations, like the ones gathered by the Lunar Orbiter Laser Altimeter (LOLA), provide precise measurements (±0.1 m) of the distance between the Lunar Reconnaissance Orbiter (LRO) spacecraft and the lunar surface [1]. These observations are reduced into regional digital elevation models (DEMs) and other products depicting surface slopes, roughness, and reflectance.

The precision of the LOLA altimetric measurements (±0.1 m) is defined by performance of the LOLA electronics, while the accuracy of the observations is dictated by how well the position of the LRO spacecraft is known and the modeling of the thermal effects on LOLA transmitter optics [1]. Recent work by Mazarico and co-workers [2] has improved the known position of LRO through precision orbit determination using radiometric data and altimetric crossovers. With this improved ephemeris, the horizontal accuracy of the orbits improves from ~300 m to ~14 m [2,3].

The LRO spacecraft also includes the Lunar Reconnaissance Orbiter Camera (LROC), which includes a single Wide Angle Camera (WAC) and two Narrow Angle Cameras (NACs) [4]. From an altitude of 50 km (common during the mapping phase) the NAC images have a pixel scale of 0.5 m. Although not designed for stereo observations, off-nadir slews of the spacecraft enable stereo NAC observations acquired from adjacent orbits. These stereo images are later reduced into DEMs with a typical post spacing of 2.0 m.

Registration of Altimetric Observations to DEMs: When producing DEMs using NAC stereo data, elevations derived from image pairs are tied to overlapping LOLA tracks to ensure the absolute elevation and horizontal accuracy of the model [5]. However due to offsets in the spacecraft location when acquiring the NAC images and the LOLA measurements, which may be acquired over many orbits, offsets (±15 m) between the datasets are common. The LROC team is currently developing a tool to automatically register altimetric observations to high-resolution digital elevation models.

Typically when tying a DEM to a set of altimeter spots that include latitude, longitude, and radius measurements, the DEM is semi-manually adjusted by rotating and displacing the model until the root-mean-squared (RMS) of the difference between the elevation of altimeter spot and the image derived DEM at the same spot location is minimized. After successful registration, the RMS error along the LOLA profile is typically <1.0 m for a DEM produced at 2.0 m per post [5].

However, mis-registrations in the products are generally due to differences in the known and actual position and rotation of the spacecraft and instruments. Using a generalized pattern search (GPS) algorithm, the new automatic registration adjusts the position and pointing information for the times when the LROC NAC images are acquired as well as when LOLA was collecting measurements of the same region. **Figure 1** shows how the RMS error improves as the GPS algorithm identifies the proper spacecraft position and rotation offsets. By registering multiple LOLA tracks across a NAC DEM, the model can be adjusted to provide a very precise and accurate elevation model of the region.

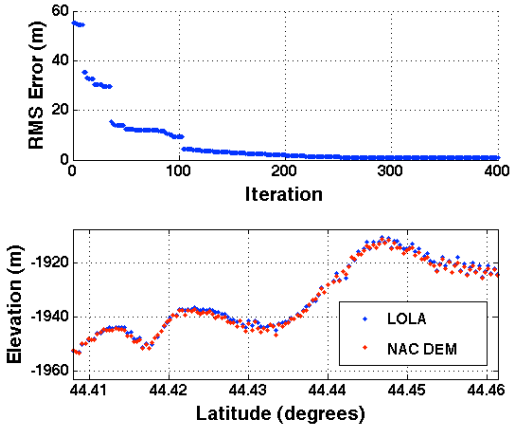

Figure 1- *Output of registration program identifying the improvement in the RMS error and a portion of the final registration.*

Further Applications: An automatic registration algorithm can also be used to improve the thermal pointing model of the LOLA instrument. When LRO passes over the terminator, typically in the polar regions, the thermal blanket contracts and causes the transmitter optics to be pulled off axis [1]. This "LOLA Anomaly" reduces the number of spots LOLA is able to acquire during a single shot (5 to 2) [1]. By tracking the rotation adjustment for each individual beam and receiver channels, one can accurately model the magnitude of this shift over a range of temperatures. This information can later be used to improve the defined pointing of LOLA instrument and thus improve the gridded data product as well as improve the altimetric data used in the precision orbit determination.

References: [1] Smith D.E. et al. (2010) Space Sci. Rev., 150, 209-241. [2] Mazarico E. (2012) J. Geod., 86, 193-207. [3] Zuber et al. (2010) Space Sci. Rev., 150, 63-80. [4] Robinson et al. (2010) Space Sci. Rev., 150, 81-124. [5] Tran T. et al. (2010) ASPRS/CaGIS.

GENE BANK IN LUNAR POLAR PSRs. Swain, R. K.[1], Behera, D.[2] [1]Student, Kendriya Vidyalaya, Sambalpur, Orissa, India. Email: Rkswain28@ovi.com, [2]PGT(Biotechnology), Kendriya Vidyalaya, Sambalpur, Orissa, India. Email: deep130784@yahoo.co.in,

Introduction: The genetic heritage on the earth is at risk under the prevailing endangered global environmental conditions. As we have observed, adequate conservation of habitat is unfeasible and active breeding programs cover only a handful of the many thousand species threatened. The gene pools of many human ethnic groups are also threatened. Apart from the financial implications for constructing gene banks on earth, the climatic as well as the very human factor also pose a great concern in future which calls for further planning for a safer location for storage of biologically vital germplasms.

Against such indispensable losses scientists are starting cryopreservation of germplasms by creation of gene banks. It is proposed to construct a cDNA library based gene bank for endangered species in the permanently shadowed polar lunar craters that would provide immunity from both natural disadvantages and humanitarian intrusions [4].

Rationale: In the pursuit of conservation of biodiversity, enormous money is spent all over the globe but they are unable to address the severity of the problem. Under such alarming circumstances, we turned to cryopreservation as an option but over thousands of years economic depressions, sabotage, conflicts, warfare or even a brief disruption to the precise cryopreservation can hamper the storage of genetic samples.When we are considering conservation it is always preferable to go for a more secure and permanent solution that would involve one time expenditure rather than repetitive attempts. It was found out that the climatic and strategic location of the lunar polar craters are adequately hospitable, remote and free of maintenance and human observation as they provide naturally cryogenic temperature, reduced gravity and vacuum environment, non-reactive surface, safety from celestial intrusion and permanent shadow which doesn't allow the temperature to fluctuate thus providing most suitable storage facilities for the germplasms. PSRs provide steady temperature of 40-60K and immunity to earthquakes due to low seismic activity. At these sites, burial in one meter or more of the regolith will provide protection against the solar wind, solar and galactic cosmic rays and micrometeorite impact. It provides the minimum necessary barrier from human intervention and at the same time enables easy retrieval for future usage. Genetic samples of endangered species can enable restoration even after its extinction. Preserved tissues can secure the genetic heritage of species, and may allow future restoration of those species. Furthermore, there would be no scientific extinction [4].

Biological Processes: For storage of a huge number of genetic samples, we need to follow the basic protocols of construction of a cDNA library based gene bank. The cDNA library represents the genes that were being actively transcribed in that particular source under the physiological, developmental, or environmental conditions that existed when the mRNA was purified [2]. Total RNA can be extracted from plants by using LiCl method [5]. The message RNA can be isolated and purified double-strand cDNA can be synthesized using the cDNA Library Construction Kit in a PCR machine. Five microliters of PCR products can be labeled with α32PdATP)fractionated by electrophoresis in 1.0% alkaline agarose gel to check the ds-cDNA quality along with the single stranded cDNA. One microliter of the purified cDNA can be ligated into the predigested vector (1 µg) digested by EcoR I-Xho I following the protocol of ovenright ligation at 16 ºC in a sense orientation. The lambda library can be packaged in a high-efficiency system and plated on the E. coli cell line .After amplification of the library titre can be calculated as per the manufacturer's recommendation and it came to 1 X 107cfu. The library can be stored in 7% DMSO at -80ºC until further screening of the gene of interest. The size of the insert fragments can be measured by PCR method using random selection of 10-15 clones from the SOLR infected positive clones (growing in LB ampicillin agar plates) [5].Using 0.1 gram of genetic material from about 20 individuals per species can allow the future restoration of a species. A realistic payload of 2,000 kg can save one million species. The storage medium would contain liquid nitrogen [4].

Location: After a thorough search, it has been concluded that the gene bank containing container should be buried under the regolith of the PSR of the base of Shoemaker Crater located near the Lunar South Pole, centered at 88.1 S, 45E[1]. It provides diameter of 20-51km with an immense 100m^2 of PSR [6].

The physical properties of the floor material can be modeled. This floor is known to be flat, providing simple geometry for understanding impact dynamics and the Ejecta plume in case required. In addition, about half of the crater floor is invisible from earth but access from polar lunar orbiter is good because a spacecraft would pass overhead every two hours[6]. Hence, it enables easy storage, surveillance and prolonged retention of the proposed gene bank.

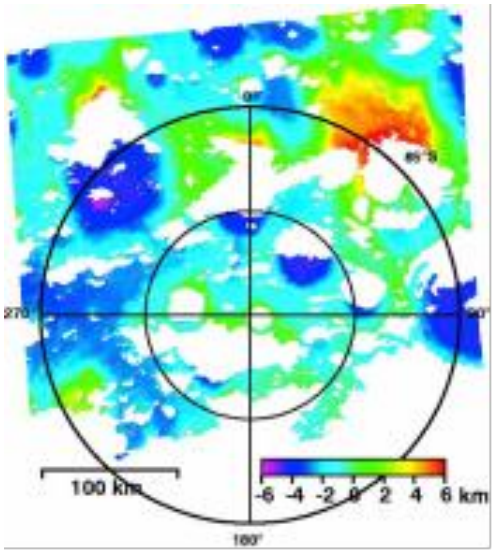

Figure 1.Radar DEM of south polar craters, maker crater indicated by arrow; white – permanent shadow (calculated), gray – no radar return; from [3]

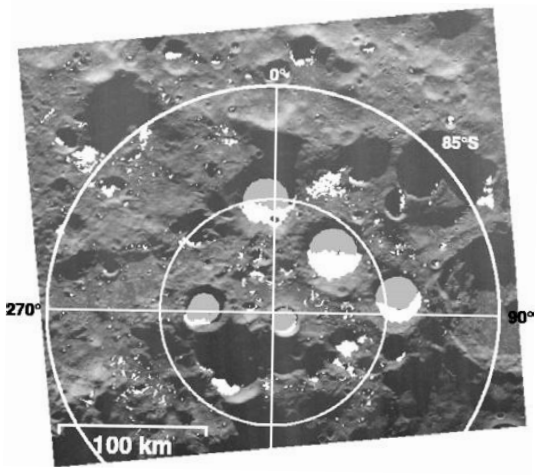

Figure 2. Radar DEM of south polar Shoemaker crater indicated by arrow; from [3].

Conclusion: Cryoconservation can add an important ethical component to the space programme and help raising public support. Conversely, such an option of conserving the vital biodiversity by developed countries on a permanent basis can also make cryoconservation more attractive and fundable. Many nations may wish to participate to secure the genetic heritage of their unique biota and ethnic groups[4]. It is highly advisable that developed countries associate with biologically rich countries and biotechnologists all over the world to collect as many genetic samples as possible which they can include in their future lunar missions to secure the future of the living world. Until habitat losses are controlled, cryoconservation may provide the best chance to secure and eventually revive many endangered species. For this purpose, space-based depositories in remote locations like the lunar polar PSRs can provide precise conservation ,the most cost-effective and secure means for permanent storage of irreplaceable genetic materials with a single one time expenditure for ages instead of the prevalent ineffective innumerable conservation programs.

References:

[1] Allen, C. C., NASA Johnson Space Center, Mail Code KT, Houston, TX 77058 carlton.c.allen@nasa.gov. Shoemaker crater – going where we can "see". [2] Anonymous, http://en.wikipedia.org/wiki/Library_(biology) [3] Margot J. L. et al. (1999) *Science*, *284*, 1658-1660 [4] Mautner, M.N. (1996) Space-based Genetic Cryoconservation of Endangered Species. *Journal of The British Interplanetary Society*. , Vol. 49, pp 319-320 [5] Sambrook J, Fritschi EF and Maniatis T (1989) Molecular cloning: a laboratorymanual, Cold Spring Harbor Laboratory Press, New York [6] Shevchenko, V.V. and E.A.Kozlova, Sternberg State Astronomical Institute, Moscow University, 13 Universitetsky pr., 119992 Moscow, Russia; e-mail: shev@sai.msu.ru Permanently shadowed areas at the lunar poles: nature and possible utilization.

MoonRise: SAMPLE RETURN FROM SOUTH POLE-AITKEN BASIN. T. D. Swindle[1], B. L. Jolliff[2], D. A. Papanastassiou[3], and C. K. Shearer[4]. [1]Lunar and Planetary Laboratory, University of Arizona, Tucson AZ 85721-0092 USA, tswindle@lpl.arizona.edu, [2]Earth and Planetary Sciences and The McDonnell Center for the Space Sciences, Washington University, St. Louis MO 63130 USA, blj@levee.wustl.edu, [3]Jet Propulsion Laboratory, Caltech, M/S 183-335, 4800 Oak Grove Drive, Pasadena, CA 91109-8099, dap@jpl.nasa.gov, [4]Institute of Meteoritics, University of New Mexico, Albuquerque NM 87131, cshearer@unm.edu.

Introduction: South Pole-Aitken Basin (SPA) is unique on the Moon in its chronology and chemistry, and can provide insight into early lunar and Solar System processes and history. A sample return from SPA would address fundamental questions about the Moon and advance our knowledge of impact bombardment and early Solar System dynamics. MoonRise, a mission that would have returned samples from SPA, was a finalist in NASA's recent round of New Frontiers proposals. Here we describe some of the scientific justifications for such a mission and the approach taken by MoonRise.

Lunar chronology: One of the key questions about the Moon with Solar System implications is whether there was a "lunar cataclysm," a period of greatly increased impact rate, at approximately 3.9 Ga. Such a period was suggested based on early analyses of the Ar-Ar and U-Th-Pb systems in Apollo samples [1, 2]. Arguments for a cataclysm have been strengthened more recently by a dearth of pre-4.0 Ga ages in recrystallized impact melt clasts in lunar meteorites [3], or in shocked eucrites or H chondrites from the Main Asteroid Belt [4, 5], and by the discovery of a dynamical mechanism to produce such a cataclysm [6]. However, most samples do not show a sharp end to the period of increased impact rate, as predicted by some cataclysm models [3-5], and coupled with the discovery of older impact ages, particularly in zircons [7, 8], the original idea of a brief cataclysm has been called into question.

SPA is stratigraphically the oldest multi-ringed basin on the Moon, and it contains several other impact basins and very large craters within it [9]. Since the Apollo samples come from a relatively restricted region on the nearside, and could all have been affected by the (relatively late) Imbrium impact, SPA samples would be extremely valuable because they would sample a different portion of lunar impact history. If SPA formed near 4.0-4.1 Ga, that would indicate that there was some form of cataclysm, regardless of how fast the rate declined after Imbrium. On the other hand, if one of the intermediate-aged basins within SPA (it would be logical to sample an area where the impact materials from such a basin would be sampled as well as those of SPA) is considerably older than 3.9 Ga, it would suggest that the Apollo data were overwhelmingly affected by Imbrium, rather than a cataclysm.

Lunar chemistry: As seen from orbit, SPA has a chemical composition distinct from either the nearside maria or the feldspathic highlands that make up most of the rest of the farside [10]. Its distinctive composition presumably results from mixing of ancient volcanic materials with deeply excavated rocks (deep crust and/or upper mantle) that differ from nearside basin ejecta, which are rich in KREEP.

Models of the chemical evolution of the Moon have been primarily based on the Apollo samples, well-studied rocks coming from known locations. A sample return mission to SPA would provide a way to gain the same level of understanding of a completely different part of the Moon, and help determine how lunar evolution differed with time and location. Similarly, because basalts (mare and cryptomare) are more common in SPA than elsewhere on the farside, an SPA sample return mission would bring back samples that reflect the farside mantle, which can be used to determine if mantle heterogeneity also reflects global asymmetry.

MoonRise mission: To accomplish SPA sample return within New Frontiers constraints, MoonRise chose a simple and straightforward implementation, with a single lander going to a location near the center of the SPA basin [11]. The concept is to use the impact process (as opposed to surface mobility) to do the job of sampling. The development of regolith combines impact-ejected materials that, from Apollo experience, we know represent well the surrounding region, including abundant small rock fragments that can be concentrated by sieving. The central regions of SPA basin have been resurfaced by basalts (mare and cryptomare), so we rely on the fact that many large impacts penetrated this veneer and excavated the underlying SPA impact-melt complex. The center of the basin is where we are most likely to find these materials, along with impact-melt rocks formed by the smaller basins and large craters within SPA. Together, these materials will provide a spectrum of ages reflecting SPA-basin and post-SPA impact chronology of the Moon, with a definitive test for the beginning of the cataclysmic bombardment interval.

References: [1] Turner G., et al. (1973) *Proc. LSC 4th*, 1889-1914. [2] Tera F., et al. (1974) *EPSL. 22*, 1-21. [3] Cohen B.A., et al. (2000) *Science. 290*, 1754-1756. [4] Bogard D.D. and Garrison D.H. (2003) *MAPS. 38*, 669-710. [5] Swindle T.D., et al. (2009) *MAPS. 44*, 747-762. [6] Gomes R., et al. (2005) *Nature. 435*, 466-469. [7] Grange M.L., et al. (2011) *GCA. 75*, 2213-2232. [8] Norman M.D. and Nemchin A.A. (2012) *LPSC. 43*, Abstract #1368. [9] Wilhelms, D. (1987) *USGS Prof. Paper 1348*. [10] Jolliff B.L., et al. (2000) *JGR. 105*, 4197-5216. [11] Jolliff B. L. et al. (2010) *LPSC 41*, Abstract #2450.

Study of the last 3 billion years lunar cratering chronology from small size crater density.

B. Trey[1], C. Quantin[1], P. Allemand[1], [1]Laboratoire de Géologie de Lyon Terre, Planètes, Environnement, France (2 rue Raphaël Dubois 69622 Villeurbanne Cedex, bertrand.trey@univ-lyon1.fr).

1. Introduction

The lunar cratering chronology was defined using the radiometric ages of the Apollo samples and terrestrial Phanerozoic craters correlated with crater counts on the Apollo landing sites (LS) and on terrestrial shields [1], [2], [3], [4], [5], [6], [7], [8], [9], [10] and [11]. The time dependence mathematical expression proposed by [6] lies the cumulative number of crater larger than 1 km per surface units (N>1km) to the radiometric age obtained on returned samples. To constrain the last three billion years lunar chronology, only four lunar sites are available [9]. All are impact craters: Copernicus crater that would occur 800 My ago, Tycho crater 109 My ago, North ray crater 50 My ago and Cone crater 26 My ago [10]. Taking into account the size of these impacts and the image resolution available at that time [6], the crater density superimposed to these 4 impact craters has been sampled on their ejecta and their rays [6]. The 800 My age of Copernicus has been obtained on a rock sampled on its ray 25 km away from the impact. Copernicus age is nevertheless widely accepted [10]. However, a rock sampled on a 2250 km distant landslide has been attributed to Tycho crater based on two major arguments: the landslide is near a Tycho's cluster and the crater density on this landslide would be the same as the one superimposed on Tycho's ray [12]. This link keeps to be equivocal. On these 4 anchor points of the lunar chronology, only Copernicus age is out of the curve (Figure 10, [9]).

The Lunar Reconnaissance Orbiter Camera (LROC) onboard Lunar Reconnaissance Orbiter (LRO) provides us high resolution images down to 50 cm per pixel. We are now able to assess the size frequency distribution (SFD) of small craters (down to few meters) on the Moon.

We performed crater counts on LROC images inside Copernicus and Tycho craters and on the landslide that served to date Tycho. The resolution of the images allows us to observe the SFD from 4 m to 1 km. We then compared our results to the lunar chronology model proposed by [6] at different crater sizes.

2. Dataset and method

We constructed a Geographic Information System (GIS) to combine lunar data set at a wide range of spatial resolution. Our GIS includes: global data set released to public by the United States Geological Survey (USGS), as well as geo-processed LROC images: the wide angle LROC images (LROC WA) at around 60 m per pixel and the LROC narrow angle images (LROC NA) at 50 cm per pixels [13]. All these data allow us to document the SFD down to 4 m of diameter. We plotted our result as incremental representation of crater size vs crater density from [14]. The incremental diagram being more sensitive to slope variations of the distribution than cumulative plots [15].

Diameter range	4 m to 100 m	100 m to 2 km
Image type and resolution	Images LROC_NA (50 cm/pixels)	Images LROC_WAC (100 m/pixels)
Tycho	M129363095RC M119929934RC M119929934RC M122284637RC M129363095RC	M119929852ME
Copernicus	M116445887RC M117630388RC M117630388RC	M119985095ME
Apollo 17 LS	M159746082RC	

Table 1: Identification of the used images to assess the SFD as well as the diameter range they cover.

3. Measured SFDs

We performed crater counts inside Tycho crater, inside Copernicus crater and on the Apollo 17 LS whose exposure age would be linked to Tycho event. The Bright mantle (or Light mantle) on the Apollo 17 LS, comes from the South massif and its shape orientation is linked to Tycho's ray [16]. We performed counts on the Bright mantle and on the surrounding floor north to the Light mantle for comparison. All the crater density data were plotted in incremental diagram [14] and the plotted isochrons in this diagram correspond to the age model proposed in Table 2 by [15].

The Copernicus SFD follows the 1 Gy isochron for the largest diameters to finally reach the saturation equilibrium curve in the small diameter ranges. The study of Copernicus SFD is crucial to constrain the lunar cratering chronology because Copernicus is the only event with a radiometric age between 3 Gy and 0.1 Gy (see next section).

The Tycho SFD and the counts done on both surfaces on the Apollo 17 LS follow the 10 My isochron. This would confirm the hypothesis that both events are contemporaneous. However, in detail, the crater density on the Bright mantle is higher

than the one measured on the surrounding floor north to the Light mantle.

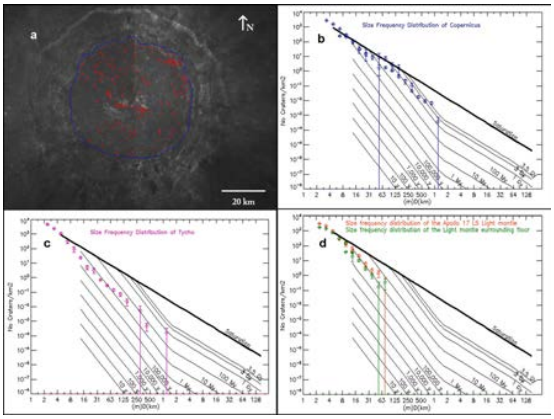

Figure 1: (a) Map of craters on the Copernicus inner floor; (b) SFD on the Copernicus melt pond; (c) SFD on the Tycho melt pond; (d) Comparison of the SFDs on the landslide covered by the light mantle and the one uncovered.

As it has been proposed by [15] the Light mantle may be related to Tycho's ejecta impact and be contaminated by Tycho's secondary craters.

4. Comparison to the age model (Neukum 1983)

The figure 2 presents a comparison of our results of crater density on Copernicus and Tycho craters superimposed with the mathematical expression proposed by [6]. The mathematical expression has been obtained at N(>1km) but can be calculated for different crater diameters. The curves at N(>500m), N(>200m) and N(>100m) are plotted as well as the value of N(>1km) that serve to construct the mathematical expression. These points are represented in black. The N(>1km) of Tycho is on the Neukum curve while Copernicus would have too high crater density in that diameter range (Figure 10, [9]). We have to keep in mind that this value of N(>1km) have been measured on the ejecta of the craters. We plotted also the results of this study, the cumulative crater density at different sizes (1km, 500m, 200m and 100m) that superimposes the interior of both Copernicus and Tycho craters. The diagram makes the assumption that the radiometric age attributions are correct for both Tycho and Copernicus impact. Our results may be discussed at different sizes:

-at N(>1km): our result are poorly liable because only one impact existed on Tycho's floor or on Copernicus's floor. Tycho would have a higher crater density than expected while Copernicus would have a lower one what is the inverse tendency compared to the data from [6].

-at N(>500m): Tycho would have a lower crater density than expected while Copernicus would have a higher one.

-at N(>200m): Both Tycho and Copernicus would have a lower crater density than expected.

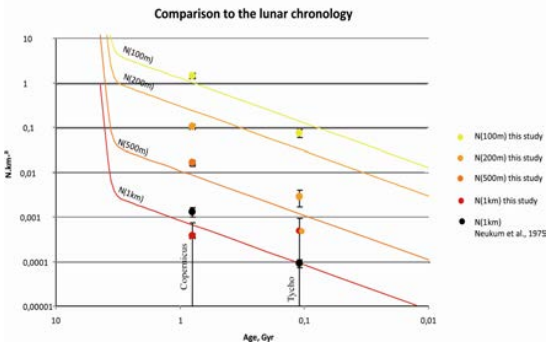

Figure 2: Comparison of the lunar chronology at different cratering sizes.

-at N(>100m): Tycho would have a lower crater density than expected while Copernicus would have a higher one.

The crater densities we observe are different from the ones predicted by the age model, and this whatever the crater size.

5. Discussion-conclusion

The SFDs measured in this work may confirm that the Bright mantle sampled to date Tycho impact event is contemporaneous of Tycho impact. Using radiometric ages of both Tycho and Copernicus, we compared the crater density of both sites to the age model proposed by [6] at different crater sizes. The results demonstrate that the use of the age model for young surfaces affected by low crater densities is equivocal.

Acknowledgements

We thank the USGS, the LRO team and the NASA for the open access to lunar data. This work is supported by ISSI (International Space Science Institute). The research leading to these results has received funding from the European Research Council under the European Union's Seventh Framework Programme (FP7/2007-2013) / ERC Grant agreement n°280168.

References

[1] Shoemaker et al. (1970a), Science, 167:452. [2] Shoemaker, E.M. et al. (1970b), Geology of the Apollo 12 landing site, Apollo 12 Preliminary Science Report, NASA SP-235. [3] Baldwin, R.B. (1971), Icarus 14, 36–52. [4] Hartmann, W.K. (1972), Astrophys. Space Sci. 17, 48–64. [5] Neukum, G. (1977), The Moon 17, 383–393. [6] Neukum, G. (1983), Univ. of Munich, 186 pp. [7] Neukum, G. et al. (1975), The Moon 12, 201–229. [8] Neukum, G. et al. (1994), in T. Gehrels (ed.), Hazards due to Comets and Asteroids, Univ. Arizona Press, Tucson, pp. 359–416. [9] Neukum, G. et al. (2001), Space Sci. Rev., Vol. 96, pp.55-86. [10] Stöffler, D. et al. (2001), Space Sci. Rev., Vol. 96, pp. 9-54. [11] Le Feuvre et al. (20011), Icarus, 214 , 1-20, doi:10.1016/j.icarus.2011.03.010. [12] Lucchitta, B.K. (1977), Icarus 30, 80–96. [13] Robinson, M.S. et al. (2010), Space Sci. Rev. 150, 81-124 [14] Hartmann, W.K.(1969), Icarus 10, 201. [15] Hartmann, W.K. (2005), Icarus 174, 294–320. [16] Arvidson, R. (1976), LPSC VII, 2817-2832.

Hydrogen and lead isotopic characteristics of lunar meteorite MIL 05035. R. Tartèse[1], J. J. Barnes[1], M. Anand[1,2], N. A. Starkey[1], I. A. Franchi[1], K. Terada[3] and Y. Sano[4], [1]Planetary and Space Sciences, The Open University, Walton Hall, Milton Keynes, MK7 6AA, UK (Romain.Tartese@open.ac.uk). [2]The Natural History Museum, Cromwell Road, London, SW7 5BD, UK. [3]Department of Earth and Planetary Systems Science, Hiroshima University, Higashi-Hiroshima 739-8526, Japan. [4]Atmosphere and Ocean research institute, The University of Tokyo, 5-1-5, Kashiwanoha, Kashiwa-shi, Chiba, 277-8564, Japan.

Introduction: Hydroxyl content and H isotope composition have been measured in apatite crystals from several Apollo mare basalts [1-2]. However, Apollo sampling is unlikely to be representative of the diversity of lunar rock-types. We report here the first H isotopic measurement in apatites from a lunar meteorite, the very low-Ti gabbroic MIL 05035 sample, together with new phosphate U-Pb data.

Methods: Phosphates were located using backscatter images and EDS elemental X-ray mapping. OH contents and H isotope measurements in apatites were carried out using the Cameca NanoSIMS 50L at the Open University. A large Cs^+ primary beam of ~ 260 pA current was rastered over a 10 × 10 µm area. A 3 minute pre-sputter was followed by the simultaneous collection of secondary ions $^1H^-$, $^2D^-$, $^{13}C^-$ and $^{18}O^-$ from a central 5 × 5 µm area. OH contents and D/H ratios were normalised against the Morocco apatite (OH = 2640 ppm, δD = -85 ‰). U-Pb dating was carried out using the SHRIMP II ion microprobe at the Hiroshima University. A O^{2-} primary beam of ~ 1 nA excavated ca. 10 µm spots, from which secondary ions were collected during ~ 120 minutes after a 2 minute pre-sputter.

Results: For U-Pb dating, 11 analyses performed on phosphates yielded a total Pb/U isochron age of 3.85 ± 0.07 Ga (2σ, MSWD = 0.62), consistent with the reported ages of 3.80-3.90 Ga for MIL 05035 [3-5]. For OH content and H isotope composition, 4 analyses carried out on 3 grains yielded OH contents and δD values ranging between 2000-4600 ppm and 320-540 ‰, respectively (Fig. 1).

Discussion: δD values measured in MIL 05035 apatites show a rough inverse correlation with their OH content (Fig. 1). Such a trend could reflect contamination by low δD terrestrial water. For example, mixing 2000 ppm lunar OH with a δD of 600 ‰ with 2000 ppm terrestrial OH with a δD of -200 ‰ (similar to the Antarctic ice δD in the Miller Range area [6]) results in 4000 ppm OH with a δD of 200 ‰. In the high-OH apatites, around half of the OH may thus be terrestrial hydroxyl. Considering that low-OH apatites are least contaminated, they provide a minimum δD estimate of ~ 500-600 ‰ for the lunar hydroxyl, which is consistent with measurements made on Apollo mare basalts.

MIL 05035 has been paired with Asuka 881757, Yamato 793169 and MET 01210 [e.g. 7], forming the 3.9 Ga old YAMM group of lunar meteorites.

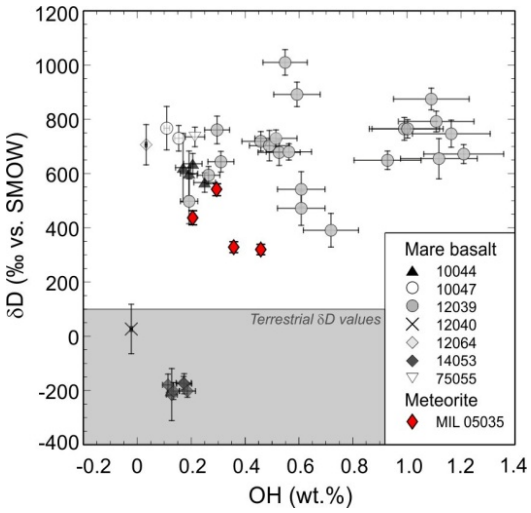

Figure 1: δD vs. OH content of lunar apatites. Apollo samples data are from [1-2]. Errors are 2σ.

In MIL 05035, phosphate Pb-Pb data yield initial $^{206}Pb/^{204}Pb$ and $^{207}Pb/^{204}Pb$ ratios of ~ 18.2 and 24.0, resp., corresponding to a μ ($^{238}U/^{204}Pb$) value of ~ 40, which is consistent with the low μ sources of ~ 10-20 of the paired meteorites [8-10]. This confirms that the impact that launched them sampled rocks derived from a primordial lunar source not sampled by the Apollo missions, possibly early cumulates of the Lunar Magma Ocean (LMO) [6].

Conclusion: Lunar H isotope composition in apatites in MIL 05035 is comparable with H isotope composition in Apollo mare basalts, although MIL 05035 is apparently derived from a very different and more primordial source. This suggests 1) that H has been added to the lunar interior after the LMO solidification, and 2) that added materials had a homogeneous H isotopic composition.

References: [1] Greenwood, J. P. et al. (2011) *Nat. Geosci., 4,* 79-82. [2] Greenwood, J. P. et al. (2012) *LPS XLIII,* Abstract #2089. [3] Nyquist L. E. et al. (2007) *LPS XXXVIII,* Abstract #1702. [4] Fernandes V. A. et al. (2009) *Meteoritics & Planet. Sci., 44,* 805-821. [5] Zhang A. (2010) *Sci. China Earth Sci., 53,* 327-334. [6] Masson-Delmotte, V. (2008) *J. Climate, 21,* 3359-3387. [7] Joy, K. H. et al. (2008) *Geochim. Cosmochim. Acta, 72,* 3822-3844. [8] Kita, N. T. et al. (1995) *Geochim. Cosmochim. Acta, 59,* 2621-2632. [9] Misawa, K. et al. (1993) *Geochim. Cosmochim. Acta, 57,* 4687-4702. [10] Terada, K. et al. (2007) *Earth Planet. Sc. Lett., 259,* 77-84.

CONSTRAINING MODELS OF WATER MIGRATION IN THE LUNAR SUBSURFACE Luís F. A. Teodoro[1], Richard C. Elphic[2], Vincent R. Eke[3], Matthew Siegler[4], Norbert Schörghofer[5], [1]BAER Inst., NASA Ames Research Center, Moffett Field, CA 94035-1000, USA; luis.f.teodoro@nasa.gov; [2]NASA Ames Research Center, Moffett Field, CA 94035-1000, USA, [3]Department of Physics, Durham University, Science Laboratories, South Road, Durham DH1 3LE, UK, [4]Jet Propulsion Laboratory, California Institute of Technology, Pasadena, CA, USA, [5] Institute of Astronomy, University of Hawaii at Manoa, Honolulu, Hawaii 96822, USA

The main aim of this research is to constrain models of the ice distribution with state-of-art lunar data and to improve our understanding of the water melecule dynamics in the lunar sub-surface throughout the lunar history. Although controversial in its physical form (e.g., crystalline as opposed to amorphous), there is increasing evidence of water ice at the lunar poles cold traps (e.g. [1]). Such locations plausibly hold not only water ice but also other volatiles of economic and scientific value. Future missions may include rovers with the ability to sample materials from the top metre of the lunar surface. This requires the identification of regions to explore and sample with the highest likelihood of finding water ice. Cold traps, including those a few cm below the surface, are the most plausible candidates. To understand the current distribution of water ice in the polar neighbourhoods, one needs to study the dynamics of the water molecules in the top layer of regolith throughout lunar history. In a seminal paper, [2] investigated the migration of H_2O molecules in the lunar regolith by random hops within the pores. In the current study, we have been developing more realistic diffusion models than the ones used in [2] to regions of the lunar surface where the measured temperatures (from LRO/Diviner) and the hydrogen maps (from Lunar Prospector) suggest that the water ice has been stable over the last few billion years.

Subsurface water ice migration and stability revisited: Water molecules move through the interstices in a porous regolith. In the Knudsen diffusion regime, the molecules do not interact with one another, but move in straight lines between points on the pore channel surface. Upon collision with the surface, a molecule adsorbs for some time, the residence time, that depends on the local temperature. An irregular surface can be considered as a perturbation on the top of a pore with a smooth surface. Along the pore, there are a large number of voids with a power law size distribution that describes the regolith at the Apollo sites [3]. In order to produce more realistic water ice distributions the effects of a fractal grain surface specifications are included in our novel analysis. This requires the tracking of the water molecules in three dimensions. We also study the implications of considering that the water molecules deposition and sublimation rates on the surface of a regolith grain to be the same [2]. This is justifiable if the water vapor is in equilibrium with the ice mono-layers on the grain surface. However, at locations where the density of water molecules in the vapor phase is larger (smaller) than the equilibrium vapor density [2] one expects deposition (sublimation) at a rate larger than the one predicted by equilibrium. An accurate understanding of the temperature profile in the sub-surface is central to the modelling of the water ice distribution with depth since the molecules mobility is controlled not only by the pore size and geometry but also by the residence time. We use temperature maps constrained by the latest LRO Diviner measurements [4]. However, besides the physical conditions for ice stability one needs also to consider the places where there had been a delivery of volatiles over the last two and half billion years. The best candidates are the regions that present the highest hydrogen concentrations as seen by the joint analysis of Lunar Prospector Neutron Spectrometer and topography datasets [5]. Currently, we are implementing the weathering and/or gardening introduced by [6] in our 3-d numerical diffusion code using a stochastic prescription.

References: [1] A. Colaprete, et al. (2010) *Science* 330:463 doi. [2] N. Schörghofer, et al. (2007) *Journal of Geophysical Research (Planets)* 112(E11):2010 doi. [3] G. H. Heiken, et al. (1991) *Lunar sourcebook - A user's guide to the moon*. [4] D. A. Paige, et al. (2010) *Science* 330:479 doi. [5] L. F. A. Teodoro, et al. (2010) *Geophys. Res. Lett.* 37:12201 doi. [6] D. H. Crider, et al. (2003) *Advances in Space Research* 31:2293 doi.

MID- AND FAR-INFRARED LABORATORY MEASUREMENTS IN SUPPORT OF THE DIVINER LUNAR RADIOMETER. I. R. Thomas[1], N. E. Bowles[1], T. J. Warren[1], B. T. Greenhagen[2] and K. L. Donaldson-Hanna[3]. [1]Atmospheric, Oceanic and Planetary Physics Dept., University of Oxford, Oxford, UK (Thomas@atm.ox.ac.uk), [2]Jet Propulsion Laboratory, California Institute of Technology, Pasadena, CA, USA, [3]Dept. of Geological Sciences, Brown University, Providence, RI, USA.

Introduction: The Diviner Lunar Radiometer is a high-resolution, nine-channel mapping radiometer currently orbiting the Moon onboard NASA's Lunar Reconnaissance Orbiter (Table 1). Channels 3-5 are used to map the spectral location of the Christiansen Feature (CF), a mid-infrared emissivity maximum, the wavelength of which is highly dependent on surface composition [1]. The Planetary Spectroscopy Facility (PSF) at the University of Oxford continues to support the interpretation of Diviner observations through the development of new laboratory experiments and measurements of mineral analogue, rock and lunar soil samples.

Channel	Wavelength	Purpose
1	0.35 – 2.8μm	High Sensitivity Solar
2	0.35 – 2.8μm	Mid Sensitivity Solar
3	7.55 – 8.05μm	Christiansen Feature
4	8.1 – 8.4μm	Christiansen Feature
5	8.4 – 8.7μm	Christiansen Feature
6	13 – 23μm	Thermal
7	25 – 41μm	Thermal
8	50 – 100μm	Thermal
9	100 – 400 μm	Thermal

Table 1: Diviner channel descriptions [2].

Simulated Lunar Environment (SLE) Chamber: Many spectral libraries exist at present, some of which include lunar soils and terrestrial analogues measured in the mid-infrared. However, the lunar environment induces a large temperature gradient in the surface affecting the shape and wavelength of the CF [e.g. 3,4,5,6 etc.], making it difficult to compare Diviner observations to spectral libraries where samples have been measured under 'ambient' laboratory conditions. For direct comparisons to be made, new spectra of samples measured in a SLE were required, leading to the construction of an environment chamber for performing high-spectral resolution measurements under lunar conditions (Figure 1).

This chamber has been used to measure a diverse range of materials including pure mineral particulates [7] and lunar soils [8], and is currently being upgraded with a sample-changer to increase the sample measurement rate.

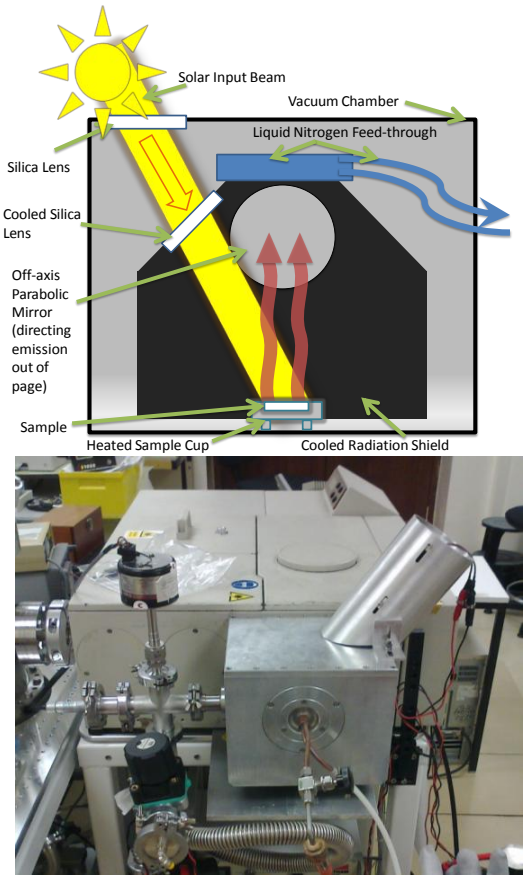

Figure 1: The SLE chamber: schematic (top) and photo (bottom). Samples are heated by solar-like illumination in a very low pressure (<10^{-3} mbar) atmosphere, whilst surrounded by a cooled (<150K) radiation shield.

Multiple-angle Infrared Reflectance: The SLE chamber measures continuous spectra, but illuminates the sample and measures emitted radiation with a fixed geometry only. To determine scattering properties of lunar soils at mid- and far-infrared wavelengths (which are poorly constrained at present) to allow further interpretation of the Diviner dataset, an infrared goniometer has been constructed [See the abstract and poster of Tristram Warren for more details]. The goniometer is capable of making measurements with variable illumination and emission angles, but is capable of

measuring emission in passbands only, similar to Diviner's channels (Table 1).

For investigations into the scattering and surface roughness properties across a continuous wavelength range, samples were measured using a Specac Monolayer Grazing Angle Accessory. This setup consists of two independently controllable arms: one directs the beam from an FTIR spectrometer onto a sample, while the other directs the reflected radiation to a detector (Figure 3) [9], allowing continuous spectra to be measured at variable incidence and emission angles.

Unlike the SLE chamber and goniometer, the lunar thermal environment is not simulated during these measurements; however the results provide a good middle-ground between the two experiments.

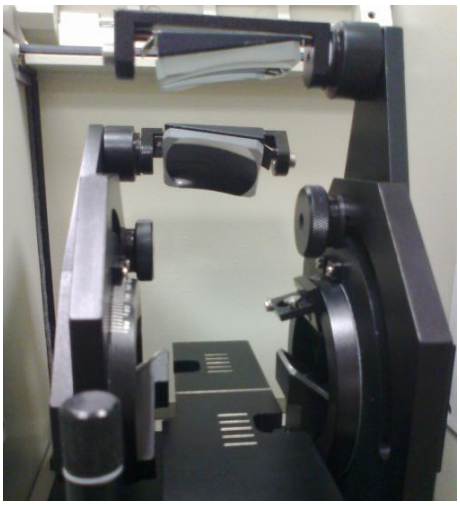

Figure 3: Multiple-angle reflectance accessory

Conclusion: The PSF continues to lead the development and execution of laboratory experiments necessary for the correct interpretation of mid-infrared observations of the Moon by Diviner [e.g. 7, 10]. This presentation will include new measurements highlighting the capabilities of the PSF, including:

- A chamber for measuring the mid- and far-infrared emissivity of minerals and lunar samples under lunar environmental conditions
- A multiple-angle infrared reflectance accessory
- A mid- and far- infrared goniometer.

References: [1] Greenhagen B. T. et al. (2010) Science, 329, 1507; [2] Paige D. A. et al. (2009) The Diviner Lunar Radiometer Experiment, Space Sci. Rev. 150, 125-160; [3] Nash D. B. et al. (1993) J. Geophys. Res., 98, 23535-23552; [4] Henderson & Jakosky (1997) J. Geophys. Res., 102, 6567-6580; [5] Logan et al. (1973) J. Geophys. Res., 78, 4983-5003; [6] Henderson et al. (1996) J. Geophys. Res., 101, 14969-14975; [7] Donaldson-Hanna, K. L. et al. (2012), J. Geophys. Res., doi:10.1029/2011JE003862, in press. [8] Greenhagen B. T. et al. (2012) LPSC 43; [9] Specac Ltd. (2011) "Monolayer Grazing Angle Accessory", Retrieved from: http://www.specac.com/products/ft-ir-specular-reflectance-accessory; [10] Glotch T. D. et al. (2010) Science, 329, 1510.

AN EXPERIMENTAL STUDY ON HUMAN AND ROBOTIC PARTNERSHIPS TO REALISE LUNAR OUTPOST STRATEGIES. Mohamed Peer M. Varman, Department of Aerospace Engineering, Hindustan Institute of Technology & Science, India. E-mail: peer.aerospace@gmail.com.

Introduction: Colonizing the Moon requires a long term and sustainable strategy be developed and executed such that it acts an outpost to explore our next destination: Mars. The debate on whether humans or robots should be employed for space exploration is nothing but a futile argument. This study will address the need for Human-Robot partnership in setting up the lunar base.

Objectives: The Moon's proximity and accessibility allows us to conduct a significant amount of exploration in relative safety with robotic machines teleoperated remotely from Earth and from cislunar space prior to human arrival [1]. The objectives of this discussion is to find out the role of human as well as robotics in setting up the lunar colony, the challenges involved in Human-robotic interaction and to find the potential implication in employing both human and robots in exploring moon.

Role of Human and Robotics in establishing Lunar base:

Why robots? Robot reduces human workload (by easing the burden of manual and repetitive tasks), cost, fatigue-driven errors and risks. To establish navigation and communication satellite system; to conduct demonstration experiments in finding the potential of water extraction; to make initial preparation of outpost site. It can perform even non-scientific works (field labor) under human control and autonomously. It can support long duration manned expedition by surveying and servicing equipments. It can assist in site preparation, sample collection and transport. It can also monitor human partner's health and provides life contingency support.

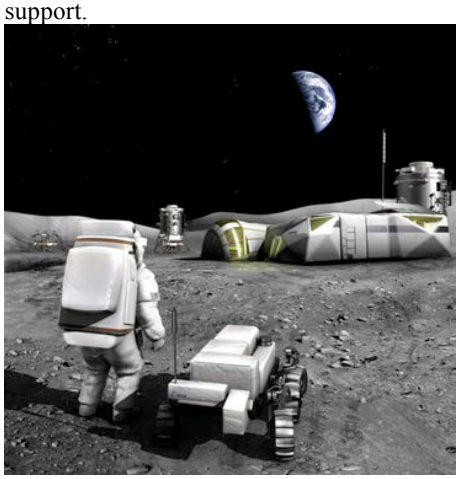

Why Human? To maintain, repair the processing machines; to expand and extend surface operations; to conduct local exploration; to work with robots in mining, collecting and transport, process materials and increase productions; to fix problems and to perform logical and developmental fuctions that humans do best.

Why Human-Robot Partnership?

- It eliminates the need for relying only on robots & automation, since the role of the humans will shift exclusively to tasks of greater complexity as the capabilities of robots become more sophisticated [2] and,
- It avoids complete reliance on humans, as humans are limited by strength, vigilance, fatigue and reaction speed [3].

Challenges involved: Some of the challenges involved in human-robotic partnerships are enabling robot to perform tasks as autonomously as possible, requesting human assistance and expertise only when needed [4]; enabling voice based commands, gestures and wireless digital communication; enabling robots to ask questions so that they can get assistance with cognition and perception; enabling constrained and standardized user interfaces.

Results of the Study: There are specific tasks that are suited to robotics as well as tasks that require only human supervision.

Conclusion: Employing both human and robots in setting up the lunar base has potential implications on realizing the strategies involved effectively and efficiently.

References: [1] Paul D. Spudis and Anthony R. Lavoie. AIAA 2011-7185. [2] Ellery, A. (2001). A robotics perspective on human spaceflight. *Earth, Moon & Planets* 87 (3), 173-190 . [3] Ellery, A. *What is a robotic spacecraft?*, Space robotics, 119 [4] Terrence Fong and Illah Nourbakhsh, *Interation challenges in human-robot space exploration*, Intelligence Div., NASA Ames Research Center.

ORIENTALE IMPACT MELT LAKE: DEPTH AND DIFFERENTIATION. W. M. Vaughan[1], J. W. Head[1], P. C. Hess[1], L. Wilson[2], G. A. Neumann[3], D. E. Smith[4], and M. T. Zuber[4]. [1]Department of Geological Sciences, Brown University, Providence, RI 02912, USA, Will_Vaughan@brown.edu. [2]Lancaster Environment Centre, Lancaster University, Lancaster, LA1 4YQ, UK. [3]Solar System Exploration Division, NASA Goddard Space Flight Center, Greenbelt, MD 20771. [4]Department of Earth, Atmospheric, and Planetary Sciences, MIT, Cambridge, MA 02139.

Introduction: Impact melt emplacement and evolution in lunar multi-ring basins is poorly understood since impact melt deposits in basins are generally buried by mare basalt fill and obscured by subsequent impact cratering. The relatively young Orientale basin [1-3], which is only partially flooded with mare basalt [4-5], opens a rare window into basin-scale impact melts.

We describe the geology of impact melt-related facies in Orientale and suggest that the central depression of Orientale may represent a solidified impact melt lake that vertically subsided shortly after basin formation due to solidification and cooling [6]. We use Lunar Orbiter Laser Altimeter (LOLA) data to measure the depth (~1.75 km) and diameter (~350 km) of this central depression. If all the observed subsidence of the central depression is due to solidification and cooling, the melt lake should be ~12.5-16 km deep, far more voluminous (~10^6 km^3) than the largest known differentiated igneous intrusions on Earth [7-8]. We investigate the possibility that the Orientale melt lake has differentiated and model 1) the bulk composition of the melt lake, 2) the operation of melt mixing in the melt lake, and 3) the chemical evolution of the resulting liquids on the An-Fo-Qz ternary in order to predict the lithologies that might be present in the solidified Orientale melt lake. Finally, we consider the possible significance of these lithologies.

Geology of melt-related facies in Orientale: The topography of the Orientale basin is shown in Figure 1. The Inner Rook Ring, at a radius of 480 km from the basin's center, and the Outer Rook Ring, at a radius of 620 km, are interpreted respectively as the peak ring [9] and an approximation of the rim crest of the transient cavity prior to cavity collapse [1, 10]. Models of impact melt production suggest that most melt is formed in a hemispherical or spherical melt cavity interior to the peak ring [11]. Assuming that only a small proportion of melt is completely ejected by the collapse of the melt cavity during crater modification [12], most impact melt should remain interior to the Outer Rook Ring [12-13].

In fact, the Maunder Formation, which lies inside the Outer Rook Ring, comprises two facies which have been interpreted as impact-melt related [1-2, 14-15]. A smooth inner plains facies, exposed through thin mare fill [5, 16] and interpreted as a pure impact melt sheet [1-3], occupies the central depression of the Orientale basin. Near the edges of the central depression, wrinkles, fractures, and polygonal cracks are apparent in the smooth facies and overlying mare. About 175 km from the center of the Orientale basin, the topography abruptly rises ~1.75 km from the central depression along a series of marginal normal faults to a corrugated, rough fissured facies. This corrugated facies is interpreted as clast-rich impact melt draping the Inner Rook Ring peaks [1-3].

Depth of the Orientale melt lake: What caused the substantial (~1.75 km) vertical subsidence of the Orientale basin's central depression? One possibility is that the vertical subsidence of the smooth facies is related to thermal stresses resulting from impact-generated heat and uplift of crustal isotherms [17]. This model predicts gentle radial vertical subsidence. However, new, high-resolution LOLA altimetry [18] shows that the vertical subsidence of the central depression is abrupt: along the west edge of the depression, the topography drops ~2 km over a radial distance of ~20 km. The model of [17] cannot fully explain this abrupt vertical subsidence. The fractures of the smooth inner plains facies bear resemblance to the deformed surfaces of terrestrial lava lakes [19]; if the smooth facies is an impact melt sheet, these fractures could result from lateral shrinkage upon solidification and cooling. The vertical subsidence of the central depression could similarly result from solidification and cooling of the impact melt sheet [6]. This constrains the depth of the impact melt sheet: a body of hot magma emplaced on the lunar surface should undergo ~11-14% vertical subsidence [6] upon solidification and cooling. ~1.75 km average vertical subsidence is observed (Fig. 1), implying the melt sheet is up to ~12.5-16 km deep.

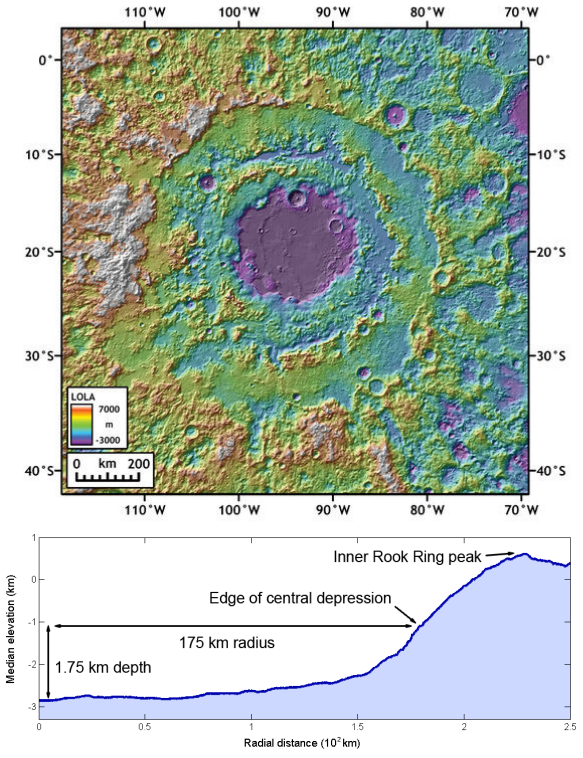

Figure 1. Topographic map (top) and average radial topographic profile (bottom) of the Orientale basin.

Differentiation of the Orientale melt lake: The Orientale melt sheet (which, volumetrically, may be better described as a lake) is ~350 km in diameter and may be up to ~12.5-16 km deep, implying a volume of ~10^6 km^3, far greater than the largest differentiated igneous intrusions known on Earth [7-8]. Could the Orientale melt sheet have differentiated? Previous work [20] has argued that impact melt sheets do not differentiate since 1) few or no differentiated impact melt sheets are known on Earth, 2) impact "melt" sheets are better described as magmas carrying cold clasts, assimilation of which rapidly depresses liquid temperature. However, mounting evidence suggests that several large terrestrial impact melt sheets have differentiated (namely, the Sudbury Igneous Complex [21-22], Manicouagan [23], and Norokweng [24]). Also, the volume of shock melt produced by an Orientale-size impact is so enormous [11] that huge clast-free volumes seem likely to exist. We therefore develop a simple model to predict the lithologies that might crystallize from the Orientale melt lake and other solidified multi-ring basin impact lakes based on 1) the bulk composition of the melt lake, 2) the operation of melt mixing in the melt lake, and 3) the chemical evolution of the resulting liquids on the An-Fo-Qz ternary.

Bulk composition of the melt lake. We model the lunar crust as a planar layer of anorthosite ~26.9 km thick overlying an anorthositic norite layer extending to a depth of 52.0 km based on the dual-layered crustal thickness model presented in [25]. The anorthosite layer has a density of 2.82 g/cm^3 and a composition of 86 wt. % anorthite, 10.5 wt. % enstatite, and 3.5 wt. % forsterite; the anorthositic norite layer has a density of 3.04 g/cm^3 and a composition of 60 wt. % anorthite, 30 wt. % enstatite, and 10 wt. % forsterite. These compositions are highly approximate; the modal anorthosite is based on [25] and the modal mafic minerals are calculated based on a 3:1 enstatite:forsterite proportion by weight.

The melt cavity has a complex geometry [11] which we approximate as a hemisphere with its largest cross section coincident with the top of the anorthosite crustal layer. M^3 [16] and Kaguya [26] spectra of the Orientale region detect no evidence for the presence of subcrustal mafic mantle material in Orientale basin deposits, so we assume that the Orientale impact did not sample the upper mantle. Therefore, we choose the radius of our modeled melt cavity to be 50 km, slightly less than the thickness of the far side crust [25]. The mass of each layer melted was calculated as the product of the volume of the melt cavity hemisphere intersecting the anorthosite and anorthositic norite layers and the density of these layers.

Melt mixing. Impact melt is vigorously mixed and may therefore be homogenous; i.e., the composition of any small volume of melt will be identical to the bulk composition of the melt lake. However, even a well-mixed melt lake may not be homogenous [22]: impact-melted liquids with very different viscosities may be effectively immiscible on short timescales and stratify according to density contrasts. In the Orientale melt lake, viscous anorthosite liquid and fluid mafic liquid could be effectively immiscible and separate by density to produce anorthosite liquid overlying dense mafic, pyroxenitic liquid.

Igneous differentiation. We treat igneous differentiation of the homogenous melt lake on the well-known An-Fo-Qz ternary phase diagram at 1 atm (since lunar crustal pressures are low). Impact melt has an initial temperature well above the liquidus at 1400 °C. Upon crystallization, the processes of crystal settling and convection operate to fractionate and mix crystals and liquid. We consider homogenous and density-stratified liquids operated upon by fractional crystallization and equilibrium crystallization to bound the resulting lithologies (Fig. 2).

Implications. Three puzzles in lunar petrology are young anorthosites [27], the provenance of Mg-suite rocks [28], and the provenance of Mg-spinel lithologies [29]. Young anorthosites could have crystallized from melt sheets. Mg-suite norites and troctolites could form in melt sheets, although their distinctive geochemical signature [28] would be hard to explain. Mg-spinel lithologies could form from mixing of anorthosite and olivine-rich mantle liquids. We continue to investigate remotely-sensed data and the lunar sample suite in order to identify possible impact melt differentiates.

Figure 2. Model differentiated melt lake lithologies.

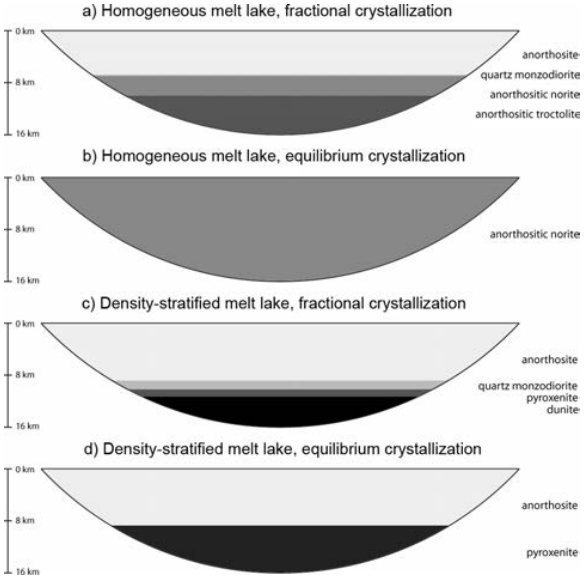

References: [1] Head J. W. (1974) *The Moon, 11,* 327-356. [2] Howard K. A. et al. (1974) *Rev. of Geophys., 12,* 309-327. [3] McCauley J. F. (1977) *PEPI*, *15*, 220-250. [4] Greeley R. et al. (1993) *JGR, 98,* 10873-10882. [5] Whitten S. J. et al. (2010) *LPS,* 41. [6] Head J. W. and Wilson L. (2011) *LPS, 42*. [7] Nielsen T. F. D. (2004) *J. Pet., 45,* 507-530. [8] Bonini W. E. (1982) *Mag. Proc. of Early Plan. Crusts*, 53-55. [9] Baker D. M. H. et al. (2011) *Icarus, 214,* 377-393. [10] Head J. W. (2010) *GRL, 37.* [11] Cintala M. J. and Grieve R. A. F. (1998) *MAPS, 33*, 889-912. [12] Hawke B. R. and Head J. W. (1976) *Imp. and Expl. Cratering,* 815-841. [13] Osinski G. R. et al. (2011) *EPSL*, *310*, 167-181. [14] Spudis P. D. (1993) *The geology of multi-ring impact basins,* Cambridge. [15] Head J. W. and Wilson L. (1992) *GCA, 55,* 2155-2175. [16] Head J. W. et al. (2010) *LPS, 41.* [17] Bratt S. R. et al. (1985) *JGR, 90*, 12415-12433. [18] Smith D. E. et al. (2010) *GRL, 37.* [19] Barberi F. and Varet J. (1970) *Bull. Volc., 34,* 848-917. [20] Warren P. H. et al. (1996) *GSA Special Papers, 307*, 105-124. [21] Therriault A. M et al. (2002) *Econ. Geo.*, *97,* 1521-1540. [22] Zieg M. J. and Marsh B. D. (2005) *GSA Bull., 117,* 1427-1450. [23] Spray J. G. and Thompson L. M. (2008) *MAPS, 43,* 2049-2057. [24] Hart R. J et al. (2002) *EPSL, 198,* 49-62. [25] Wieczorek M. A. et al. (2006) *RIMG, 60,* 221-364. [26] Yamamoto S. et al. (2010) *Nature Geo., 3,* 533-536. [27] Borg L. E. et al. (2011) *Nature Geo.*, *477,* 70-72. [28] Hess P. C. (1994) *JGR*, *99,* 19083-19093. [29] Pieters C. M. et al. (2011) *JGR, 116.*

THE SPACE ENVIRONMENT GONIOMETER. T. J. Warren[1], I. R. Thomas[1] and N. Bowles[1], [1]Atmospheric, Oceanic and Planetary Physics, University of Oxford, Department of Physics, Clarendon Laboratory, Parks Road, Oxford, OX1 3PU, United Kingdom, (warren@atm.ox.ac.uk, thomas@atm.ox.ac.uk, bowles@atm.ox.ac.uk).

Introduction: This paper describes work currently under way in the Atmospheric, Oceanic and Planetary Physics Dept. to develop the 'Space Environment Goniometer' designed to support thermal infrared remote sensing measurements of airless bodies in the Solar System. In particular, it will be used to support measurements currently being made by the Diviner Lunar Radiometer ('Diviner'), a nine-channel mapping radiometer currently in orbit around the Moon as part of NASA's Lunar Reconnaissance Orbiter mission.

The Diviner channels range from the visible to the far infrared (>400μm) [1,2], with three channels centred around the mid-infrared (8μm). Although significant progress is being made in determining the scattering properties of the lunar soil in the visible and near-infrared [e.g. 3,4], there is still limited or no data available on the scattering or emission phase functions in the thermal infrared, required by 3D thermal-physical models of the lunar surface [5] to accurately reproduce the brightness temperatures observed by instruments such as Diviner. To fill this gap, we are developing an automated, vacuum compatible goniometer system capable of making measurements under lunar conditions in the laboratory at the same wavelengths as Diviner.

Once built the goniometer will be able to measure full bidirectional reflectance functions (BDRF) and emission phase functions (EPF) of lunar analogue minerals and Apollo samples, allowing Hapke [6] or similar parameters to then be fitted to the measurments, creating a new library of BDRF and EPF measurements directly comparable to the Diviner dataset.

Goniometer: Detailed design work for the goniometer has been completed and the instrument is currently under construction. Presently, the goniometer setup (Figure 1) is being tested in the visible on an optical bench in air. In the future the goniometer will make measurements in the mid-infrared surrounded by a cold shield (Figure 2) inside the vacuum chamber (Figure 3). The cold shield and vacuum chamber simulate the lunar environment, by creating a temperature gradient within the sample. For intercomparison, the new goniometer has been designed to have a similar angular range and accuracy as other infrared goniometers [e.g. 7]. The physical design of the goniometer is described below:

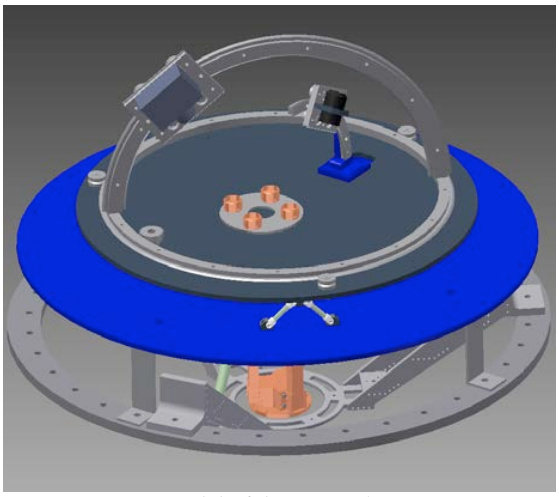

Figure 1: CAD model of the internal goniometer setup

Light Source: This initial goniometer uses a high temperature 75W quatz halogen bulb and reflector to provide a well controlled light source. In future the light source will be upgraded to a solar-like lamp to more closely simulate the environment on the near lunar-surface.

Radiometer: The radiometer will be based on a high performance pyro-electric detector (Infratec LIE-312F) with a reference chopper [4] and views of a calibrated blackbody target. Wavelength selection will be provided by spare Diviner filters [2]. In the future the system will be coupled to a FTIR spectrometer to allow full spectro-goniometric measurement to be made.

Mechanical Components: Two stepper motors are used to control the position of the radiometer's azimuthul and emission angles, while another stepper motor controls the position of the light source (i.e. incidence angle). The incident angle can be varied between 0-74^o, emission angle from 0-84^o and the azimuth angle from 0-180^o. The angular accuracy of the goniometer will be ~0.01^o. A PC with Labview^{TM} software will automate the measurement process.

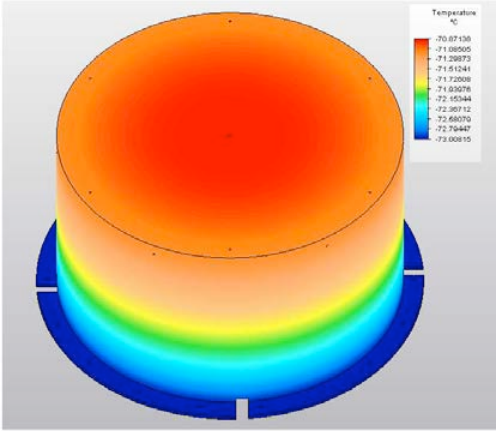

Figure 2: A thermal model of the cold shield

Cold Shield and Vacuum Chamber: The goniometer will make measurements in a lunar simulated environment. To achieve this, the whole system is enclosed in a $<10^{-3}$ mbar vacuum chamber (Figure 3) and surrounded by a <150K cold shield powered by a 140W cold head. The cold shield is made from thermally conducting 2mm copper, and has a diameter of 0.8m and height of 0.5m. Thermal models have shown this will cool uniformly, with any temperature gradient between top and bottom <8K (Figure 2). It is also important to cool the experiment down to reduce stray infrared radiation inside the goniometer. Critical components will be coated in high-emissivity paint (e.g. NEXTEL Black velvet) to prevent stray light reflections etc. from affecting the measurements where appropriate.

Figure 3: Vacuum chamber that will enclose the goniometer and cold shield

References: [1] Thomas I. R. et al. (2012) LPSC XXXXIII abstract #2637; [2] Paige D. A. et al. (2009) The Diviner Lunar Radiometer Experiment, Space Sci. Rev.150, 125-160; [3] Foote, E. J. (2012) LPSC XXXXIII abstract #2357; [4]Foote, E. J. (2009) LPSC XXXX abstract #2500; [5] D. A. Paige *et al*., The Lunar Reconnaissance Orbiter Diviner Lunar Radiometer Experiment. Space Sci. Rev. 150, 125 (2010); [6] Hapke, B. (1993) Theory of Reflectance and Emittance Spectroscopy, Cambridge Univ. Press. [7] Shepard, M. K. (2001) LPSC XXXII abstract #1015; [8] InfraTec Ltd. (2012) LIE-312f datasheet, retrieved from: http://www.infratec-infrared.com/Data/LIE-312f.pdf.

LUNAR MARE PHOTOMETRY FROM SMART-1/AMIE DATA. O. Wilkman[1], K. Muinonen[1,2], A. Penttilä[1] and H. Parviainen[3], [1]Department of Physics, University of Helsinki PL 64 00014 Finland (olli.wilkman@helsinki.fi) [2]Finnish Geodetic Institute, Kirkkonummi, Finland, [3]Instituto de Astrofisica de Canarias, La Laguna, Tenerife, Spain.

The SMART-1 spacecraft pioneered European lunar exploration with its orbiting mission in 2004–2006. Among its instruments was the optical/near-infrared camera AMIE which mapped a significant part of the lunar surface with a resolution between 40–200 metres per pixel.

We have taken a sample of 821 AMIE frames, representing most of the mare regions of the near side. We then extracted multi-angular photometry from the images by sampling the brightness of the surface and estimating the local observational geometry. The present work is an extension of an earlier study using a smaller data set [1][2].

We make the assumption that the photometric properties of mare surfaces are similar in all the regions studied and consider the entire data set as representing "average" mare properties. Mare surfaces were chosen because they are smooth, making the estimation of the observational geometry simple, and also because they are dark, justifying the use of the Lommel-Seeliger scattering law.

We use a numerical ray-tracing code with a simulated regolith medium consisting of spherical particles to compute the effect of mutual shadowing of surface particles. This simulation considers the full observational geometry and includes azimuthal shadowings effects. The contribution of the shadowing function can then be removed from the data, resulting in a phase function for the lunar mare surfaces.

In all cases, the reduced phase function shows a significant opposition brightening, indicating that the lunar opposition effect is not explainable through shadowing effects only.

Physical properties of the surface such as porosity and surface roughness affect the shadowing function. By varying these properties in the ray-tracing simulation, some information of the corresponding properties of the lunar surface may be gained.

[1] Muinonen, K et al. (2011), *A&A, 531,* A150.

[2] Wilkman, O (2011), Master's thesis, University of Helsinki

EXTRA HIGH UNDERGROUND TEMPERATURE OF OCEANUS PROCELLARUM REVEALED BY CHANG'E-1 LUNAR MICROWAVE RADIO METER DATA. W. Zhang[1] and N. E. Bowles[2], [1] University of Oxford, Department of Physics, Clarendon Laboratory, Parks Road, Oxford, OX1 3PU, United Kingdom, zhangw@physics.ox.ac.uk , [2] University of Oxford, Department of Physics, Clarendon Laboratory, Parks Road, Oxford, OX1 3PU, United Kingdom, n.bowles1@physics.ox.ac.uk.

Lunar soil temperature profile, including surface and interior, is an important parameter in lunar exploration. The lunar surface temperature has been measured by Diviner but the deep temperatures have only been measured at the Apollo 15 and 17 landing sites until the recent launch of the Chang'e-1 (CE-1) mission. The CE-1 Lunar orbiter is equipped with Microwave Radio Meter (MRM) instrument, which is a full-power 4 frequency microwave radiometer, and it is mainly used to detect the brightness temperature of lunar surface. The penetrating depth is generally less than 0.5 m at 37.0 GHz, 1.0 m at 19.35 GHz, and 2.0 m at 7.8 GHz, and the 3 GHz frequency channel can penetrate to a depth of 5 m or more [1]. Using data from this instrument we have successfully plotted the spatial variation of lunar surface temperature at 5 meter depth (Figure 1, left).

Studying the brightness temperature distribution data of lunar surface obtained by ChangE-1, it appears to closely follow the topographic information of the lunar surface. For example, in the 37.0 GHz brightness temperature map, we can distinguish the impact craters on the moon, while in the 3.0 GHz brightness temperature map we can distinguish mare and highlands. Thus we can link MRM temperature data with topography and geological features.

Through the comparison of the brightness temperature map and geological conditions on lunar surface, we can see an interesting phenomenon. In the Channel 4 and 3's brightness temperature maps, the Oceanus Procellarum (North 18.4°, East 57.4°), which is the largest of the lunar maria, shows nothing special. But if we look at Channel 1 (3.0GHz, 5m depth)'s brightness temperature map, which indicates deep underground temperature of the lunar surface, we instantly notice that the Oceanus Procellarum has the highest underground temperature, and can thus be significantly noticed from the map, see enlarged Figure 1 below. This means underground temperature is quite different with surface ones, as it is not expected to be influenced by solar radiation at these depths but by underground heat flow.

Oceanus Procellarum might be the possible location of the youngest basalts on the lunar nearside.The existence of this Procellarum basin is not completely accepted because the geochemical arguments for such a basin as well as the identification of ring structures of this basin are subject to alternative interpretation [3]. However, as we presented above, ChangE-1 MRM data are consistent with a Procellarum basin. Since Procellarum basin concentrates more Thorium and FeO [2], there may be evidence for further melting and differentiation after the intial formation of the lunar crust (e.g. Glotch et al 2010), and may retain a higher sub-surface temperature, as thorium is a well-known magmatophile element [4].

What's the geophysics mechanism behind such phenomena? It deserves our further consideration.

References: [1] Wang Z. Z. et al. (2010) *Science China Earth Sciences*, 53, 1392- 1406. [2] Hiesinger H. et al. (2003) *Journal of Geophysical Research*, 108, 5065, doi:10.1029/2002JE001985. [3] Spudis P. D. and Schultz P. H. (1985) *Lunar Planet. Sci.*, XVI, 809– 810, 1985. [4] Sclater J.G., Jaupart C., Galson D. (1980) *Rev. Geophys. Space Phys.* 18, 269-311.

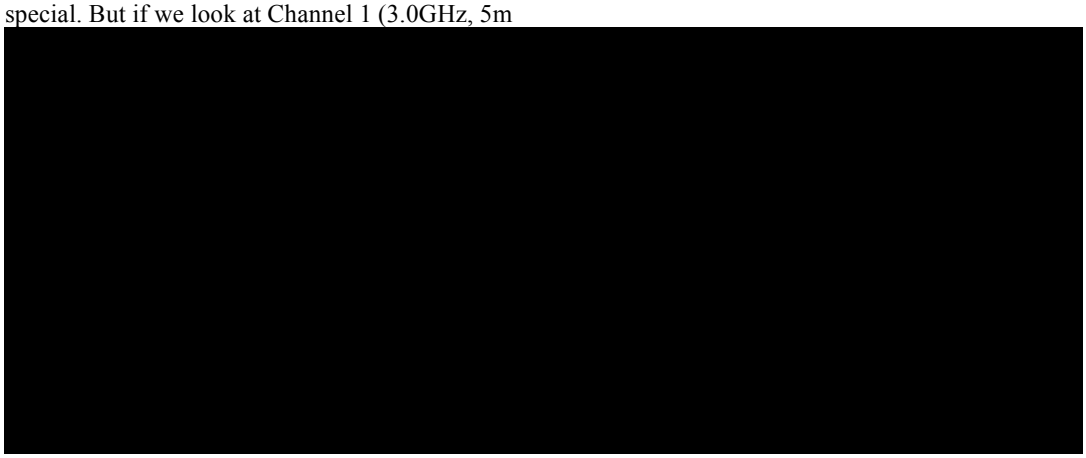

Figure 1. Enlarged lunar deep brightness temperature map at 5 meter depth (Left) shows clearly the shape and position of Oceanus Procellarum. The right Map of the lunar surface showing the location of the investigated basins, the Apollo and Luna landing sites, are cited from Ref [2]'s figure 1.

CHANG'E-1 LUNAR MICROWAVE RADIO METER DATA ANALYSIS AND COMPAREATION WITH DIVINER DATA. W. Zhang[1] and N. E. Bowles[2], [1] University of Oxford, Department of Physics, Clarendon Laboratory, Parks Road, Oxford, OX1 3PU, United Kingdom, zhangw@physics.ox.ac.uk, [2] University of Oxford, Department of Physics, Clarendon Laboratory, Parks Road, Oxford, OX1 3PU, United Kingdom, n.bowles1@physics.ox.ac.uk.

China's first lunar probe CE-1was successfully launched on Oct. 24th, 2007 in Xichang, and controlled to impact on the lunar surface On March 1, 2009. During its operation period, CE-1 obtained a large number of valid scientific data from the eight instruments in its scientific payload, including the Microwave Radio Meter (MRM). The MRM is a full-time 4 frequency microwave radiometer, and it is mainly used to detect the brightness temperature of lunar surface, to retrieve lunar regolith thickness, temperature, dielectric constant and other related properties. The MRM's has four channels working a frequencies 3.0GHz，7.8GHz，19.35GHz and 37GHz. Its observing directions are consistent with the fixed CE-1 track directions. Details of instruments and ground calibrations are described in ref [1].

Figure 1 and Figure 2 show the cover times of MRM data in homolographic grid (each grid in the equatorial region is 2 ° × 2 °, about 3678km2) during the whole detection phase, reflecting data distribution on lunar surface.

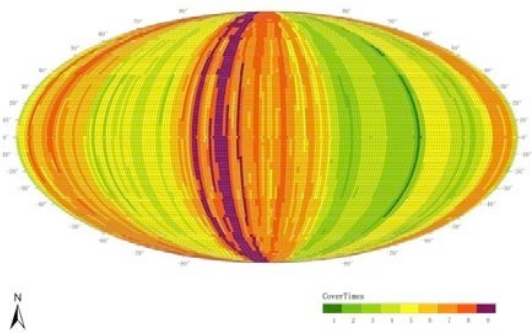

Figure 1. MRM data cover on lunar day during CE-1 detection period,In this figure, lunar surface is divided into 11306 homolographic grids, and the colors of the grid stand for the cover time.

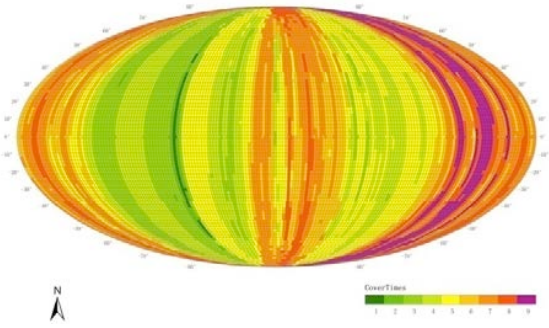

Figure 2. MRM data cover at lunar night during CE-1 detection period.

Since the 3.0GHz channel can penetrate up to 5 meter below the lunar surface, it is really interesting if we could compare such data with previously derived surface temperature data from instruments such as the Diviner radiometer on NASA's Lunar Reconnaissance Orbiter [2]. Therefore, on the basis of MRM data and the ephemeris of ChangE-1 spacecraft, we successfully plotted a 3-dimensional Lunar Brightness Temperature map for 5 meter deep lunar soil (Figure 3).

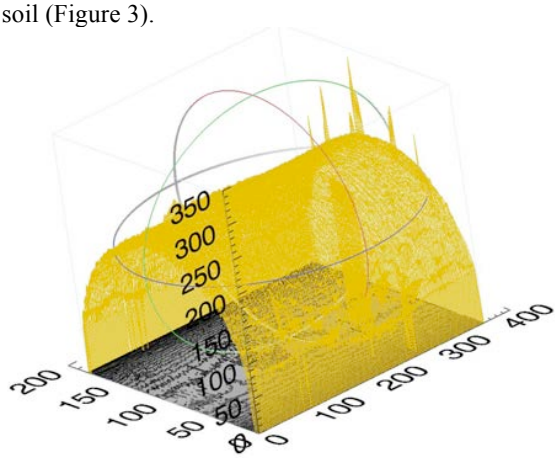

Figure 3. Moon's 5m-depth brightness temperature 3-D map derived from ChangE-1 MRM data.

Then we looked for some overlaps between the Chang'e data and Diviner's coverage, we extracted Diviner data with local times and latitude/longitude co-ordinates derived from the region with most ChangE-1 flyby times (0-5degrees North and 40-35degrees West for midday (11am – 1pm local time) and 0-5 degrees North and 140-145degrees East for midnight (11pm – 1am)). We show that the two spacecrafts' data are in accordance (Figure 4 and Figure 5).

References: [1] Wang. et al. (2010) *Science China Earth Sciences*, 53, 1392- 1406. [2] Paige. et al. (2010) *Space Science Reviews*, 150 (1-4), 125-160.

Supporting Mars exploration: BIOMEX in low Earth orbit as first step to start further astrobiological experiments on the Moon by the use of Raman and PanCam technology

Jean-Pierre de Vera[1], Ute Boettger[1], Nicole Schmitz[1], Heinz-Wilhelm Hübers[1,2], Ralf Jaumann, Tilman Spohn[1] and Co-I team of BIOMEX

[1]German Aerospace Center (DLR) Berlin, Institute of Planetary Research, Rutherfordstr. 2, 12489 Berlin
[2]Technische Universitaet Berlin, Institut für Optik und Atomare Physik, Hardenbergstr. 36, 10623 Berlin, Germany

The low earth orbit (LEO) experiment BIOMEX is an interdisciplinary and international space research project selected by ESA. The experiment will take place on the space exposure facility EXPOSE-R2 on the International Space Station (ISS) and is foreseen to be launched in 2012. The prime objective of BIOMEX is to measure to what extent biomolecules like pigments and cellular components are resistant to and able to maintain their stability under space and Mars-like conditions. The results of BIOMEX will be relevant for space proven biosignature definition and for the formation of a biosignature data base (e.g. the proposed creation of an international Raman library). The library will be useful for future space missions like in "Search for Life" missions to Mars. The secondary scientific objective is to analyze to what extent terrestrial extremophiles are able to survive in space, and which interaction between biological samples and selected minerals (including terrestrial, Moon- and Mars analogue varieties) can be observed under space- and Mars-like conditions. In this context the Moon will be a promising further platform to perform similar experiments with less shielding influence due to periodical absence of Earths' magnetic field and higher solar irradiation. Hence, using the Moon as a second astrobiological exposure platform to the existing LEO investigations would provide us with additional knowledge about the stability of biomarkers under different environmental conditions to effectively support the preparation towards "Life-detection" missions to Mars and beyond. A possible approach to efficiently combine a Lunar BIOMEX-like experiment with existing plans for Lunar exploration is to realize in-situ measurements of exposed bio-relevant material by making use of instruments which are likely anyway a part of the scientific payload of future lunar landers. Here, we propose to use a combination of Raman spectroscopy with multispectral and high-resolution imagery for in-situ measurements on a proposed astrobiological exposure platform on a possible lunar lander. The strawman payload for ESA's Lunar Lander includes a Raman spectrometer as well as a mast-mounted multispectral Panoramic Camera with a high-resolution channel [1].
This technology combination might increase significantly the scientific outcome and would provide more knowledge about the Moon's surface itself as well as about the stability of life-markers in an extraterrestrial environment with much closer relations to the radiation properties of the surface of Mars. A Raman data base collecting data of the mineral composition close to the lunar landing site and collecting data of spectra changes of the exposed geo-biological samples together with data from LEO and space simulation experiments will lead to further progress on analysis and interpretation of data we will get during future Mars exploration missions.

[1] Carpenter et al., Objectives and Model Payload for Human Exploration Preparation on ESA's First Lunar Lander, 61st International Astronautical Congress, Prague, CZ.

THE DORN EXPERIMENT: AN ALPHA SPECTROMETER DEDICATED TO THE CHARACTERIZATION OF THE TRANSPORT OF LUNAR VOLATILES. P.-Y. Meslin[1], J.-C. Sabroux[2], J.-F. Pineau[3], G. Deprez[1], O. Gasnault[1], N. Michielsen[2], P. Richon[4], E. Chassefière[5], E. Seran[6], N. Renno[7], N. Yamashita[8]. [1]Recherche en Astrophysique et Planétologie (IRAP), 9 avenue Colonel Roche, BP 44346, 31028 Toulouse, France ; pmeslin@irap.omp.eu; +33 (0)5-61-55-75-53, [2]Institut Radioprotection et de Sûreté Nucléaire (IRSN), Saclay, France, [3]ALBEDO Technologies, Razès, France, [4]Commissariat à l'Energie Atomique (CEA), France, [5]IDES, CNRS, Orsay, France, [6]LATMOS, IPSL/CNRS, Paris, France, [7]University of Michigan, Ann Arbor, USA.[8]Planetary Science Institute, Albuquerque, USA.

Introduction: We have been developing an instrument named DORN (Detection of Outgassing RadoN, after the name of the German physicist who first discovered this gas) for ESA's Lunar Lander. It is an alpha spectrometer that will work very much like previous Alpha Particle Spectrometer (APS or APXS) that have flown on other planetary missions (on Surveyor, MER, Rosetta), but it is dedicated to the measurement of radon and its decay products. Radon is a key tracer of the transport of gases in the lunar environment (regolith and exosphere), which explains why it has been targeted by several lunar missions since the very early stages of the exploration of the Moon (Explorer 35, Surveyor 5, 6, 7, Apollo 15, 16, Lunar Prospector, Kaguya-Selene, Chandrayaan-1). Past measurements revealed time and space variations of its surface activity, possibly related to the existence of episodic release of volatiles during seismic events or TLPs, through conducts or fracture networks possibly at mare boundaries and young and massive craters [1]. But they have raised more questions than answers, in part because of their limited quality, or limited spatial or temporal coverage.

Objectives: Long-term monitoring of its surface activity, in particular in the South polar region, would considerably increase our understanding of its cycle and would enable us to achieve the following objectives: study the transport of gases through the lunar regolith; monitor the venting activity of the Moon and identify active outgassing spots; study the transport of volatiles in the lunar exosphere; detect an effect of the soil water content on the exhalation rate (direct effect or indirect effect due to its role as a weathering agent); study the transport of lunar dust over time scales of the order of the hal-life of ^{210}Pb (~22.3 y); and establish ground truth for orbital measurements of radon, polonium (from Apollo15,16, Lunar Prospector and Kaguya-Selene APS) and uranium (from Kaguya-Selene Gamma Ray Spectrometer), the measurement of the latter being possibly biased by the mobility of radon [2].

Some interesting properties: Radon as a tracer has many advantages as a tracer. It has a well-identified source term, intrinsic to the regolith: uranium-238, which has been mapped by Kaguya-Selene Gamma Ray Spectrometer [3]. Its only significant loss process is its radioactive decay. The temperature dependence of its adsorption is the strongest of all noble gases, which could lead to a pronounced diurnal cycle, as was observed for argon-40 by Apollo 17 mass spectrometer [4]. It has a limited lifetime (~5.5 days), which is an advantage in the search for active degassing spots. Moreover, it is not subject to chemical contamination issues (radon is necessarily endogeneous). Finally, remote measurements are made possible owing to the infinite range of alpha particles in the lunar exosphere. Therefore, radon appears to be an interesting "benchmark" tracer to study the fragile lunar exosphere before it is polluted by human exploration, and to understand the transport of other volatiles of interest for this exploration.

The DORN instrument: The DORN instrument is made of two independent subsystems, with different objectives, although their detection unit is identical. The first subsystem, DORN-1, is aimed at measuring ^{222}Rn, ^{218}Po, ^{214}Po and ^{210}Po deposited around the lander and originating from a region of radius ~30° in latitude/longitude (approximate distance crossed by radon atoms during their average lifetime of 5,5 days, assuming no reincorporation into the regolith). It is composed of 4 sets of double-sided silicon detectors, measuring alpha particles over the energy range [~1-10MeV] (one side to measure the surface activity, the other one to reject part of the background ionizing radiations). It is ideally located on the edge of the lander, pointing towards different directions (e.g., illuminated and shadowed targets) The second subsystem, DORN-2, is designed to measure directly the exhalation rate of radon from the subsurface, at the landing site. It is composed of a a microcooler fixed to a cup layed on the ground, bringing the temperature of a cold finger to ~90K in order to trap escaping atoms by adsorption. Two silicon detectors face this cold finger to measure the activity deposited on it.

We are currently developing a global thermal and transport model to predict the radon cycle at the surface of the Moon, in particular at the South Pole, to validate the design of the instrument in terms of surface area of the detectors. DORN objectives and technical solutions will be presented, together with results of this model.

References:

[1] Crotts, A. P. S (2008), *Astrophys. J.* 687, 692–705. [2] Meslin, P.Y. and Déprez, G. (2012), *43rd LPSC Conference*, Abstract #2800. [3] Yamashita, N. et al. (2010), *GRL*, 37, L10201. [4] Hodges R. R. (1977), *Physics Earth Planet. Sci. Interiors*, 14, 282-288.

RADIOGENIC HEAT PRODUCTION IN THE MOON CONSTRAINED BY PLAGIOCLASE-MELT PARTITIONING OF URANIUM AND THORIUM. J. de Vries[1,2], W. van Westrenen[1] and A. van den Berg[2], [1]VU University Amsterdam, Netherlands, j.de.vries@vu.nl, [2]Utrecht University, Netherlands

Introduction: Accurate knowledge of global heat budgets is essential for the development of planetary thermal evolution models. In contrast to Earth, the lunar heat budget is at present poorly constrained. Only four heat flow measurements have been performed on the Moon [1], and the concentrations of U, Th and K in the Moon are not well constrained. Here, we explore a method of estimating radiogenic heat production in the Moon, and its depth distribution, based on combining recent observations of the surface concentrations of U, Th and K in the highlands regions of the Moon with experimental constraints on the distribution of these elements between anorthositic plagioclase and silicate melt at high temperature.

Background: Remote sensing data on the composition of the lunar surface, combined with data from samples returned with the Apollo and Luna missions and meteorite data, has led to improved estimates of the potassium, thorium and uranium concentrations of the lunar surface, e.g. [2-6]. Most studies to date have focused on the resulting concentrations of radiogenic heat producing elements in the Procellarum KREEP terrane on the lunar near side, which shows pronounced enrichments in K, U and Th concentrations due to the influence of the enriched KREEP source. Our focus here is on the concentrations of the main heat producing elements derived for the Feldspathic Highlands Terrane (FHT), composed mostly of anorthite-rich plagioclase, as the Lunar Magma Ocean (LMO) concept provides a direct link between surface remote sensing data and the Moon's interior heat budget. These data, together with mineral-melt partition coeffients for Th, U and K constrain the concentrations of these elements in the main lunar silicate reservoirs, from which the bulk Moon concentrations can be determined.

Crystallisation of the LMO resulted in a layered mantle with olivine and orthopyroxene-rich layers at the bottom, followed by clinopyroxene-rich materials and a dense ilmenite-rich layer at shallow depth below the plagioclase flotation crust [7]. To combine surface concentration observations with this petrological model for LMO crystallisation and thus provide information about the Moon's heat budget, information is required on the partitioning behaviour of U, Th and K between plagioclase and melt. Although some preliminary models for the behaviour of U and Th in plagioclase-melt systems were developed in the past [8], the experimental database used for these models is small - mostly due to the fact that on Earth, plagioclase is not a relevant reservoir for these elements.

Previous studies on trace element incorporation into plagioclase [9-14] did not focus on the radioactive elements Th and U (although some of these studies did include these elements in their experiments). As a result the spread in partition coefficients for U and Th is very large. For U, plagioclase-melt partition coefficients reported in the literature vary from 0.00004 to 0.5. For Th, the variation also covers several orders of magnitude ($0.0004 < D_{Th} < 0.38$).

We experimentally determined the partitioning of U, Th, K and a suite of other trace elements between anorthite-rich plagioclase and silicate melt at high temperature and atmospheric pressure. The lattice strain model [15] was used to rationalise plagioclase-melt partition coefficients for 1+, 2+, 3+ and 4+ trace elements. Our data are used to provide new estimates for the concentrations of U, Th and K in the lunar interior, which can serve as input parameters for models of lunar thermo-chemical evolution.

Methods: To separate the effect of composition from the possible effects of temperature and pressure, we chose compositions in the anhydrous simple system anorthite-albite-diopside, enabling synthesis of a range of plagioclase-melt pairs at a constant pressure of 1 bar and near-constant temperature of 1200-1230 ºC with different compositions. Experiments were performed in air in a box furnace. Run products (Fig. 1) were analysed by electron microprobe for major elements and laser ablation-ICP-MS for trace elements using methods described elsewhere [16].

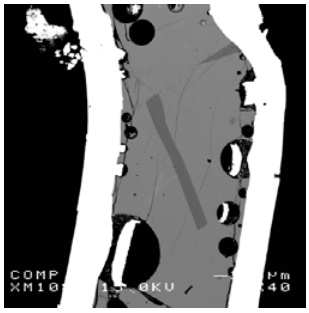

Fig. 1. Back-scattered electron image of typical polished run product. Plagioclase laths in dark grey, co-existing glass in light grey, Pt capsule in white.

Results: A range of plagioclase compositions between An58 and An81 was produced, enabling us to study the influence of the plagioclase anorthite content on partition coefficients. Our results for univalent, divalent and trivalent trace elements (not shown) are in

good agreement with previous plagioclase-melt partitioning experiments performed at similar conditions. Data for 1+, 2+, and 3+ elements are all amenable to lattice strain modeling treatment, and resulting lattice strain model parameters are in exellent agreement with previous work (not shown). We do not find any significant effect of plagioclase composition on D values. Figure 2 shows our partitioning values for Zr, Hf, U, and Th, together with lattice strain model fits. Fits to D_{Zr}, D_{Hf} and D_{Th} result in very similar ideal ionic radii r_0 values for all experiments, with a mean value of 0.925 Å.

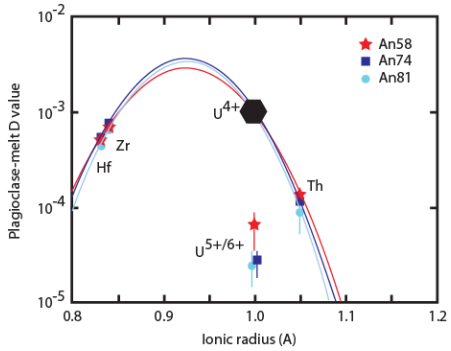

Fig 2. Measured plagioclase-melt D values for Zr, Hf, U and Th (small symbols), lattice strain models(curves) and predicted U4+ partition coefficient (large symbol).

Measured D_U values consistently fall significantly below the best-fit curves. It is important to note that our experiments were performed in air, in the absence of an oxygen fugacity buffer. At these conditions (log fO_2 approximately -0.7), uranium is not quadruvalent, but present mostly as pentavalent or hexavalent cations [17]. It is therefore not surprising that our U partitioning data do not fit the parabolic trends defined by the Zr, Hf and Th data. The fact that our measured D_U values lie significantly below the curve derived from the other elements is consistent with the fact that D for trace elements with charges >3+ decrease with increasing charge [18]. Our fits make it possible to estimate a partition coefficient for U^{4+} of approximately 0.00103. This estimate is required as, at the oxygen fugacity in the Moon, uranium is likely to be present in the 4+ state. The predicted D is an order of magnitude larger the the measured D. The fits indicate that the U^{4+} D is independent of plagioclase composition, enabling use of this value for models of lunar magmatic systems where the exact plagioclase composition and its variation are not perfectly known.

Implications for lunar heat budget: Our data on partitioning of U, Th and K between plagioclase and melt, combined with partitioning data for these elements in other minerals and an LMO crystallization sequence, can be used to estimate the total lunar heat budget. A sample calculation, using Apollo-derived surface plagioclase concentrations of 84 ppb for Th and 13 ppb for U, is shown in Fig. 3.

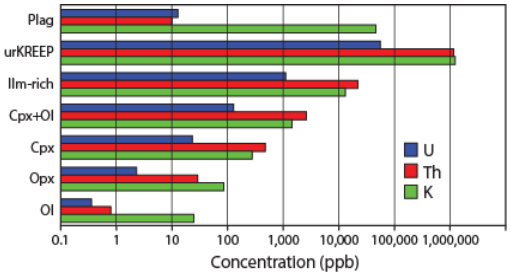

Fig 3.Sample calculation of spatial distribution of K, U and Th after solidification of the LMO using our plagioclase-melt D values for U and Th (Fig. 2)

A major result from our modeling is that resulting estimated bulk Moon Th and U levels are unrealisticially high. This indicates that plagioclase Th and U concentrations as taken from Apollo rock measurements, cannot represent concentrations in true primary plagioclase that crystallised from the LMO. To improve the calculation on heat production in the lunar minerals, accurate knowledge of trace element concentrations for pure LMO-derived anorthosites is essential, likely requiring new sample return missions. Furthermore, additional work on partitioning of 4+ elements under reducing conditions is needed to to determine the Th and U^{4+} D values for lunar applications with higher accuracy.

References: [1] Langseth M. et al. (1976) *LPSC 7*, 3143 [2] Takeda, H. et al. (2006) *EPSL 247*, 171 [3] Prettyman T. et al. (2007) *JGRP 111*, E12007 [4] Yamashita N. et al. (2010) *GRL 37*, L10201 [5] Kobayashi S. et al. (2010) *SSR 154*, 193 [6] Jolliff B.L. et al. (2011) *Nat Geo 4*, 566 [7] Snyder, G. et al. (1992) *GCA 56*, 3809 [8] Blundy J.D. and Wood B.J. (2003), *RMG 52*, 59 [9] Drake M. and Weill D. (1975) *GCA 39*, 689 [10] Bindeman I. et al. (1998) *GCA 62*, 1175 [11] Bindeman I. and Davis A. (2000) *GCA 64*, 2863 [12] Miller S. et al. (2006) *GCA 70*, 4258 [13] Aigner-Torres M. et al. (2007) *CMP 153*, 647 [14] Tepley III F. et al. (2010) *Lithos 118*, 82 [15] Blundy J.D. and Wood B.J. (1994) *Nature 372*, 452 [16] Van Kan Parker M. et al. (2011) *GCA 75*, 4179 [17] Berry A. et al. (2008) *GCA 12S1*, A79 [18] Wood B.J. and Blundy J.D. (2001) *EPSL 188*, 59.

Acknowledgement and Dedication: We thank Helen de Waard (Utrecht) for help with the laser ablation analyses.

TITANIUM-RICH MELTS ARE NEUTRALLY BUOYANT IN THE DEEP LUNAR INTERIOR. W. van Westrenen[1], M. van Kan Parker[1], C. Sanloup[2,3], N. Sator[4], B. Guillot[4], E. J. Tronche[1], J.-P. Perrillat[5], M. Mezouar[6], and N. Rai[1], [1]VU University Amsterdam, De Boelelaan 1085, 1081 HV, Amsterdam, the Netherlands, e-mail w.van.westrenen@vu.nl, [2]UPMC Université Paris 06, and CNRS, UMR 7193, Paris, France, [3]SUPA, School of Physics and Astronomy, and Centre for Science at Extreme Conditions, The University of Edinburgh, Edinburgh EH9 3JZ, UK, [4]Laboratoire de Physique Théorique de la Matière Condensée (UMR7600), Université Pierre et Marie Curie (Paris 6), 4 Place Jussieu, 75252 Paris, France, [5]Laboratoire de Géologie de Lyon, UMR5276, Université Claude Bernard Lyon 1, CNRS and ENS Lyon, Villeurbanne, France, [6]European Synchrotron Radiation Facility, Grenoble, France.

Introduction: The absence of moonquakes originating deeper than ~1100 km [1] has been used to suggest that the lower mantle of the Moon is partially molten, with recent estimates suggesting up to 30 volume per cent melt between 1200 and ~1350 km depth [2]. The absence of recent surface volcanic activity implies that such deep partial melts must be as dense as or denser than their solid surroundings. We determined [3] the density of a range of primitive lunar melts at lunar interior pressures by combining *in situ* synchrotron X-ray absorption measurement [4] with molecular dynamics computer simulations [5].

In situ measurements: To determine melt densities at high pressure (P) and high temperature (T), in situ synchrotron X-ray absorption experiments were conducted at beamline ID27 of the European Synchrotron Radiation Facility (Grenoble, France) on synthetic equivalents of two end-member compositions bracketing the unusually broad range of titanium contents in Apollo samples: Apollo 15C "green" glass (low titanium content of 0.23 wt% TiO_2) and Apollo 14 "black" glass (high titanium content of 16.4 wt% TiO_2). These glasses, thought to have formed in fire-fountaining eruptions [6], represent the most primitive lunar magmas sampled to date [7].

Powdered starting material was inserted into cylinders prepared from natural single crystal diamonds with graphite end caps, surrounded by low atomic number pressure-transmitting materials including a graphite heater, boron nitride insulating material, and boron epoxy pressure medium [4]. After pressurization, temperatures were increased until samples were fully molten. The intensity of the X-ray beam was measured with two photodiodes before and after crossing the cell assembly. Sample densities were obtained from fitting observed absorption patterns to simulated patterns that change as a function of sample density.

For molten green glass at P = 1.6 ± 0.3 GPa we obtained densities (ρ) of 2.87 ± 0.03 g cm^{-3} at T = 1908 ± 50 K and 2.84 ± 0.04 g cm^{-3} at T = 1983 ± 50 K. Molten black glass experiments yielded ρ = 3.15 ± 0.14 g cm^{-3} at P = 1.0 ± 0.3 GPa, T = 1854 ± 50 K; ρ = 3.11 ± 0.03 g cm^{-3} at P = 1.6 ± 0.3 GPa, T = 1775 ± 50 K; and ρ = 3.14 ± 0.03 g cm^{-3} at P = 1.7 ± 0.3 GPa, T = 1850 ± 140 K [3].

Molecular dynamics simulations: To enable extrapolation of our measurements to the pressure-temperature conditions in areas of the deep lunar mantle where melt was identified (P > 4.5 GPa), and to better quantify the effect of composition on melt density, we performed molecular dynamics (MD) simulations to evaluate the density of molten low (green), intermediate-high (orange) and high titanium (black) bearing lunar glass compositions at conditions bracketing those relevant to the Moon (pressures between 0 and 10 GPa and temperatures of 1723, 2073 and 2423 K). Melt densities were calculated by classical MD simulations [5], using a simple force field to describe the silicate melt structure.

Results of the MD simulations are well described by third-order Birch-Murnaghan equations of state. Calculated 1-bar densities of these lunar melts, at a reference temperature of 1673 K, increase from ρ = 2.83 ± 0.01 g cm^{-3} for the molten green glass composition and ρ = 2.96 ± 0.02 g cm^{-3} for the molten orange glass composition, to ρ = 3.04 ± 0.01 g cm^{-3} for the molten Ti-rich black glass composition [3]. These values are within error of predicted values based on 1-bar density measurements in simple silicate systems, and clearly show the strong effect of composition on melt density. Isothermal bulk moduli at a reference temperature of 1673 K, are 18.2 ± 0.2 GPa for molten green glass, 20.4 ± 0.9 GPa for molten orange glass, and 19.6 ± 0.3 GPa for molten black glass [3], again in excellent agreement with empirical relations. Corresponding pressure derivatives, K′, are similar for all three compositions at 8.5 ± 0.2, 7.4 ± 0.5, and 9.2 ± 0.3, respectively. The combined effect of increasing Ti content, concomitant decreasing Si content, and nearly constant Ca+Fe+Mg content in the sequence green-orange-black glass is an increase in 1-bar melt densities at similar K and K′ values.

Figure 1 summarizes our results. Our in situ measurements agree well with our MD simulations, especially considering the fully independent nature of the techniques. Small density differences between the two data sets are likely due to (1) small differences between

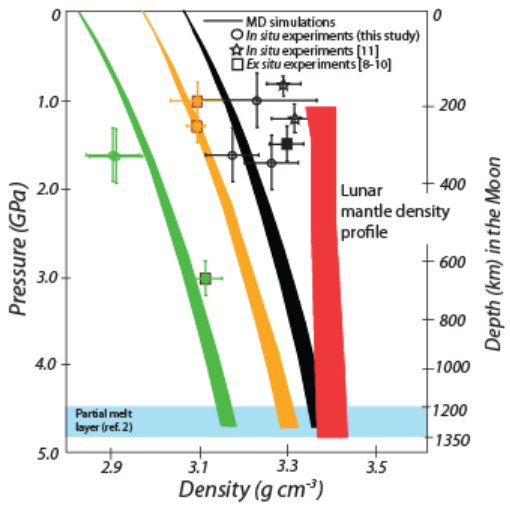

Fig. 1. *Density evolution of studied lunar glass compositions with P at estimated liquidus temperature and estimated liquidus T gradients of 70-100 K GPa^{-1}. Results from sink/float experiments are indicated with squares [8-10], in situ experiments are indicated with stars [11] and circles (this study). Blue bar gives area of partial melt according to [2]. Red field gives recent estimates of the density profile in the lunar mantle from seismic data and thermodynamic modeling [12,13]. Figure modified after [3].*

the ideal glass compositions used in the simulations and the experimental compositions; (2) the relatively large P-T uncertainties of the in situ experiments.

Ex situ high-pressure, high-temperature so-called sink/float experiments were previously performed on synthetic analogues of the green, orange, and black glass composition [8-10] (squares in Fig. 1). Sink/float data are in excellent agreement with our results for the green glass and orange glass. For the black glass composition, sink/float data suggest slightly higher density values than obtained from our in situ data or MD results. Within the lunar pressure regime, the sink/float density results agree with MD results to within 1.3 % for the green, 0.7 % for the orange and 2.8 % for the black glass composition.

One other study recently reported the results of in situ experiments on the density of molten black glass [11]. These results suggested higher densities than both our in situ and MD data (Fig. 1). As ref. [11] did not report the chemical compositions of their run products, it is difficult to assess the extent of the deviation of their sample composition from ours.

Discussion: The recent re-evaluation of the Apollo seismic data set by Weber et al. [2] suggests the presence of 5 to 30% melt in the lowermost 150 km of the lunar mantle. The density at this depth range is estimated to be 3.39-3.44 g cm^{-3} [12,13]. Figure 1 shows that only melts with TiO_2 contents above ~ 16 wt%, coinciding with the maximum TiO_2 content of melts erupted on the lunar surface, can be neutrally or negatively buoyant in the lunar interior. The seismically observed presence of partial melt [1,2] thus suggests the presence of very Ti-rich melts in the present-day Moon. Such melts can only plausibly be formed from titanium-rich source rocks, as thought to be formed in the Moon towards the end of initial magma ocean crystallization. Previous work has shown that Ti-rich cumulates form near the base of the lunar crust, and that the relatively shallow presence of this dense cumulate leads to a gravitationally unstable cumulate pile conducive to convective overturn [14,15]. Our data imply that sinking Ti-rich cumulates stay hot enough over the course of lunar history to remain partially molten to the present day near the bottom of the lunar mantle.

Partial melting of Ti-rich cumulates at high pressure requires temperatures in excess of ~ 1750 K [16]. Such high temperatures are consistent with recent models of the distribution of heat-producing elements between lunar magma ocean cumulate reservoirs [17,18]. These models show that Ti-rich cumulates are enriched in uranium and thorium compared to all other mantle reservoirs due to their relatively high modal abundance of pyroxene and the enriched nature of the residual magma ocean at the time of crystallisation of these cumulates. The resulting elevated heat production levels could lead to the present-day presence of partial melt in the deep lunar mantle. In addition, high lunar lower mantle temperatures would induce low cooling rates of a metallic lunar core, consistent with the proposed presence of a partially molten core today [2].

References: [1] Nakamura Y 2005) *JGR* 10, E01001 [2] Weber RC et al. (2011) *Science* 331, 309 [3] Van Kan Parker M et al. (2012) *Nature Geosci*., in press [4] Sanloup C et al. (2000) *GRL* 27, 8114 (2000 [5] Guillot B & Sator N (2007) *GCA* 71, 1249 [6] Elkins-Tanton LT et al. (2003) *GRL* 30, 1513 [7] Wagner TP & Grove TL (1997) *GCA* 61, 1315 [8] Smith JR & Agee CB (1997) *GCA* 61, 2139 [9] van Kan Parker M et al. (2011) GCA 75, 1161 [10] Circone S & Agee CB (1996) *GCA* 60, 2709 [11] Sakamaki, T., Ohtani, E., Urakawa, S., Suzuki, A., Katayama, Y. & Zhao, D (2010) *EPSL* 299, 293 [12] Garcia RF et al. (2011) *PEPI* 188, 96 [13] Khan A et al. (2006) JGR 111, E05005 [14] Hess PC & Parmentier EM (1995) *EPSL* 134, 501 [15] de Vries J et al. (2010) *EPSL* 292, 139 [16] Wyatt B (1977) *CMP* 61, 1 [17] van Kan Parker M (2011) PhD Thesis, VU University Amsterdam, ISBN 978-90-8659-542-6 [18] de Vries J et al. (2011) *LPSC* 42, 1745